

**ENGAGING IMMUNE CELLS WITHIN THE TUMOR MICROENVIRONMENT TO  
ENHANCE EFFICACY OF ONCOLYTIC VIROTHERAPY**

By

**Divya Priya Ravirala**

A dissertation submitted to the Department of Biology and Biochemistry,  
University of Houston  
in partial fulfillment of the requirements for the degree of

**DOCTOR OF PHILOSOPHY**

in Biology

Chair of Committee: Xiaoliu Zhang

Committee Member: Qin Feng

Committee Member: Weiyi Peng

Committee Member: Navin Varadarajan

University of Houston  
August 2021

Copyright 2021, Divya Priya Ravirala

## DEDICATION/EPIGRAPH

I dedicate this work to my *amma* and *bapa* who gave me all their love and care.

No words can express my gratitude for them, for all the sacrifices they have made and have  
always supported and encouraged me.

\*\*\*\*\*

## ACKNOWLEDGMENTS

I would like to express my sincere thanks to my advisor, Dr. Shaun Zhang, for his relentless support, guidance, and valuable inputs throughout this endeavor. I am immensely thankful to him for investing his time, providing all the required resources in the lab towards my research work. I would like to specially thank him for his valuable input in reviewing my manuscripts and submitting it to various high impact journals. His readiness to discuss the progress of my work and his expert suggestions helped me to complete my studies in relatively short time.

I am also thankful to Dr. Fu for generously sharing with me his technical expertise in oncolytic viral research. In many of my conversations we have had over the last three and half years, he was always available for trouble shooting experiments and offered helpful solutions in many of the experiments in the lab.

I would also like to sincerely thank my committee members, Dr. Navin Varadarajan for his scientific advice and his questions probed me in exploring my research to achieve much deeper insight. I would like to thank Dr. Weiyi Peng for her enormous support and assistance in some of my experiments that led to publications. I would also thank Dr. Qin Feng, who has been extremely supportive, giving me constant encouragement throughout my research work.

I would like to acknowledge our collaboration with the University of Houston Sequencing and Editing Core (UH-SNEC), Dr. Preeti Gunaratne and Dr. Brandon Mistretta for assistance with pre-processing and upstream analysis of the scRNA-seq data. I would like to extend my sincere thanks to our collaborators, at UT Health, Dr.

Zhongming Zhao and Dr. Guangsheng Pei, without which this work would have not been complete. I would like to extend my special thanks to Dr. Pei for all the help with the Bioinformatics and scRNA seq analysis. He was always available to answer my questions at any time of the day and has been extremely patient with me.

I would like to also thank our Lab Manager, Aiwu Jin. She has been very kind, highly cooperative, taking care of my needs in the lab on a day to day basis. I would also thank our lab technician, Lihua Tao who is amazing with her lab skills, some of which she had taught me during my period here.

The friendly and co-operative working environment at the Center for Nuclear Receptors and Cell Signaling (CNRCS) was a great help during the past few years of my time here. I also want to extend my thanks to my friends in the center, Charles, Esra, Siddharth, Bilqees, Shivangi, Rick, Nick, Chunyu and others who offered their help whenever needed.

This journey would have been impossible without the support of my family. My mom has been the most important influence in my life. It is impossible to describe her contribution in a few words. Her excellent vision and constant encouragement have helped me in becoming what I am today. My dad has always been a silent supporter throughout my career. I am also indebted to all my sisters, Akka, Suman and Devi for their support and encouragement. I would also like to thank my parents-in-law for supporting me in this journey.

Lastly but not least, thanks to my beloved husband, Naveen, who has been nothing but supportive and without which, I would not have been able to accomplish this goal. His Love, encouragement and help with taking care of our daughters while I am at work, helped me to achieve my goals. I thank him from the bottom of my heart for playing such a huge part and I am proud to share my accomplishment with him today. I would want to shower my love to my two daughters, Nivea and Nishta, to whom I went back to seek solace after an exhausted day in the lab. They are and will be the source of my motivation and commitment in finishing this journey and many more in the future.

This work was supported by the CPRIT grant RP200464 and a grant from the William and Ella Owens Medical Research Foundation (to X.Z.).

## ABSTRACT

Oncolytic viruses are particularly attractive for many of the current cancer-immunotherapeutic modalities in their capacity to simultaneously cause direct lysis of tumor cells and indirect augmentation of host anti-tumor immunity. Despite widespread interest in the direct anti-cancer activity of oncolytic viruses, only limited attention has been paid to the interaction between viral therapy and the tumor microenvironment. We studied the impact of FusOn-H3 (HSV-2 oncolytic virus) on the tumor microenvironment (TME), using single-cell RNA sequencing (scRNAseq) to investigate the infiltration and functionality within global populations or at the single-cell level. Our data show that FusOn-H3 can induce significant infiltration of both innate and adaptive immune cells. Detailed analysis by scRNAseq revealed the influx of T cells, B cells, NK cells, and Neutrophils into the TME, contributing to the conversion of cold tumors into hot ones. Moreover, we harnessed the immune modulation potential of oncolytic viruses by engaging the immune cells within the TME, using chimeric engagers for improved anti-tumor efficacy. To accomplish this, we have generated two chimeric proteins, the Bispecific and Trispecific engagers (BiCEP and TriCEP), the genes encoding for which were delivered by an HSV amplicon system, packaged with the oncolytic virus as a helper virus. The release of these chimeric engagers by the co-delivered amplicons mediate cytotoxicity against tumor cells by crosslinking them with the immune cells via the overexpressed EGFR. Our data demonstrate that HSV-1 amplicon encoding Bi- and TriCEP combined with the oncolytic virus (Synco-2D) lead to durable remissions and protective anti-tumor immunity in an immunocompetent mouse model. These findings give us an understanding of changes in the immune cell

landscape and viral-host interactions in complex tumor microenvironment and open new avenues for virotherapy.

# TABLE OF CONTENTS

<b>DEDICATION/EPIGRAPH .....</b>	<b>III</b>
<b>ACKNOWLEDGMENTS .....</b>	<b>IV</b>
<b>ABSTRACT.....</b>	<b>VII</b>
<b>TABLE OF CONTENTS .....</b>	<b>IX</b>
<b>LIST OF TABLES.....</b>	<b>XIII</b>
<b>LIST OF FIGURES.....</b>	<b>XIV</b>
<b>LIST OF ABBREVIATIONS .....</b>	<b>XVI</b>
<b>1. ONCOLYTIC VIRUSES- A GENERAL INTRODUCTION.....</b>	<b>19</b>
1.1 Oncolytic viruses.....	20
1.2 Herpes Simplex Virus (HSV).....	22
1.3 Type I HSV .....	23
1.3.1 Synco-2D, an HSV-1 virus.....	26
1.4 Type II HSV .....	27
1.4.1 FusOn-H2, an HSV-2 virus.....	28
1.5 HSV as an attractive oncolytic agent .....	32
1.6 HSV Amplicon vectors .....	33
1.7 Cancer and the immune system.....	35
1.8 Current strategies in engaging oncolytic viruses with antitumor immunity .....	36
1.8.1 Oncolytic viruses enhance antigen presentation .....	39
1.8.2 OV's can enhance dendritic cell trafficking to the TME and cross- presentation to CTLs .....	40
1.8.3 Armed OV's can cause the release of ligands of T cell costimulatory receptors .....	47
1.8.4 OV's induce the release of cytokines that support CTL expansion and function.....	50
1.8.5 OV's can induce the release of chemokines that attract CTLs to the TME	53
1.8.6 OV's can support CTL activity by inhibiting T regulatory cells.....	55
1.8.7 Oncolytic virotherapy is enhanced by targeting CTL checkpoints .....	56
1.8.8 OV's can also be engineered to mediate direct engagement of tumor cells with immune cells in the TME .....	62
1.8.9 Ongoing OV Trials .....	70
1.9 Oncolytic virotherapy in combination with immunotherapy .....	73
1.10 Goals, and overall aim of the current study.....	75
<b>2. SINGLE CELL RNA SEQUENCING REVEALS PROFOUND AND DISTINCT CHANGES IN THE TUMOR IMMUNE LANDSCAPE FOLLOWING TREATMENT WITH AN HSV-2 BASED ONCOLYTIC VIRUS.....</b>	<b>77</b>
2.1 Abstract .....	78

2.2	Introduction .....	79
2.3	Materials and Methods .....	82
2.3.1	Cell lines and oncolytic viruses .....	82
2.3.2	Tumor transplantation and treatment .....	82
2.3.3	Tumor dissociation and single-cell processing .....	83
2.3.4	scRNA-seq library preparation and sequencing .....	83
2.3.5	Transcriptome analysis .....	84
2.3.6	Single-cell data analysis .....	85
2.3.7	Lymphoid population analysis .....	86
2.3.8	Immunohistochemistry protocol .....	86
2.3.9	Immunofluorescence staining .....	87
2.4	Results .....	88
2.4.1	scRNA-seq data collection on tumor samples obtained from a “hEGFR tagged” murine colon cancer model .....	88
2.4.2	The overall impact of FusOn-H3 virotherapy on the immune cell landscape in TME .....	93
2.4.3	Comparison of subset composition of the infiltrated T cells between the PBS control and FusOn-H3 treatment groups .....	98
2.4.4	Further characterization on the infiltrated B cells following FusOn-H3 virotherapy .....	103
2.4.5	Changes in the infiltration of other immune cells induced by FusOn-H3 virotherapy .....	106
2.4.6	Complex immune landscape change in the TME following FusOn-H3 virotherapy predicted by interactions among the infiltrated immune cells .....	111
2.5	Discussion .....	117
2.6	Supporting information .....	120
2.6.1	scRNA sequencing raw and meta data .....	120
<b>3.</b>	<b>CO-DELIVERY OF NOVEL BI-SPECIFIC AND TRI-SPECIFIC ENGAGERS BY AN AMPLICON VECTOR AUGMENTS THE THERAPEUTIC EFFECT OF AN HSV-BASED ONCOLYTIC VIROTHERAPY .....</b>	<b>121</b>
3.1	Abstract .....	122
3.2	Introduction .....	123
3.3	Materials and Methods .....	127
3.3.1	Cell lines and oncolytic virus .....	127
3.3.2	Plasmid construction .....	128
3.3.3	Amplicon plasmid cloning and amplicon production .....	128
3.3.4	In vitro detection of transgene expression in mammalian cells .....	129
3.3.5	Binding assays by flow cytometry analysis .....	129
3.3.6	In vitro co-culture killing assay .....	130
3.3.7	FACS based cleaved caspase 3 cytotoxicity assay set-up, antibody staining and flow cytometry analysis .....	131
3.3.8	Oncolytic virus and amplicon titration .....	132
3.3.9	Western blot .....	132

3.3.10	Animal studies .....	132
3.3.11	H & E staining and immunohistochemistry .....	133
3.3.12	Tumor dissociation and single-cell processing .....	133
3.3.13	scRNA-seq library preparation and sequencing .....	134
3.3.14	Transcriptome analysis .....	135
3.3.15	Single-cell data analysis .....	135
3.3.16	Statistical analysis .....	136
3.4	Results .....	137
3.4.1	Design of a novel engager that can engage both infiltrating NK cells and CD8+ T cells to enhance the antitumor effect of an HSV-based oncolytic virus .....	137
3.4.2	In vitro characterization of BiCEP and TriCEP .....	140
3.4.3	In vitro assay on the ability of BiCEP and TriCEP to engage NK cell with tumor cells and to induce cytotoxicity .....	145
3.4.4	Insertion of BiCEP and TriCEP coding sequences into an amplicon vector for in vivo delivery .....	149
3.4.5	Therapeutic impact of BiCEP and TriCEP co-delivered by amplicon during Synco-2D virotherapy .....	152
3.4.6	Characterization of immune cell landscape in TME during virotherapy with or without co-delivery of TriCEP by single-cell RNA sequence (scRNA-seq) .....	154
3.4.7	Oncolytic vectors for expression of chimeric engagers .....	161
3.5	Discussion .....	164
3.6	Supporting information .....	167
3.6.1	scRNA sequencing raw and meta data .....	167
<b>4.</b>	<b>COMPREHENSIVE CHARACTERIZATION OF ONCOLYTIC VIRUS INFECTION WITHIN THE TUMOR MICROENVIRONMENT BY SINGLE CELL RNA SEQUENCING .....</b>	<b>168</b>
4.1	Introduction .....	169
4.2	Materials and Methods .....	171
4.2.1	Cell lines and oncolytic viruses .....	171
4.2.2	Tumor transplantation and treatment .....	172
4.2.3	Tumor dissociation and single-cell processing .....	172
4.2.4	scRNA-seq library preparation and sequencing .....	173
4.2.5	scRNA-seq data process .....	174
4.2.6	scRNA-seq data analysis .....	174
4.2.7	Statistical analysis .....	175
4.3	Results .....	176
4.3.1	Dissecting oncolytic HSV infection of tumor with FusOn-H3 using combined single-cell mapping of host and viral transcriptome .....	176
4.3.2	Correlation of known antiviral genes and tumor infection status .....	183
4.3.3	Correlation of other cellular genes and tumor infection status .....	186
4.3.4	Oncolytic HSV infection of immune cells .....	188
4.3.5	CellChat analysis .....	191
4.4	Discussion .....	194

4.5	Supporting information .....	195
4.5.1	scRNA sequencing raw and meta data .....	195
4.5.2	Additional figures.....	196
<b>5</b>	<b>FUTURE DIRECTIONS .....</b>	<b>199</b>
<b>6</b>	<b>BIBLIOGRAPHY .....</b>	<b>201</b>
	<b>APPENDIX I: LIST OF GLOSSARY (SOURCE: MARY CROWLEY CANCER RESEARCH) .....</b>	<b>222</b>

## LIST OF TABLES

Table 1.1: OVs in combination with the immune modulators .....	67
Table 1.2: Current ongoing clinical trials involving oncolytic viruses .....	72
Table 3.1: p-values for the violin plots .....	157
Table 4.1: Immediate early ( $\alpha$ ), early ( $\beta$ ), and late ( $\gamma$ ) HSV gene expression .....	189

## LIST OF FIGURES

Figure 1.1: HSV-1 infection.....	25
Figure 1.2: HSV-2 infection.....	28
Figure 1.3: Therapeutic effect of FusOn-H2 against established mammary tumor after a single intratumoral infection.....	30
Figure 1.4: Attractant effect of FusOn-H2 on OT1 cell migration to the tumor site and the subsequent in situ expansion of OT-1 cells.....	31
Figure 1.5: Amplicon plasmid and amplicon vectors .....	34
Figure 2.1: scRNA-seq setup and data collection .....	90
Figure 2.2: Quantification of the signature genes of various immune cell subsets by scRNA-seq.....	92
Figure 2.3: Characterization of the composition of infiltrated immune cells via scRNA-seq data analysis and substantiation by IHC staining on the same tumor tissues after virotherapy .....	95
Figure 2.4: CD45+ cell sorting data on the single cell suspensions used for scRNA-seq expression and IHC staining on the same tumor tissues .....	97
Figure 2.5: Compositional and qualitative characterization of the infiltrated T lymphocytes in TME.....	101
Figure 2.6: Quantification of some key genes in the T cell sub-clusters .....	102
Figure 2.7: FusOn-H3 induces significant infiltration of B cells to the TME .....	105
Figure 2.8: NK cell infiltration and activation status upon FusOn-H3 treatment.....	108
Figure 2.9: Other innate immune cell infiltration and activation status upon FusOn-H3 treatment.....	110
Figure 2.10: Cell-to-cell communications among the infiltrated immune cells in the TME predicted by the CellChat software.....	115
Figure 2.11: Comparison of the overall information flow/interaction strength of each signaling pathway within the inferred network.....	116
Figure 3.1: Design of bispecific and trispecific engagers, their anticipated mechanism of action and expression in-vitro .....	139
Figure 3.2: Binding specificity of BiCEP and TriCEP to NKG2D and EGFR .....	143

Figure 3.3: In-vitro cytotoxic activity of TALL-104 cells against EGFR-expressing SKOV3 cells in the presence of chimeric engagers .....	147
Figure 3.4: Characterization of amplicon plasmids the chimeric engagers and production of the packaged amplicon .....	151
Figure 3.5: Therapeutic evaluation of co-administration of the chimeric engagers with Synco-2D in a murine colon cancer model .....	153
Figure 3.6: scRNA-seq characterization of infiltrating immune cells in TME after different treatment .....	158
Figure 3.7: Quantification of the signature NK and T cell activation and cytotoxic genes by scRNA-seq .....	160
Figure 3.8: Quantification of key cytokine genes within NK and T cell clusters by scRNA-seq.....	162
Figure 3.9: Oncolytic Herpes viruses encoding chimeric engagers (BiCEP/ TriCEP). Proposed mechanism of action of HSV amplicon vector encoding chimeric engagers.....	163
Figure 4.1: scRNA-seq experiment and data analysis .....	180
Figure 4.2: Cell-to-cell variability in infection dynamics and viral gene expression	181
Figure 4.3: viral gene expression according to their infection status.....	182
Figure 4.4: The anti-viral program is initiated in cells irrespective of their infection status .....	185
Figure 4.5: Differential expression of cellular genes between infected and uninfected cells.....	187
Figure 4.6: FusOn-H3 specifically infects tumor cells sparing other cells in the TME .....	190
Figure 4.7: Cell-to cell communications among the infected and uninfected cells with the cells in the TME .....	193
Figure 4.8: Differential expression of viral genes between infected and uninfected cells.....	196
Figure 4.9: Common signaling pathways for IL-1 family of cytokines .....	197
Figure 4.10: Therapeutic impact of FusOn-H3 in two mouse tumor models .....	198

## LIST OF ABBREVIATIONS

<b>APC</b>	Antigen Presenting Cells
<b>ATP</b>	Adenosine Triphosphate
<b>BCR</b>	B-Cell Receptor
<b>BiCEP</b>	Bispecific Chimeric Engager Protein
<b>BiTE</b>	Bispecific T Cell Engager
<b>CAFs</b>	Cancer Associated Fibroblasts
<b>CAR-T</b>	Chimeric Antigen Receptor – T cells
<b>CD</b>	Cluster of Differentiation
<b>CPE</b>	Cytopathic Effect
<b>CTLs</b>	Cytotoxic T-Lymphocytes
<b>DAMPs</b>	Damage Associated Molecular Patterns
<b>DC</b>	Dendritic Cell
<b>ECM</b>	Extracellular Matrix
<b>EGFR</b>	Epidermal Growth Factor Receptor
<b>FACS</b>	Fluorescence Activated Cell Sorting
<b>FDA</b>	U.S. Food and Drug Administration
<b>FITC</b>	Fluorescein Isothiocyanate
<b>GALV.fus</b>	Gibbon Ape Leukemia Virus Envelope Fusogenic Membrane Glycoprotein
<b>GEM</b>	Genetically Engineered Mouse
<b>GFP</b>	Green Florescent Protein
<b>GMCSF</b>	Granulocyte Macrophage Colony-Stimulation Factor
<b>GZMB</b>	Granzyme B
<b>HSV</b>	Herpes Simplex Virus
<b>HVEM</b>	Herpes Virus Entry Mediator
<b>ICIs</b>	Immune Check Point Inhibitors
<b>IFC</b>	Immunofluorescence
<b>IFN</b>	Interferon- $\gamma$

<b>IHC</b>	Immune Histochemistry
<b>IL</b>	Interleukin
<b>ISGs</b>	Interferon-Stimulated Genes
<b>MDSC</b>	Myeloid-Derived Suppressor Cells
<b>MHC</b>	Major Histocompatibility Complex
<b>MIF</b>	Macrophage Inhibitory Factor
<b>MOI</b>	Multiplicity of Infection
<b>MTD</b>	Maximum Tolerated Dose
<b>MWCO</b>	Molecular Weight Cut-Off
<b>NK</b>	Natural Killer Cells
<b>NKG2D</b>	Natural Killer Group 2D Receptor
<b>NT</b>	Non-Transfected (Control)
<b>OMCP</b>	Orthopox Major Histocompatibility Class I-like Protein
<b>oriS</b>	Origin of Replication
<b>OVs</b>	Oncolytic Viruses
<b>p.i</b>	Post-infection
<b>pac</b>	Packaging Signal
<b>PAMPs</b>	Pathogen Associated Molecular Patterns
<b>PCA</b>	Principle Component Analysis
<b>pfu</b>	Plaque Forming Units
<b>PKR</b>	Protein Kinase R
<b>Prf1</b>	Perforin I
<b>PTEN</b>	Phosphatidylinositol 3,4,5-Trisphosphate 3-Phosphatase
<b>RAS</b>	Rat Sarcoma
<b>RB1</b>	Retinoblastoma I
<b>RCC</b>	Renal Cell Carcinoma
<b>scRNA-seq</b>	Single-Cell RNA Sequencing
<b>SNN</b>	Shared Nearest Neighbor
<b>TAA</b>	Tumor Associated Antigens

<b>TCR</b>	T-Cell Receptor
<b>TGFb</b>	Transforming Growth Factor B
<b>TK</b>	Thymidine Kinase
<b>TME</b>	Tumor Microenvironment
<b>TP53</b>	Tumor Protein 53
<b>TriCEP</b>	Trispecific Chimeric Engager Protein
<b>T-VEC</b>	Talimogene Laherparepve
<b>UMAP</b>	Uniform Manifold Approximation and Projection
<b>VEGF</b>	Vascular Endothelial Growth Factor
<b>WNT</b>	Wingless-Int
<b>WT</b>	Wild Type

## **1. ONCOLYTIC VIRUSES- A GENERAL INTRODUCTION**

## 1.1 Oncolytic viruses

Oncolytic viruses (OVs) are self-replicating, tumor specific, and directly lyse the tumor cells.<sup>1</sup> These viruses may be tumor selective in wild-type (WT) or attenuated forms. OVs present two distinct, although not mutually exclusive, advantages by which they can target specific cells. The first is the basic principle of viral infection, that viruses naturally exploit permissive cells for infection through expression of the necessary surface receptors that allow viral entry into the cells and via the modulation of host defense pathways that allow viruses to avoid detection. Secondly, the tumor selectivity of OVs is largely conferred by tumor-specific aberrations in certain signaling pathways that would otherwise sense and block viral replication. There is increasing evidence that cancer-specific aberrations in RAS, TP53, RB1, and PTEN genes encoding proteins involved in the WNT signaling pathway and other cancer-related genes can predispose cancer cells to infection.<sup>2,3,4</sup> Moreover, OVs mediate anti-tumor responses through a dual mechanism; direct viral oncolysis of cancer cells and induction of host anti-tumor immunity.

Oncolytic viruses are of special interest for their capacity to induce immunogenic cell death.<sup>5,6</sup> Upon infection, viruses hijack the host cell to make viral proteins, avoiding early cell death and simultaneously bypass immune recognition from the host.<sup>7</sup> This promotes the viral replication within, eventually lysing the cells and releasing the progeny viral particles, resulting in the amplification of the viral dose. Dying tumor cells release Tumor-associated antigens (TAA's), pathogen-associated molecular patterns (PAMPs), and damage-associated molecular pathogens (DAMPs) and encounter

Antigen Presenting Cells such as dendritic cells in the TME. Viral infection induces local inflammation, which stimulates the maturation of dendritic cells. Mature dendritic cells migrate to the lymph nodes where they present the TAA's to the T cells. This may elicit an anti-cancer CD4+ and CD8+ effector T cell response that has the potential to kill both viral infected and viral uninfected cells.<sup>8</sup> Moreover, there is an early influx of innate immune cells, including macrophages and NK cells in response to tumor viral therapy. Besides, some OV's infect tumor endothelial cells and disrupt the tumor-associated vasculature by expression of anti-angiogenic viral proteins, leading to ischemia and necrotic death of uninfected tumor cells. Collectively, these immunogenic changes within the tumor alter the cold, immune-suppressive environment, to a hot inflamed tumor. It has become evident in recent years that virotherapy can modulate the tumor microenvironment in a way favorable to many immunotherapeutic agents, thereby synergizing the effects of both therapies.

Oncolytic virus immunotherapy (OVIT) is a therapeutic approach to cancer treatment that utilizes native or genetically modified viruses that selectively replicate within tumor cells and has shown promising results in the clinic. Moreover, these viruses have demonstrated favorable toxicity and safety profiles.<sup>9</sup> Talimogene laherparepvec (T-VEC; Imlygic™), is a genetically modified herpes simplex virus, type 1, supported by the expression of GM-CSF is the first oncolytic virus therapy to be approved for the treatment of advanced melanoma by the US FDA.<sup>10</sup> Despite its success in the clinic, no other oncolytic virus has been approved thus far for the treatment of cancers. Although monotherapy with T-VEC has manifested only moderate benefits against melanoma, the combination treatment with check point inhibitors has improved its overall

efficacy.<sup>11</sup> On this basis, future clinical trials of oncolytic viral therapy should be designed to exploit their immunotherapeutic as well as direct cytotoxic properties to treat cancers. In this dissertation, we have investigated the use of combination immunotherapy, combining OV's with immune modulators, which will cause a direct and targeted killing of the tumor cells and simultaneously activating the immune system to produce a more robust and sustainable anti-tumor immune response. The oncolytic viruses investigated in this study are Herpes Simplex Viruses, both Type I (Synco-2D) and Type II (FusOn-H3) viruses, which were developed in the lab.

## **1.2 Herpes Simplex Virus (HSV)**

HSV is a double stranded DNA virus and is well studied human pathogen. The genome of HSV is large, consisting of around 150 kbp and encodes approximately 84 polypeptides, several of which are essential for viral replication. The HSV genome is enclosed inside a capsid and is surrounded by a fibrous component called the integument. The virus is encapsulated within a glycolipid envelope structure and has glycoproteins attached to the surface. There are two closely related serotypes, HSV-1, and HSV-2; with HSV-1 causing oral lesions, while HSV-2 causes genital herpes in humans. HSV infect the host through skin or mucosal surfaces, with the initial interaction between the glycoproteins and the cellular receptors. HSV encodes four glycoproteins (A-D) that mediate the attachment of the target cell through heparin sulfate (HS).<sup>12</sup> Following which, the virus envelope binds to the cellular receptors leading to the fusion of the viral envelope with the cellular membrane. The capsid is transported to the nucleus where the genome is released. Immediate early genes are

transcribed first, initiating the transcription of early and late genes. Early genes are the genes encoding for viral ribonucleotide reductase (ICP6), thymidine kinase (TK), and DNA polymerase (UL30), all of which initiate viral DNA synthesis. Late genes encode for structural proteins and form capsid, during this process, often called hijacking, host defenses are inhibited against viral replication and spread. HSV enters sensory nerve endings after infection, where its replication is restricted and often culminates in a latent infection, associated with the transcription of latency associated transcript (LAT) proteins. A variety of stimulus can reactivate the latent virus, resulting in recurrent infections throughout a person's lifetime.

### 1.3 Type I HSV

HSV-1 is a major human pathogen that causes cold sores, skin lesions or rashes and has been extensively researched as a candidate for oncolytic viral therapy. The prominent approach of converting a wild-type HSV-1 virus into an oncolytic agent is to delete the viral genes necessary for efficient replication in normal cells but not in tumor cells. Early research of the virus as an oncolytic agent included deletions of the  $\gamma 34.5$  gene and *ICP6*.<sup>12</sup> By deleting the  $\gamma 34.5$  gene, infections of the nervous system were prevented since this gene encodes for neuro-virulence factor.<sup>13,14</sup> When infected with HSV-1, normal cells shut down protein synthesis because of an activated protein kinase R (**Figure 1.1**). ICP34.5 will reactivate a downstream phosphatase which revives protein synthesis in infected cells allowing for viral proliferation. Because there is limited activation of protein kinase R in cycling cells, replication of HSV-1 with a deleted  $\gamma 34.5$  will be specific in those cells with activated protein kinase R, abundant in dividing cells

but not in non-dividing cells.<sup>15</sup> Removal of the *ICP6* also induces the virus to divide specifically in tumor cells. Because *ICP6* encodes for a ribonucleotide reductase and its deletion constrains the virus to divide in cells which express mammalian ribonucleotide reductase, which is abundantly expressed in tumor cells.<sup>16,17</sup> Consequently, any mutations within these genes would also render the virus replicate specifically in tumor cells.

T-VEC is a modified HSV-1, developed by Robert Coffin and colleagues from a clinical isolate of HSV-1 (strain JS1) which includes deletions of both copies its  $\gamma 34.5$  as well as a replacement of the *ICP47* gene with *GM-CSF*.<sup>18</sup> This modification would help enhance the virulence of the virus, increasing its oncolytic potential and to potentiate the ability to induce anti-tumor immunity (with the insertion of GMCSF).<sup>12</sup> With its excellent safety profile and efficacy against melanoma, T-VEC remains the first live virus to be approved by FDA for clinical use as a therapeutic against malignant melanoma.

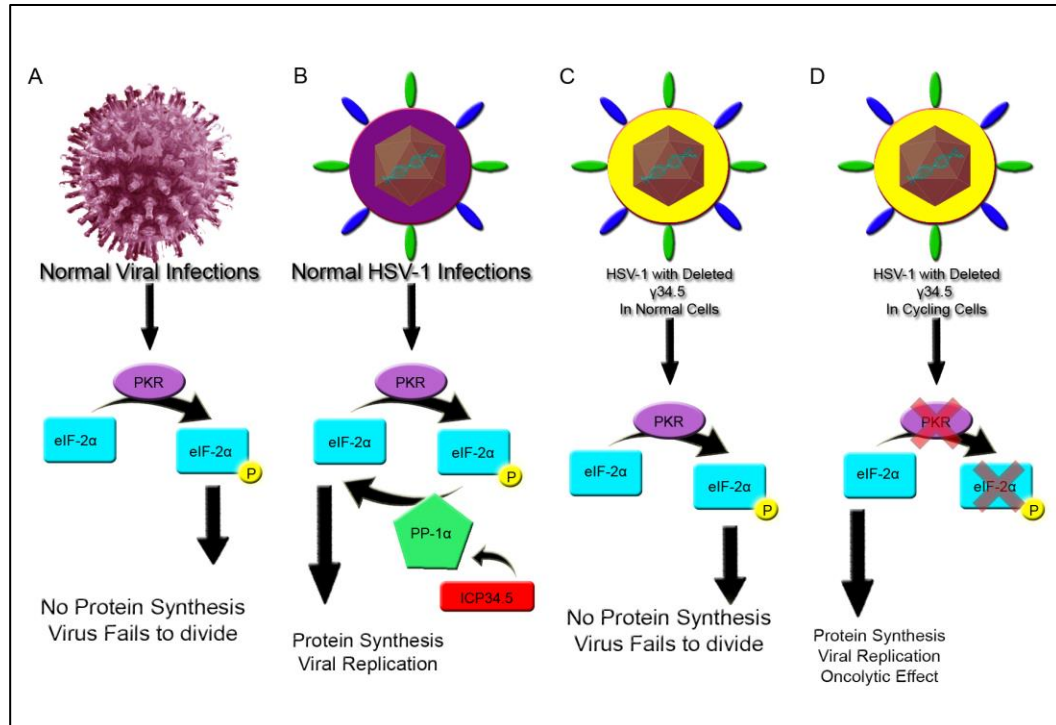


**Figure 1.1: HSV-1 infection**

**A.** In normal viral infections, protein kinase R (PKR) activation leads to the phosphorylation of eukaryotic initiation factor-2 $\alpha$  (eIF-2 $\alpha$ ) and causes the cell to stop producing protein. This is a cell's natural defense against invasion of foreign molecules.

**B.** HSV-1's ICP34.5 will activate protein phosphatase-1 $\alpha$  which will in turn dephosphorylate the eIF-2 $\alpha$  and allow protein synthesis in the cell. With protein production functioning, the virus will be able to divide.

**C.** HSV-1 with a deleted  $\gamma$ 34.5 will not divide in normal cells as eIF-2 $\alpha$  will remain phosphorylated and cellular protein synthesis is halted.

**D.** In cells that are constantly dividing, PKR function is limited and eIF-2 $\alpha$  remains in the unphosphorylated form. This allows for viral replication in cells that are cycling.<sup>15</sup>

### 1.3.1 Synco-2D, an HSV-1 virus

Synco-2D is an HSV-1 based oncolytic virus developed in the lab. Its construction has been described in our previous publications.<sup>19</sup> Briefly, it has both copies of the *ICP34.5* gene deleted. Additionally, it contains two membrane fusion mechanisms - the syn phenotype through mutagenesis and insertion of the truncated form of the gibbon ape leukemia virus envelope fusogenic membrane glycoprotein (GALV.fus) into the virus genome.<sup>19</sup> The envelope glycoprotein of GALV is the only viral protein required for both viral and cellular membrane fusion. PiT1, a type III sodium-dependent phosphate transporter is the cellular receptor for GALV.<sup>20</sup> The membrane fusion induced by HSV is more complex, requiring the participation of multiple viral glycoproteins and at least two specific receptors on the cell surface, heparan sulfate and HVEM [herpesvirus entry mediator].<sup>21</sup> Therefore, it is possible that tumor cells that become resistant to one fusion protein (*e.g.*, due to the lack of a requisite cellular receptor) will still be destroyed by syncytial formation resulting from expression of the other fusion protein, which uses a totally different cellular receptor to initiate the membrane fusion process.

Synco-2D produced superior cytolytic activity when tested against two human renal carcinoma cell lines, ACHN and A-498.<sup>22</sup> Moreover, systemic delivery of Synco-2D led to initial shrinkage of the tumors in RCC (renal cell carcinoma) xenografts. In-vitro characterization of Synco-2D in Vero and ovarian cancer cells showed that this virus produces a distinct syncytial phenotype, leading to a significantly increased tumor killing compared to non-fusogenic virus.<sup>19</sup> The efficacy of Synco-2D against human

ovarian cancer was evaluated in a peritoneal metastasis model with Xenografted Hey8 cells. Intraperitoneal administration of Synco-2D virus to mice with disseminated ovarian cancer led to dramatic eradication of tumors in 75% of mice.<sup>21</sup> Overall, the clear anti-tumor effect of the Synco-2D virus suggest that this virus might be useful in therapy against various cancers.

In the present study, we have employed the use of Synco-2D in combination with the amplicon virus derived from Synco-2D as a gene delivery tool. Subsequently, the amplicon virus was packed with several copies of genes encoding the bispecific and trispecific chimeric engagers that can engage immune cells with the tumor cells, detailed in Chapter 3 of this dissertation.

#### **1.4 Type II HSV**

The current generation of oncolytic HSVs are constructed from HSV-1, yet HSV-2 offers several unique advantages that makes it an attractive candidate as an oncolytic agent. Although HSV-1 and HSV-2 have about 50% sequence identity, one gene that interested researchers was ICP10 gene. ICP10 is an analogue of ICP6 in HSV-1, the N-terminus domain of the ICP10 binds to and phosphorylates the GTPase activating Ras-GAP and turns on the Ras pathway which is essential for HSV-2 replication. Deletion of the protein kinase excerpt on ICP10 gene prevents replication of the virus in non-mitotic cells but not in Ras activated tumor cells.<sup>23</sup> This deletion allows for the selective replication of the virus in tumor cells, which have constitutively active Ras- signaling pathway (**Figure 1.2**).<sup>12</sup>

A

B

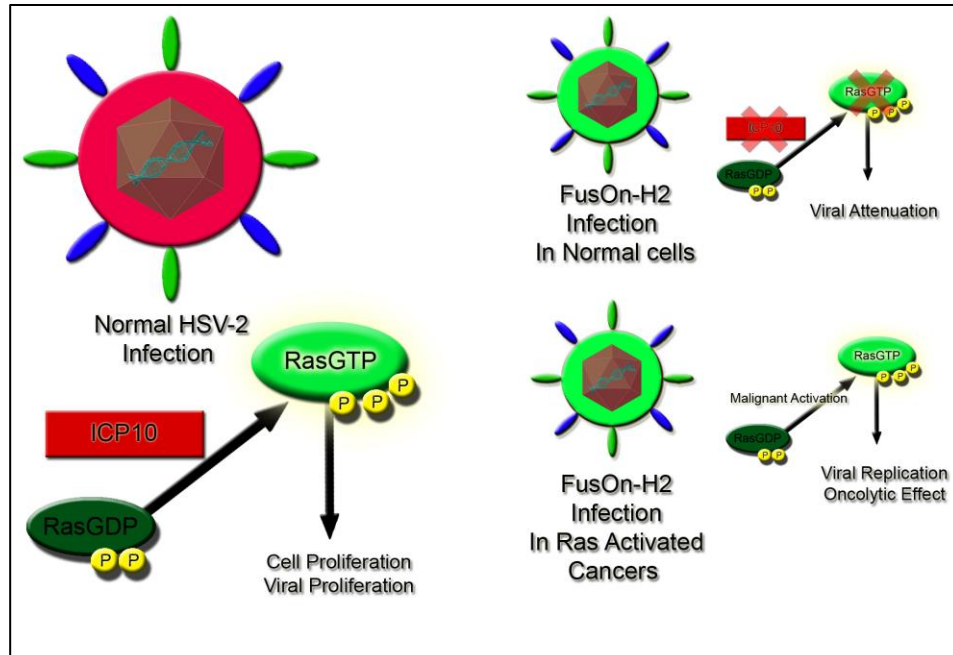


**Figure 1.2: HSV-2 infection**

**A.** In normal HSV-2 infections, ICP10 phosphorylation of RasGDP triggers viral proliferation. **B.** FusOn-H2 viruses have a deletion of ICP10 gene, which in turn only allows it to divide in cells with an activated Ras pathway.

#### 1.4.1 FusOn-H2, an HSV-2 virus

Based on the reasoning that deletion of N-terminal domain of ICP10 gene from the viral genome, would render virus incapable of replicating in normal cells. We constructed a mutant virus of HSV-2, by replacing the N-terminal region of ICP10 with the gene encoding for Green Florescent protein (GFP). As hypothesized, the mutant virus failed to replicate in normal cells, however, its replication in malignant cells is almost as efficient as parental WT virus.<sup>24</sup> Infection with FusOn-H2 induced syncytia formation and apoptosis of tumor cells, further enhancing the anti-tumor effect of the virus. When evaluated *in vivo*, the antitumor effect of FusOn-H2 was previously tested in syngeneic

murine tumor models, in comparison with other oncolytic HSVs derived from HSV1. Our results showed the FusOn-H2 have greater oncolytic activity, causing tumor destruction, leading to the activation of anti-tumor immunity, which together contributed to the overall anti-tumor immune responses.<sup>25</sup> Moreover, FusOn-H2 induced strong T cells responses against primary and metastatic mammary tumors in vivo (**Figure 1.3**). We demonstrated that FusOn-H2 induced a significantly stronger antitumor effect compared to its HSV-1-based oncolytic virus (Baco-1) in several xenograft models of human tumors, including breast cancer,<sup>24</sup> pancreatic cancer,<sup>26</sup> ovarian cancer,<sup>27</sup> and renal cell carcinoma.<sup>28</sup>

The lab has also explored the possibility of FusOn-H2 as an attractant for T-cell adoptive therapy, which can help guide adoptively transferred T cells to the site of infection. The data suggests that FusOn-H2 can initially guide the migration of adoptively transferred T cells towards the treated tumor (**Figure 1.4**). The migrated cells persisted and proliferated upon arrival at the tumor site. Many of the migrated cells that persisted eventually changed to a T cell memory phenotype.<sup>29</sup> Moreover, splenocytes adoptively transferred from FusOn-H2 treated mice effectively prevented metastasis in naïve mice bearing mammary tumors.<sup>29</sup>

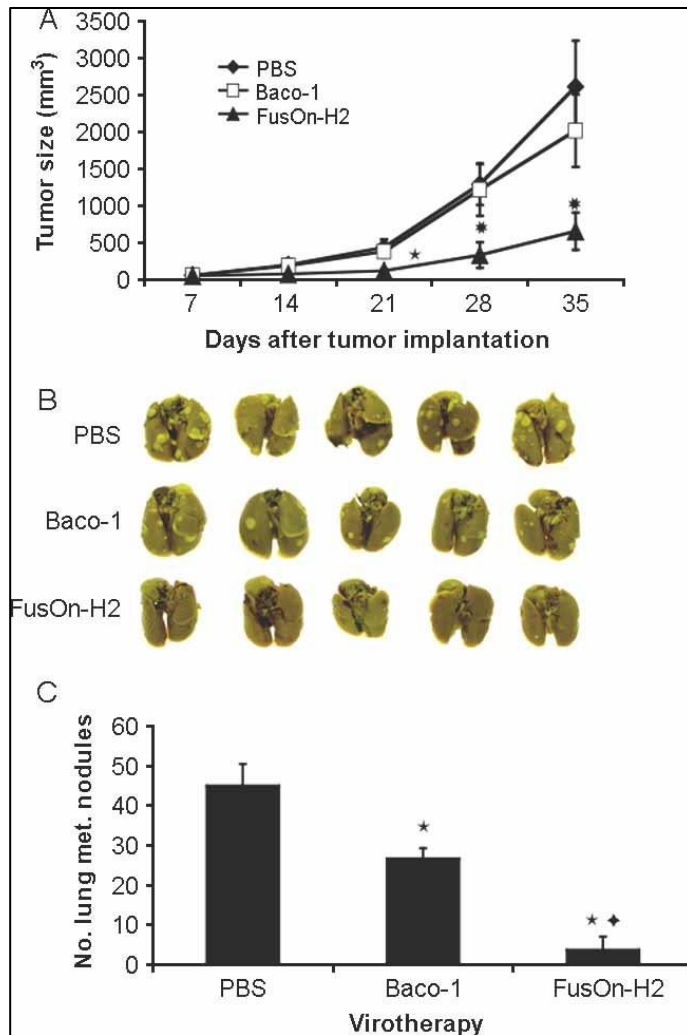


**Figure 1.3: Therapeutic effect of FusOn-H2 against established mammary tumor after a single intratumoral infection**

Tumors were established orthotopically in the mammary fat pads of immune-competent BALB/c mice by subcutaneous implantation of 4T1 cells. Seven days later,  $1 \times 10^7$  pfu of oncolytic virus or PBS were injected into the tumor nodule (n= 8), and tumor size was measured weekly for 4 weeks. All the mice euthanized; their lungs collected for examination of lung metastasis. **A.** Orthotopic tumor volume after virotherapy. **B.** gross

appearance of lung metastatic tumor nodules. C. Enumeration of lung metastatic tumor nodules.

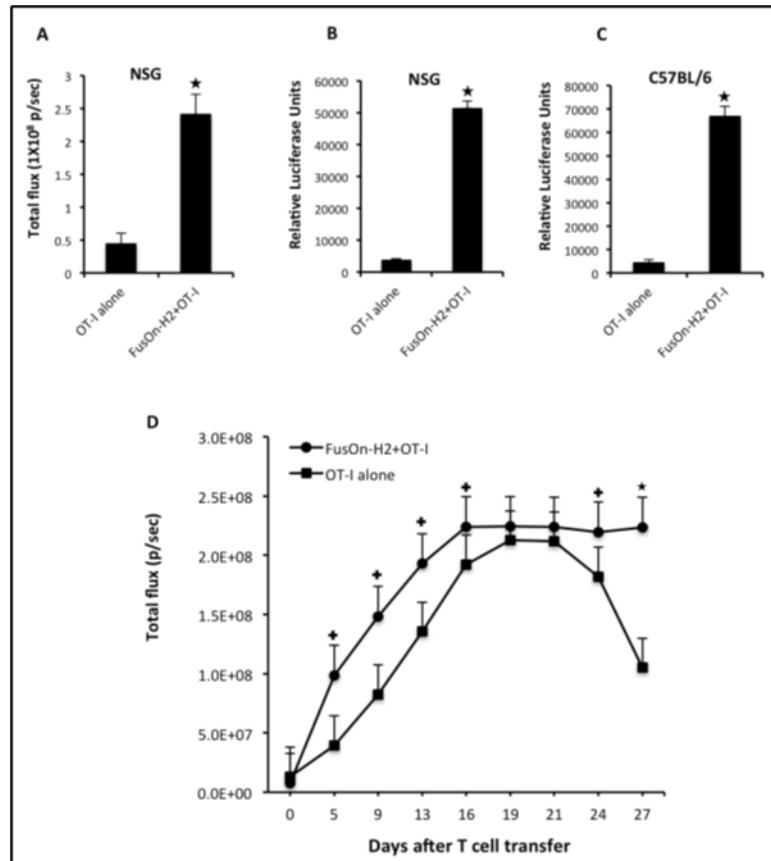


**Figure 1.4: Attractant effect of FusOn-H2 on OT1 cell migration to the tumor site and the subsequent in situ expansion of OT-1 cells**

Murine pancreatic tumors were established by implanting Panco2-H7-OVA cells in the right flank of both immunodeficient NSG mice (A, B and D) and syngeneic C57BL/6 mice. Once tumor reached the approximate size of 5mm in diameter, mice received intratumoral infections of either PBS or 5X10<sup>6</sup> pfu of FusOnH2. Twenty-four hours later, all mice received an intravenous infusion of 2X10<sup>6</sup> OT-1 cells that has been transduced with a luciferase-containing retroviral vector. The abundance of OT-1 cells that had migrated to tumor sites was determined either by IVIS imagine (A and D)

and/or luciferase assay (B and C). A and B were from the same animals. The IVIS image in A was taken at day 28 (after adoptive cell transfer). +p<0.05, \*p<0.01 as compared to OT-1 alone.

In the current study, we explored the immune modulation of the tumor microenvironment by FusOn-H3 (FusOn-H2 without the GFP) in a murine colon cancer model by means of high dimensional scRNA sequencing analysis detailed in chapter 3 of this dissertation.

## **1.5 HSV as an attractive oncolytic agent**

Some of the intrinsic features of HSV that makes it an attractive candidate as an oncolytic agent are 1) Its pathogenicity is restricted and self-limiting local disease with only rare episodes of life-threatening disease in immune-competent adults. (2) There are effective anti-HSV medications such as acyclovir and famciclovir that are available and can be administered in the event of undesired infection or toxicity from the virus. (3) the virus has wide tropism; in that it can enter cells by binding to any one of the four cellular receptors and thus can be applied in attacking many different types of tumors. In principle, this property gives an advantage to HSV against the rapid development of resistance to virotherapy in contrast to other oncolytic viruses. (4) HSV lyses and kills the tumor cells much more rapidly than some other oncolytic viruses. For example, HSV can form visible plaques in cultured cells in only 2 days, in contrast to 7 to 9 days for an adenovirus. Moreover, the multiplicity of infection (MOI) of HSV is much lower at 0.01, where it can kill almost 100% of cultured cancer cells in 2 days,<sup>30</sup> while a much higher dose or a longer infection time is needed to achieve equivalent cell killing with

a conditionally replicating adenovirus.<sup>31</sup> Upon infection, the virus replicates rapidly in the target cells, allowing the virus to execute its fully oncolytic potential *in vivo*, thus can escape the immune system, as it is known that the body's immune system is more likely to restrict the spread of a slower growing virus. Lastly, (5) HSVs rarely integrate into the cellular DNA, thereby, minimizing the risk of introducing an insertional mutation during HSV oncolytic therapy.

## **1.6 HSV Amplicon vectors**

Amplicon viruses are defective, helper dependent vectors that carry no viral genes and take advantage of the large carrier capacity of the virus particle to deliver long transgenic sequences. Amplicon vectors are one of the most powerful and versatile tools for gene transfer.<sup>32</sup> Amplicon vectors of HSV-1 viruses that are identical to WT HSV-1 from the structural, immunological, and host-range points of view, but carry a concatemeric form of a DNA plasmid, named the amplicon plasmid, instead of the viral genome.<sup>33</sup>

Amplicon genome replicates in a mono-directional, rolling circle-like mechanism, generating long concatemers composed of tandem repeats of the amplicon plasmid.<sup>34</sup> Since infectious HSV-1 particles will always package approximately 150 kbp DNA (the size of the virus genome), the number of repeats that an amplicon vector will carry and deliver will depend on the size of the original amplicon plasmid.<sup>35</sup> Therefore, an amplicon plasmid of around 5 kbp will be repeated approximately 30 times in the amplicon vector (**Figure 1.5**).

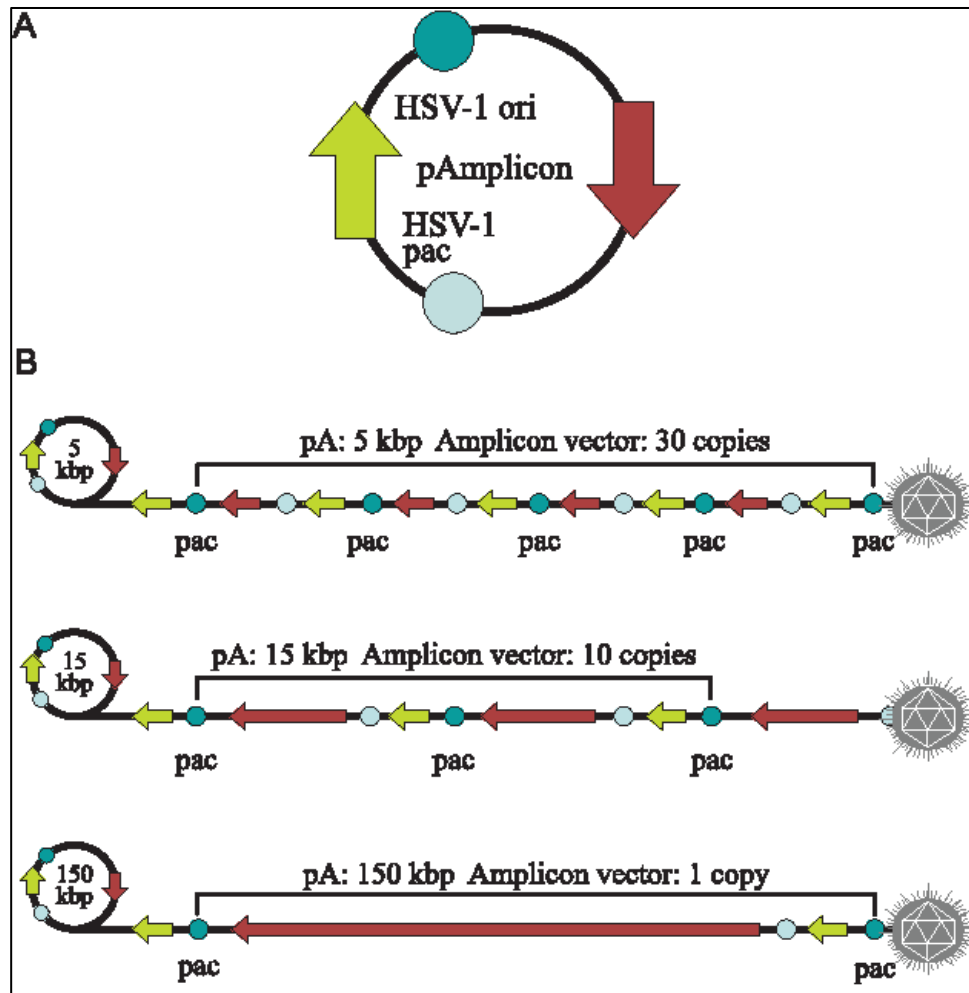


**Figure 1.5: Amplicon plasmid and amplicon vectors**

**A.** A standard *Escherichia coli* plasmid carrying one HSV-1 based Origin of replication (oriS), one HSV-1 packaging signal (pac) and the transgenic (Red arrow) and reporter gene (green arrow) of interest. **B.** an amplicon vector carrying approx. 150 kbp of a head to tail concatemer of DNA derived from the amplicon plasmids generating multiple copies of the transgene.<sup>32</sup>

Traditionally, amplicon vectors were prepared by transfecting cells with the amplicon plasmid, followed by super infection with the helper HSV-1 virus.<sup>30</sup> As a result, the amplicon stocks are a mixture of amplicon viruses and the helper viruses. Although

various approaches are in practice to generate helper-virus free stocks, for the purpose of our study, we employed the use of the stocks containing the helper virus and the amplicon vectors. Although these helper virus free amplicon vectors can efficiently deliver genes to cancer cells, they are diluted during successive cell divisions, for which reason, most studies have used acute approaches, such as anti-angiogenic therapy, immunotherapeutic approaches,<sup>36</sup> indirect cell killing using pro-drugs together with vectors expressing pro-drug-modifying proteins, or direct cell killing using vectors expressing a variety of anti-tumor gene products (proteins or shRNA).<sup>37,38</sup>

In this study, we used the amplicon stocks (helper virus + amplicon vector), where, the helper virus would infect, replicate within the tumor cells, inducing cytotoxicity and stimulating anti-tumor immunity; while amplicon virus would deliver the genes encoding the immune engagers, released into the tumor microenvironment, can engage the infiltrated immune cells with the tumor cells for an increased anti-tumor efficacy. The details of the use of amplicon as a gene delivery tool, details of which are described in chapter 3 of this dissertation.

## **1.7 Cancer and the immune system**

An important function of the immune system in the fight against cancer is surveillance and identification of foreign or non-self-antigens, which may be exogenous microbes or endogenous, altered or malignantly transformed cells. There is increasing evidence that supports the immune system can modify the immunogenicity and behavior in tumors. Several tumor-associated antigens have been identified which are abnormal proteins produced by malignant cells. These antigens expressing tumor cells are marked as non-

self and therefore, are recognized by the immune cells, and eliminates them. However, it is apparent that these cancer cells possess multiple mechanisms to evade the immune system, and form tumors. There are several proposed mechanisms by which the tumor cells escape immune responses; 1) downregulation of major histocompatibility (MHC) I expression, by which the antigen can go unrecognized. 2) lack of co-stimulatory signals for antigen presentation. 3) inhibition of immune responses by release of immune suppressive mediators, including nitric oxide, IL-10 and TGF beta and recruitment of myeloid suppressor cells. 4) modulation of the antigen, preventing it from being recognized by the immune cells. All these mechanisms played by the tumor cells renders the antitumor immune responses ineffable. According to Matzingers danger hypothesis, the prime role of immune system is to respond to cellular and tissue distress to non-self antigens. On this basis, tumor associated danger signals are critical for the generation of effective anti-tumor immune responses. In addition to the above-mentioned mechanisms of immune suppression by tumors, they also lack such danger signals and the current immunotherapeutic strategy is focused on generation of danger signals. Oncolysis results in the enhanced release of TAA, which act as danger signals for the immune system to act. Thus, oncolytic virotherapy represents a potent approach to cancer immunotherapy, combining oncolysis and generation of anti-tumor immunity.

## **1.8 Current strategies in engaging oncolytic viruses with antitumor immunity**

Nearly all cells present fragments of their endogenously synthesized proteins on major histocompatibility complex class I (MHC-1) molecules on the cell surface, allowing immune surveillance of the contents of each cell.<sup>39</sup> Cytotoxic T lymphocytes (CTLs)

can recognize viral or tumor antigens via association of the T cell receptor (TCR) with MHC-I-antigen complex and subsequently kill the infected or cancerous cell. CTLs, therefore, can be potent anticancer agents. However, most tumors have means of evading recognition by CTLs and/or suppressing their activity. Numerous current research strategies are under investigation, which utilize the highly versatile yet specific nature of these cells to target cancer cells.

Oncolytic viruses (OV), whether naturally occurring or genetically engineered, specifically infect, and lyse cancer cells without damage to normal cells and are currently under investigation as a therapeutic strategy to engage the immune response against cancer. Their means of selectivity vary among different types of viruses. Some OVs only enter tumor cells by engaging with surface receptors exclusively expressed or upregulated by tumor cells.<sup>40</sup> Others have virulence genes deleted so that they depend upon defective signaling pathways found in cancer cells to be able to replicate. Upon viral infection, normal cells inhibit viral replication by initiating apoptosis and releasing type I interferons (i.e., IFN $\alpha$  and IFN $\beta$ ). Type I IFNs activate neighboring cells to halt translation, disabling the production of viral proteins. While viral genes have evolved to inhibit apoptotic and IFN defense mechanisms, deletion of these genes renders viruses unable to replicate in healthy cells but still able to replicate in tumor cells, whose apoptotic or IFN signaling pathways are defective.<sup>18 41</sup> For example, the *ICP34.5* gene found in herpesviruses enables the virus to inhibit IFN signaling, and the gene products of the E1B region found in adenoviral genomes inhibit p53 and Rb, preventing apoptosis.<sup>18</sup> The *ICP34.5* and *E1B* genes are deleted in oncolytic herpesviruses and adenoviruses, respectively, restricting their ability to replicate in healthy cells. Other

OVs utilize cell-specific promoters so that transcription of viral genes is dependent upon whether the host cell is healthy or cancerous.<sup>18,41</sup> OVs may also depend on the activation of specific cellular pathways that may be overactivated in tumor cells, such as the Ras pathway.<sup>42</sup> A wide variety of OVs are showing promise, both in efficacy and safety, in preclinical and clinical studies. Talimogene Laherparepvec (T-VEC), a modified oncolytic herpes simplex virus type 1 (HSV-1), has produced a measurable therapeutic response in a phase III clinical trial and has been approved by the FDA for treatment of melanoma.<sup>43</sup>

The therapeutic efficacy of OVs is not only due to specific killing of tumor cells directly, but more importantly, due to the immune response elicited toward uninfected cells, especially that of tumor-specific CTLs.<sup>18</sup> Tumor infection with viruses lacking immunogenic transgenes can produce tumor antigen-specific, CTL-mediated immune responses, likely through multiple contributing factors including support of dendritic cell (DC) maturation and release of pro-inflammatory T cell cytokines.<sup>44</sup> Engineering of oncolytic viruses to express immunomodulatory transgenes holds the potential for even further enhancement of CTL-mediated tumor immunity. In general, the more effectively an oncolytic virus can transform the immunosuppressive tumor microenvironment (TME) into an immunostimulatory one, the more potent the tumor-specific immunity will be, and the greater the therapeutic benefit. Of note, attempts to activate antitumor immunity must also consider potential side effects, and genetic engineering strategies have been used to abrogate the detrimental effects of immunomodulatory transgenes. For example, an oncolytic HSV that caused rashes through the expression of tumor necrosis factor alpha (TNF- $\alpha$ ) was modified to contain

a promoter that limited TNF- $\alpha$  expression, reducing the side effects and improving anti-tumor efficacy.<sup>45</sup> While this is an important aspect of oncolytic virotherapy, this review focuses on the molecular mechanisms behind the adaptive immune response to armed and unarmed OVs.

### **1.8.1 Oncolytic viruses enhance antigen presentation**

In most instances, the process of antigen presentation begins as cytosolic proteins are degraded into peptide fragments by the proteasome, then transported into the endoplasmic reticulum by the transporter associated with antigen processing (i.e., TAP-1 and TAP-2) proteins, where they are loaded onto MHC-I molecules.<sup>46</sup> The peptide-MHC-I complex then travels to the cell surface, where MHC-I becomes anchored in the plasma membrane and the peptide fragment remains bound to the extracellular domain.<sup>39</sup> In the context of cancer, many tumor cells have lost MHC expression, which hinders recognition by immune cells.<sup>47</sup> Enhanced presentation of tumor-associated antigens on MHC-1 would render tumor cells more likely to be recognized and lysed by CTLs, and numerous strategies have been employed to increase MHC-I presentation on tumor cells for this purpose. Results from the following studies indicate that various OVs can upregulate antigen processing and presentation in cancer cells.

Infection of mouse ovarian cancer cells with oncolytic reovirus was found to induce expression of MHC-I, TAP-1 and TAP-2, all of which are downregulated in the untreated cell line.<sup>47</sup> In another preclinical study, infection with an adenovirus triggered tumor cells to upregulate uric acid, stimulating DCs to release IFN $\gamma$ , which subsequently stimulated tumor cells to upregulate PA28,<sup>48</sup> a protein known to activate proteasomal

cleavage of polypeptides to produce MHC-I antigens.<sup>49</sup> This process led to increased specific CTL lysis of infected tumor cells.<sup>48</sup> Similarly, Zamarin et al., 2014<sup>50</sup> found that infection with an oncolytic NDV stimulated uniform upregulation of MHC-I among infected and non-infected tumor cells. This was likely caused by increased type I IFNs, which are known to regulate MHC-I expression and were released by tumor cells infected by the same NDV.<sup>50</sup> A similar mechanism was observed in a murine lung cancer model treated with an adenovirus armed with an IFN $\beta$  transgene. IFN $\beta$  expression was shown to upregulate MHC-I expression in this tumor cell line. This alteration of the tumor cells was required for CTL-mediated tumor rejection.<sup>51</sup> These two studies suggest that the ability of IFN $\beta$  to upregulate MHC-I make it a promising tool to increase the immunogenicity of tumor cells in the context of virotherapy.<sup>50</sup> In addition, inhibition of certain viral genes can promote antigen processing, for example, deletion of HSV-1 gene *ICP47*, known to downregulate MHC-I expression by blocking TAP,<sup>52</sup> has successfully resulted in increased expression of MHC-I in infected tumor cells compared to mock treatment in mice.<sup>18</sup>

### **1.8.2 OV<sub>s</sub> can enhance dendritic cell trafficking to the TME and cross-presentation to CTLs**

Antigen-presenting cells, particularly DCs, have the unique ability to present antigens from exogenous proteins on MHC-I in a process known as cross-presentation.<sup>39</sup> As DCs reside in the tissues, they can take in these proteins through endocytosis and process them through various and poorly understood pathways.<sup>53</sup> Once tissue-resident DCs have matured, they travel to the draining lymph nodes to present MHC-I antigens by binding

to the TCR of naïve CTLs, a process called priming, inducing either tolerance or immunity against the presented antigen depending on the costimulatory molecules expressed.<sup>54</sup> For CD8<sup>+</sup> T cell activating costimulatory molecules to be expressed, inflammatory cytokines and other “danger” signals must be provided during the maturation of APCs.<sup>53</sup> Therefore, enhancement of antigen uptake before DC maturation and provision of the appropriate maturation signals play essential roles in the induction of tumor-specific CTL immunity.

IFN $\alpha/\beta$  signaling is required for the development of a systemic antitumor response.<sup>55</sup> It is essential for the accumulation of CD8<sup>+</sup> DCs in the TME, and therefore necessary for activation of tumor-specific naïve T cells.<sup>56</sup> *In vivo* studies have also shown IFN $\alpha/\beta$  signaling to be an important factor in generating DCs capable of efficient cross-presentation to CD8<sup>+</sup> T cells.<sup>40</sup> *In vitro* studies have elucidated some of the mechanisms behind this connection between type I IFNs and DC activity that promotes antitumor immunity. The presence of IFN- $\alpha$  during DC maturation stimulates multiple immunogenic pathways, particularly those involved in phagocytosis and antigen processing. One upregulated protein in DCs matured in the presence of IFN- $\alpha$  is the scavenger receptor LOX-1, which mediates endocytosis of apoptotic cells, a necessary step for antigen cross-presentation to occur. The LOX-1 endocytic pathway induces immunity more efficiently than the non-specific mechanisms of endocytosis used by DCs.<sup>57</sup> IFN- $\alpha$  also triggers upregulation of MHC-I and TAP-1,<sup>58</sup> the latter of which is involved in at least one of the pathways for MHC-I cross-presentation. Non-oncolytic viruses trigger the release of type I IFNs,<sup>40</sup> and oncolytic viruses can do so likewise, although the magnitude of the release may differ among types of OV, and the effects

of the IFNs may differ among types of cancer cells. Release of type I IFNs may be a mechanism through which OV infection enhances cross-presentation by DCs. Multiple studies have found that oncolytic NDV infection enhances DC cross-presentation of tumor antigens and is accompanied by increased IFN- $\alpha$  secretion, but further research is needed to confirm a direct relationship.<sup>50,59</sup> In a murine lung cancer model, treatment with an adenovirus armed with an IFN $\beta$  transgene prolonged survival significantly compared to treatment with the adenovirus lacking the transgene. Tumor-bearing mice treated with the armed virus developed tumor-specific CTLs that contributed to the therapeutic effect and protected cured mice from subsequent tumor injections. Although a mechanism involving DCs was not confirmed by this study, further investigation into the effect of IFN release by this virus on DCs could be useful.<sup>51</sup> In another study by the same group, a VV was armed with IFN $\beta$  and used to treat two different mouse lung cancer models. The transgene did not have the same treatment-enhancing effect relative to the unarmed virus as it did with the two adenoviruses, although even the unarmed virus caused IFN $\beta$  expression, which may have contributed to the CTL-mediated tumor regression observed.<sup>60</sup> Because IFN signaling also inhibits NDV replication,<sup>61</sup> future studies should consider the dual effects OV-induced type I IFN release on antitumor immunity and viral replication in order to optimize efficacy.

Granulocyte-macrophage colony-stimulating factor (GM-CSF) controls both myeloid cell differentiation and the function of mature blood cells, including CD8<sup>+</sup> DCs. It has been found to be particularly important to nonlymphoid tissue migratory DCs, regulating homeostasis and promoting the survival of these cells. GM-CSF is also essential to T cell priming by CD8<sup>+</sup> DCs.<sup>62</sup> Its overexpression in transgenic mice has

been shown to increase CD8+ DC antigen presentation to naïve CD8+ T cells, leading to enhanced proliferation of CD8+ T cells.<sup>63</sup> This effect has been replicated by treating tumors with oncolytic viruses with GM-CSF gene insertions, producing specific immunogenic antitumor responses in multiple models. For example, the inclusion of the gene coding for GM-CSF in adenovirus Ad5-D24 caused tumor cells to secrete the gene product upon infection, inducing complete tumor eradication and protection from repeated challenge with the same tumor cell line in hamsters.<sup>64</sup> Tumor-specific CTL response in human patients was also shown.<sup>64</sup> Similar *in vivo* results have been found with the inclusion of GM-CSF in modified HSV-1,<sup>18</sup> NDV,<sup>59</sup> and VV<sup>65</sup> to treat various tumor models. GM-CSF levels have even been elevated by infection of tumors with viruses lacking the transgene, including  $\Delta$ PK.<sup>66</sup> Use of this cytokine and few others described in **Table 1.1** in oncolytic virotherapy, therefore, has the potential to be a valuable contributor to long-term clinical benefits via specific antitumor immunity.

Tumor cells undergoing apoptosis or necrosis in response to effective, immune-activating cancer therapy are known to release damage-associated molecular patterns (DAMPs), which can trigger inflammatory responses from DCs and consequently CTLs.<sup>67</sup> In particular, adenosine triphosphate (ATP), high mobility group box 1 (HMGB1), and exogenous calreticulin (CALR) are considered to be important indicators of immunogenic cell death. (**Table 1.1**)<sup>68</sup> ATP released by dying cells can attract dendritic cells to the TME.<sup>69</sup> It can also interact with purinergic P2X7 receptors on DCs, triggering the NOD-like receptor family, pyrin domain containing-3 protein (NLRP3)-dependent caspase-1 activation complex (NALP3-ASC-inflammasome).<sup>67</sup> This complex is required for efficient priming of CTLs in response to dying tumor

cells.<sup>67 70</sup> Upon interaction with toll-like receptor 4 (TLR4) on DCs, HMGB1 is endocytosed and triggers signaling cascades that lead to activation of DCs.<sup>71</sup> By these respective mechanisms, the release of both ATP and HMGB1 by dying tumor cells are important for the maturation of DCs into cells capable of cross-presentation *in vivo*.<sup>69</sup> CALR marks cells to be targeted by SR-A and SREC-1 on dendritic cells for endocytosis and subsequent antigen processing and cross-presentation.<sup>72</sup> Through their interactions with antigen-presenting DCs, DAMPs are important drivers of tumor-specific immunogenicity induced by oncolytic viruses. Tumor infection with oncolytic coxsackievirus CVB3 resulted in increased tumor production of ATP and HMGB1, and DCs with significantly high expression of the maturation marker CCR7 were recruited to the TME, indicating the potential for the generation of adaptive antitumor immunity.<sup>73</sup> Similarly, infection with adenovirus dl922-947 triggered mesothelioma cell release of ATP and HMGB1, as well as increased CALR cell surface expression.<sup>74</sup> Treatment with both of these viruses induced significant tumor growth suppression and prolonged survival.<sup>74</sup> Increased ATP production has also been reported by an oHSV armed with PTEN $\alpha$ , an N-terminally extended isoform of PTEN that has the additional function of increasing electron transport chain activity by localizing to cytochrome C in the mitochondrial membrane. The PTEN $\alpha$ -expressing virus improved the survival of brain tumor-bearing mice relative to the control virus in a manner dependent on CD8+ T cells, and surviving mice were protected from tumor rechallenge. Consistent with the known effects of ATP on DCs, there was also increased DC infiltration in tumors treated with the PTEN $\alpha$ -expressing virus.<sup>75</sup>

Notably, HMGB1 secretion triggered by OV has also been shown to have other effects that may hinder therapeutic efficacy and must be weighed against the beneficial effects. For example, inhibition of HMGB1 with both a small molecule inhibitor and genetic knockdown resulted in increased spread of an oncolytic HSV among fibroblast cells, implicating a role for HMGB1 in viral restriction.<sup>76</sup> In contrast, in a study on glioma, treatment with HMGB1-blocking antibodies had no effect on oncolytic HSV spread *in vitro* and *in vivo*. However, secreted HMGB1 triggered by oncolytic HSV infection was found to increase vascular leakiness and edema *in vivo*, while HMGB1 blockade rescued both conditions and prolonged survival.<sup>75</sup>

When secreted, heat shock proteins (HSPs) are also considered to be DAMPs as they can support antitumor immunity by functioning as chaperones for receptor-mediated endocytosis of antigenic peptides by DCs.<sup>77</sup> For example, tumor-derived HSP70 can form a complex with tumor antigens and subsequently bind to various scavenger receptors, including LOX1, on the surface of dendritic cells. LOX1 is particularly active in mediating cross-presentation of HSP70-complexed tumor antigens to elicit a specific CTL response.<sup>78</sup> HSPs can also upregulate costimulatory molecules necessary for T cell activation on the surface of DCs.<sup>77</sup> Arming an oncolytic adenovirus to express HSP70 dramatically improved the virus's immune-driven therapeutic efficacy. Treatment of mice with the armed virus completely eradicated weakly immunogenic tumors and induced a specific response against tumor rechallenge, while the virus lacking the transgene merely inhibited tumor growth and had no effect on tumor rechallenge.<sup>77</sup> Cell depletion revealed CD8+ T cells to be the most important effector cells in the observed immunogenic effects of HSP70,<sup>77</sup> suggesting that viral expression of HSP70 enhanced

cross-presentation by DCs, producing a tumor-specific CTL response against these tumor models. Other groups similarly found that adenoviral expression of HSP70 produced T cell-dependent antitumor effects in gastric cancer,<sup>79</sup> and pancreatic cancer xenografts.<sup>80</sup> These findings do not contradict those that have found HSP70 to promote tumorigenesis, as it can function as an antiapoptotic factor intracellularly and an immune stimulator extracellularly.<sup>81</sup> Nevertheless, as intracellular antiapoptotic factors, HSPs have effects on viral replication that should be considered in the context of OV therapy. For example, hyperthermia-induced HSP72 synergized with an oncolytic HSV-1, enhancing viral replication and increasing cytotoxicity against pancreatic cancer cells.<sup>82</sup> In another study, HSP90 was found to be required for efficient viral DNA replication and production of viral progeny during HSV-1 infection.<sup>83</sup> While these results were obtained using non-tumor cells, HSP90 is known to be in an active state characterized by the formation of complexes with other HSPs and cochaperones in various types of tumor cells,<sup>83</sup> under which conditions it can inhibit apoptosis.<sup>44</sup> Taken together with the effects of HSP90 on HSV-1 replication, this suggests that HSP90 may play a role in promoting OV replication in tumors. Concurrently, HSP90 induction by the proteasome inhibitor bortezomib was found to synergize with oncolytic HSV-1 therapy in a variety of tumor xenografts by increasing viral replication and cell killing.<sup>84</sup> HSP transgenes in OVs merit further investigation for their dual function as immune-stimulating factors and their potential to promote OV replication by inhibiting apoptosis.

### 1.8.3 Armed OV<sub>s</sub> can cause the release of ligands of T cell costimulatory receptors

For CD8<sup>+</sup> and CD4<sup>+</sup> T cells to be primed against tumor antigens, they must receive not only an MHC-restricted TCR signal but a costimulatory signal as well, which is often provided by DCs.<sup>85-87</sup> These signals are often lacking in the TME, leaving infiltrating T cells in an anergic state.<sup>87</sup> While oncolytic virotherapy has the potential to produce an inflammatory microenvironment that recruits T cells to the tumor site and potentiates their initial priming, arming OV<sub>s</sub> with costimulatory ligands, as indicated in **Table 1.1**, can increase activation of tumor-specific T cells.<sup>85,87,88</sup>

A critical costimulatory interaction is that of B7 expressed on the surface of DCs with CD28 expressed on T cells. B7-transfected melanoma cells have been shown to successfully provide this costimulatory signal, directly activating CD8<sup>+</sup> T cells against tumor antigens without the need for CD4<sup>+</sup> T cells.<sup>86</sup> As a single agent, B7.1 expressed by an oncolytic HSV-1 was found to be relatively ineffective in boosting antitumor immunity in a murine neuroblastoma model, however it was able to significantly enhance antitumor effects in combination with HSV expression of IL-12 and/or IL-18 in a T cell-dependent manner.<sup>88</sup>

Upon TCR activation, CD8<sup>+</sup> and CD4<sup>+</sup> T cells upregulate glucocorticoid-induced tumor necrosis factor receptor (GITR), the activation of which increases their proliferation and effector functions.<sup>89</sup> One study found that treatment with an agonist of GITR produced these effects in mouse models; the agonist induced systemic CD8<sup>+</sup> T cell-mediated, tumor-specific immunity against secondary tumors, although significant effects on primary tumors were not observed.<sup>90</sup> Another group reported tumor growth

inhibition or regression in nearly all treated mice, increased proportions of tumor antigen-specific CD8<sup>+</sup> T cells, and protection from tumor rechallenge in response to GITR agonism.<sup>91</sup> Notably, these results were obtained using CT26 cells, which are known to naturally induce priming of naïve T cells against their own antigens, albeit insufficiently for inducing tumor rejection. Upon repeating the experiment with a less immunogenic tumor cell line (E7), the same group observed that GITR agonism alone did not produce significant effects on tumor-specific CD8<sup>+</sup> T cells or tumor regression.<sup>91</sup> To produce a significant antitumor response against E7 tumors, GITR agonism had to be combined with a peptide vaccination, indicating that GITR stimulation could activate antitumor immunity but was only effective when accompanied by a T cell-priming mechanism.<sup>91</sup> Thus, as oncolytic viruses have been shown to enhance T cell priming, incorporation of GITR into the genome of an OV can be rationally hypothesized to enhance its antitumor effects. Concurrently, arming an oncolytic adenovirus with GITR ligand significantly prolonged survival of glioma-bearing mice compared to treatment with the parental virus, and the armed virus produced both cytotoxic and memory CD8<sup>+</sup> T cell responses against tumor antigens.<sup>87</sup>

Tumor-specific CTL activity can also be potentiated by stimulation of CD4<sup>+</sup> T helper cells.<sup>85</sup> Major histocompatibility complex class II (MHC-II)-restricted TCR engagement on the surface of CD4<sup>+</sup> T cells induces upregulation of the costimulatory receptor OX40, the ligand for which (OX40L) is expressed by DCs. Tumor cell expression of OX40L mediated by an oncolytic adenovirus led to enhanced infiltration of CD4<sup>+</sup> and CD8<sup>+</sup> T cells to the tumor site. This resulted in improved tumor-specific lysis by CTLs, inhibition of tumor growth, and improved survival in mice with melanoma and colon

adenocarcinoma. Tumor expression of OX40L significantly increased CD4<sup>+</sup> T cell IFN- $\gamma$  production, and the antitumor effects of the OX40L-expressing adenovirus could not be replicated in either CD4<sup>+</sup> T cell or CD8<sup>+</sup> T cell-deficient mice, indicating both cell types were required. These findings suggested that OX40L-OX40 interaction on CD4<sup>+</sup> Th cells specific for the treated tumors stimulated IFN- $\gamma$  release, which in turn activated tumor-specific CTLs, although more research is needed to confirm this mechanism.<sup>85</sup>

4-1BB is a tumor necrosis factor family receptor (TNFR) expressed on activated CD4<sup>+</sup> and CD8<sup>+</sup> T cells. 4-1BB stimulation results in enhanced proliferation of activated CD8<sup>+</sup> T cells *in vitro* and subsequent generation of CTLs *in vivo*.<sup>92</sup> The expression of 4-1BBL in tumor cells has been shown to provide a costimulatory signal that drives both CD4<sup>+</sup> and CD8<sup>+</sup> T cell proliferation, leading to their expansion in the tumor site.<sup>93</sup> Although 4-1BB/4-1BBL interaction has this effect on isolated colonies of both CD4<sup>+</sup> and CD8<sup>+</sup> cells, optimal expansion of CD8<sup>+</sup> T cells in response to this costimulatory signal requires the presence of CD4<sup>+</sup> T cells. The ability of CTL effector cells to specifically lyse tumor cells can also be enhanced by 4-1BB stimulation.<sup>93</sup> As an adenoviral transgene, 4-1BBL has been found to significantly enhance the tumor-shrinking effect of virotherapy. While 4-1BBL did not produce as strong an effect as an IL-12 transgene, the two transgenes were found to work synergistically to enhance tumor regression, likely by activating CD4<sup>+</sup> T helper cells which in turn activated CTLs.<sup>94</sup>

NDV infection has been shown to stimulate CD8<sup>+</sup> and CD4<sup>+</sup> T cell upregulation of various co-receptors, especially the inducible costimulator (ICOS). Compared to its

wild-type counterpart, an NDV modified to express the ligand for this receptor enhanced CD8<sup>+</sup> and CD4<sup>+</sup> T cell infiltration as well as tumor regression in sites not directly treated with the virus. Viral ICOSL expression enhanced CTL expression of ICOS, suggesting increased activation. Increased CTL release of granzyme B was also observed in response to ICOSL expression, suggesting increased lytic function.<sup>95</sup>

#### **1.8.4 OV<sub>s</sub> induce the release of cytokines that support CTL expansion and function**

IL-12 and type I IFNs have similar functions as inflammatory stimulators required for optimal CD8<sup>+</sup> T cell activation.<sup>96,97</sup> Capable of functioning alone or synergistically, these signal 3 cytokines play important roles in T cell expansion, effector function, and ultimately in generating an antigen-specific response (**Table 1.1**). However, it has been noted that their requirement for optimal T cell expansion and effector function varies among different types of infections. For example, optimal expansion of T cells responding to vesicular stomatitis virus (VSV) infection depends on both signals, while only type I IFN is required in lymphocytic choriomeningitis virus (LCMV) infection. Neither IL-12 nor type I IFNs are necessary for the development of antiviral CTLs in VV infection.<sup>97</sup> Nonetheless, IL-12 and/or type I IFN signaling during CD8<sup>+</sup> T cell activation enhances the accumulation of effector cells by prolonging expression of the high-affinity IL-2 receptor CD25, the presence of which increases cell sensitivity to IL-2. In the presence of IL-2, increased CD25 expression results in prolonged PI3K-dependent cell division.<sup>96</sup> Thus, both IL-12 and IL-2 are potentially important factors for the accumulation of tumor-specific CTLs in the tumor site. Multiple studies with

NDV have found that viral IL-2 expression increased infiltration of CD4+ and CD8+ T cells into TME, tumor-specific T cell function, and tumor regression in mice following infection compared to the virus lacking the transgene.<sup>98</sup> Oncolytic HSV-1 expression of IL-12 yielded similar results, enhancing the survival of tumor-bearing mice as well as tumor infiltration of NK cells, CD4+ and CD8+ T cells.<sup>99</sup> Tumor infection with a reovirus, without the need for a transgene, has been shown to increase levels of IL-12, suggesting IL-12 signaling to be one important factor in tumor-specific immunity induced by unarmed reoviruses.<sup>100</sup>

IL-15 binds to the same receptor as IL-2, which is commonly expressed on NK cells and T cells. Both cytokines activate, expand, and increase the cytolytic activity of these cells, but IL-15 lacks some of the immunosuppressive properties and clinical side effects of IL-2.<sup>101</sup> IL-15 treatment, especially with the IL-15 superagonist ALT-803, has shown promising preclinical results against cancer. Treatment of an experimental mouse glioblastoma with ALT-803 led to enhanced tumor growth inhibition and animal survival, which were found to be mediated by CD4+ and CD8+ T cells. Aligning with the known functions of IL-15, increased tumor-infiltrating CD8+ T cells, as well as the increased function of these cells was observed.<sup>101</sup> Editing a VSV and vaccinia virus (VV) to express IL-15 and an IL-15 super agonist, respectively, significantly increased infiltration of tumor-antigen specific CD8+ T cells, tumor regression, and survival upon infection.<sup>102</sup> Cell-depletion assays in the second study revealed CD8+ T cells to be more critical than NK or CD4+ T cells in the observed therapeutic effects of the virus.<sup>103</sup>

Studies on the effects of IL-10 on the TME have yielded contrasting findings. In context with a persistent viral infection, IL-10 deficiency or IL-10R blockade was found to increase the number of virus-specific CD8<sup>+</sup> T cells, the function of CD8<sup>+</sup> and CD4<sup>+</sup> T cells, and viral clearance, suggesting that IL-10 suppressed antiviral CD8<sup>+</sup> T cell-mediated antiviral immunity.<sup>104</sup> Taking advantage of these immunosuppressive effects, arming an oncolytic VV with IL-10 enhanced the oncolytic effect of the virus by reducing anti-viral CTLs without reducing antitumor CTLs. Specific antitumor immunity was also observed and attributed to increased release of tumor-associated antigens via enhanced viral oncolysis.<sup>105</sup> In another study, tumor-infiltrating DCs did not respond to the presence of molecules able to stimulate IL-12 and TNF $\alpha$  secretion in typical immature DCs. Blockade of IL-10/IL-10R signaling, when combined with TLR-9 activation, was able to restore the normal response, and the treated DCs were able to stimulate a tumor-specific CTL response, suggesting that IL-10 signaling was a contributor to inhibition of antitumor immunity.<sup>106</sup> In melanoma models, high levels of IL-10 can also inhibit antitumor CTLs by deregulating the CTL-activating ligand MICA.  $\Delta$ PK infection inhibited IL-10 secretion by melanoma cells, leading to restored expression of MICA.<sup>66</sup>

In contrast, tumor expression of IL-10 has also been shown to cause inhibition of tumor growth, with CD8<sup>+</sup> T cells playing a crucial role in the observed antitumor effects,<sup>107</sup> although these studies did not clearly prove that IL-10 acted directly on CD8<sup>+</sup> T cells. In a more recent study, however, IL-10 treatment was shown to enhance tumor rejection by increasing tumor-specific CTL proliferation and cytotoxic activity without the need for migration of new CD8<sup>+</sup> T cells to the tumor site. These immunogenic effects were

shown to require IL-10 interaction with IL-10Ra on the surface of CD8+ T cells only.<sup>108</sup> The effect of IL-10 likely depends on the environment in which it is expressed, and more research will be needed to elucidate its mechanisms of immune activation and/or suppression to inform the development of more effective oncolytic viruses.

### **1.8.5 OVs can induce the release of chemokines that attract CTLs to the TME**

The IFN- $\gamma$ -inducible chemokines CXCL9, CXCL10, and CXCL11 are known to directly attract effector CTLs to sites of infections or tumors via their interaction with CXCR3, which is highly expressed on activated T cells.<sup>109</sup> Downregulation of these chemokines is one way in which tumors evade immune responses,<sup>110</sup> and restoring their expression has consequently been considered as a possible way that oncolytic viruses can engage tumor-specific CTLs. Listed in **Table 1.1** are some reports of the effects of chemokines induced or expressed by OVs on the TME.

In one preclinical study, infection with an oncolytic HSV-2 triggered the release of CXCL9 and CXCL10, increasing migration of tumor-specific CD4+ and CD8+ T cells to the TME. This migratory effect enhanced tumor-specific immunity *in vivo*.<sup>29</sup> An oncolytic HSV-1 was found to similarly enhance CD8+ T cell migration to murine ovarian carcinoma tumors via upregulation of CXCL9 and CXCL10 by both tumor cells and DCs, which also migrated to the tumor site in response to infection.<sup>111</sup> In yet another study, CXCL9 was inserted into the genome of an oncolytic VSV in an attempt to enhance migration of CTLs to the tumor site upon infection. While this gene insertion increased tumor expression of CXCL9, it failed to increase CXCR3+ T cell infiltration over that observed in response to treatment with the virus lacking the transgene.

However, treatment with either virus increased both CXCL9 expression and CXCR3+ T cell infiltration, and the authors hypothesized that oncolytic viral activity likely produced a sufficient chemokine gradient to optimally attract T cells to the TME, without the need for additional chemokine expression.<sup>110</sup> However, further research would be needed to definitively prove this, and chemokine gene insertion may have more immunostimulatory effects in the context of different oncolytic viruses or different tumor models.

Expression of CXCL11 by an oncolytic VV enhanced the therapeutic efficacy of the virus against mesothelioma via increased migration of tumor-specific T cells to the TME as well as increased activation of systemic tumor-specific CD8+ T cells.<sup>29</sup> In a murine colorectal cancer model that is weakly immunogenic, the induced CXCL11 enhanced tumor infiltration of CD8+ T cells, but therapeutic efficacy was not significantly increased compared to treatment with a virus lacking the transgene.<sup>112</sup> However, the CXCL11-expressing virus was shown to enhance therapeutic efficacy when combined with a cytokine modulating drug cocktail (CKM) capable of increasing intratumoral CCL5 and CXCL9. Combination therapy induced greater CXCL11 levels, more CD8+ T cell infiltration, and longer survival than either therapy alone. Although further study would be required to fully elucidate the mechanism of the synergy between these two therapies, the viral therapy likely induced activation of CTLs, and both therapies likely played a role in enhancing CTL migration to the tumor site, while the CKM functioned by promoting prolonged T cell activity in the tumor site.<sup>112</sup>

### **1.8.6 OVs can support CTL activity by inhibiting T regulatory cells**

T regulatory (Treg) cells often characterized as CD4<sup>+</sup>CD25<sup>+</sup>Foxp3<sup>+</sup> T cells are particularly active toward self-antigens. By expressing cytotoxic T lymphocyte-associated antigen 4 (CTLA-4), they can decrease APC expression of the costimulatory ligands CD80 (B7-1) and CD86 (B7-2), resulting in apoptosis, anergy, or dormancy in CD4<sup>+</sup> and CD8<sup>+</sup> T cells.<sup>113</sup> They also induce immune tolerance via their high-affinity IL-2 receptors, which deprive responder T cells of IL-2 signaling.<sup>113</sup> While these functions are essential to prevent autoimmunity, they can be detrimental to antitumor immunity, and have been associated with poor prognosis.<sup>113</sup> For example, one study found that infection with a particular virus increased CD4<sup>+</sup> T cell populations expressing T regulatory markers, and that these cells inhibited the ability of mice to reject tumors that could otherwise be rejected through CD8<sup>+</sup> T cell activity.<sup>114</sup> Injection of a splenic cell suspension depleted of CD25<sup>+</sup> cells into athymic mice followed by injection of leukemia cells resulted in tumor-specific rejection requiring the presence of CD8<sup>+</sup> CTLs.<sup>115</sup> Similar results were obtained by systemic administration of antibodies against CD25 in immunocompetent mice, using a variety of tumor cell lines.<sup>115</sup> It is therefore reasonable to expect that Treg-targeting strategies could prove effective in enhancing the adaptive immune effects of virotherapy.

Tregs highly express GITR. A study found that tumor infection with an adenovirus containing the gene for the GITR ligand could augment tumor infiltration of CD4<sup>+</sup> and CD8<sup>+</sup> T cells.<sup>116</sup> Another study similarly found that tumor-bearing mice treated with a GITRL fusion protein had decreased proportions of Tregs with respect to total

lymphocytes, as well as increased antigen-specific CD8+ T cells in the tumor site, leading to tumor rejection and protection from rechallenge.<sup>91</sup> Taken together with the findings that Treg immunosuppressive activity can be inhibited by GITR-specific agonists,<sup>91</sup> the expansion of antigen-specific T cells was likely due at least in part to Treg inhibition. *In vitro*, the GITR ligand could enhance proliferation of CD4+ and CD8+ T cells in the presence and absence of T regs, allowing the possibility that the proliferative effect was mediated by a direct action of GITRL with GITR expressed by T cells,<sup>116</sup> and further research is required to clarify which mechanisms contribute to the therapeutic effects of GITR therapy.

A myxoma virus armed with a PD-1/PD-L1 blocking molecule, while able to regress the injected tumor via CD8+ T cell activity, was ineffective against metastatic lesions. However, when CD4+ T cells were depleted, the virus had enhanced efficacy against the injected tumor, and could significantly reduce the number and size of metastatic lesions. This was likely due to inhibition of Treg-mediated suppression of CTLs, although more data is needed to confirm this mechanism.<sup>117</sup> In a study that found anti-PD-1 treatment to synergize with oncolytic VV therapy to elicit tumor-specific immunity, anti-PD-1 decreased the proportion of total CD4+ T cells characterized as Tregs.<sup>118</sup>

### **1.8.7 Oncolytic virotherapy is enhanced by targeting CTL checkpoints**

Throughout the past decade, various antibodies that target immune checkpoint molecules CTLA-4 and PD-1 have been approved by the FDA for the treatment of certain types of cancer.<sup>119</sup> Because immune checkpoint molecules are often highly

expressed by tumor-infiltrating T cells, and their ligands are often expressed by tumor cells, oncolytic virotherapy may be more efficacious in combination with these immune checkpoint inhibitors (ICIs) or as gene delivery vehicles of immune checkpoint antagonizing molecules (**Table 1.1**).<sup>95</sup>

CTLA-4 is expressed by T cells upon TCR activation. It binds B7, competitively inhibiting it from interacting with the costimulatory receptor CD28.<sup>119</sup> CTLA-4 antagonism prevents suppression of CD8<sup>+</sup> and CD4<sup>+</sup> T cell activity and deactivates T-regulatory cells.<sup>120</sup> Tumor treatment with NDV has resulted in an inflammatory response in both directly treated and distal tumors characterized by increased infiltration of various immune cells, including CD8<sup>+</sup> T cells. This was accompanied by increased CD8<sup>+</sup> T cell expression of activation marker ICOS, proliferation marker Ki-67, and lytic function marker granzyme B. The immunosuppressive marker CTLA-4 was also upregulated. While the immune activity triggered by NDV mediated some tumor regression and protective antitumor memory, these therapeutic benefits are limited in NDV treatment alone but were profoundly enhanced by combination treatment with anti-CTLA-4 monoclonal antibodies (mAbs). The combination treatment also yielded more favorable results than the antibody alone.<sup>50</sup> Similarly, in a study of ICOSL-expressing NDV, the highest CD8<sup>+</sup> T cell tumor infiltration was achieved with combination therapy with anti-CTLA-4.<sup>95</sup> Systemic CTLA-4 blockade has also produced synergistic therapeutic benefits with an oncolytic VV at least in part by increasing the presence and activity of tumor-specific CTLs.<sup>121</sup> Combinations of OVs with CTLA-4 blockade is therefore an attractive prospect for cancer treatments that optimally activate the adaptive immune system. However, systemic delivery of anti-

CTLA4 produces adverse side effects; a better approach to combination therapy may be to modify an OV to express anti-CTLA-4. This has been shown to increase tumor concentrations of the antibody without affecting systemic levels, and the blockade was shown to successfully activate tumor-resident T cells.<sup>120</sup>

PD-L1 interaction with PD-1 expressed on the surface of T cells has been shown to promote apoptosis and suppress activation.<sup>118</sup> Despite the ability of virotherapy to engage the immune system therapeutically, an optimal CTL response can be suppressed by tumor expression of PD-L1.<sup>117</sup> Various OVs have been shown to upregulate tumor expression of PD-L1.<sup>118</sup> Combined with knowledge of the ability of OVs to attract T cells to the tumor site, these data have led researchers to hypothesize that PD-1 blockade would synergize with oncolytic virotherapy by enhancing the antitumor immune response.<sup>117</sup> In one study, PD-L1 knockout in a melanoma model was shown to increase the efficacy of an oncolytic myxoma virus, resulting in complete tumor eradication in almost all treated mice, while the OV treatment in wild type mice merely stabilized tumor growth.<sup>117</sup> Blockade of PD-1/PD-L1 interaction has been shown to restore CD8+ T cell function during viral infection,<sup>118</sup> and to enhance immune responses to cancer by preventing exhaustion of antitumor T cells.<sup>117</sup> Antibodies against PD-1 have been approved for the treatment of some malignancies, though they are only therapeutically effective in a relatively small proportion of patients, particularly those whose tumors highly express PD-L1 and have high T cell infiltration.<sup>117</sup> Virotherapy has the potential to modify the TME to resemble that of patients who respond to checkpoint blockade treatment, as has been suggested by multiple studies reporting synergistic effects between virotherapy and PD-1/PD-L1 blockade.<sup>117</sup> For example, a study in which

tumor-bearing mice were treated with a combination of anti-PD-L1 and an oncolytic vaccinia virus reported that the vaccinia virus was capable of attracting T cells to the tumor site and causing various types of tumor cells to upregulate PD-L1 on the cell surface. Combination therapy with the virus and immune checkpoint blockade reduced tumor burden, improved survival, increased the ratio of CD8<sup>+</sup>/Tregs, and significantly increased cytolytic activity compared to either monotherapy. The increased immune response was shown to be specific to tumor antigens.<sup>118</sup> Another VV armed with IL-2 and TNF $\alpha$  was proven to work synergistically with PD-1 blockade to increase the presence of CD8<sup>+</sup> T cells in the tumor site, shrink tumors, and increase long-term survival to 100% of mice treated with combination virotherapy and anti-PD-1.<sup>122</sup> Delivered before surgical tumor resection, an oncolytic Maraba virus was shown to improve survival, and the response of tumor-specific T cells rendered the mice significantly more responsive to post-surgery PD-1 blockade therapy.<sup>123</sup>

While combination virotherapy and immune checkpoint blockade have shown promising therapeutic results in preclinical studies, systemic administration of PD-1 has been associated with toxicity and autoimmunity. As such, PD-1-antagonizing molecules have been incorporated into the genome of OVs to attempt to mitigate these side effects while maintaining or improving therapeutic efficacy. In one such study, treatment of melanoma with a myxoma virus armed with a soluble splice variant of PD-1 with similar blocking effects to an antibody led to significantly better tumor regression than the combination of the parental virus with the antibody or with either monotherapy. CD8<sup>+</sup> T cells were the most responsible for the observed therapeutic effects of the recombinant

virus, and while all viral therapies produced similar infiltration of these cells, their activation was highest in mice treated with the armed virus.<sup>117</sup>

The ability of various oncolytic adenoviruses, HSV-1s, VVs, coxsackieviruses, reoviruses, VSVs, and maraba viruses to activate antitumor immunity in preclinical and clinical studies has recently led to a plethora of clinical trials that combine OV with immune checkpoint inhibitors.<sup>124</sup> The two treatments are expected to work synergistically, with the general hypothesis that virotherapy will trigger an inflammatory response in the tumor microenvironment that includes increased infiltration of tumor-specific CTLs, and ICI therapy will enhance the immune response by preventing those CTLs from becoming anergic.<sup>124</sup> Many of these trials are still underway and have not yet published results, although some have released limited interim results. A few completed clinical trials of this nature have also been published. Although melanoma is the most frequent cancer type among these trials, combination treatment is also being tested on others including pancreatic cancer, liver cancer, glioma, and advanced solid tumors.<sup>124</sup>

A 2016 clinical trial in which patients with advanced melanoma were treated with a combination of the approved OV T-VEC and the CTLA-4 inhibitor ipilimumab reported an objective response rate (ORR) of 50%, while the ORR for previous phase III trials for monotherapy with T-VEC and ipilimumab were 26.4% and 10.9%, respectively.<sup>125</sup> While a direct comparison of these values suggests that the combined therapy may be more efficacious against melanoma than either monotherapy, such a conclusion cannot be definitively made without further evidence, because there were differing patient

characteristics between the studies, and the dual therapy trial had a very small sample size (n=19).<sup>125</sup> A 2018 phase II trial in which 198 melanoma patients were placed into randomized groups to receive either T-VEC plus ipilimumab or ipilimumab alone reported a significant increase in ORR in the combination arm versus the monotherapy arm (39% vs. 18%), providing stronger evidence for the higher efficacy of the combination therapy relative to monotherapy.<sup>126</sup> A 2019 trial on a mutant HSV-1 known as C-REV combined with ipilimumab reported that the virus alone resulted in significantly increased infiltration of CD4+ and CD8+ in over half of melanoma patients and that the combination therapy provided an ORR of 41% and disease control rate of 68%, which were higher than the corresponding values of 4% and 16% observed in a trial of ipilimumab monotherapy.<sup>124</sup> The trial also found that responders had higher levels of ICOS on CD4+ T cells, which has been indicated as a pharmacodynamic biomarker for anti-CTLA therapy.<sup>67</sup> Another trial for the treatment of advanced melanoma with coxsackievirus A21 (CVA21) combined with ipilimumab released interim results stating that tumors had increased immune cell infiltration and expression of genes associated with INF- $\gamma$  and immune checkpoints, supporting the rationale behind the combination therapy.<sup>127</sup>

In a small (n=21) but promising 2017 phase 1b clinical trial, patients with metastatic melanoma were treated with T-VEC followed by a combination of T-VEC and the anti-PD-1 antibody pembrolizumab.<sup>128</sup> The ORR was 62% and the complete response rate was 33%. Biopsies from patients who responded to this dual therapy revealed an increased density of infiltrating CD8+ T cells, increased tumor cell expression of PD-L1, and increased T cell expression of PD-1. Increased IFN- $\gamma$  mRNA and granzyme B

post-treatment specifically indicated an increase in cytotoxic T cell activity. These trends were observed from biopsies taken between virotherapy and combination therapy, as well as those taken after both therapies had been administered. Thus, this study supports the hypothesis that oncolytic virotherapy leads to recruitment of cytotoxic T cells that could be further activated by PD-1 blockade and that combination therapy modulated the tumor microenvironment to favor antitumor immunity.<sup>128</sup> Interim results of a phase II study of treatment of recurrent glioblastoma with the oncolytic adenovirus DNX-2401 combined with pembrolizumab has also reported that the therapy is generally well tolerated with promising effects on disease control and survival.<sup>129</sup>

### **1.8.8 OVs can also be engineered to mediate direct engagement of tumor cells with immune cells in the TME**

Studies in recent years from us and others have shown that virotherapy can impact the immune cell landscape by attracting the migration of immune cells to TME,<sup>29</sup> the so-called converting “cold tumors” to hot ones.<sup>128</sup> Other studies have shown that there is an early influx of innate immune cells, including macrophages and NK cells, in response to tumor virotherapy. Several strategies have been developed to exploit the changes in the immune landscape during virotherapy by engaging the infiltrating immune cells to attack tumor cells (**Figure 3.9**). First amongst them, are the Bispecific T cell engagers (BiTEs), which are bispecific antibodies, consisting of two single-chain variable fragments, one that bind to CD3 receptor on the surface of T cells and the other specific to a target antigen on the surface of cancer cells, mediating direct engagement independent of the MHC-peptide-TCR complex. BiTEs have shown impressive results

in the treatment of hematological malignancies,<sup>130, 131, 132</sup> however, their application in the treatment of solid tumors is limited. This may be due to penetration issues into the TME or toxicities associated with off-target activity. These problems can potentially be overcome by encoding BiTEs in OVs.<sup>133</sup>

The possibility of tumor-restricted expression, combined with the infiltration of immune cells into the TME, render OVs as promising gene delivery tools for intratumoral expression of BiTEs. The first BiTE-armed OV to undergo preclinical evaluation was a double TK deleted vaccinia virus with a secretory bispecific T-cell engager (BiTE), specific for CD3 and the tumor cell surface antigen EphA2, and has been demonstrated to significantly enhance antitumor immunity.<sup>134</sup> BiTE has since been incorporated into other oncolytic viruses such as adenovirus,<sup>135</sup> measles virus,<sup>136</sup> and others that have been described in *Table 1.1*. The dynamic design of BiTEs offers flexibility in replacing scFvs, to target various receptors on immune cells and various antigens on the tumor cells. Freedman and colleagues modified the oncolytic group B adenovirus EnAdenotucirev (EnAd) with BiTEs targeting EpCAM, and crosslinking them to CD3 on T cells, and demonstrated clustering and activation of CD4 and CD8 T cells. Taking a similar approach, another group<sup>137</sup> have armed an oncolytic adenovirus (ICOVIR-15K) with an EGFR targeting BiTE. The authors reported improved efficacy in two xenograft mouse tumor models. Other BiTE-armed OVs which are currently under investigation are the oncolytic measles virus, encoding CEA-<sup>138</sup> and CD20-targeting BiTEs.<sup>139</sup>

In 2017, FDA approved the use of BiTE targeting both CD19 and CD3, Blinatumomab, for the treatment of a rare type of acute lymphoblastic leukemia (ALL).<sup>132</sup> Moreover, trispecific antibodies binding to NK or T cells have also been explored to treat cancer. Vallera and group designed IL-15 Trispecific killer engagers, TriKE, that contains a single-chain scFv against CD16 and CD33, linking NK cell with CD33+myeloid targets, creating an immunological synapse, combined with an IL-15 crosslinker that promotes NK cell expansion and survival. With the clinical success of OV-BiTEs, similar strategy was explored, where OVs are used to express a T cell activating molecules on infected cells. These activating molecules are called membrane-integrated T cell engagers (MiTes), which were expressed in an oncolytic adeno virus, selective to CD46 expressing tumor cells.<sup>140</sup> This approach can potentially overcome immune suppression in the TME, by antigen independent activation of T cells. MiTes, thus can mediate the engagement of infected cells with the tumor cells, sparking the host immunological responses, leading to a broader anti-tumor immune response. We have shown in our recent studies that arming an oncolytic HSV with a novel chimeric molecule that can engage natural killer (NK) cells with tumor cells via Protein L and a TAA ligand can also enhance the antitumor efficacy of the virotherapy.<sup>141</sup>

Although arming OVs with cancer-cell targeting BiTEs/ TriTEs or BiKes/ Trikes is promising, there is a risk of premature clearance if infected tumor cells, interfering with OV replication and spread. An alternate approach is to target non-transformed cells (Cancer-associated fibroblasts, adipocytes, endothelial cells, as well as a range of immune cells such as macrophages, myeloid-derived suppressor cells, T regulatory cells and neutrophils), all in co-existence in the TME, that play critical role in enhancing

tumor growth, immune suppression and metastasis. Therefore, targeting the TME using armed OV's encoding BiTEs is a viable option yet challenging due to the lack of tumor-restricted surface antigen of TME cells. Fibroblast activation protein- $\alpha$  (FAP) is overexpressed in cancer-associated fibroblasts (CAFs), represents an attractive target for TME-focused generation of OV's. Consequently, scientists investigated the use of FAP as a target for BiTE, to which, X-T Song and team<sup>142, 143</sup> constructed an oncolytic vaccinia virus encoding BiTE specific for CD3 and FAP (mFAP-TEA-VV). It has proven to exhibit potent antitumor activity in an immunocompetent mouse melanoma model, which is a result of BiTE armed OV spread and destruction of tumor stroma. Based on the same principle, another group,<sup>144</sup> also constructed an OV encoding a BiTE that targeted FAP on CAFs and Cd3e on T cells, leading to the death of the fibroblasts and simultaneously activating T cells within the TME. Another BiTE targeting FAP on CAFs and CD3e on T cells, was inserted into the oncolytic adenovirus (ICO15K-BiTE). The engagement of CD3 T cell with the CAF's led to T cell activation, proliferation, and the cytotoxic death of FAP+ CAF's in the TME. Overall, BiTE armed OV enhanced intratumoral infiltration/accumulation of T cells and decreased the FAP expression in the treated tumors.<sup>145</sup> Engineering OV's to express TME-targeted BiTEs, offers a unique advantage and synergizes the immune stimulating activities of the OV, and direct oncolysis from viral spread and infection. Scott et al., 2019 developed BiTE and TriTE armed adenoviruses, in which the molecules were designed to recognize CD3e on T cells and CD206/folate receptor b on M2- like macrophages/tumor associated macrophages (TAMs).<sup>146</sup> This opened an avenue to direct these molecules to eradicate non-transformed cells in the TME, improving the therapeutic benefit.

Few other investigators explored the possibility of combining armed OV's in combination with CAR-T cell therapy. Suzuki and team constructed a BiTE molecule designed to target CD44v6 on cancer cells, crosslinking with native TCR on CAR-T cells and incorporated in an OV (CAAdTrio) that simultaneously produced IL2, an Anti-PD-L1 antibody, making it a CAAdTrio. CD44v6 BiTE expressed from CAAdTrio engaged HER2-specific CAR T cells with CD44v6+ cancer cell lines, induced cytotoxicity to produce more rapid and sustained disease control of orthotopic HER2+ and HER2- CD44v6+ tumors. This approach ensured dual targeting for two tumor antigens by simultaneously engaging native TCR and CAR, resulting in improved therapeutic efficacy.<sup>147</sup>

Although BiTEs and TriTEs armed OV's are a promising approach for the treatment of solid tumors, owing to the possibility of tumor restricted expression combined with the infiltration of immune cells into the TME. Regardless, there are many challenges for OV's clinical evolution as immunotherapies including but not limited to tumor antigenic heterogeneity, insufficient OV dose, immune escape, evasion, and suppression in the TME.

Efforts are made in our lab in designing novel chimeric molecules that engage NKG2D expressing T and NK cells with EGFR on the target cells. Instead of using the traditional single chain antibodies (scFvs), we chose to use ligands as the targeting moieties. The reason for such a design is the concern on the high binding affinity of scFvs used in either BiTE or CAR-T cells and its potential link to the enhanced release of cytokines and the consequential cytokine storms.<sup>148</sup> The affinity of ligand binding is usually

significantly lower than that of a scFv. As such, this design mimics “affinity tuning” that has been applied for increasing the safety of BiTE.<sup>149</sup> This approach is now under investigation in our laboratory and will soon be published.

All of these studies suggest that the arming OV with immune cell engagers (BiTEs, TriTEs), immune cell stimulators (MiTEs), killer engagers (BiKEs, TriKEs) can target both cancer cells and tumor-associated stroma to promote anti-tumor immunity, resulting in enhanced therapeutic efficacy.

**Table 1.1: OVs in combination with the immune modulators**

Transgene	Type of OV	Effect on Tumor Microenvironment	Cancer Type (preclinical model unless specified otherwise)	References
<b>Cytokines</b>				
<b>IFN<math>\beta</math></b>	AdV	Upregulates MHC1 in tumor cells	Mesothelioma, bronchogenic lung cancer	51
	MV	Triggered CD68-positive immune cell infiltration; innate immune cell infiltration	Non-small cell lung cancer	150
	VV		Mesothelioma	151
	VSV		Non-small cell lung cancer	152
	NDV		Pancreatic adenocarcinoma	153
<b>IFN<math>\gamma</math></b>	NDV	Increased cytokine expression; maturation of DC's	Melanoma	154
	VSV	Increased T cell infiltration	Mammary and colon carcinoma	95
<b>GM-CSF</b>	AdV	Promotes DC survival and T cell priming; CD3+ T cell infiltration	Solid tumors (clinical)	64, 155
	HSV-1		Colon, adenocarcinoma, hypopharyngeal carcinoma, Glioma, breast cancer	18
	NDV	Improved peripheral blood mononuclear cell response	Fibrosarcoma	59
	VV		Melanoma, mammary carcinoma, colorectal carcinoma	65
<b>IL-12</b>	HSV-1	Prolongs expression of IL-2 receptor on CD8+ T cells; infiltration of T helper, CTL, NK cells and macrophages	Glioma	99
	Reovirus (unarmed)		Melanoma	156
	AdV	Stronger antitumor activity; DC maturation	Melanoma	157

**Table 1.1. Continued**

	VSV		Squamous cell carcinoma	158
<b>IL-2</b>	NDV	Promotes expansion and effector function of CD8+ and CD4+ T cells	Colon carcinoma	98
	HSV		Hepatocellular carcinoma, melanoma	79
<b>IL-15</b>	VSV	Increase in tumor specific T cells	Colon adenocarcinoma	102
	VV	Infiltration of T helper and CTLs	Colon carcinoma, ovarian cancer	103
	NDV		Melanoma	159
	IAV	Anti-tumor immunity against rechallenge	Melanoma	160
	HSV	Increased survival, NK mediated cytotoxicity	Glioma	69
<b>Chemokines</b>				
<b>CCL5</b>	VV	Improved DC maturation. Improved infiltration of T helper and CTLs	Colon carcinoma	161
<b>CCL2</b>				162
<b>CCL19</b>				163
<b>CXCL9 (OV-induced)</b>	HSV-2	Triggers migration of activated T cells to tumor site	Pancreatic cancer	29
	HSV-1		Ovarian carcinoma	111
<b>CXCL10 (OV-induced)</b>	HSV-2	Triggers migration of activated T cells to tumor site	Pancreatic cancer	29
	HSV-1		Ovarian carcinoma	111
<b>CXCL11</b>	VV	Triggers migration of activated T cells to tumor site	Mesothelioma	164
<b>Checkpoint inhibitors</b>				
<b>CTLA4</b>	NDV	Reverses inhibition of B7 costimulatory activation of CD8+ T cells	Melanoma	50 95
	AdV	Decreased infiltration of Tregs		120
	MV	Infiltration of T helper and CTL		165
<b>PD-1/PD-L1</b>	VV	Decreased infiltration of Tregs	Renal adenocarcinoma, colon adenocarcinoma	121
	MV	Infiltration of T helper and CTL	Melanoma	165
	MYX V	antitumor CD8+ T-cell responses		117
<b>Co-stimulatory ligands</b>				
<b>B7</b>	HSV-1	Costimulatory activation of CD8+ T cells	Neuroblastoma	88 166
	VV	Anti-tumor immunity	Melanoma	167
<b>GITRL</b>	AdV	Increases proliferation and effector functions of CD8+ and CD4+ T cells	Glioma	87
<b>CD40L</b>	AdV	Inhibits Tregs immunosuppressive activity	Melanoma	116 168
	VV	Infiltration of T helper, CTL., NK, DCs and MDSCs	Melanoma	169
	VSV	Significant priming of T cells directed against TAAs		170

**Table 1.1. Continued**

<b>OX40L</b>	AdV	Costimulatory activation of CD4+ T cells	Melanoma, colon adenocarcinoma	85
<b>4-1BBL</b>	AdV	Increases proliferation and effector functions of CD8+ and CD4+ T cells	Melanoma	94
	VV	Infiltration of CTLs	Melanoma	171
<b>LIGHT</b>	AdV	Reduced Treg suppression	Prostate	172
<b>CD70</b>	VV	Tumor reduction	Colon adenocarcinoma	173
<b>Combinations</b>				
<b>GMCSF+ IL-12</b>	AdV	Shift from Th2 to Th1 response, infiltration of T helper, CTL, NK and DC	Melanoma	174
<b>4-1BBL+IL-12</b>		Infiltration of T helper, CTL, DCs and NK cells		94
<b>B7.1+IL-12</b>				175
<b>B7.1+ GMCSF</b>				176
<b>IL-12+ IL-18</b>				63
<b>B7.1+ IL-18</b>	HSV	Reduced tumor growth	Prostate, neuroblastoma	166
<b>IL-12+CCL2</b>			Neuroblastoma	162
<b>Immune cell engagers</b>				
<b>CD3/EphA2</b>	VV	Induced T cell activation, increased cytotoxicity of target cells and bystander killing of non-infected tumor cells.	Human lung cancer	143
			Colorectal Carcinoma	134
<b>CD3/EGFR</b>	Ad	T cell activation, proliferation and bystander cell-mediated cytotoxicity, enhanced antitumor efficacy	Human lung and colorectal cancer	112
<b>CD3/EpCAM</b>	EnAd	T cell activation	Primary pleural effusions and peritoneal malignant ascites	137
<b>CD3/CEA or CD20</b>	MV	Increased therapeutic efficacy	Patient derived primary colorectal carcinoma	135
<b>CD3/FAP</b>	VV	T cell activation and killing of stromal fibroblasts	B16 models, Human colon and lung cancers	143
	AdV			144 145
<b>CD3, CD206 folate receptor B</b>	EnAd	T cell activation with preferential killing of M2-like macrophages.	Human cancer samples tested in vitro	146
<b>Others</b>				
<b>ATP (OV-induced)</b>	coxsackieviruses	Promotes DC maturation and T cell priming	Lung adenocarcinoma	73
	AdV		Mesothelioma	74

**Table 1.1. Continued**

	HSV-1		Breast cancer, brain metastasis, glioblastoma	76
<b>HMGB1 (OV-induced)</b>	coxsackieviruses	Promotes DC maturation and T cell priming	Lung adenocarcinoma	73
	AdV		Mesothelioma	74
<b>CALR (OV-induced)</b>	AdV	Increases DC antigen processing and cross-presentation	Mesothelioma	74
<b>HSP70</b>	AdV	Increases DC antigen uptake, upregulates T cell costimulatory molecules on surface of DCs	Prostate adenocarcinoma, melanoma	77
			various forms of gastric cancer	177
			Pancreatic cancer	80
<b>HPGD</b>	VV	Expression of Th1 cytokines, secretion of IL-12	Solid tumors, Renal cell carcinoma	178
<b>TRIF</b>				
<b>DAI</b>				

### 1.8.9 Ongoing OV Trials

From a recent article by Kaufman et al., 2020 a total of 97 independent clinical trials reporting OV studies from 2000 to 2020 that included treatment of 3233 patients with various cancers have been reported (*Table 1.2*). Majority of these clinical trial were phase I. There were very few (6.2%) phase I/II ongoing clinical studies.

Although both DNA and RNA viruses have been deployed for OV therapy, the majority of clinical studies were DNA-based viruses, with the most common one being adenovirus, followed by HSV-1, reovirus and pox viruses.

Native viruses were commonly used in about one-third of the ongoing clinical trials where as two-thirds of the studies were genetically modified viruses, The modification are usually deletion of the viral genes to promote selective tumor cell replication and at the same time attenuate viral pathogenicity, GMCSF was the most common transgene

which is designed to promote and mature local dendritic cells to help stimulate the host immune responses against the tumor. Second in the list, is LacZ, which encodes the bacterial b-galactosidase, and is used for selection of recombinant virus and can be used as a maker to identify OVS after treatment,

The most common tumor evaluated using oncolytic viruses are melanoma and GI cancers, The largest number of patients (n=1000) were accrued for clinical studies involving melanoma patients, part of which are the patients (n=436) were from the phase III TVEC clinical trial, . Other common cancers include head and neck cancer, breast and gynecological cancers, genitourinary cancers, and sarcomas.

Based on encouraging preclinical data, numerous combination studies are under way using small molecules and chemotherapy.

**Table 1.2: Current ongoing clinical trials involving oncolytic viruses**

Patient characteristics in oncolytic virus clinical trials	
<i>Characteristic</i>	<i>N</i>
<b>Cancer type</b>	
Brain	154
Breast	136
Gastrointestinal	577
Genitourinary	207
Gynecologic	185
Head and neck	106
Lung	197
Melanoma	1000
Pediatric	62
Sarcoma	44
Other solid tumors*	494
Hematological tumors	71
Total	3233
<b>Delivery route</b>	
Intratumoral	1482
Intravenous	1147
Multiple†	54
Other‡	550
Total	3233
<b>Study phase</b>	
I	1008
I/II	92
II	714
III	477
Not specified	942
Total	3233

\*includes studies enrolling solid tumors

†patients received virus by both intratumoral and intravenous

‡includes intravesical, intraperitoneal, intradermal, hepatic artery infusion, convection-enhanced delivery, and direct injection of resected tumor bed.

(Reprinted by permission from Copyright © 2020, BMJ Publishing Group Ltd & Society for Immunotherapy of Cancer.<sup>180</sup>)

## **1.9 Oncolytic virotherapy in combination with immunotherapy**

Although monotherapy approach is still very common treatment for many different types of cancer, this method is generally deemed ineffective than the combination therapy approach. The conventional therapeutic techniques non-selectively target actively proliferating cells, which ultimately leads to the destruction of both healthy and cancerous cells, e.g., chemotherapy can be toxic to the patient with multiple side effects and risks and can also reduce their immunity and increased susceptibility to host diseases. Therefore, better strategies need to be developed to decrease the toxic effects on normal cells while simultaneously producing cytotoxic effects on cancer cells.

The amalgamation of anti-cancer agents enhances both efficacy and tolerability compared to monotherapy because it targets multiple key pathways in a synergistic/additive manner. This approach also potentially reduces drug resistance, that's one of the limitations that we can overcome with combination therapy and simultaneously providing anti-cancer benefits by reducing tumor growth and metastatic potential.

While, only a minor group of cancer patients respond to monotherapy, it may be relatively ineffective to most patients with advanced cancers. Moreover, to achieve complete remission of cancer, the combination of two or more therapeutic approaches may be required.<sup>181</sup> This field is progressing fast, and researches are focused on improving current strategies, combined with novel scientific discoveries.

Although the combination of check point inhibitory antibodies may enhance anti-tumor immunity, it is coupled with side effects and toxicities including autoimmune disorders like dermatitis and inflammatory colitis. To minimize the risk, dosing and timed administration of product need to be carefully assessed for clinical efficacy. In addition, combining immunotherapy with other conventional treatments like chemotherapy, radiation therapy and targeted therapies including CAR-T's can also be considered. Immunotherapy combined with the other types of therapies have demonstrated promising synergistic effects in early clinical trials.

The rationale behind my research proposal is that combination therapy, a treatment modality that combines two or more therapeutic agents is a cornerstone of cancer therapy. The future of immuno-oncology drug development is positioned to combination therapy, where immunotherapy is combined in rational combinations with targeted therapy, cell therapy, viral therapy for synergistic effects.

In this research study, we explored the possibility of combining oncolytic viruses with immune modulators to achieve a synergistic effect and this is illustrated in Chapter 3 of this dissertation. Moreover, the targeted infection of the tumor with the oncolytic viruses not only kills the tumor cells, but also has the potential to create an “inflammatory storm” that arouses the innate and adaptive immune responses against tumors. The immune modulation using an HSV-2 based oncolytic virus is extensively studied in Chapter 2 of this dissertation.

### **1.10 Goals, and overall aim of the current study**

The overall goal of this study is to potentiate the therapeutic benefit of oncolytic viruses by integrating immune cell engagers into OV's for application in the cancer setting. The study focusses the use of oncolytic HSV-1 and HSV-2 as potent anti-cancer agents. The research work in this dissertation are the result of our previous efforts where FusOn-H3 (HSV-2 based oncolytic virus) showed potent anti-cancer properties. Moreover, we have demonstrated the generation of robust anti-tumor immune responses from the host upon oncolytic virotherapy in various animal models. The study focusses on harnessing the immune modulation potential of the oncolytic viruses and by arming the viruses with immune stimulating/activating agents.

In Chapter 2 of this dissertation, we studied the modulation of intratumoral immune landscape upon oncolytic virotherapy with our FusOn-H3, our lab's HSV-2 based oncolytic virus. We demonstrated that, the virus infection caused the massive infiltration of immune cells including T/NK cells. Moreover, we also observed the activation of the immune cells towards developing robust anti-tumor immune responses in the host. This proves the synergistic benefit of the virus in combination with other immune cell stimulating agents.

In Chapter 3 of the dissertation, we designed novel immune cell engagers: BiCEP and TriCEP that can actively engage T/NK cells with tumor cells via overexpressed EGFR. This engagement potentially activated the immune cells and further caused the infiltrated immune cells activate, act upon tumor cells, and persist in the harsh TME.

We have demonstrated in this study the reduction of tumor growth in mouse colon cancer model and demonstrated the increased infiltration of tumor cells into the TME.

**2. SINGLE CELL RNA SEQUENCING REVEALS PROFOUND AND DISTINCT CHANGES IN THE TUMOR IMMUNE LANDSCAPE FOLLOWING TREATMENT WITH AN HSV-2 BASED ONCOLYTIC VIRUS**

## 2.1 Abstract

Oncolytic virotherapy can reinvigorate cancer immunotherapy by directly inducing a robust anti-tumor immune response as well as turning a cold immunosuppressive environment into a hot inflamed tumor. Oncolytic viruses are particularly attractive for many of the current cancer-immunotherapeutic modalities in their capacity to simultaneously induce both anti-viral and anti-tumoral immunity. Despite widespread interest in the direct anti-cancer activity of oncolytic viruses, only limited attention has been paid to the interaction between viral therapy and the tumor microenvironment. FusOn-H3 is a novel HSV-2 based oncolytic virus created by deleting the N-terminal domain of the ICP10 genes of HSV-2, which enables the virus to selectively replicate in tumor cells with activated Ras pathway. We have previously demonstrated the anti-tumor activity of FusOn-H3, particularly its role in the induction of strong T cell responses against primary and metastatic mammary tumors *in vivo*. However, the mechanism of its immunomodulatory function and the immune cell engagement upon viral infection in the tumor microenvironment has not been explored. In this study, we investigated the impact of FusOn-H3 virotherapy on the tumor microenvironment, using single-cell RNA sequencing (scRNAseq) to investigate the infiltration and functionality within global populations or at the single-cell level. Our data show that FusOn-H3 can induce significant infiltration of both innate and adaptive immune cells. Detailed analysis by scRNAseq revealed the influx of T cells, B cells, NK cells, and Neutrophils into the TME, contributing to the conversion of cold tumors into hot ones. Moreover, tracking immune gene signatures of these infiltrating immune cells by scRNAseq revealed that this virotherapy also activated these cells, allowing them to fight cancer

more effectively. This study thus gives us an insightful as well as an overall understanding of how FusOn-H3 can impact the tumor immune landscape. These findings are important in guiding the clinical translation of the virotherapy, particularly in the context of combining it with other immune-therapeutics such as check-point blockers in the treatment of solid tumors.

## **2.2 Introduction**

Oncolytic viruses (OVs) represent a new class of therapeutic agents that can be applied for the treatment of many malignancies. With the FDA approval of talimogene laherparepvec (T-VEC or Imlygic) that is a herpes simplex virus type I (HSV-1) based oncolytic virus, virotherapy has become a therapeutic option for melanoma.<sup>182</sup> Several clinical trials are currently underway at testing the efficacy of virotherapy for treating other malignancies either as a monotherapy or in combination with other treatments such as immune checkpoint inhibitors (ICIs). Although virotherapy was originally designed for the intrinsic ability of OVs to infect and lyse cancer cells, it has become increasingly clear that the engagement of OVs with the host's immunity system and the consequential elicitation of antitumor immunity is a key part of the overall antitumor activity. It is believed that the lysed tumor cells by the applied virotherapy can release abundant tumor antigens in the infectious milieu, which favors tumor antigen presentation.<sup>183</sup> The unique way of tumor cell destructions by certain oncolytic viruses, such as the cell-membrane fusion induced by some fusogenic oncolytic viruses or the so-called "immunogenic cell death" by many other types of OVs, may contribute further to the efficient generation of tumor-specific immune responses.<sup>184</sup> OVs have also been

armed with a variety of cytokines and other immune modulators that are crucial for eliciting effective immune responses.

Immune landscape is an important determining factor dictating the effectiveness of cancer immunotherapy.<sup>185</sup> For example, it has been reported that, among the immune cells, the number and quality of the infiltrating T cells are a key indicator for the effectiveness of check-point blockade treatment.<sup>186</sup> Low T cell infiltration into the tumor is a limitation for poor outcomes of immunotherapy. Previous studies have indicated increased T cell infiltration to be an indispensable predictive biomarker for better prognosis.<sup>186</sup> Hence, therapies to increase T cell infiltration would theoretically exhibit a synergetic effect with anti-PD-1 immunotherapy.<sup>128</sup> Infection with an oncolytic virus induces highly dynamic and interactive immune changes within the tumor microenvironment.<sup>187</sup> Therefore, oncolytic virotherapy is a potential approach to increase T cell infiltration of tumor resulting in host anti-tumor immunity. Thus, OVs provide an ideal way to reverse the immunosuppressive tumor microenvironment and render tumors sensitive to the immune check point treatment.

More recently, it has also become clear that oncolytic virotherapy can impact cancer immunotherapy through altering the immune landscape within the tumor microenvironment (TME). Immune landscape is an important determining factor dictating the effectiveness of many cancer immunotherapies.<sup>185</sup> For example, it has been reported that the number and subtype of the infiltrated T cells are a key indicator for the effectiveness of checkpoint blockade inhibitor (CBI) treatment.<sup>186</sup> TMEs with low T cell infiltration are considered cold tumors and they usually serve as a strong indicator

for poor outcomes of immunotherapy. In contrast, tumors with high T cell infiltration are considered hot tumors and they intend to respond more favorably to CBI treatment.<sup>186</sup> Studies from us and others have shown that OVs can impact the immune cell landscape by attracting the migration of T cells to TME,<sup>29</sup> which indicates that it has the ability to convert cold tumors to hot ones and paves the way for combining virotherapy with CBIs.<sup>188</sup>

However, the studies reported so far on analyzing the impact of virotherapy on TME are fragmented. A comprehensive and detailed analysis on how virotherapy may impact the entire immune landscape in TME has not been reported. We took the advantage of single cell RNA sequencing (scRNA-seq) on its ability to unbiasedly profile the entire cell population in TME, to extensively monitor the immune profile changes during virotherapy. For this study, we focused on an HSV-2 based oncolytic virus, FusOn-H3, which was originally constructed in our lab and is currently in the process of being translated into clinical application. The virus was constructed by a unique strategy, via deleting the N-terminal domain of the ICP10 gene and insertion to the locus of the green fluorescent protein (GFP) gene (for the construction of FusOn-H2). FusOn-H3 was derived from FusOn-H2 by deleting the GFP gene (necessary for clinical application). Our data reveal that, despite their significant sequence homology, these two oncolytic HSVs displayed a substantial difference in impacting the TME immune landscape, with the HSV-2 based virus showing more preferential immune cell infiltration for cancer immunotherapy.

## **2.3 Materials and Methods**

### **2.3.1 Cell lines and oncolytic viruses**

The mouse colon cancer cell line CT26-EGFR was established in the lab as previously described.<sup>141</sup> Tumor cells were propagated in vitro in Dulbecco's Modified Eagle Medium (Gibco) supplemented with 10% fetal bovine serum (FBS, Gibco). FusOnH3 is derived from an HSV-2 based oncolytic virus, FusOn-H2. The details of FusOn-H2 construction and its antitumor properties have been described in our previous studies.<sup>24</sup> FusOn-H3 was constructed from FusOn-H2 by deleting the inserted *GFP* gene at the N-terminus of the *ICP10* gene locus.

### **2.3.2 Tumor transplantation and treatment**

Immune-competent female BALB/c mice (4 - 6 weeks old) were purchased from Charles River Laboratories. All animal experiments were approved by the University's Institutional Animal Care and Use Committee (IACUC). Right flanks of mice were shaved the day before tumor cell injection. CT26-hEGFR cells were washed extensively, resuspended in endotoxin-free phosphate-buffered saline (PBS) for tumor implantation in mice. The next day,  $3 \times 10^5$  CT26-EGFR cells were injected subcutaneously to the shaved right flank. Once the tumor volumes reached the approximate size of 8-10 mm in diameter, mice were randomized into different groups to receive either PBS control or FusOn treatment at the dose of  $5 \times 10^6$  pfu per mouse. The mice were euthanized on day three after virotherapy to collect tumor tissues for scRNA-seq or histology exam and spleens for other immune assays.

### **2.3.3 Tumor dissociation and single-cell processing**

For scRNA-seq studies, the freshly collected tumors were immediately immersed in a tissue storage medium (Miltenyi, San Diego, CA) and kept at 4 °C until ready for dissociation. Within 24 h, tissues were processed to single-cell suspensions using the human tumor dissociation kit from Miltenyi and the gentleMACS apparatus and this was done by following the manufacturer's protocol. Single-cell suspensions were then stained with a fluorescently conjugated antibody specific to CD45 (BioLegend) for 30 min at 4 °C. The cells were washed with cell staining buffer (BioLegend) and CD45<sup>+</sup> live cells were sorted on a FACS Melody cell sorter (BD) into 2% FBS in PBS, which were kept on ice until the cells were further processed for scRNA-seq.

### **2.3.4 scRNA-seq library preparation and sequencing**

Cell suspensions were washed 2–4 times and manually counted twice to assure cell viability was >90% before loading onto the Chromium platform. The libraries were created from the cells by successfully capturing cells inside gel beads in emulsion (GEM) by passing cells through a microfluidic channel. Library fragmentation size and quantification were measured before sequencing to ensure that the cDNA has been fragmented and barcoded correctly. The cDNA libraries were assessed while using an Agilent TapeStation 4200 High sensitivity DNA tape. On the day of single-cell capture and library preparation, the cells were resuspended in PBS containing 0.04% bovine serum albumin (BSA) (Ambion, Foster City, CA) to a final concentration of 200 cells per  $\mu\text{L}$ . This cell suspension was used as an input for automated single-cell capture and barcoding using the 10X Genomics Full Chromium platform. Approximately 700 single

cells were captured for each sample while using the 10X Genomics Single Cell 3' Chip at the university's Seq-N-Edit Core per standard protocols. Single-cell GEMs were generated, and the single cells were uniquely barcoded. The cDNA was recovered and selected using DynaBead MyOne Silane Beads (Thermo Fisher Scientific, Carlsbad, CA) and SPRIselect beads (Beckman Coulter, Brea, CA). The sequencing libraries were generated and the quality was assessed using a high-sensitivity DNA tape on TapeStation 4200 (Agilent, Santa Clara, CA), and the fragments were counted with Qubit Fluorometer (Thermo Fisher Scientific, Carlsbad, CA) and Kapa Library Quantification Kit (Kapa Biosystems, Wilmington, MA) using the AriaMX instrument (Agilent, Santa Clara, CA). The libraries were sequenced using NextSeq 500 (Illumina, San Diego, CA) in stand-alone mode to obtain pair-end sequencing 26 bp (read1) X 98 bp (read2) and a single index 8 bp in length.

### **2.3.5 Transcriptome analysis**

Single-cell sequencing data downstream analysis was performed on the Maxwell Cluster high-performance research computing center at the University of Houston, using the analytical program, Cell Ranger 4.0.0 Single Cell Analysis Pipelines (10X Genomics, Pleasanton, CA, USA). Raw base call files that were generated by NextSeq 500 were demultiplexed using the "cellranger mkfastq" function to generate FASTQ files. The reads were aligned to the mouse (mm 10) genome using "cellranger count" function by STAR aligner.<sup>189</sup> The feature-barcode matrices across different samples were aggregated by "cellranger aggr" function, leading to an aggregated read count table.

### 2.3.6 Single-cell data analysis

After constructing the single-cell gene expression count matrix, we used the R package Seurat (v3.1.1) for downstream analysis on R platform (v3.5.2). Transcription noise cells were firstly filtered by several criteria, including minimal expression of 300 genes per cell and mitochondrial read percentage >30%. All cells passing quality control were merged into one count matrix and normalized and scaled using Seurat's `NormalizeData` and `ScaleData` functions. The reduced set of consensus highly variable genes was used as the feature set for independent component analysis on ~3000 genes using Seurat's `RunPCA` function. A UMAP dimensional reduction was performed on the scaled matrix (with most variable genes only) using the first 40 PCA components to obtain a two-dimensional representation of the cell states. Cell clustering was performed using the function `FindClusters` that implements SNN (shared nearest neighbor) modularity optimization-based clustering algorithm on 40 PCA components with resolution 0.8, leading to 22 clusters. For each cluster, only genes that were expressed in >25% of cells with at least 0.25-fold difference were considered.

To aid the assignment of cell type to clusters derived from unsupervised clustering, we performed cell-type enrichment analysis. Cell-type gene signatures obtained from BlueprintENCODE, Monaco Immune references from SingleR and human cell landscape. Mouse gene symbols were capitalized to map to human gene symbols. Each gene signature obtained from our clustering was statistically evaluated for overlap with gene signatures contained in these two resources.

### **2.3.7 Lymphoid population analysis**

To further explore lymphoid cells, clusters expressing CD45 were extracted from aggregated samples. Most variable genes, PCA, UMAP, clustering (resolution 1 on 40 first PCAs) and marker selection analysis was performed as described above.

### **2.3.8 Immunohistochemistry protocol**

Immunostaining was performed on paraffin-embedded tumor tissues harvested 48 hours after virotherapy. In brief, the paraffin blocks were sliced into thin sections, deparaffinized with xylene, and rehydrated with decreasing concentrations of ethanol in water (100%, 90%, 70%). Antigen retrieval was achieved by incubating the slides for 20 min in the hot (95 °C) citrate buffer in a steamer, followed by 20 min of slow cooling at room temperature. Endogenous peroxidases were quenched by incubating the slides in 3% hydrogen peroxide for 20 min. The sections were then washed three times with phosphate-buffered saline (PBS) for 10 min. The sections were blocked using 3% BSA for 1 h at RT, followed by three times washes with PBS for 5 min each wash. Primary antibodies were applied O/N at room temperature in a humidified chamber (rabbit anti-CD4 antibody (ab183685, Abcam), rabbit anti-CD8 antibody (ab203035, Abcam), goat anti-CD3 antibody (SC-1127, SantaCruz), mouse Anti-CD20 antibody (ab9475, Cell Signaling Technology)). After rinsing the slides in PBS, they were incubated in fluorophore secondary antibodies for 1 h at room temperature. After washing with PBS for 10 min, the slides were incubated with Vectastain ABC reagent (Vector Laboratories) for 30 min. After washing with PBS for five min, color development was achieved by applying diaminobenzidine tetrahydrochloride (DAB) solution (Vector

Laboratories) for two to five min, depending on the primary antibody. The duration of DAB incubation was held constant for all the slides for that antibody. After washing in distilled water, the sections were counterstained with hematoxylin, dehydrated through ethanol and xylene, and cover-slipped using a xylene-based mounting medium.

### **2.3.9 Immunofluorescence staining**

To stain for HSV antigens, the tumor sections were rehydrated with decreasing concentrations of ethanol, blocked with 3% BSA for 1 h at RT and incubated with a human anti-HSV serum (prepared by our own lab at a 1:100 dilution), overnight at RT. After washing, fluorescein isothiocyanate (FITC)-conjugated goat anti-human IgG antibody (Sigma-Aldrich, St Louis, MO), diluted at 1:200, was added to the tissue section and incubated at 37 °C for 60 min, followed by three washes with PBS. The slides were then dehydrated in an ascending series of ethanol for 5 min each, cleared in xylene for 5 min, mounted in UltraCruz aqueous mounting medium with DAPI (sc-24941), and observed under a fluorescence microscope. To stain for CD3, CD4, CD8, and CD20, a similar IFC procedure was followed for CD3, CD4, CD8, and CD20 antigens. The same antibodies used for IHC were used for IFC with compatible fluorophore-conjugated secondary antibodies.

## 2.4 Results

### 2.4.1 scRNA-seq data collection on tumor samples obtained from a “hEGFR tagged” murine colon cancer model

To fully characterize the immune landscape within the tumor microenvironment (TME) and the potential impact of virotherapy on it, we used high-dimensional scRNA-seq analysis to reveal the complex transcriptomes and compositions of cells in the collected tumor tissues. The experimental procedure is summarized in **Figure 2.1A**. It started with the establishment of tumors at the right flank by implanting the CT26 murine colon cancer cell line that had been stably transduced with the encodes the human epidermal growth factor receptor (hEGFR).<sup>141</sup> The transduced *hEGFR* gene would allow the tumor cells to be clustered. When the tumors reached an approximate size of 8-10 mm in diameter, tumors were injected either with PBS as a control or with  $5 \times 10^6$  plaque-forming-unit (pfu) of FusOn-H3, an HSV-2 based oncolytic virus.<sup>190</sup> The tumors were collected 48 h post virotherapy and were divided into halves, with one half for single cell preparation and the other half for immunohistochemistry (IHC). The single cell preparations were then sorted into CD45<sup>-</sup> and CD45<sup>+</sup> populations. The CD45<sup>-</sup> and CD45<sup>+</sup> cells from each tumor sample were mixed at a 3:1 ratio before they were processed for single-cell RNA sequencing (scRNA-seq) on the 10x Genomics Chromium platform and sequenced by Illumina NextSeq at recommended sequencing depth to provide information for both gene expression and paired immune repertoire. The sequencing yielded gene expression profiles from over 12,232 cells in total with a coverage of over 14,492 reads per cell post normalization. The breakdown details for

each treatment group are: 1) Control group (n= 7,013 cells sequenced, 11,605 mean reads per cell) and 2) FusOn treatment group (n= 5,229 cells sequenced, 17,379 mean reads per cell). The data was normalized with the Seurat V4.0.<sup>191</sup> After clustering and annotation analysis in the aggregated datasets, the 22 cell clusters were initially classified into two distinct groups: CD45<sup>+</sup> leukocytes (containing all the immune cells) based on CD45 (*Ptprc*) expression (**Figure 2.1B**) and EGFR<sup>+</sup> tumor cells based upon hEGFR expression (**Figure 2.1C**). There were two distinct clusters of epithelial and adipocytes which are CD45<sup>-</sup> and EGFR<sup>-</sup> and were separately clustered at the top left in the Uniform Manifold Approximation and Projection (UMAP) plots. The CD45<sup>+</sup> cells were reanalyzed at a high-resolution by performing sub-clustering of immune cells and mapped them to the Monaco Immune fine reference panel by SingleR<sup>189</sup>. This yielded nine distinct CD45<sup>+</sup> subpopulations (CD4 T cells, CD8 T cells, NK cells, B cells, neutrophils, monocytes/macrophages, progenitors, dendritic cells, and basophils (**Figure 2.1D**), which are broadly defined by the distribution of the classical marker genes (**Figure 2.2**).

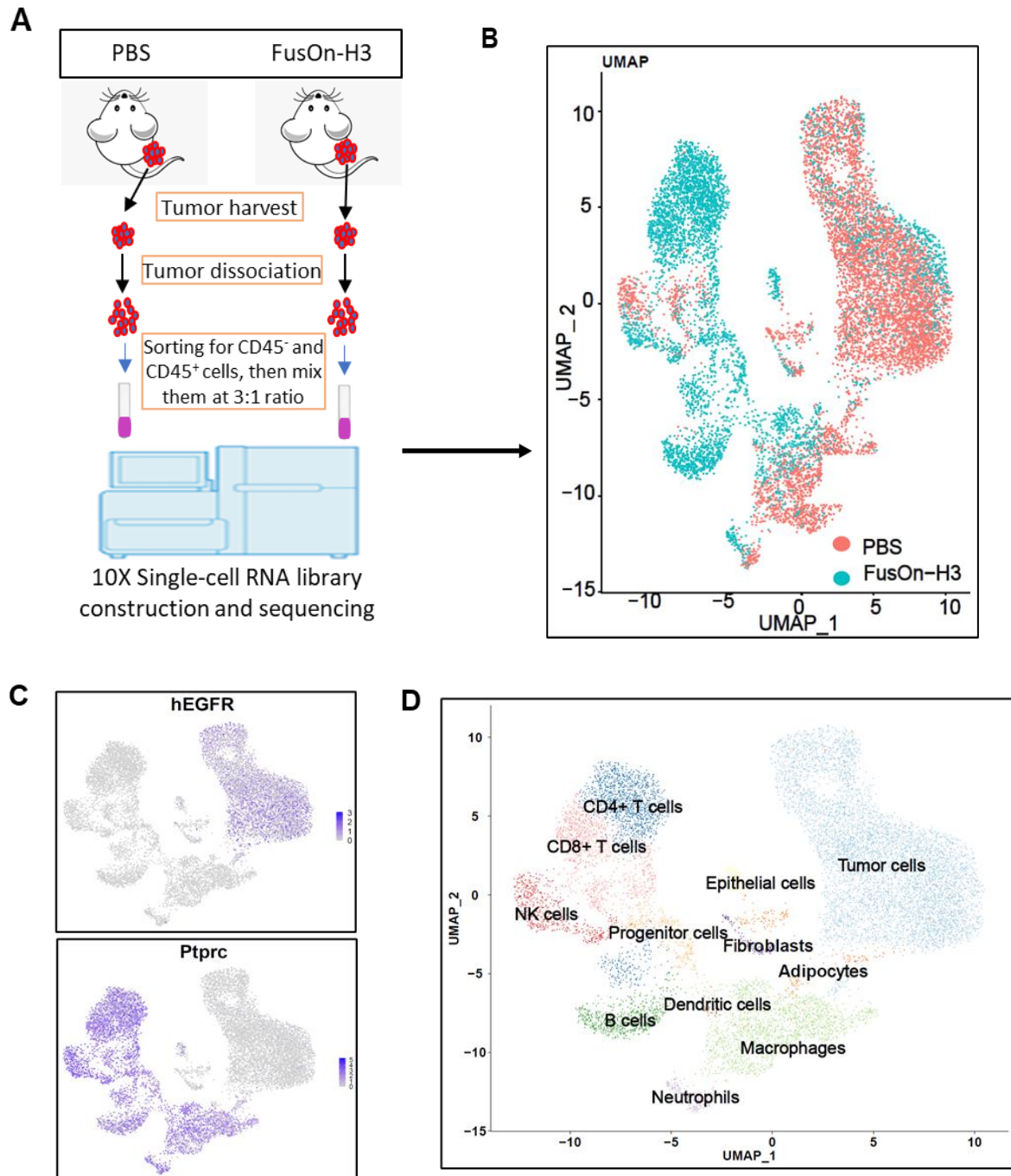


**Figure 2.1: scRNA-seq setup and data collection**

**A.** Single cell preparation and scRNA-seq. Tumors were explanted from three mice in each group at 48 h after receiving the indicated treatment. The pooled tumors were digested and dissociated into single cells, which were subsequently sorted into CD45<sup>-</sup>

and CD45<sup>+</sup> populations and then mixed at a 3:1 ratio for scRNA-seq using a 10X Genomics pipeline. **B.** Aggregated UMAP (Uniform Manifold Approximation and Projection) of total sequenced cells, with PBS group labeled red and FusOn-H3 group green. **C.** Classification of cells into immune cells (CD45<sup>+</sup>/*Ptprc*) and tumor cells (hEGFR<sup>+</sup>) based on *Ptprc* and *hEGFR* expression, respectively. **D.** UMAP plot showing the merged data of all the cell types annotated as per Monaco cell immune database.

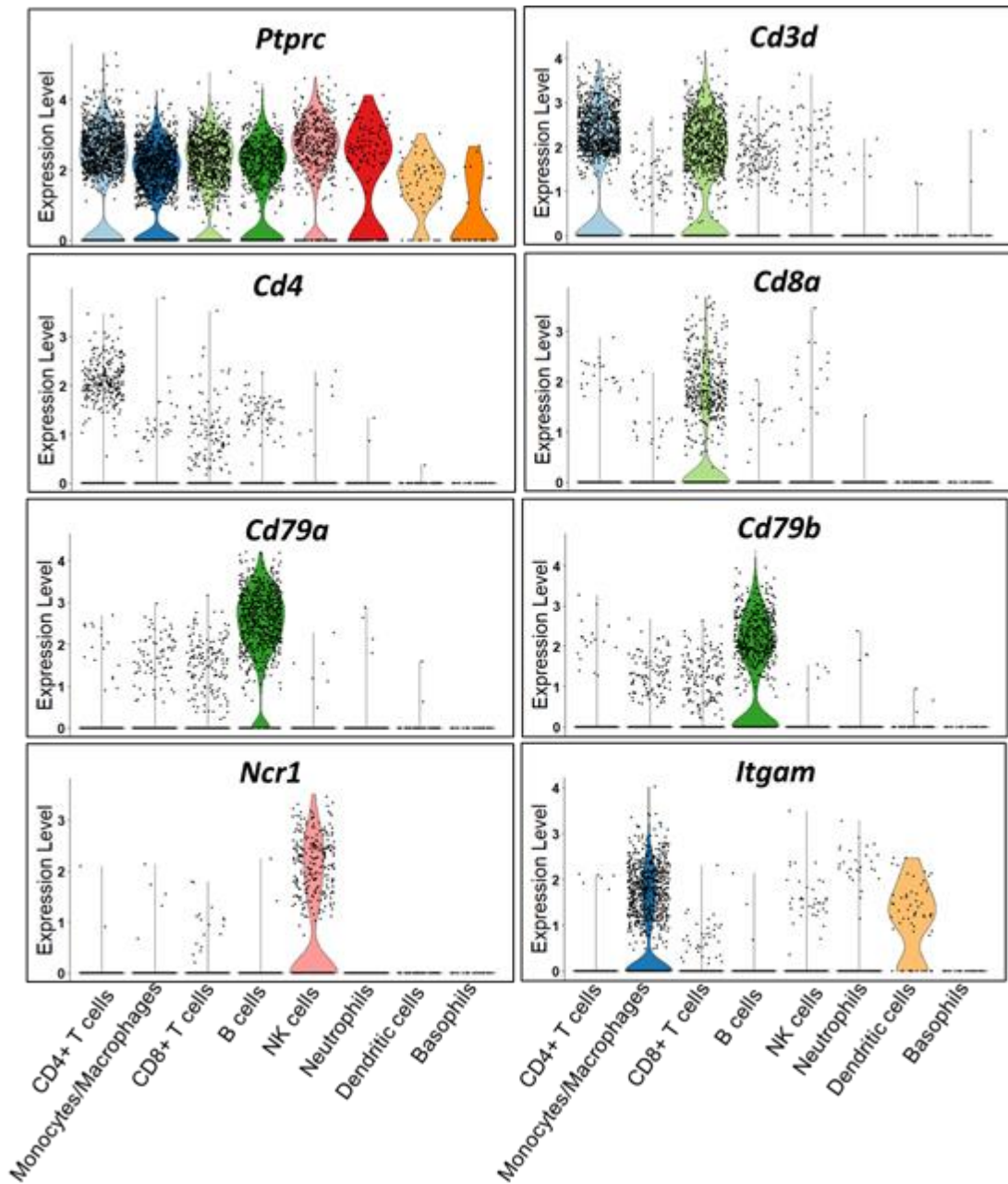


**Figure 2.2: Quantification of the signature genes of various immune cell subsets by scRNA-seq**

Violin plots showing the expression of *Ptprc*, *Cd3d*, *Cd4*, *Cd8a*, *Cd79a*, *Cd79b*, *Ncr1*, and *Itgam* genes within the stratified CD45<sup>+</sup> cell population. In a standard workflow on Seurat-v2, the expression level on y-axis in the violin plots represents the Log2

transformed value (readcount+1). A higher expression level represents more read count (or percentage, as it is scaled by total read count).

#### **2.4.2 The overall impact of FusOn-H3 virotherapy on the immune cell landscape in TME**

The cell clusters in **Figure 2.1D** were stratified into individual groups (PBS control and FusOn-H3 treatment) and the distribution of CD45<sup>+</sup> subpopulations in both groups are illustrated in **Figure 2.3A**. The UMAP of each subtype of these infiltrated immune cells in each group is shown in **Figure 2.3B**, and their relative composition is shown in **Figure 2.3C**. The data show that FusOn-H3 treatment has resulted in some significant changes in the relative composition of the immune cells. Notable among them is the significant increase in the relative composition of both CD4 and CD8 T cells in the FusOn-H3 treatment group, while the overwhelming majority of the infiltrated CD45<sup>+</sup> cells in the PBS group are monocytes/macrophages. Another cell subtype that also shows a significant increase following FusOn-H3 treatment is the B cell. Indeed, B cells were barely datable in the PBS group, but they presented as a significant portion of the infiltrated CD45<sup>+</sup> cells in the FusOn-H3 treated tumors (approx. 20%). In contrast, the composition of several cell subtypes showed a noticeable decrease during FusOn-H3 virotherapy. They include monocytes/macrophages, NK cells, dendritic cells, and neutrophils. However, considering that FusOn-H3-treated tumors showed more than 6-fold higher percentage of CD45<sup>+</sup> cells than in the PBS control group (3.03% vs. 0.49%, **Figure 2.4A**), the absolute number of the immune cells showing increased composition is even more profound. Even for those cells showing the decreased composition, the

absolute numbers of their presence in TME might be higher than in the PBS control group. Overall, the data suggest that FusOn-H3 virotherapy significantly changed the immune cell landscape in TME. It induced a vastly enhanced infiltration of CD45<sup>+</sup> cells, with a predominant increase on CD4<sup>+</sup>, CD8<sup>+</sup>, and B cells.

We conducted immunohistochemical staining on the same collected tumor tissues for the predominant immune cells identified in **Figure 2.3B**. Shown in **Figure 2.3D** are staining for CD3, CD4 and CD8 T cells. While the staining for CD3<sup>+</sup>, CD4<sup>+</sup>, and CD8<sup>+</sup> cells could be identified in the control tumors treated with PBS, there are significantly more of them in the FusOn-H3 treated tumors (**Figure 2.4D**). The CD20 staining (and CD19 staining in **Figure 2.4D**) showed the same trend. While CD20<sup>+</sup> (and CD19<sup>+</sup>) cells are largely undetectable in the control tumors, they were readily detected in tumors treated with FusOn-H3 (**Figure 2.3D** and **Figure 2.4B**). These immunohistochemical stainings thus provide corroborative support to the immune cell clustering as stratified in **Figure 2.4B**. We also conducted immunohistochemical staining for HSV antigens (**Figure 2.4C**), which showed clear positive staining only in tumors treated with FusOn-H3.

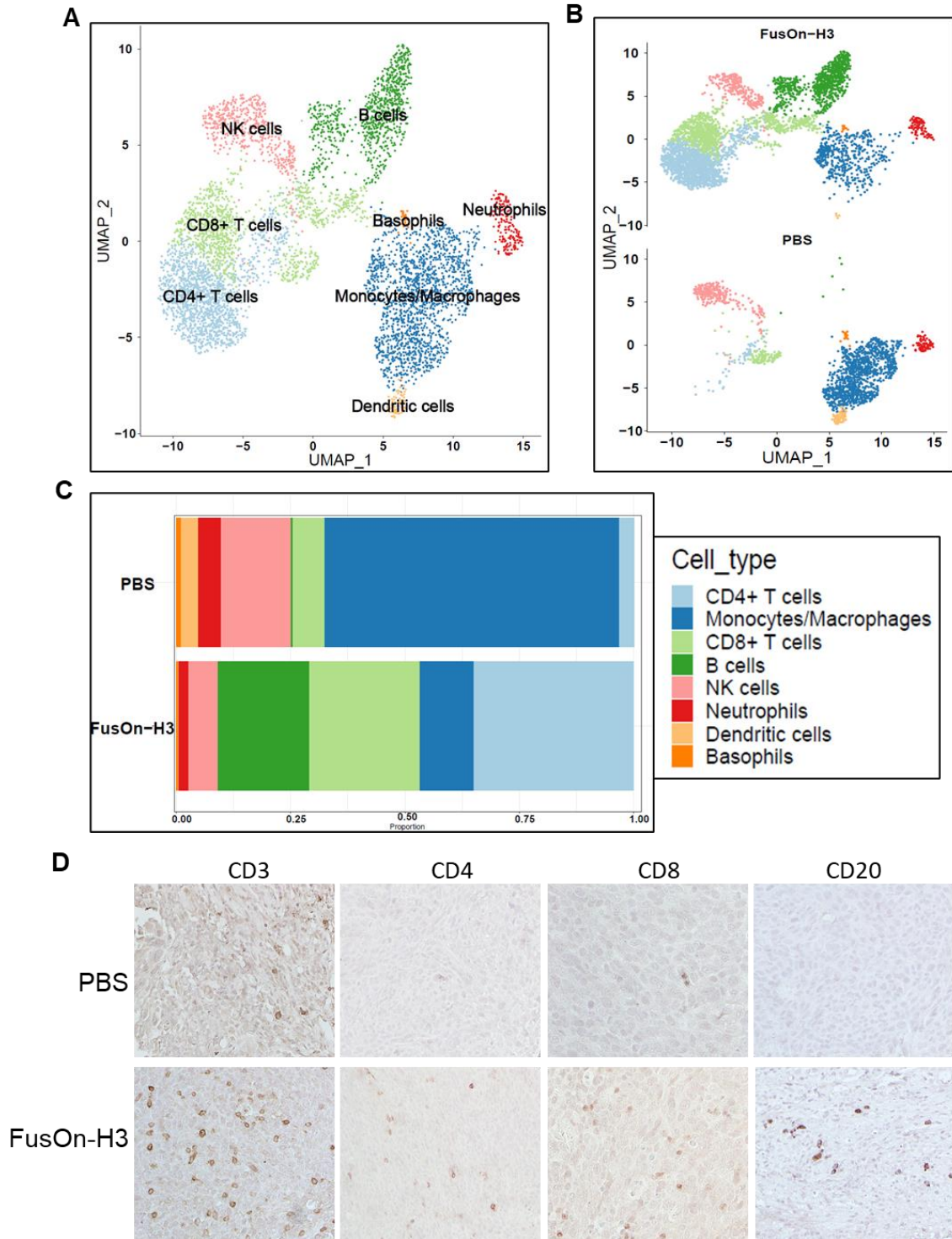


**Figure 2.3: Characterization of the composition of infiltrated immune cells via scRNA-seq data analysis and substantiation by IHC staining on the same tumor tissues after virotherapy**

**A.** UMAP plot showing the merged data of immune cells in TME. The CD45<sup>+</sup> cells were annotated into eight distinct sub-clusters. **B.** UMAP representation of the CD45<sup>+</sup> subsets stratified by the treatment group. **C.** The relative composition and proportion of CD45 sub-clusters within each treatment group. **D.** Immunohistochemical staining for the expression of CD3, CD4, CD8, and CD20 on sections of the same tumor tissues used for scRNA-seq. Original magnification: 20X.

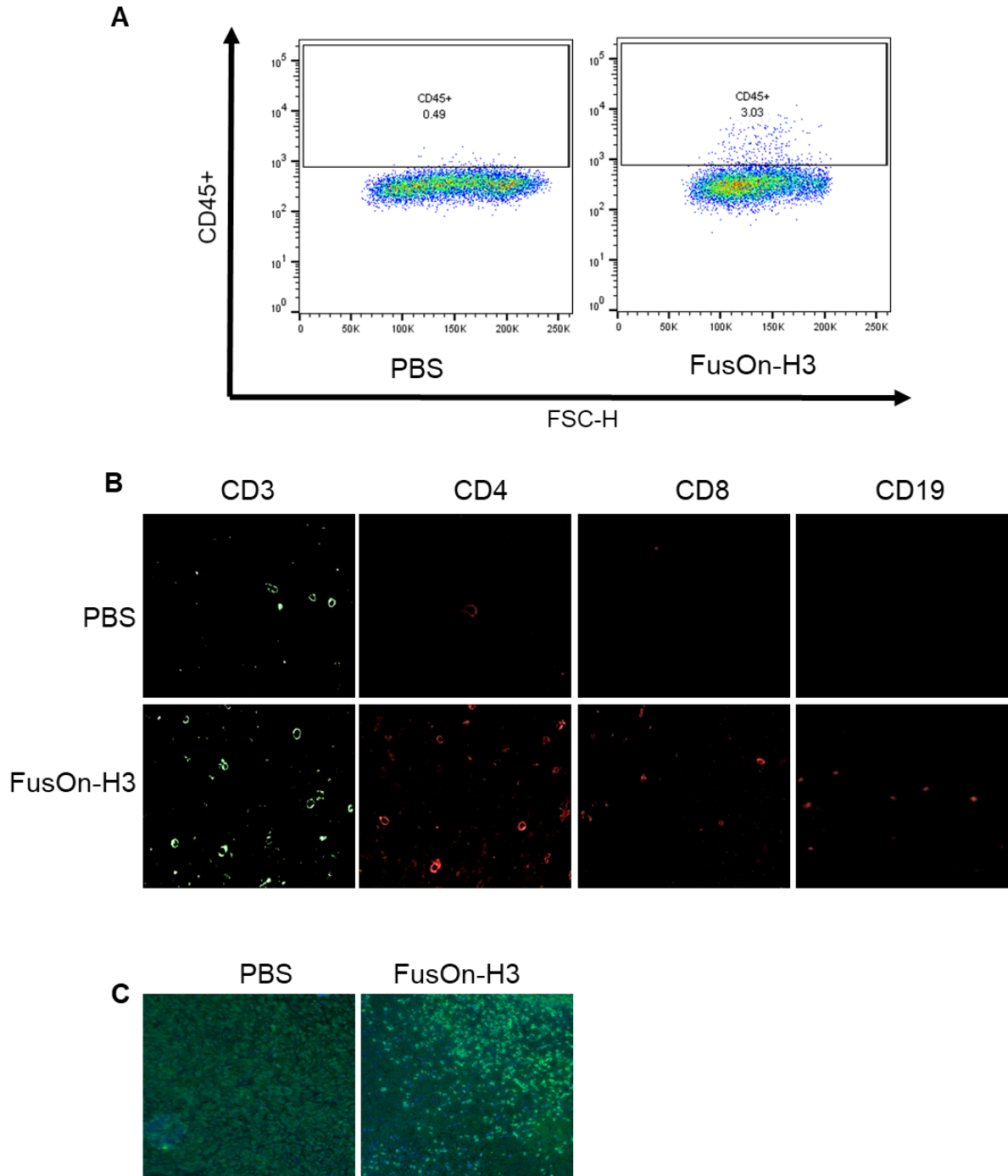


**Figure 2.4: CD45<sup>+</sup> cell sorting data on the single cell suspensions used for scRNA-seq expression and IHC staining on the same tumor tissues**

**A.** CD45<sup>+</sup> cell composition in the single cell suspensions of PBS and FusOn-H3 treated tumors, as revealed by flow cytometry analysis. **B.** Immunofluorescence staining for the expression of CD3 (green), CD4 (red), and CD19 (red) on tumor sections from the same tumor tissues used in **Figure 2.3D**. Original magnification: 20X. **C.** Immunohistochemical staining of HSV antigens (using a human anti-HSV polyclonal antibody as the first antibody and FITC-conjugated goat anti-human IgG as the second antibody) of tumor sections prepared as described in materials and methods. Original magnification: 40X

### **2.4.3 Comparison of subset composition of the infiltrated T cells between the PBS control and FusOn-H3 treatment groups**

To further characterize the infiltrated T cells and their activation status, we extracted the CD4 and CD8 T cells from the CD45<sup>+</sup> cluster from the UMAP plot shown in **Figure 2.3A** and conducted sub-clustering of T cells. Five distinct sub-clusters (naïve CD4<sup>+</sup> T cells, central memory CD8 T cells, Th17 cells, Th1 cells, and v $\delta$ 2  $\gamma\delta$  T cells) were identified (**Figure 2.5A**). These clusters were then stratified by treatment groups as illustrated in **Figure 2.5B**, and the relative composition of each sub-cluster is shown in **Figure 2.5C**. The sub-clustering analysis reveals that within the T cell population that had infiltrated to the FusOn-H3 treated TME, naïve CD4 and central memory CD8 T cells were the dominant cell subtypes. This revelation is in line with studies by Nakanishi et al., 2009 who showed that regional inoculation of HSV-2 could actively “pull” both naïve and virus-specific effector T cells towards the infected area. Another interesting revelation is the relatively high presence of Th1 cells in the FusOn-H3

treatment group, which are considered to be desirable for cancer immunotherapy. In contrast, the predominant T cell subtypes in the PBS group are  $v\delta 2 \gamma\delta$  T cells and Th17 cells, both of which have been reported to be highly represented in CT26 tumors. To further characterize these infiltrated T cells, we compiled the gene expression profile on the top 10 genes for each of the major T cell subsets shown in **Figure 2.5D**. Although some of these gene expression profiles displayed across all cell types due to the fact that they are either the discrete sub-population specific genes or continuous T cell development/activation genes, the intensity on the rest of these gene transcripts correlates reasonably well with the relative composition of these individual T cell subset. These gene profiling data thus support the validity of the T-cell subset clustering. We also stratified some of these gene expression profiles into treatment groups (**Figure 2.6**) and, in general, the results are in line with this conclusion.

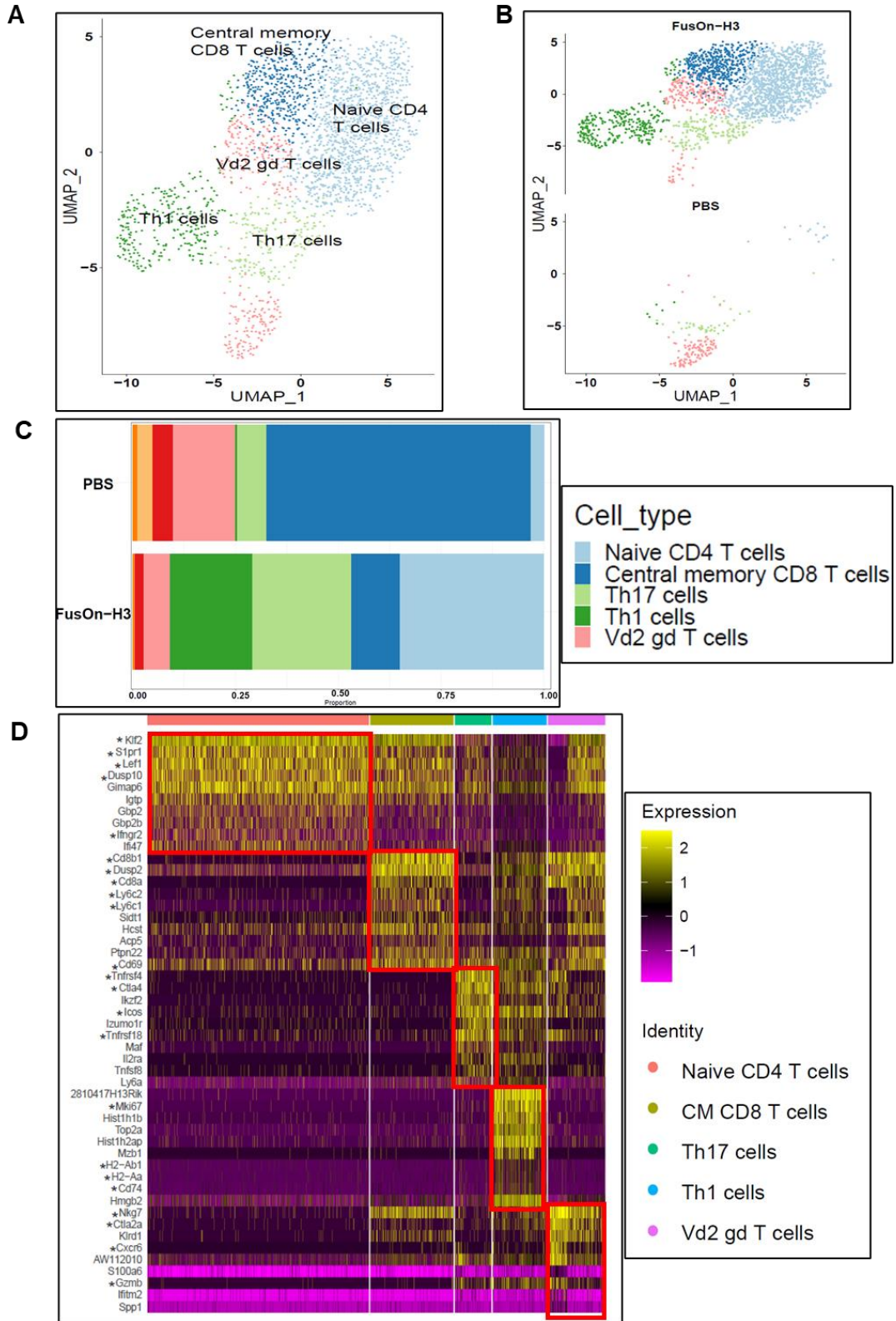
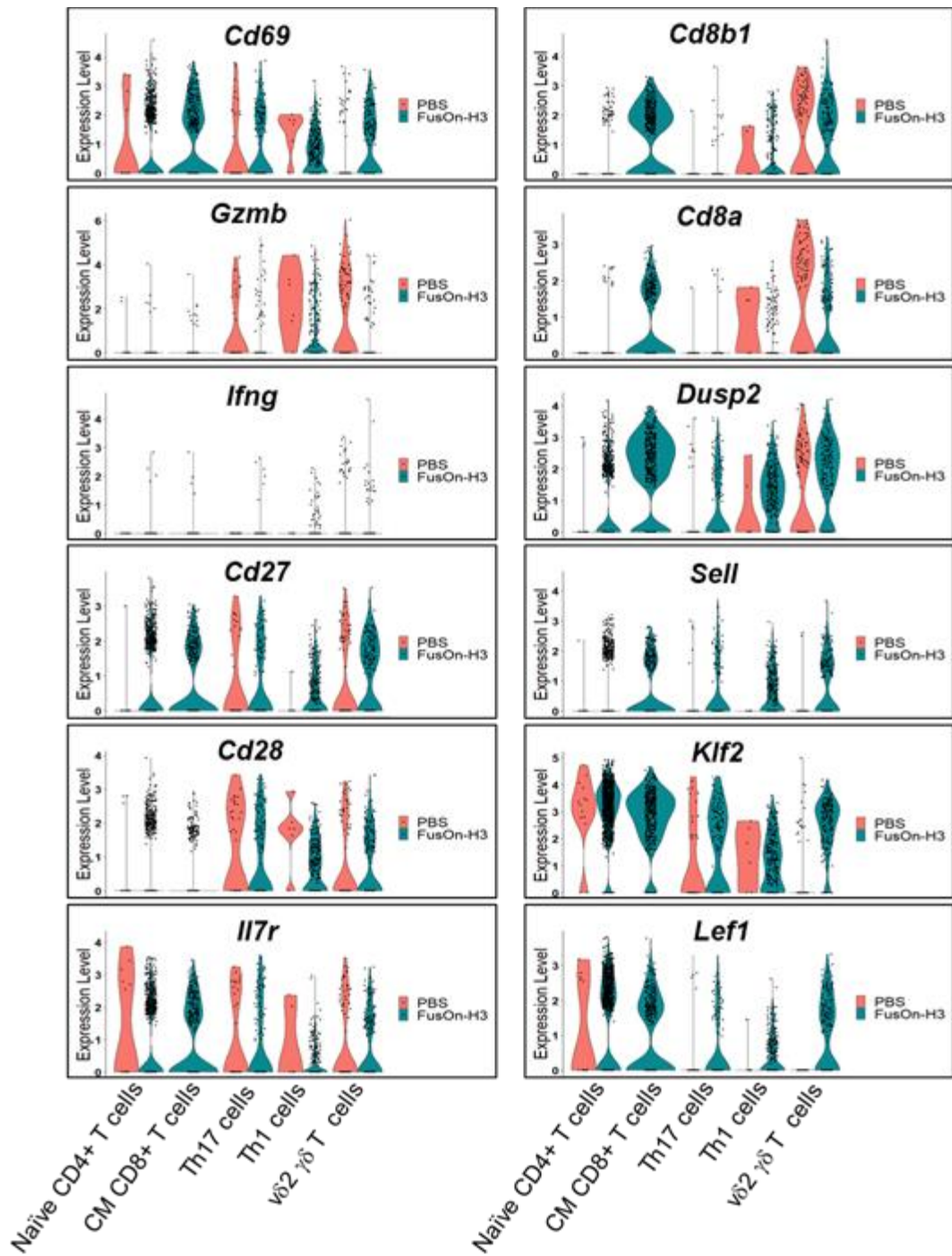


Figure 2.5

**Figure 2.5: Compositional and qualitative characterization of the infiltrated T lymphocytes in TME**

**A.** UMAP plots from merged data of the sub-clustered T cells annotated into five distinct T cell subclusters upon mapping the scRNA-data to Monaco Immune database. **B.** UMAP representation of the T cell subsets stratified by the treatment group. **C.** The relative composition and of T cell subclusters within each treatment group. **D.** Heat map displaying normalized expression level for the top expressed genes in each subcluster. The expression level is calculated based on their PCA (Principal Component Analysis) scores derived from the expression of the integrated most variable gene, with each PC essentially representing a “metagene” that combines the information across a correlated gene set.



**Figure 2.6: Quantification of some key genes in the T cell sub-clusters**

A. Violin plots showing the expression of *Cd69*, *GZMB*, *Ifng*, *Cd27*, *Cd28*, *Il7r*, *Cd8b1*, *Cd8a*, *Dusp2*, *Sell*, *Klf2*, and *Lef1* genes within Naïve CD4<sup>+</sup> T cells, CM CD8<sup>+</sup> T cells,

Th17 cells, Th1 cells and  $v\delta 2 \gamma\delta$  T cell clusters and further stratified as per the treatment group (PBS or FusOn-H3). In a standard workflow on Seurat-v2, the expression level on y-axis in the violin plots represents the Log2 transformed value (readcount+1). A higher expression level represents more read count (or percentage, as it is scaled by total read count).

#### **2.4.4 Further characterization on the infiltrated B cells following FusOn-H3 virotherapy**

One of the distinct findings shown in **Figure 2.3B** is the significant increase of B cell infiltration in TME from FusOn-H3 treatment. Recent studies have suggested that an increased presence of B cells in tumors is a unique biomarker for immunotherapies such as ICIs. For example, gene expression profile studies in 608 patients with sarcoma showed that B cell infiltration in TME are the strongest prognostic factor for improved survival and a high response rate to PD1 blockade with pembrolizumab in a phase 2 clinical trial, regardless if the patients had high or low CD8<sup>+</sup> T cells and cytotoxic contents. Studies by Helmink et al., 2020 and Cabrita et al., 2020 have reached an identical conclusion in patients with melanoma, and the increased B cell infiltration is predominately through tertiary lymphoid structures.<sup>192</sup> Preclinical studies in a high mutation burden mouse model of breast cancer have also shown that B cells and T follicular helper cells played a major role in a positive response to ICIs.<sup>193</sup> In particular, in the studies by Helmink et al., 2020 they performed bulk RNA sequencing to profile B cell markers that were the most differentially expressed genes in the tumors of responders versus non-responders.<sup>192</sup>

To further characterize the infiltrated B cells, we first plotted the total B cell cluster as well as its stratification based on treatment groups (**Figure 2.7A**). The plots show that, while B cells were detected only sparsely in the TME of the PBS control group (just 6 B cells), they were abundantly detected in the tumors treated with FusOn-H3 (788 B cells). This represents a more than 130-fold increase in B cell infiltration following FusOn-H3 treatment. Considering that FusOn-H3-treated tumors showed more than 6-fold higher percentage of CD45<sup>+</sup> cells than in the PBS control group, this difference is even more significant. The identity of the infiltrated B cells in the FusOn-H3 treated tumors was further confirmed by the overlapping plotting with the expression profile of 4 important genes associated with B cells (**Figure 2.7B**). Among them, CD79A and CD79B form part of the B cell receptor (BCR) complex while CD19 and CD20 are signature biomarkers for B cells. The property of these infiltrated B cells was further characterized by analyzing the gene expression profile of another four genes that control several aspects of B cell functions including their homing/ migration (CXCR4), development (PAX5), co-receptor formation (CD2), and B-cell receptor-induced calcium mobilization (BANK1). All these genes showed enhanced expression in these B cells (**Figure 2.7C**), indicating their full functionality in the infiltrated TME.

Studies by Helmink et al., 2020 have shown that the infiltrated B cells with either memory or plasma cell property are closely related to a favorable response to ICIs and could function as a biomarker for this immunotherapy.<sup>192</sup> Hence, we further characterized the infiltrated B cells in the TME treated with FusOn-H3 by clustering them into subsets. Indeed, memory and plasma B cells account for more than 50% of the total infiltrated B cells in the tumor treated with FusOn-H3 (**Figure 2.7D**). These

data suggest that this resulting change on the immune landscape triggered by FusOn-H3 virotherapy may create a particularly favorable TME for combinational treatment with ICIs, which is currently being tested on several clinical trials.<sup>124</sup>

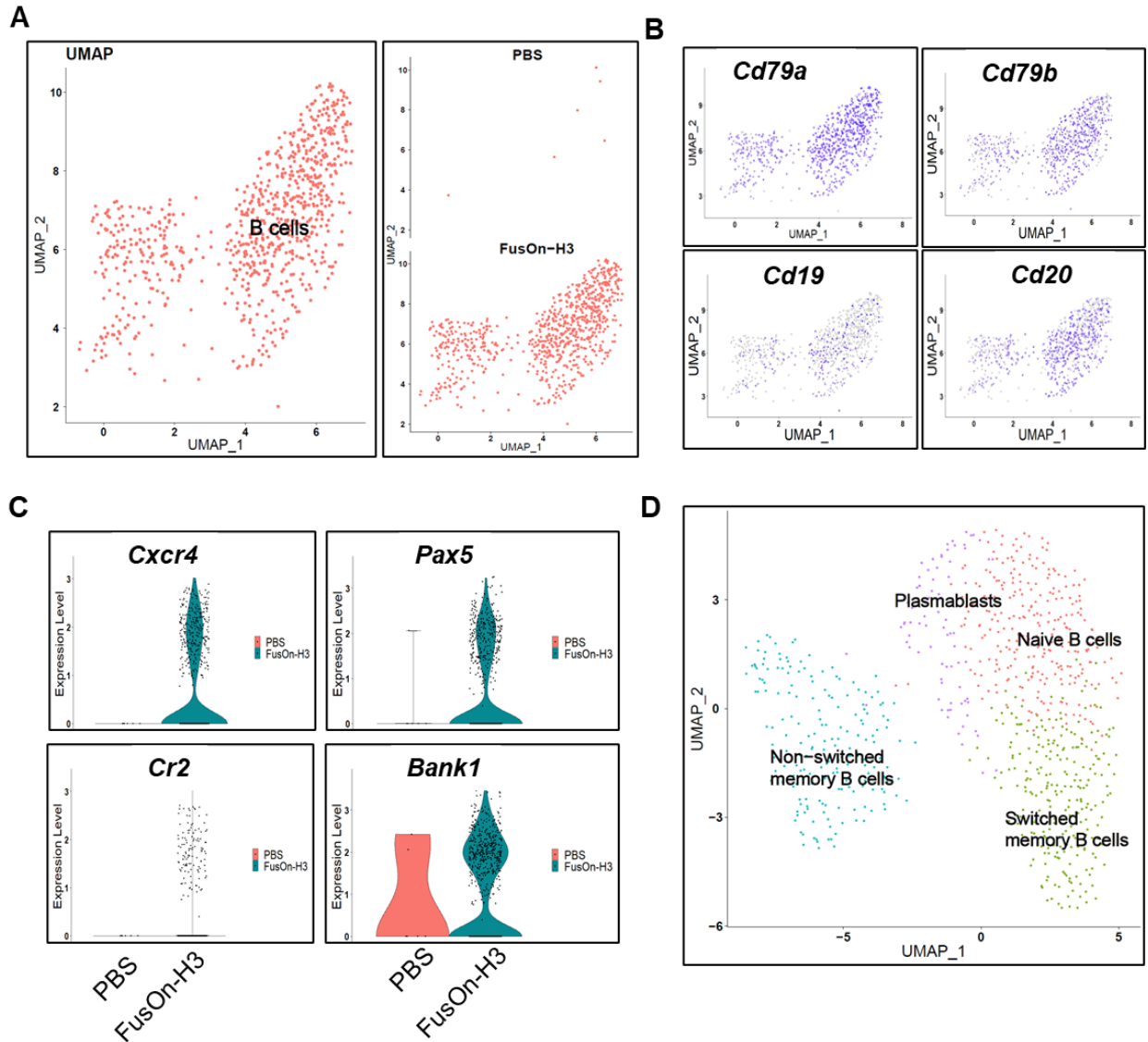


**Figure 2.7: FusOn-H3 induces significant infiltration of B cells to the TME**

**A.** UMAP plot representing the B cell cluster. The left panel shows the merged plot and the right panel showed the stratified plot (with the PBS control group at the top and the

FusOn-H3 treated group at the bottom). **B.** Feature plots showing the expression of key B cell genes (*Cd79a*, *Cd79b*, *Cd19*, and *Cd20*) **C.** Violin plots showing the expression of B cell activation genes *Cxcr4*, *Pax5*, *Cr2*, and *Bank1* within the B cell cluster stratified as per treatment group. In a standard workflow on Seurat-v2, the expression level on y-axis in the violin plots represents the Log2 transformed value (readcount+1). A higher expression level represents more read count (or percentage, as it is scaled by total read count). **D.** UMAP plot with annotated B cell sub-clusters in the FusOn-H3 treated group, including Naïve B cells, plasmablasts, non-switched memory B cells and switched memory B cells.

#### **2.4.5 Changes in the infiltration of other immune cells induced by FusOn-H3 virotherapy**

The NK cell cluster was plotted in **Figure 2.8A**, which was further stratified into treatment groups (**Figure 2.8B**). Although the plots showed that the number of the infiltrated NK cells in the FusOn-H3 treatment group is only slightly higher than in the PBS control group (251 vs. 245), the actual number of the infiltrated NK cells in the former should be significantly higher if taking into consideration that FusOn-H3-treated tumors showed more than 6-fold higher percentage of CD45<sup>+</sup> cells than in the PBS control group. The functional status of the infiltrated NK cells was evaluated by examining the expression profile of 6 genes whose expressions are the indicators for NK cell cytotoxicity (*Prfl* gene for perforin and *Gzmb* gene for granzyme B), activation (*CD69* and *Ifng* gene for interferon- $\gamma$ ), and the NKG2D-DAP10 activation receptor (*Klrk1* and *Hcst* genes) that signals to induce cytotoxicity and cytokine production in

NK cells. The results in **Figure 2.8C** showed that all these genes are expressed at a higher level in NK cells from FusOn-H3-treated tumors than in the tumors of PBS control. Thus, FusOn-H3 virotherapy not only enhanced the migration of NK cells to the tumor site but also led to their activation.

The data in **Figure 2.9A** showed that the composition of myeloid cell infiltration in tumors treated with FusOn-H3 is approximately 1/5 of that in the PBS control tumors. Considering the 6-fold difference of CD45<sup>+</sup> cells between these two groups, the FusOn-H3 treatment did not significantly increase the actual number of myeloid cells. To further analyze these infiltrated myeloid cells, we sub-clustered the myeloid cells using the SingleR Monaco immune cell reference and distinguished them into five sub-clusters: macrophage/monocytes, dendritic cells, neutrophils, progenitor cells, and Basophils (**Figure 2.9A**). Monocytes/macrophages represented the largest proportion of these infiltrated myeloid cells (**Figure 2.9C**). We then further characterized the macrophage/monocyte cluster by comparing for expression profile of signature genes for either M1 and M2 and the results are shown in **Figure 2.9D**(for M1 genes) and **Figure 2.9E** (for M2 genes), respectively. The data showed that, while the M1 genes are expressed in roughly the same level between myeloid cells of either the control or the FusOn-H3 treated tumors, the M2 gene expression is lower in the latter. Together, these data suggest that FusOn-H3 treatment did not significantly change the total number of myeloid cells in the TME, but the presence of the virus tilted the subpopulation of monocyte/macrophage towards M1 phenotype that is considered to be more favorable for the function of cancer-specific immune cells.

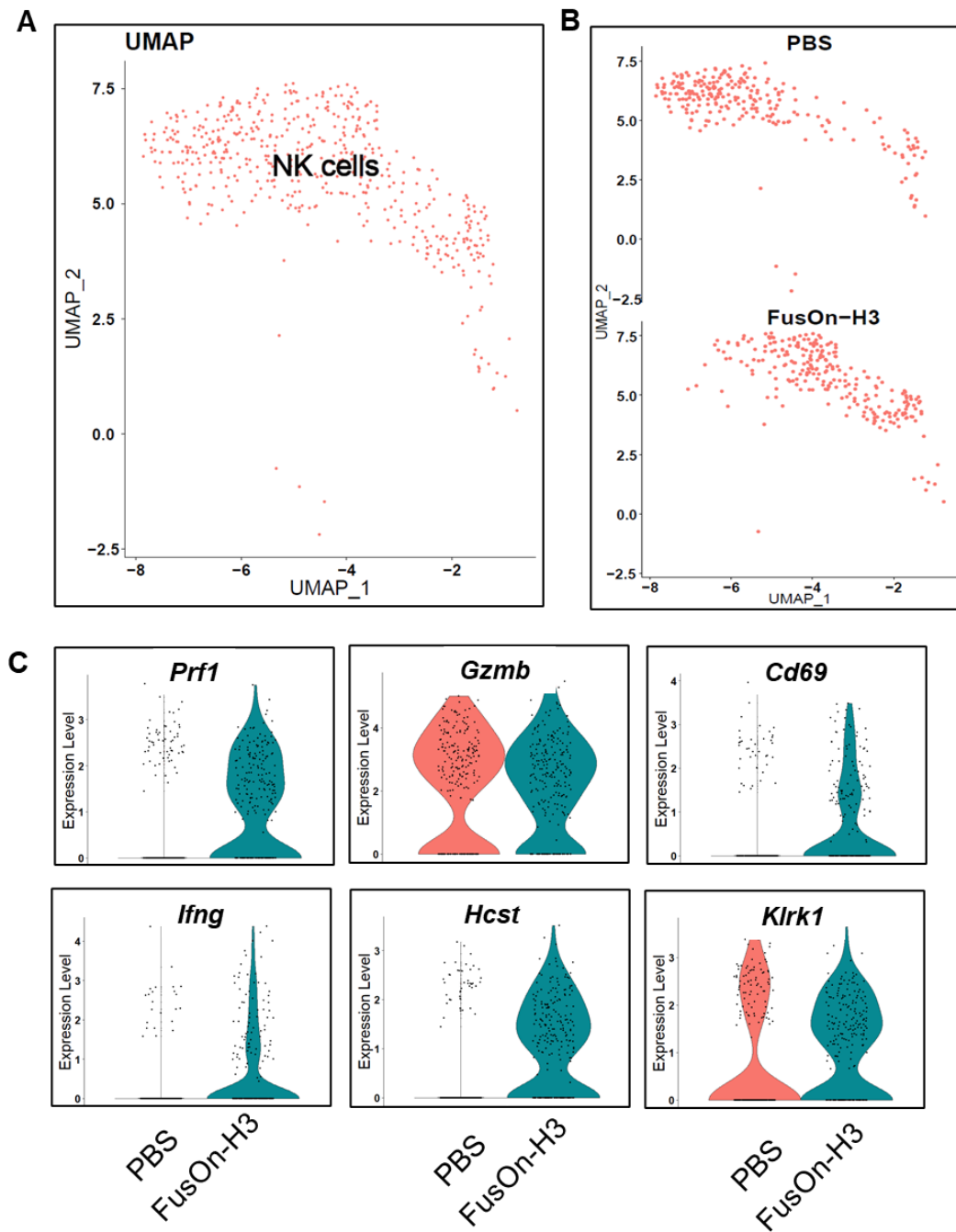


**Figure 2.8: NK cell infiltration and activation status upon FusOn-H3 treatment**

**A.** UMAP plot representing the merged data of the NK cell population. **B.** UMAP plot showing NK cell clusters stratified as per treatment group (Top panel: PBS; bottom panel: FusOn-H3). **C.** Violin plots showing the comparison of expression of key NK

cell activation genes (*Prf1*, *GZMB*, *Cd69*, *Ifng*, *Hcst*, and *Klrk1*) between the PBS and the FusOn-H3 treated group. In a standard workflow on Seurat-v2, the expression level on y-axis in the violin plots represents the Log2 transformed value (readcount+1). A higher expression level represents more read count (or percentage, as it is scaled by total read count).

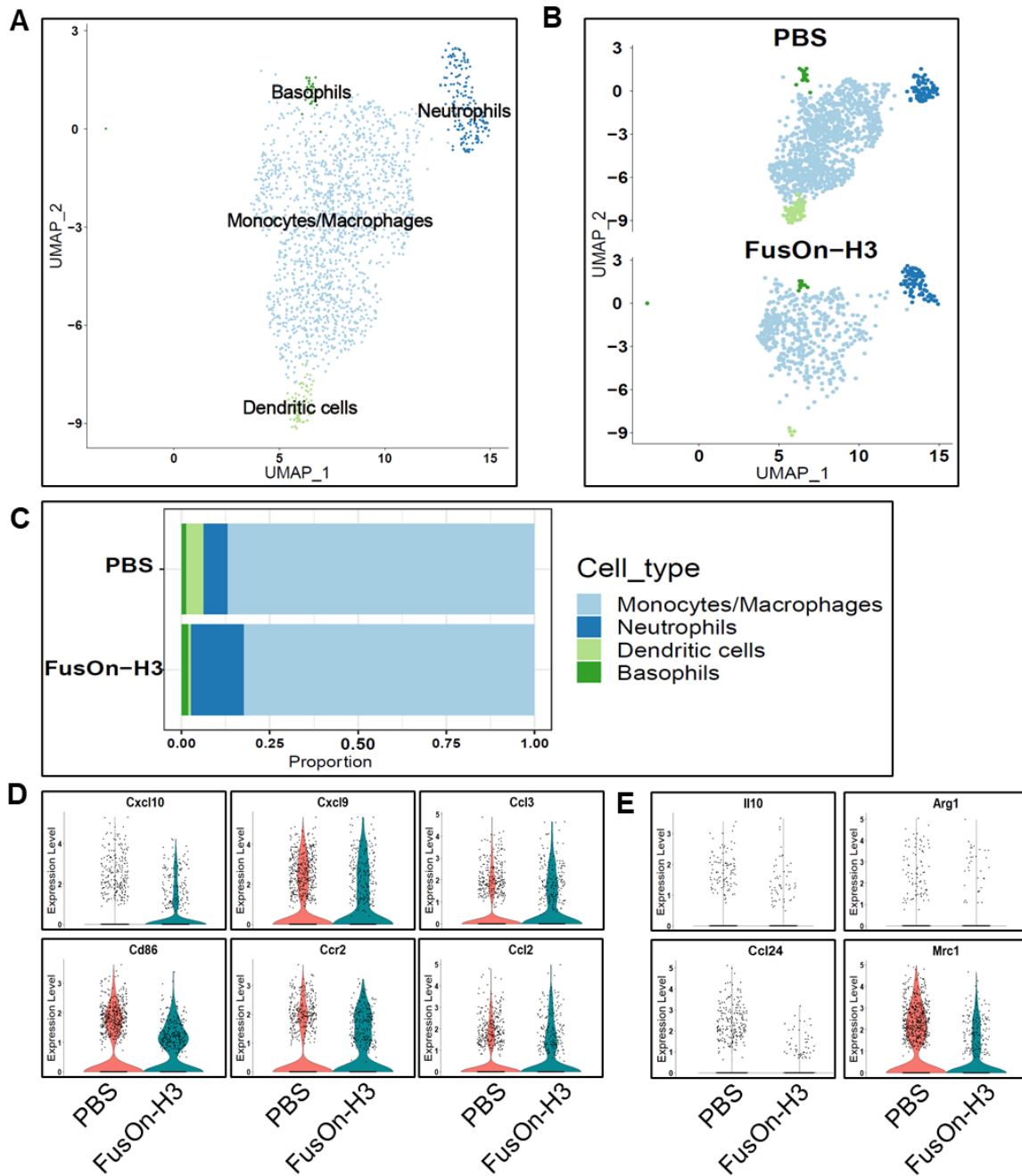


**Figure 2.9: Other innate immune cell infiltration and activation status upon FusOn-H3 treatment**

**A.** Merged UMAP plot showing four cell clusters of other innate immune cells, including monocytes/macrophages, neutrophils, basophils, and dendritic cells. **B.**

Stratified UMAP plot showing the same innate immune cells (Top panel: PBS; bottom panel: FusOn-H3). **C.** The relative composition of these innate immune cells in each treatment group. **D** and **E.** Violin plots showing the comparative expression of key M1 type macrophage genes (*Cxcl10*, *Cxcl9*, *Ccl3*, *Cd86*, *Ccr2*, and *Ccl2*) and M2 type macrophage genes (*Il10*, *Arg1*, *Ccl24*, and *Mrc1*) within this cell cluster stratified by the treatment group. In a standard workflow on Seurat-v2, the expression level on y-axis in the violin plots represents the Log2 transformed value (readcount+1). A higher expression level represents more read count (or percentage, as it is scaled by total read count).

#### **2.4.6 Complex immune landscape change in the TME following FusOn-H3 virotherapy predicted by interactions among the infiltrated immune cells**

The data presented so far have indicated that FusOn-H3 treatment induced a significant change on the immune cell landscape in TME, in both the composition of immune cell subsets and the activation status. It is expected that these changes can result in the alteration of the complex intercellular communication networks among these immune cells. Recently, Jin et al., 2021 have reported a CellChat program that quantitatively networks the intercellular communication through methods abstracted from graph theory, pattern recognition, and manifold learning.<sup>194</sup> CellChat predicts how cells work together to coordinate activities and the ability of the cells to perceive and respond correctly to their tumor microenvironment and how these may be relevant to the generation of antitumor immunity. We used CellChat prediction to compare the number of interactions and the interaction strength among different cell populations in PBS and

FusOn-H3 treatment groups (**Figure 2.10A**). The analysis shows a more than 2-fold increase in the total number of interactions and a significant increase in the interaction strength in the FusOn-H3 treatment group over the PBS control. The predicted interaction details among the immune cells are elaborated in **Figure 2.10B**, from which it is inferred that cells in the FusOH3 treatment group generally displayed a higher level of connectivity and an increased number of interactions between various cell types. In particular, immune cells including B cells, CD4<sup>+</sup> T cells, CD8<sup>+</sup> T cells, dendritic cells, and macrophages interacted within themselves and also with the non-immune cells. In contrast, the interactions and the interaction strength were more limited in the PBS group, with the B cell cluster distinctly disconnected from the rest of the clusters. The intensive interaction between the innate and adaptive immune cells in the FusOn-H3 treatment group shown in **Figure 2.10B** is interesting as it is known that, in order to generate an effective immunity against infection and malignancy, these two immune components need to act together in concert.<sup>195</sup>, [Brücher, 2014 #269}

Next, we compiled the information flow (i.e., the overall communication probability across the two datasets, PBS vs. FusOn-H3). This predicts the information flow for a given signaling pathway that is defined by the sum of communication probability among all pairs of cell groups in the inferred network.<sup>194</sup> Intriguingly, 47 out of 77 pathways are highly active, albeit at different levels, in the FusOn treated group (**Figure 2.11**). Among those pathways showing significantly enhanced information flow upon FusOn treatment as compared to PBS is MIF (macrophage migration inhibitory factor) (**Figure 2.10C**), which is expressed by myeloid and lymphocyte cells in response to stress or infection. MIF is a pro-inflammatory cytokine and it plays a crucial role as a regulator

of innate and acquired immunity. Indeed, the information flow maps in **Figure 2.10D** show that it acts heavily through CD4<sup>+</sup>, CD8<sup>+</sup> T cells and B cells as senders during FusOn-H3 virotherapy to impact additional innate and adaptive immune cells in the TME (**Figure 2.10D**). The heatmap in **Figure 2.10E** illustrates the details of the predicted information flow among the individual cellular components in the TME during FusOn-H3 virotherapy.

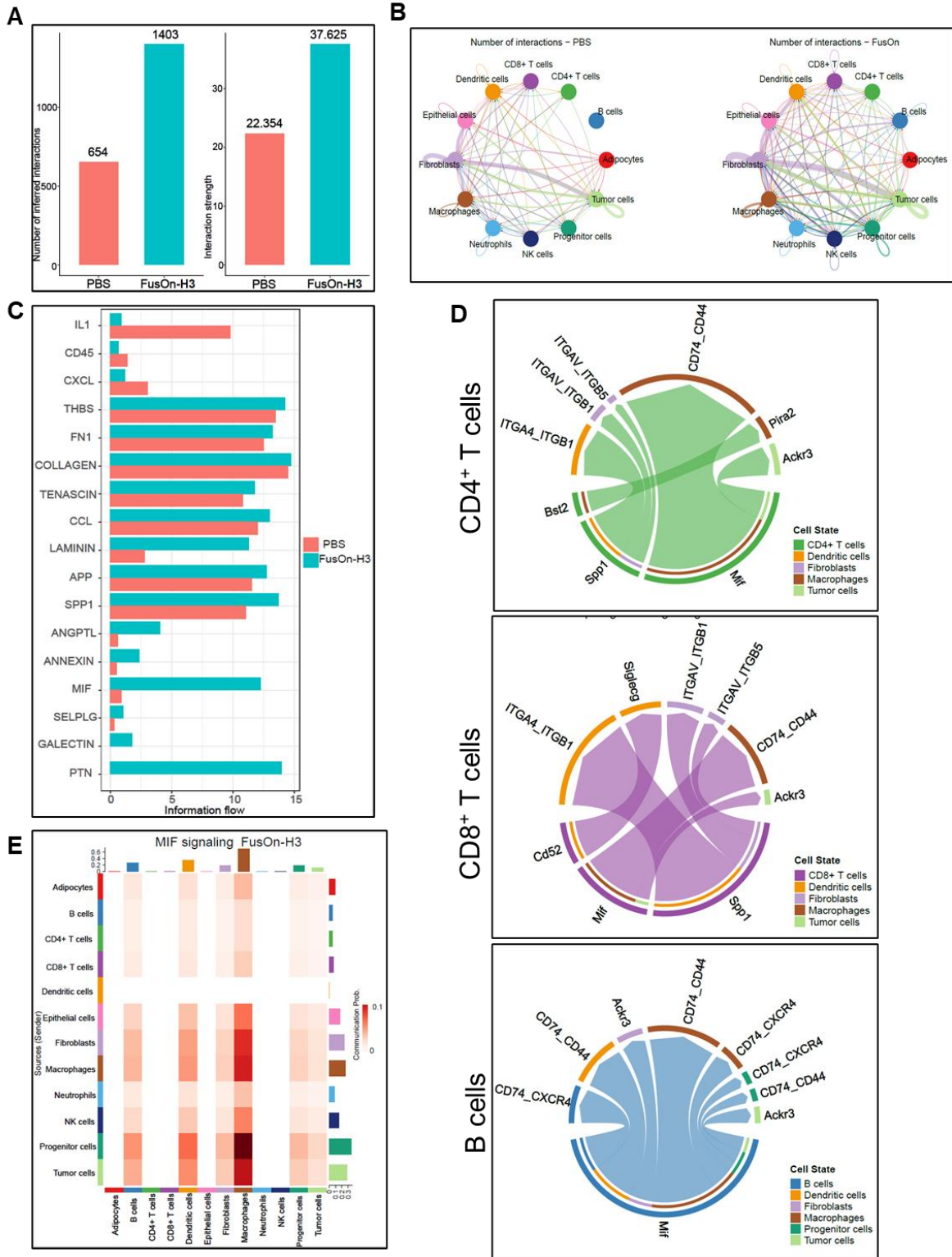
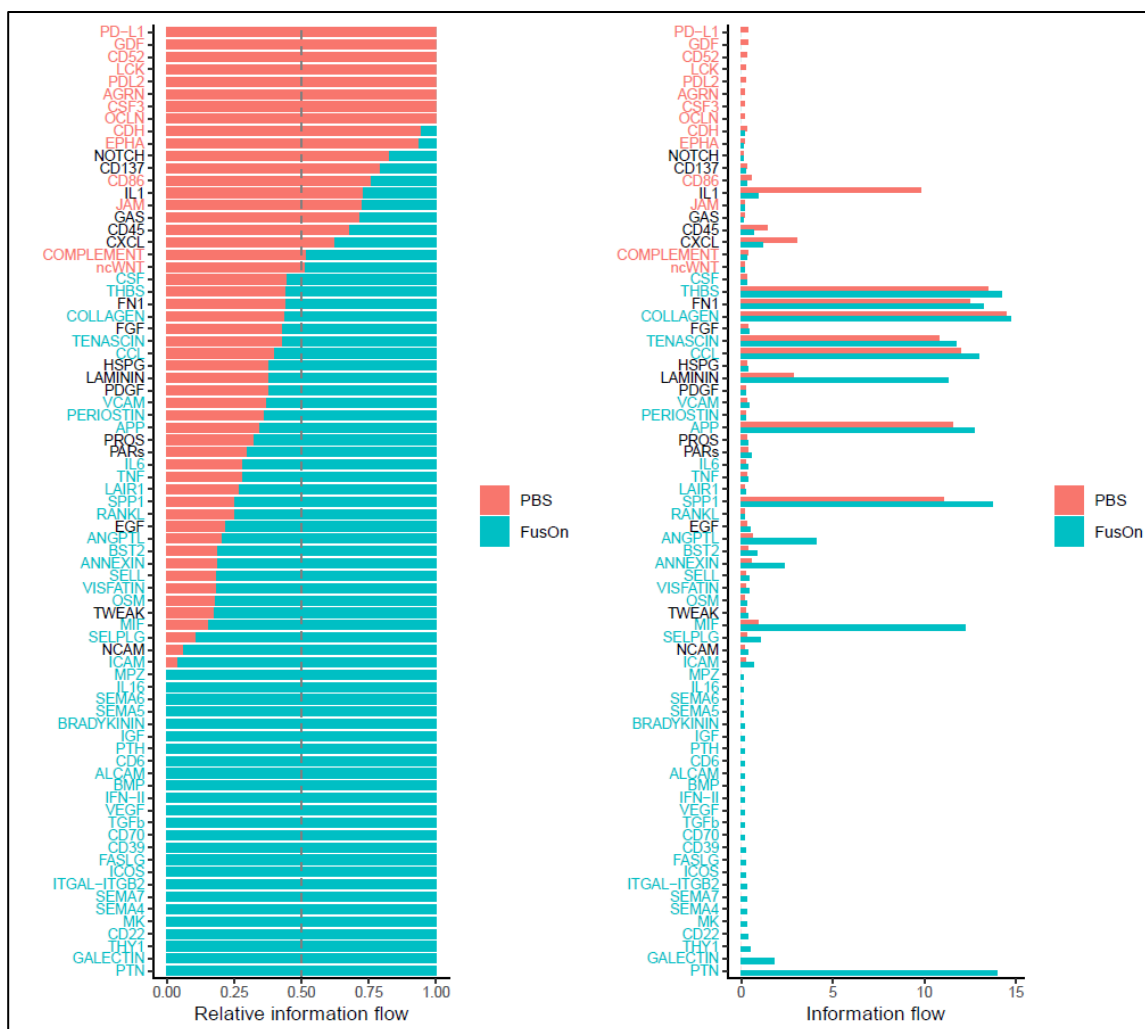


Figure 2.10

**Figure 2.10: Cell-to-cell communications among the infiltrated immune cells in the TME predicted by the CellChat software**

**A.** Bar plot showing the total number of interactions and interaction strength of the inferred cell-cell communication networks from PBS and FusOn-H3 treated groups. **B.** Circle plot summarizing the maximum number of interactions among individual cell types in each treated group. The thickness of the lines connecting cells indicates the interaction strength. **C.** Selected signaling pathway networks that are strongly active in either group based on the differences of overall information flow as predicted by CellChat. The overall information flow of a signaling network is calculated by summarizing all the communication probabilities in that network. **D.** Summary chord plots showing the interactions; from CD4+ T cells, CD8+ T cells and B cells as senders via ligand-receptor pair (Mif- (Cd74\_Cd44) to Macrophages contributing to the overall communication network of MIF signaling pathway. **E.** Heatmap showing the relative contribution of each cell group based on the computed four network centrality measures of MIF signaling network.



**Figure 2.11: Comparison of the overall information flow/interaction strength of each signaling pathway within the inferred network**

The bar graph representing significant signaling pathways ranked based on the differences in the overall information flow within the inferred networks between PBS and FusOn-H3 treated groups. The top signaling pathways in red are enriched in PBS, and those in green were enriched in the FusOn-H3 treated group.

## 2.5 Discussion

It is becoming increasingly clear that, in addition to directly lyse tumor cells, oncolytic viruses can significantly change the immune cell landscape in TME during virotherapy. Studies on preclinical models and on tumor samples collected from clinical patients following virotherapy have shown that intratumoral administration of oncolytic viruses can attract the migration of important immune cells such as T cells and NK cells to the tumor site,<sup>29</sup> which converts “cold” tumors into hot ones. However, these studies on characterizing the infiltrated immune cells during virotherapy are largely fragmented, as they were designed to focus on a certain population of immune cells. Herein we report our studies using scRNA-seq to comprehensively characterize immune cell landscape during a HSV-based oncolytic virotherapy. Our data reveal that the virotherapy induced a significant change in both the number and composition of immune cells in TME in a clear pattern of favoring the therapeutic benefit of antitumor immunity. First of all, FusOn-H3 virotherapy induced a 6-fold increase in the infiltration of CD45<sup>+</sup> leukocytes as compared to the control group. Second, the composition of the infiltrated immune cells is quite different between the control and the treatment groups, with CD4, CD8, and B cells as the dominant ones in the FusOn-H3 treated tumors, in contrast to the overwhelming presence of monocytes/macrophages in the control group. Third, despite the overall increased infiltration of the CD45<sup>+</sup> cell infiltration following FusOn-H3 virotherapy, the composition of the myeloid cells, especially monocytes/macrophages, is similar to that in the control tumor. Moreover, the macrophages in the FusOn-H3 treated tumors are mostly M1 phenotype as compared to the control tumor.

In one of our previous studies, we showed that this same virotherapy could attract the migration of adoptively transferred tumor-specific T cells of both CD4 and CD8 subsets to the tumor site,<sup>29</sup> a result that was reproduced by this scRNA-seq analysis. At that study, we also analyzed the chemokine profile within the TME after virotherapy. This virotherapy induced the production of several chemokines in addition to CXCL9, CXCL10, and CXCL11 that have been shown to play a role in mediating the T cell homing to the site of HSV-2 infection.<sup>196</sup> These increased chemokines induced by FusOn-H3 virotherapy include CCL2, CCL3, CCL4, and CXCL1. At times, we were puzzled by the changes of these chemokines. Our data showing a dramatic increase in B cell infiltration after FusOn-H3 virotherapy may explain the source of the increased CCL3 and CCL4 expression, as B cells and their activation are known to result in the secretion of these two chemokines. The increased CCL-2 secretion in the TME following FusOn-H3 treatment may explain the M1 macrophage polarization as seen in this study, as such an effect has been reported in the literature.<sup>177</sup> Using the most recently developed CellChat software, we further analyzed the predicted interactions of the infiltrated immune cells following FusOn-H3 virotherapy. It seems that the enhanced interactions among the infiltrated immune cells, partly prompted by MIF, might have further shaped the immune landscape in TME, particularly on the activation and functional status of the immune cells.

While this manuscript was in preparation, Ramelyte et al., 2021 published their analysis of scRNA-seq on cutaneous B lymphoma samples collected by fine-needle aspiration following intratumor injection of T-VEC in three patients.<sup>197</sup> Their results show that T-VEC virotherapy induced a significant increase in the number of CD4+ and CD8+ T

cells, NK cells, and monocytes in the tumor lesions. While our data are largely consistent with these observations, our studies went further to analyze the subsets and the functional status of the infiltrated T cells, NK cells, and myeloid cells. For T cells, FusOn-H3 virotherapy induced infiltration of mainly naïve CD4 cells, central memory CD8 T cells and Th1 cells. Although FusOn-H3 did not significantly induce the infiltration of monocytes/macrophages, the virotherapy impacted these myeloid cells by driving them toward M1 polarization. These are considered as overall in favor of cancer immunotherapy, especially in combination with ICIs.

However, one key difference is on B cells. While our data showed a dramatic increase in B cell infiltration following FusOn-H3 treatment, the scRNA-seq data from the studies by Ramelyte et al., 2021 demonstrate that the number of B cells decreased in all subsequent FNA samples of the injected lesions. Recent studies have suggested that an increased presence of B cells in tumors is an important biomarker for a favorable therapy response to immunotherapies such as ICIs. As such, FusOn-H3 virotherapy is able to induce additional change on the immune cell landscape in TME that further favors the therapeutic outcome of antitumor immunity. The differential effect on inducing B cell infiltration between the two different virotherapy is probably due to the fact that T-VEC and FusOn-H3 are based on different serotypes of HSV – T-VEC is a HSV-1 based oncolytic virus while FusOn-H3 is constructed from HSV-2. Although HSV-1 and HSV-2 genomes share extensive homology (approximately 50%) and many of the genes are co-linear, there are also substantial differences between these two viruses. It has been reported that, in HSV-2-exposed mice, B cells infiltrate into the infected mucosa area. Regardless of the mechanism, the vastly increased B cell infiltration seems to be unique

for the HSV-2 based FusOn-H3 and this may make it more suitable for combination with ICIs. We are currently conducting additional preclinical studies to investigate this probability.

## **2.6 Supporting information**

### **2.6.1 scRNA sequencing raw and meta data**

The raw data files and the processed data files will be loaded on GEO website.

**3. CO-DELIVERY OF NOVEL BI-SPECIFIC AND TRI-SPECIFIC ENGAGERS  
BY AN AMPLICON VECTOR AUGMENTS THE THERAPEUTIC EFFECT  
OF AN HSV-BASED ONCOLYTIC VIROTHERAPY**

### 3.1 Abstract

Despite striking success in hematologic malignancies, immunotherapy has limited efficacy against solid tumors. Whereas, oncolytic viruses (OVs) have shown considerable promise for the treatment of solid tumors. Incorporation of immune modulators into oncolytic virotherapy represents a modality that combines direct and targeted killing of the tumor cells with simultaneous activation of the immune system to produce a more robust and sustainable anti-tumor response for a safe and effective treatment against solid tumors. To accomplish this, we have generated two chimeric proteins, the bispecific and trispecific engagers (BiCEP and TriCEP), both of which are composed of OMCP (orthopoxvirus major histocompatibility complex (MHC) class I-like protein, cowpox virus-encoded NKG2D binding protein), which binds to NKG2D (Natural Killer Group 2D) receptor on immune cells and a mutated form of epidermal growth factor (EGF $\alpha$ ) which binds to epidermal growth factor receptor (EGFR) on tumor cells. In addition to the dual specificity of BiCEP to the tumor and the immune cells, the TriCEP contains a uniquely modified IL-2 that can selectively activate the engaged immune cells via IL2R $\alpha$  to enhance their proliferation and activation. Oncolytic virotherapy can recruit NKG2D bearing NK or T cells to the tumor site, and the simultaneous release of these chimeric engagers by the co-delivered amplicons mediate cytotoxicity against tumor cells by crosslinking them with the immune cells via the overexpressed EGFR. The genes encoding these two chimeric engagers were delivered by an HSV amplicon system, which was packaged with the oncolytic virus as the helper virus, and as such, they can be conveniently co-administered. We hypothesize that the combination of the engagement effects of the locally released Bi-/TriCEPs and

the direct oncolysis by the virus forms a formidable viro-immunotherapeutic synergy for the treatment of solid tumors. Indeed, our data demonstrate that HSV-1 amplicon encoding Bi- and TriCEPs combined with the oncolytic virus (Synco-2D) lead to durable remissions and protective anti-tumor immunity in an immunocompetent mouse model. Our study thus validates this combined approach strategy, by leveraging that the specifically designed immune engagers and oncolytic virotherapy would act together to elicit a robust antitumor immune response in addition to the direct oncolysis for efficient treatment of solid tumors.

### **3.2 Introduction**

The intrinsic propensity of the oncolytic viruses to selectively infect, replicate in, and kill malignant cells makes them attractive candidates as emerging anti-cancer agents. Considerable progress has been made in recent years on oncolytic virotherapy research, which has led to preclinical and clinical evaluation of a range of oncolytic viruses, including those derived from Herpes Simplex Virus (HSV),<sup>187</sup> vesicular stomatitis virus (VSV),<sup>198</sup> adenovirus,<sup>199</sup> vaccinia virus,<sup>200</sup> and measles virus.<sup>201</sup> Talimogene laherparepvec (T-VEC or Imlygic™) is a genetically modified type I herpes simplex virus (HSV-1) and is the first and only oncolytic virus therapy to be approved for the treatment of advanced melanoma by the US FDA.<sup>182</sup> However, despite these exciting developments, it is noticeable that T-VEC has manifested only moderate benefits in patients with advanced melanoma. Thus, there is a need to further improve the efficacy of oncolytic virotherapy. One plausible way of achieving this is to combine virotherapy with other common therapeutic strategies, particularly with immunotherapy.<sup>181</sup> Indeed,

recent clinical studies have shown that the therapeutic effect can be significantly improved by combining virotherapy with checkpoint inhibitors.<sup>202</sup> Oncolytic virotherapy interacts with the host's immunity in many ways, and a full understanding of these interactions will likely lead to the design of new strategies for synergizing viro-immunotherapy.

One way that oncolytic viruses interact with the host's immune system is to induce immunogenic death of tumor cells.<sup>203</sup> Upon infection, viruses hijack the host cell to make viral proteins, avoiding early apoptotic cell death.<sup>204</sup> This allows the oncolytic viruses to replicate within, and eventually lyse the tumor cells and release large quantities of the progeny viral particles. Dying tumor cells release tumor-associated antigens (TAA's) and neoantigens, as well as pathogen-associated molecular patterns (PAMPs) and damage-associated molecular pathogens (DAMPs). Together, they promote antigen presentation to dendritic cells (DCs) in the tumor microenvironment (TME). Viral infection induces local inflammation, which can stimulate DC maturation. Mature DCs then migrate to the lymph nodes where they present the tumor antigens to the T cells, and the activated CD4<sup>+</sup> and CD8<sup>+</sup> effector T cells can potentially kill both infected and uninfected tumor cells.<sup>8</sup> To enhance the antitumor immune responses, OVs have been armed with a variety of immunostimulatory genes. For example, GM-CSF has been inserted into several oncolytic viruses, including HSV-1-based T-VEC, adenovirus-based CG0070, Vaccinia virus-based JX-594<sup>205</sup> Oncolytic viruses carrying other immunostimulatory genes include Tanapoxvirus (TANV) expressing IL2,<sup>206</sup> VV expressing IL24,<sup>65</sup> and HSV-1 expressing IL2 and IL12,<sup>207</sup> adenovirus expressing OX-40.<sup>208</sup> Through the expression of these immunostimulatory genes, tumor antigen

presentation (e.g., through the local expression of GM-CSF and OX-40), and the function of the activated CD8<sup>+</sup> T and CD4<sup>+</sup> T cells (through the local expression of IL-2, IL-12, and IL-24) can be further potentiated.

Studies in recent years from us and others have shown that virotherapy can also impact the immune cell landscape by attracting the migration of immune cells to TME,<sup>29</sup> the so-called converting “cold tumors” to hot ones.<sup>128</sup> Other studies have shown that there is an early influx of innate immune cells, including macrophages and NK cells, in response to tumor virotherapy. Besides, some OV’s infect tumor endothelial cells and disrupt the tumor-associated vasculature by expression of anti-angiogenic viral proteins, leading to ischemia and necrotic death of uninfected tumor cells.<sup>209</sup> Collectively, they also contribute to the immunogenic changes within TME that convert the cold, immune-suppressive environment to a hot and inflamed tumor. Several strategies have been developed to exploit the changes in the immune landscape during virotherapy by converting the infiltrating immune cells to attack tumor cells. For example, it was reported that arming an oncolytic vaccinia virus with a secretory bispecific T-cell engager (BiTE) consisting of two single-chain variable fragments specific for CD3 and the tumor cell surface antigen EphA2 can significantly enhance antitumor therapy.<sup>134</sup> BiTE has since been incorporated into other oncolytic viruses such as adenovirus,<sup>135</sup> and measles virus.<sup>136</sup> Our recent studies show that arming an oncolytic HSV with a novel chimeric molecule that can engage natural killer (NK) cells with tumor cells via Protein L and a TAA ligand can also enhance the antitumor efficacy of the virotherapy.<sup>141</sup>

Here we report a novel strategy to engage both the infiltrating T cells and NK cells in TME to kill tumor cells during virotherapy. The molecule on immune cells that we chose to engage is NKG2D, an activating receptor that is abundantly expressed on human NK and CD8<sup>+</sup> T cells, murine NK cells and activated murine CD8<sup>+</sup> T cells.<sup>210</sup> In addition to engaging both NK and T cells, choosing NKG2D over the traditional CD3 allows the engagement of mainly CD8<sup>+</sup> subpopulation of T cells. On the other hand, the TAA that we chose to engage is epidermal growth factor receptor (EGFR) that is overexpressed on many solid tumors.<sup>211</sup> Instead of using the traditional single chain antibodies (scFvs), we chose to use ligands as the targeting moieties. The reason for such a design is the concern on the high binding affinity of scFvs used in either BiTE or CAR-T cells and its potential link to the enhanced release of cytokines and the consequential cytokine storms.<sup>212</sup> The affinity of ligand binding is usually significantly lower than that of a scFv. As such, this design mimics “affinity tuning” that has been applied for increasing the safety of BiTE.<sup>149</sup> For engaging to the NKG2D molecule, we chose to use orthopoxvirus major histocompatibility complex class I-like protein (OMCP), which is a small polypeptide encoded by monkeypox and cowpox virus that can selectively bind to NKG2D with an affinity equal to, or greater than, all other known NKG2D ligands.<sup>183</sup> For engaging EGFR, we chose to use a mutant form of EGF (m123) that has an enhanced binding affinity and dynamic to both murine and human EGFR.<sup>213</sup> Another advantage of the design of this unique chimeric molecule is that it can be used for evaluating both human and murine immune setting. We constructed this chimeric molecule in two different forms. A bispecific chimeric engager (BiCEP) is composed of OMCP at its N-terminus and EGF (m123) at the C-terminus with a flexible linker

between these two components. A trispecific chimeric engager (TriCEP) was constructed by incorporating a mutated IL2 to the N-terminus of BiCEP so that it may bind to the IL-2 receptor on the engaged NK or T cells to potentiate their proliferation and functionality. Both BiCEP and TriCEP showed the capability of engaging NK or T cells to kill tumor cells when evaluated in vitro. When co-delivered together with an HSV-based oncolytic virus in vivo, they enhanced the antitumor therapeutic activity. Furthermore, our single-cell RNA seq data indicate that co-delivery of these chimeric molecules can dramatically change the immune cell landscape within TME, as evidenced by increased infiltration of NK/T cells. Together, our data suggest that co-administration of these uniquely designed chimeric engagers represents a viable way of potentiating virotherapy for solid tumors.

### **3.3 Materials and Methods**

#### **3.3.1 Cell lines and oncolytic virus**

HEK293, SKOV3, CT26, Vero, BHK, and TALL-104 cells were obtained from ATCC. CT26-EGFR cells were established from CT26 cells by stably transducing the cells with a lentiviral vector that contains EGFR extracellular and transmembrane domains without the intracellular sequence.<sup>141</sup> All cells were maintained in DMEM medium with 10% FBS, except TALL-104 cells, which were cultured in RPMI medium supplemented with HI-FBS and IL-2 at 100 ng/mL concentration at 37 °C with 10% CO<sub>2</sub>.

Primary human NK cells were isolated from leukapheresis using NK cell isolation kit (Stem cell technologies). The isolated NK cells were expanded using irradiated K562-mIL15 cells for 2-3 weeks and frozen until further use in the cytotoxicity assays.

Synco-2D is an HSV-1–based oncolytic virus. Its construction has been described in our previous publications.<sup>19</sup> Briefly, it has both copies of the *ICP34.5* gene deleted. Additionally, it contains two membrane fusion mechanisms - the syn phenotype through mutagenesis and insertion of the truncated form of the gibbon ape leukemia virus envelope fusogenic membrane glycoprotein (GALV.fus) into the virus genome.<sup>19</sup>

### **3.3.2 Plasmid construction**

For building the BiCEP, the coding sequence for OMCP (1–152) and the mutated form of EGF $\alpha$  (m123), together a glycine/serine linker and a Myc tag was synthesized by GenScript (U0596DB120; U0596DB130) is inserted in the frame for ease of detection. TriCEP coding sequence was similarly synthesized, except that the coding sequence for a mutated form of IL-2 was added to the 5' end. Both synthesized sequences were cloned into pcDNA3.1 plasmid to generate pcDNA3.1-BiCEP and pcDNA3.1-TriCEP, respectively.

### **3.3.3 Amplicon plasmid cloning and amplicon production**

The pcDNA3.1 plasmids containing the BiCEP and TriCEP sequences were constructed as mentioned above. For constructing amplicon plasmids containing these two chimeric engagers, the key components of an HSV amplicon, the Ori and the Pac signals, together with the EGFP coding sequence, were cut from pW7-EGFP, which is an amplicon that our lab had constructed and used in many of our previous studies.<sup>214</sup> The cut-out fragment containing the amplicon components was then cloned into pcDNA3.1-BiCEP and pcDNA3.1-TriCEP, to generate Amplicon-BiCEP and Amplicon-TriCEP, respectively. For packaging the amplicon plasmids into HSV viral particles, Amplicon-

BiCEP and Amplicon-TriCEP were transfected to BHK cells with Fugene HD (Promega, Madison, WI). pW7-GFP amplicon vector was included as a control. The transfected cells were infected with Synco-2D at 0.1 pfu/cell 24 h later. The cells were harvested when full cytopathic effect (CPE) was detected. Synco-2D and the packaged amplicon were released by three cycles of freeze-thaw, followed by centrifugation. The generated stocks were labeled as Synco-2D-GFP, Synco-2D-BiCEP, and Synco-2D-TriCEP, respectively, and stored at -80 °C until use.

#### **3.3.4 In vitro detection of transgene expression in mammalian cells**

For determining the transgene expression from either the amplicon plasmids or from the packaged amplicons, HEK293 cells were transfected with pW7-GFP, Amplicon-BiCEP and Amplicon-TriCEP, and BHK cells were infected with the corresponding packaged amplicons. The supernatants were collected 48 and 72 h later. The collected supernatants were either used directly or concentrated using 10,000 MWCO Millipore spin-columns and stored at -80 °C before they were used for Western blot detection or other quantitative assays.

#### **3.3.5 Binding assays by flow cytometry analysis**

The binding of OMCP to NKG2D was determined by incubating TALL-104 cells with the supernatants collected from HEK293 cells transfected with the amplicon plasmids or BHK cells infected with the packaged amplicon as described above. After 1 h incubation at room temperature with the fusion proteins containing supernatants, the cells were stained for NKG2D (with APC conjugated anti-human CD314 (NKG2D) antibody (BioLegend, San Diego, CA) and Myc-tag with PE-conjugated Myc-tag

mouse mAb (Cell Signaling Technology, Danvers, MA) for 30 min at 4 °C. Post staining, the cells were washed three times with 2% FBS containing PBS to remove any excess antibody. After the final wash, the cells were resuspended in flow staining buffer and analyzed immediately for the double staining for OMCP to NKG2D (determined by detection of NKG2D<sup>+</sup>/Myc<sup>+</sup> double-positive cells) by flow cytometry. Similarly, binding of EGF $\alpha$  to EGFR on SKOV3 cells and on CT26-EGFR cells is determined by incubating the cells with the supernatants collected from HEK293 cells transfected with the amplicon plasmids or BHK cells infected with the packaged amplicon respectively, for 30 min at RT. The cells were then stained for EGFR with Brilliant Violet-421 conjugated anti-human EGFR antibody (BioLegend, San Diego, CA) and Myc tag with PE-conjugated Myc-tag mouse mAb (Cell Signaling Technology, Danvers, MA). The binding of EGF $\alpha$  to EGFR on the cells is determined by the detection of EGFR<sup>+</sup>/Myc<sup>+</sup> double-positive cells by flow cytometry.

For cell surface staining, cells were washed with PBS and blocked with Fc blocker (BD Biosciences, San Jose, CA). Fluorochrome labeled antibodies (EGFR, Annexin-V, CD45, CD3, CD4, CD8, CD11b, CD56, NKG2D, and Myc) were obtained from BD Biosciences (Franklin Lakes, USA), added and stained for 30 min, washed 3X with 2% FBS containing PBS and analyzed. All samples were analyzed on a BD FACS Aria flow cytometer.

### **3.3.6 In vitro co-culture killing assay**

Ovarian cancer cells (SKOV3) were co-cultured with TALL-104 cells, at a different effector to target ratios (1:1, 2:1, and 5:1) for 2-3 d. Tumor cell lysis was monitored in

real-time using real-time fluorescent microscopy (IncuCyte; Essen Biosciences). The cytotoxicity is reported by the percentage of viable cells/percentage of confluence remaining at the end of 48 h co-culture.

### **3.3.7 FACS based cleaved caspase 3 cytotoxicity assay set-up, antibody staining and flow cytometry analysis**

DDAO-SE (CellTrace Far Red dye- C34564) labeled target cells (CT26-EGFR) were seeded at 100,000 cells per well in a 96-round bottom tissue culture plate. The cells were incubated O/N at 37 °C, 5% CO<sub>2</sub> in a humidified incubator. Following day, primary human NK cells were added to the target cells at various E:T ratios (1:1, 3:1 and 5:1) and were incubated at 37 °C for 3 h to 4 h). The cells were washed with D-PBS, 1% BSA at room temperature (RT) and either fixed and permeabilized with Fix/Perm solution (BD Biosciences, Mississauga, ON) 20 min at RT immediately or fixed in 1% paraformaldehyde for 20 min at RT and then stored at 4 °C for up to 24 h. Fixed and stored cells were centrifuged and re-suspended in Fix/Perm buffer at RT for 20 min. Cells were then washed 2 times with staining buffer (2% FBS in PBS) and re-suspended in 0.1 ml staining buffer. The cells were stained for 30 min at 4 °C with 2 µl of PE-conjugated anti-active caspase 3 monoclonal antibody (BD Biosciences) in 50 µL Perm buffer per well. The cells were washed in staining buffer 2 times and re-suspended in D-PBS, 1% BSA for analysis on a flow cytometer.

The stained cells were analyzed in a FACS Fortessa flow cytometer (BD Biosciences, Mississauga, ON). 100 thousand events were collected for each sample. Live cells and target cells were gated using the forward and side scatter parameters followed by gating

of the DDAO-SE-labeled target cell population on the APC channel (see also **Figure 3.3D**). Cleaved caspase-3 expression (PE channel) was then determined using the DDAO-SE gated target cells in an APC versus PE dot plot.

### **3.3.8 Oncolytic virus and amplicon titration**

Vero cells in 12-well plates were infected with serially diluted stocks in triplicates. The titer of Synco-2D is determined by plaque-forming units counted 24 to 48 h later. The amplicon titer is determined by counting the number of GFP<sup>+</sup> cells. In most stock preparations, the Synco-2D to amplicon ratio is approximately 8-10:1.

### **3.3.9 Western blot**

Whole-cell lysates and supernatants from either transfected or infected cells were prepared and loaded onto an SDS-PAGE gel. After electrophoresis, the proteins were transferred to a membrane, which was first blocked with 5% skim milk for 1 h and then incubated with the diluted primary antibody for Myc-tag (1:2000) (Cell Signaling Technology, Danvers, MA) overnight. The membrane was washed with TBS-T three times and incubated with an HRP-labeled secondary antibody (anti-rabbit IgG, HRP linked Antibody) at 1:1000 dilution for 1 h at RT. The membrane was developed using the GE ECIL developer system.

### **3.3.10 Animal studies**

Immune-competent female BALB/c mice (4 - 6 weeks old) were purchased from Charles River Laboratories. All animal experiments were approved by the University's Institutional Animal Care and Use Committee (IACUC). Right flanks of mice were

shaved the day before tumor cell injection. The next day,  $3 \times 10^5$  CT26-EGFR cells were injected subcutaneously to the shaved right flank. Once the tumor volumes reached the approximate size of 6 mm in diameter, mice were randomized into different groups to receive either PBS control or Synco-2D treatment with or without the chimeric molecule-containing amplicons, at the dose of  $5 \times 10^6$  pfu Synco-2D per mouse. Three mice from groups receiving the treatment of PBS, Synco-2D GFP and Synco-2D TriCEP were euthanized on day three after virotherapy to collect tumor tissues for scRNA-seq or histology exam and spleens for other immune assays. The rest of the mice were kept for 2 to 3 weeks to monitor tumor growth by measuring two perpendicular tumor diameters with a caliper. Tumor volume was calculated by the formula: tumor volume ( $\text{mm}^3$ ) = [length (mm)]  $\times$  [width (mm)]<sup>2</sup>  $\times$  0.52.

### **3.3.11 H & E staining and immunohistochemistry**

Tumor tissues were fixed and embedded in paraffin and sections were prepared. After de-paraffin and antigen retrieval, for H & E staining, the tissue sections were stained with Hematoxylin and Eosin following standard procedure. For IHC, the tissue sections were incubated in primary antibody GFP (Santa Cruz Biotech, Dallas, TX) overnight. After washing three times with PBS-T, the sections were incubated in secondary antibody for one h, and nuclei were stained with DAPI for 60 s. The slides were washed and analyzed under confocal or regular fluorescence microscopy.

### **3.3.12 Tumor dissociation and single-cell processing**

For scRNA-seq studies, the freshly collected tumors were immediately immersed in a tissue storage medium (Miltenyi, San Diego, CA) and kept at 4 °C until ready for

dissociation. Within 24 h, tissues were processed to single-cell suspensions using the human tumor dissociation kit from Miltenyi and the gentleMACS apparatus and this was done by following the manufacturer's protocol. Single-cell suspensions were then stained with a fluorescently conjugated antibody specific to CD45 (BioLegend) for 30 min at 4 °C. The cells were washed with cell staining buffer (BioLegend) and CD45<sup>+</sup> live cells were sorted on a FACS Melody cell sorter (BD) into 2% FBS in PBS, which were kept on ice until the cells were further processed for scRNA-seq.

### **3.3.13 scRNA-seq library preparation and sequencing**

Cell suspensions were washed 2–4 times and manually counted twice to assure cell viability was >90% before loading onto the Chromium platform. The libraries were created from the cells by successfully capturing cells inside gel beads in emulsion (GEM) by passing cells through a microfluidic channel. Library fragmentation size and quantification were measured before sequencing to ensure that the cDNA has been fragmented and barcoded correctly. The cDNA libraries were assessed while using an Agilent TapeStation 4200 High sensitivity DNA tape. On the day of single-cell capture and library preparation, the cells were resuspended in PBS containing 0.04% bovine serum albumin (BSA) (Ambion, Foster City, CA) to a final concentration of 200 cells per  $\mu\text{L}$ . This cell suspension was used as an input for automated single-cell capture and barcoding using the 10X Genomics Full Chromium platform. Approximately 700 single cells were captured for each sample while using the 10X Genomics Single Cell 3' Chip at the university's Seq-N-Edit Core per standard protocols. Single-cell GEMs were generated, and the single cells were uniquely barcoded. The cDNA was recovered and

selected using DynaBead MyOne Silane Beads (Thermo Fisher Scientific, Carlsbad, CA) and SPRIselect beads (Beckman Coulter, Brea, CA). The sequencing libraries were generated and the quality was assessed using a high-sensitivity DNA tape on TapeStation 4200 (Agilent, Santa Clara, CA), and the fragments were counted with Qubit Fluorometer (Thermo Fisher Scientific, Carlsbad, CA) and Kapa Library Quantification Kit (Kapa Biosystems, Wilmington, MA) using the AriaMX instrument (Agilent, Santa Clara, CA). The libraries were sequenced using NextSeq 500 (Illumina, San Diego, CA) in stand-alone mode to obtain pair-end sequencing 26 bp (read1) X 98 bp (read2) and a single index 8 bp in length.

#### **3.3.14 Transcriptome analysis**

Single-cell sequencing data downstream analysis was performed on the Maxwell Cluster high-performance research computing center at the University of Houston, using the analytical program, Cell Ranger 4.0.0 Single Cell Analysis Pipelines (10X Genomics, Pleasanton, CA, USA). Raw base call files that were generated by NextSeq 500 were demultiplexed using the “cellranger mkfastq” function to generate FASTQ files. The reads were aligned to the mouse (mm10) genome using “cellranger count” function by STAR aligner.<sup>189</sup> The feature-barcode matrices across different samples were aggregated by “cellranger aggr” function, leading to an aggregated read count table.

#### **3.3.15 Single-cell data analysis**

After constructing the single-cell gene expression count matrix, we used the R package Seurat (v3.1.1) for downstream analysis on R platform (v3.5.2). Transcription noise

cells were firstly filtered by several criteria, including minimal expression of 200 genes per cell and mitochondrial read percentage >10%. All cells passing quality control were merged into one count matrix and normalized and scaled using Seurat's `NormalizeData` and `ScaleData` functions. The reduced set of consensus highly variable genes was used as the feature set for independent component analysis using Seurat's `RunPCA` function. Cell clusters were identified using the shared nearest neighbor algorithm with a resolution parameter of 0.8. UMAP clusters of cells were identified based on the first 30 principal components.

To aid the assignment of cell type to clusters derived from unsupervised clustering, we performed cell-type enrichment analysis. Cell-type gene signatures obtained from BlueprintENCODE, Monaco Immune references from SingleR and human cell landscape. Mouse gene symbols were capitalized to map to human gene symbols. Each gene signature obtained from our clustering was statistically evaluated for overlap with gene signatures contained in these two resources.

### **3.3.16 Statistical analysis**

All quantitative results are displayed as the mean  $\pm$  S.D. The statistical difference between the two groups was compared using a Mann-Whitney U test or a Student's t-test. If more than two groups were compared, ANOVA was used. Statistical analysis was determined using Prism5 software (GraphPad Software, Inc., La Jolla, CA). A *p*-value of less than 0.05 was considered statistically significant.

## 3.4 Results

### 3.4.1 Design of a novel engager that can engage both infiltrating NK cells and CD8<sup>+</sup> T cells to enhance the antitumor effect of an HSV-based oncolytic virus

Previous studies from us and others have shown that chimeric molecules that engage either T cells (mostly via a scFv to CD3) or NK cells can enhance the therapeutic effect of an oncolytic virotherapy.<sup>134</sup> Here we report the design of a novel chimeric molecule that can engage both NK and T cells. As depicted in **Figure 3.1A**, the key components of this chimeric molecule are at the N-terminus is a 152 amino acid (aa) OMCP (orthopoxvirus major histocompatibility complex class I-like protein) and at the C-terminus is a mutant form of EGF (m123). OMCP is a small polypeptide encoded by monkeypox and cowpox virus that can selectively bind to NKG2D with an affinity equal to, or greater than, all other known NKG2D ligands.<sup>183</sup> The mutated EGF $\alpha$  ligand (EGFm123) has an enhanced binding affinity and dynamic to both murine and human EGFR.<sup>213</sup> It is engineered by directed evolution through yeast surface display for significantly enhanced affinity for the EGF receptor (EGFR). Compared to the wild type EGF (EGFwt), m123 bound eight-fold and 33-fold more tightly to surface EGFR on NR6WT cells and BJ-5a cells, respectively. m123 also bounds 18-fold and 8-fold more tightly to human EGFR and murine EGFR, respectively.<sup>213</sup> Interestingly, m123 showed stronger binding at low pH, which is beneficial given that the pH of the tumor microenvironment is universally acidic. Additionally, the binding of m123 to the EGFR may enhance its intracellular degradation, thus benefiting the overall antitumor activity.<sup>213</sup>

We constructed two versions of this chimeric molecule - the bi-specific and tri-specific binding engagers. In the bispecific construct, termed BiCEP (Bispecific Chimeric Engager Proteins), OMCP, and the m123 are linked via a flexible 20 residue (Gly-Gly-Gly-Gly-Ser)<sub>4</sub> linker and a Myc-tag for ease of detection. In the tri-specific construct, termed TriCEP (for Trispecific Chimeric Engager Proteins), a mutated form of IL-2 (mutIL-2) that has substitutions of alanine for arginine at the 38 position (R38A) and/or lysine for phenylalanine at the 42 position (F42K) is placed upstream of OMCP via a (Gly-Ser-Ser)<sub>4</sub> and a His8-tag for detection. These mutations decrease the affinity of IL-2 for IL-2Ra. This allows mutIL-2 to selectively activate IL2-signalling only as a tethered form without broadly activating other IL-2R bearing cells and minimizing the unwanted toxicity.<sup>215</sup> The hypothesized action mechanisms of BiCEP and TriCEP are illustrated in **Figure 3.1B**. The simultaneous binding of OMCP to NKG2D and mEGF $\alpha$  to EGFR by the chimeric engagers will efficiently engage the NKG2D bearing NK and T cells with EGFR-bearing tumor cells, bringing the two cells in proximity and creating an immunological synapse. The mutIL-2 in TriCEP would flicker on the IL2R on the engaged immune cells and enable the activation and proliferation of the engaged NK or T cell to further potentiate the immune response and improve the efficacy.

After the design and construction of BiCEP and TriCEP, we checked for the presence of steric-imposed conformational constraints on both chimeric molecules, and for that, we generated the predicted 3D structure using Robetta protein modeling software.<sup>215</sup> The 3D structure in **Figure 3.1C** predicts that all the individual components in both chimeric molecules are spatially separated by an intermittent linker, such that they can readily bind to their cognate targets without intra-domain steric hindrance. Next, we

examined the expression of both BiCEP and TriCEP by transfecting the plasmid constructs to BHK cells, followed by a Western blot analysis. The results in **Figure 3.2A** showed that both chimeric molecules are efficiently expressed in mammalian cells and are secreted to the supernatant after the molecules are synthesized. The secreted supernatants were harvested and concentrated by using amicon Ultra-15 Centrifugal Filter units of 10,000 NMWL to 10X concentration and subsequently used in the binding and cytotoxicity assays.

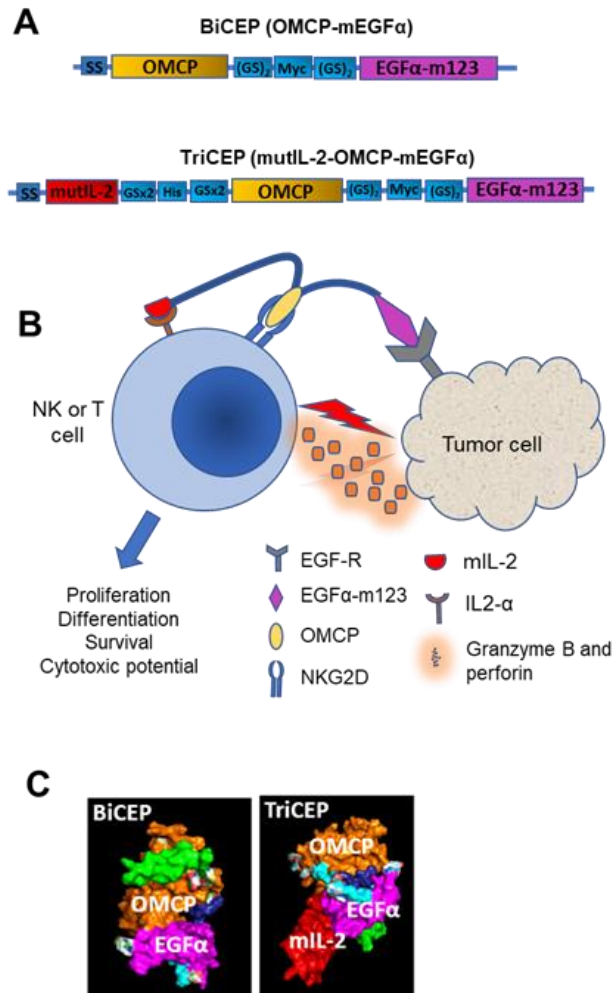


**Figure 3.1: Design of bispecific and trispecific engagers, their anticipated mechanism of action and expression in-vitro**

**A.** Schematic illustration of BiCEP and TriCEP constructs. The composition of the gene cassettes for the chimeric molecules. Each component in the BiCEP (OMCP-EGF $\alpha$ m123) and TriCEP (mutIL-2-OMCP-EGF $\alpha$ m123) is labeled accordingly. SS for signal sequence, (GS)<sub>2</sub> for two copies of GS linker. TriCEP contains the mutant IL-2 (mutIL-2) at the N-terminus. The rest is the same as BiCEP. The actual length of the coding sequence of each component is not proportional to the size of the drawn box. **B.** Perceived mechanism of action of the chimeric engagers after being expressed in TME. The chimeric molecules can engage the NKG2D bearing immune cells, including NK and T cells, with tumor cells through intermolecular binding of EGF $\alpha$ m123 (to EGFR) and OMCP (to NKG2D), and for TriCEP, the flickering action of mutIL-2 on IL-2R to NK or T cell potentiate proliferation and activation. **C.** 3D model of protein structures of BiCEP and TriCEP performed using Robetta, indicating no inter-domain hindrances. **D.** Western blot detection of transgene expression. HEK cells were transfected with pcDNA3.1 plasmids containing GFP, BiCEP, and TriCEP constructs or mock-transfected. Supernatant and cell lysate were prepared 48 h later for western blot analysis with anti-Myc tag IgG. Lanes 1 and 5, mock-transfected; lanes 2 and 6, GFP; lanes 3 and 7, BiCEP, and lanes 4 and 8, TriCEP.

### 3.4.2 In vitro characterization of BiCEP and TriCEP

Next, we conducted a series of in vitro experiments to test the binding specificity of the individual components in the chimeric molecules to their respective receptors. First, the binding affinity of OMCP to NKG2D was assessed by incubating the TALL-104 cells with the supernatants harvested from HEK293 transfected with the BiCEP and TriCEP

constructs for 1 h at RT. TALL-104 cells are a human leukemic cell line that expresses markers characteristic of both NK cells and cytotoxic T-lymphocytes with high expression of NKG2D. The binding of OMCP to NKG2D was determined by measuring the number of cells positive for both NKG2D and the Myc tag contained in both BiCEP and TriCEP (NKG2D<sup>+</sup>/Myc<sup>+</sup>) via flow cytometry analysis. Over 50-60% of NKG2D<sup>+</sup> cells are positive for Myc, indicating a good binding affinity of OMCP to NKG2D (**Figure 3.2B**).

For determining the binding activity of BiCEP and TriCEP to EGFR, we initially incubated the supernatants with SKOV3 cells for 30 min at RT. SKOV3 is a human ovarian cancer cell line with overexpression of EGFR.<sup>216</sup> The binding of the chimeric molecules to EGFR on the surface of SKOV3 cells was detected by measuring the number of cells positive for both EGFR and Myc (EGFR<sup>+</sup>/Myc<sup>+</sup>), again via flow cytometry analysis. The result in **Figure 3.2C** showed that over 80% of EGFR expressing SKOV3 cells are also positive for Myc, indicating that the mutant form of EGFm123 contained in both BiCEP and TriCEP can efficiently bind to EGFR. No binding was observed with the mock-transfected supernatants, confirming the specificity of this assay. Moreover, from **Figure 3.2C**, it can be appreciated that the about 50% of SKOV3 are EGFR negative and served as an internal control, where the negative cells do not show any bound BiCEP or TriCEP, which indicates the specificity of the chimeric molecules to its target-EGFR.

To further confirm the binding specificity of OMCP and EGFm123 in the two chimeric molecules, we also determined the co-staining positivity of EGFR in a murine colon

cancer cell line CT26-EGFR that was established in our own lab and has been used in our previous studies in an EGFR-targeted immunotherapy. We repeated the binding assay on this cell line with the cell-free supernatants collected from the amplicon infected cells (**Figure 3.2D**). From the binding assays, assessed using flow cytometry, there is increased binding of EGF to the truncated human EGFR on the CT26 cell line, evaluated by the cells positive for both Myc and the EGFR. Over 90% of the cells are double positives (EGFR<sup>+</sup>/Myc<sup>+</sup>), indicating that the EGF $\alpha$  binding affinity is retained in the supernatants collected from the amplicon infected cells (**Figure 3.2E**). Since the mutIL-2 could only bind weakly to IL-2R, we did not perform any in vitro binding assays on the TriCEP. However, as presented in the following sections, the IL2 dependent activation by TriCEP could be detected from in vivo studies by the single-cell RNA seq analysis.

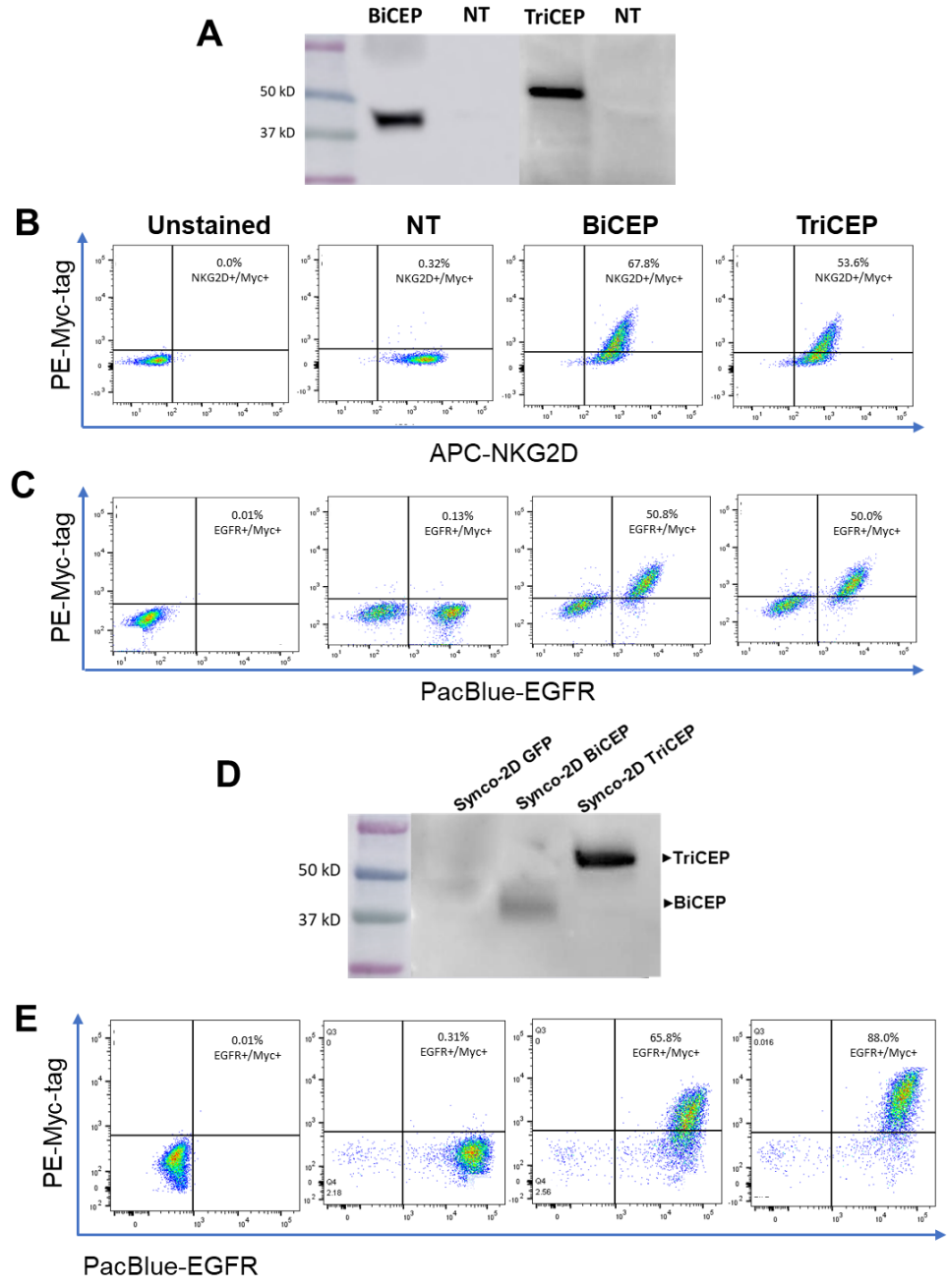


**Figure 3.2: Binding specificity of BiCEP and TriCEP to NKG2D and EGFR**

A. Western blot detection of transgene expression. HEK cells were transfected with pcDNA3.1 plasmids containing GFP, BiCEP, and TriCEP constructs or mock-transfected. Supernatant and cell lysate were prepared 48 h later for western blot

analysis with anti-Myc tag IgG. Lanes 1 and 5, mock-transfected; lanes 2 and 6, GFP; lanes 3 and 7, BiCEP, and lanes 4 and 8, TriCEP. **B.** Flow cytometry analysis of the selective binding activity of OMCP to NKG2D on TALL-104 cells. TALL-104 cells were incubated with supernatants harvested from HEK293 cells transfected with mock (NT), BiCEP or TriCEP constructs for one h at room temperature. The cells were then stained with antibodies against NKG2D and Myc-tag and subjected to flow cytometry analysis. The double-positive NKG2D<sup>+</sup>/Myc<sup>+</sup> cells indicate the specific binding of OMCP in the chimeric molecules to NKG2D on TALL-104 cell surface. **C.** Binding of EGF $\alpha$ m123 to EGFR on SKOV3 cells. SKOV3 cells were incubated with the same supernatants as in A. The cells were then stained with antibodies against EGFR and Myc-tag and subjected to flow cytometry analysis. The double-positive EGFR<sup>+</sup>/Myc<sup>+</sup> cells indicate the specific binding of EGF $\alpha$ m123 within the chimeric molecules to EGFR on the SKOV3 cell surface. **D.** Western-blot analysis to detect the transgene expression. The supernatants collected 48 h after infection were used for Western blot analysis using anti-Myc IgG and are subsequently used in the assay in the below panel. **E.** Binding of EGF $\alpha$ m123 to EGFR on CT26-EGFR cells. CT26-EGFR cells were incubated with supernatants harvested from BHK cells infected with mock, Synco-2D BiCEP or Synco-2D TriCEP, for one h at room temperature. The cells were then stained with antibodies against EGFR and Myc-tag and subjected to flow cytometry analysis. The double-positive EGFR<sup>+</sup>/Myc<sup>+</sup> cells indicate the specific binding of EGF $\alpha$ m123 within the chimeric molecules to EGFR on the CT26-EGFR cell surface.

### 3.4.3 In vitro assay on the ability of BiCEP and TriCEP to engage NK cell with tumor cells and to induce cytotoxicity

To test whether BiCEP and TriCEP could engage NK cells (TALL-104) to kill tumor cells, a real-time in vitro tumor-killing assay was performed.<sup>217</sup> Target tumor cells (SKOV3) were incubated with the effector TALL-104 cells at an increasing E:T ratio (1:1, 2:1, and 5:1) in the presence or absence of BiCEP or TriCEP. The tumor cell viability was monitored by IncuCyte, a real-time cell imaging device. Images were taken every 2 hours and the number of viable cells per well was quantified with the IncuCyte-FLR-Platform technology (**Figure 3.3A**). The cytotoxicity is reported by the percentage of viable cells/percentage of confluence remaining at the end of 24 h co-culture (**Figure 3.3B**). The results show that at the lower E:T ratios (1:1 and 2:1), there is a significant increase in the percentage killing in the presence of BiCEP and TriCEP compared to the control well with the mock-transfected supernatants. However, at the high E:T ratio (5:1), this difference became insignificant. This is probably due to the high background killing activity of TALL-104 cells.<sup>218</sup>

Moreover, we conducted a highly sensitive FACS based cleaved caspase 3 cytotoxicity assay using the cleavage of caspase-3 as a readout of cytotoxicity.<sup>219</sup> Briefly, the assay involved labelling of tumor cells (CT26-EGFR cells) with a cell tracker dye, which were then used to co-culture with primary human NK cells at different E:T ratios (1:1, 3:1 and 5:1). The cells were permeabilized and stained with an antibody recognizing cleaved caspase 3 and analyzed by flow cytometry (**Figure 3.3C**), with the detailed data in **Figure 3.3D**). The results show that at the lowest E:T ratio (1:1), there is a significant

increase on the tumor cell killing (represented as percentage caspase 3 positive cells) in the presence of BiCEP compared to the control well (NT). However, at the high E:T ratios (3:1 and 5:1), this difference became insignificant, probably due to the significant background killing in the control well. There was a significant increase on the tumor cell killing in the presence of TriCEP over the control at all the E:T ratios. Moreover, TriCEP resulted in a better killing than BiCEP at high ratios (3:1 and 5:1).

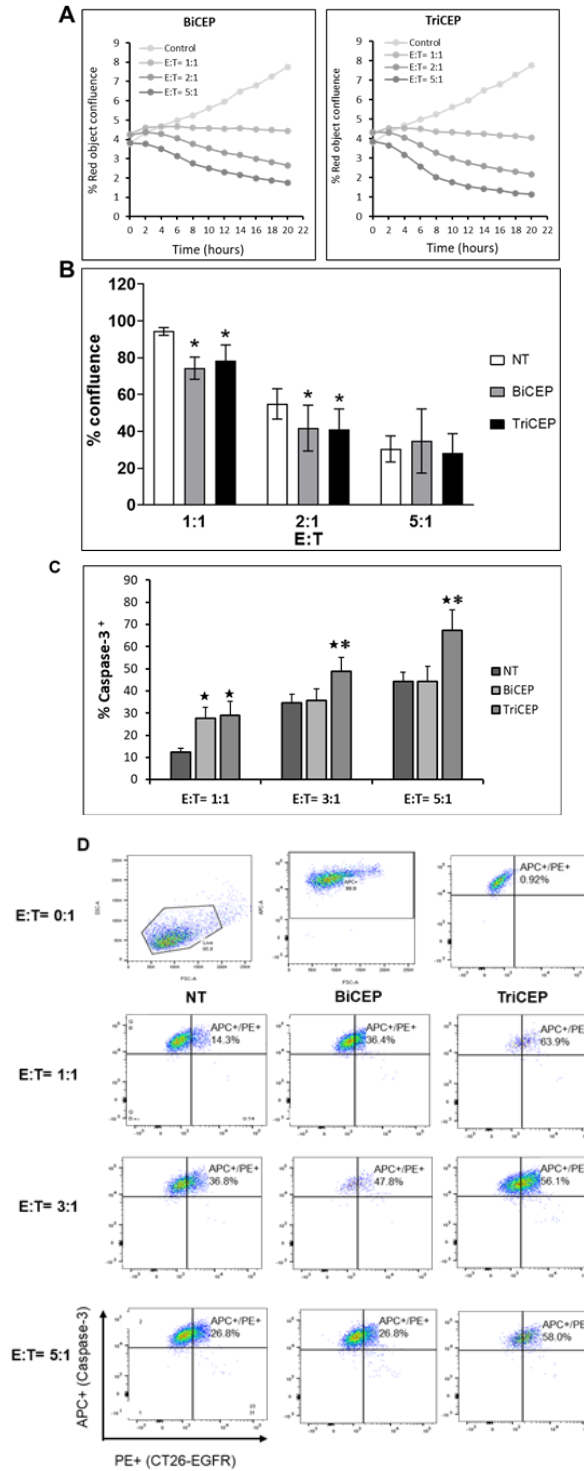


**Figure 3.3: In-vitro cytotoxic activity of TALL-104 cells against EGFR-expressing SKOV3 cells in the presence of chimeric engagers**

TALL-104 were mixed with SKOV3 tumor cells at the effector-to-target (E:T) ratio of 1:1, 2:1, or 5:1 in triplicates, in a 96 well plate, and in the presence or absence of supernatant harvested from a control vector (NT), or BiCEP and TriCEP. The plate was incubated in the IncuCyte real-time imaging system to monitor cell viability constantly for 48-72 h. **A.** The graphs show the real-time drop in the red object confluence (SKOV3 cells expressing RFP in the nuclei) over 20 h with BiCEP and TriCEP. One single red object is equivalent to a single viable tumor cell. **B.** Quantification of tumor cell killing. The experiment setting was the same as in **A.** The percentage inhibition of growth is represented by measuring the percentage confluence of the wells at the end of 24 h incubation period. The percentage confluence is the surface area of the well covered with the tumor cells, recorded by the IncuCyte as described in Materials and Methods. The results are an average of four independent assays. \* $p < 0.05$  as compared with non-transfected (NT) control. **C.** Quantification of tumor cell killing by FACS based cleaved caspase-3 cytotoxicity assay. The percentage of cleaved caspase-3 as a measure of cytotoxicity is represented by measuring the percentage of caspase-3 positive tumor cells at the end of 4 h co-culture with human primary NK cells. The results are an average of a total of six replicates from two independent assays. ★ $p < 0.05$  as compared with Non-transfected (NT) control, \*  $p < 0.05$  as compared with both NT and BiCEP. **D.** Quantification of tumor cell killing measured by caspase-3 assay. The details of the experiment were described in Section 3.3.7. CT26-EGFR target cells in the absence of NK cells are included for comparison and the gating strategy for live and APC+ tumor cells (labelled CT26-EGFR cells) are shown in the top panel. The numbers indicate the percentage of CT26-EGFR labeled cells positive for caspase 3 activation in the presence

of non-transfected supernatants (NT, first column), BiCEP (second column) and TriCEP (third column) at various E:T target ratios as indicated. Shown in the top far right quadrant of the dot plots are the percentage of CT26-EGFR labeled cells positive for caspase 3 activation at the indicated E:T ratios.

#### **3.4.4 Insertion of BiCEP and TriCEP coding sequences into an amplicon vector for in vivo delivery**

An obvious and common approach to co-delivering the chimeric molecules during virotherapy is to insert their coding sequences into the backbone of the oncolytic virus. However, as HSV has a large genome (over 150 kb) and recombination insertion of foreign genes is cumbersome and time-consuming, thus we chose to use an HSV amplicon vector to deliver these two transgenes. An HSV amplicon is a plasmid like vector that contains a copy of HSV replication origin (ori-) and packaging signal (pac). In the presence of a helper HSV (e.g., an oncolytic HSV), the plasmid gets amplified by a rolling-circle mechanism and the amplified DNA (a total of 150 kb) will be subsequently packaged into a viral particle. Depending on the size of the amplicon plasmid, many copies of the amplicon sequence (and hence multiple copies of the transgene) can be packaged into each viral particle. So it is an efficient and nimble gene delivery system that we have successfully used in several of our previous studies.<sup>214</sup> We inserted the coding sequence of either BiCEP or TriCEP, together with a copy of the EGFP gene into the amplicon construct. The inclusion of the EGFP gene allows for easy and convenient titration of the amplicon vector.

We examined the un-packaged amplicon (via transfection of the amplicon plasmid into HEK293 cells) and the packaged amplicon (via infection to BHK cells) for transgene expression (both GFP and the chimeric molecules). For packaging the amplicon plasmids into HSV particles, we initially transfected the amplicon plasmids into BHK cells, which were super-infected 24 h later with Synco-2D, which is a HSV-1-based oncolytic virus that has a clear fusogenic property.<sup>19</sup> It was constructed by deletion of the ICP34.5. Additionally, it contains two membrane fusion mechanisms - the syn phenotype through mutagenesis and insertion of the truncated form of the gibbon ape leukemia virus envelope fusogenic membrane glycoprotein (GALV.fus) into the virus genome.<sup>19</sup> The generated stock thus contains the mixture of the oncolytic virus (Synco-2D) and the packaged amplicon. The titer of Synco-2D was determined by the conventional plaque assay and the virus of the packaged amplicon was determined by GFP positive cell counts. The results in **Figure 3.4A** and **Figure 3.4B** (the top panel) showed efficient GFP expression from the amplicon plasmids when they were transfected into both HEK293 and BHK cells as they all contain the *EGFP* gene. The extensive appearance of GFP<sup>+</sup> cells after infection in the bottom panel of **Figure 3.4B** indicated that the amplicon plasmid had been efficiently packaged into viral particles when Synco-2D was used as a helper virus (as well as the oncolytic virus for the in vivo studies) in this unique delivery system, and the estimated amplicon titer from the GFP<sup>+</sup> cell counting is 1X10<sup>5</sup> per milliliter. The Western blot analysis showed that the BiCEP and TriCEP molecules were sufficiently produced from the infection of the packaged amplicons (**Figure 3.2E**), and their yield was between 1 to 3 mg/mL supernatant, as

estimated by comparison of Coomassie staining and Western blot analysis to protein standards (data not shown).

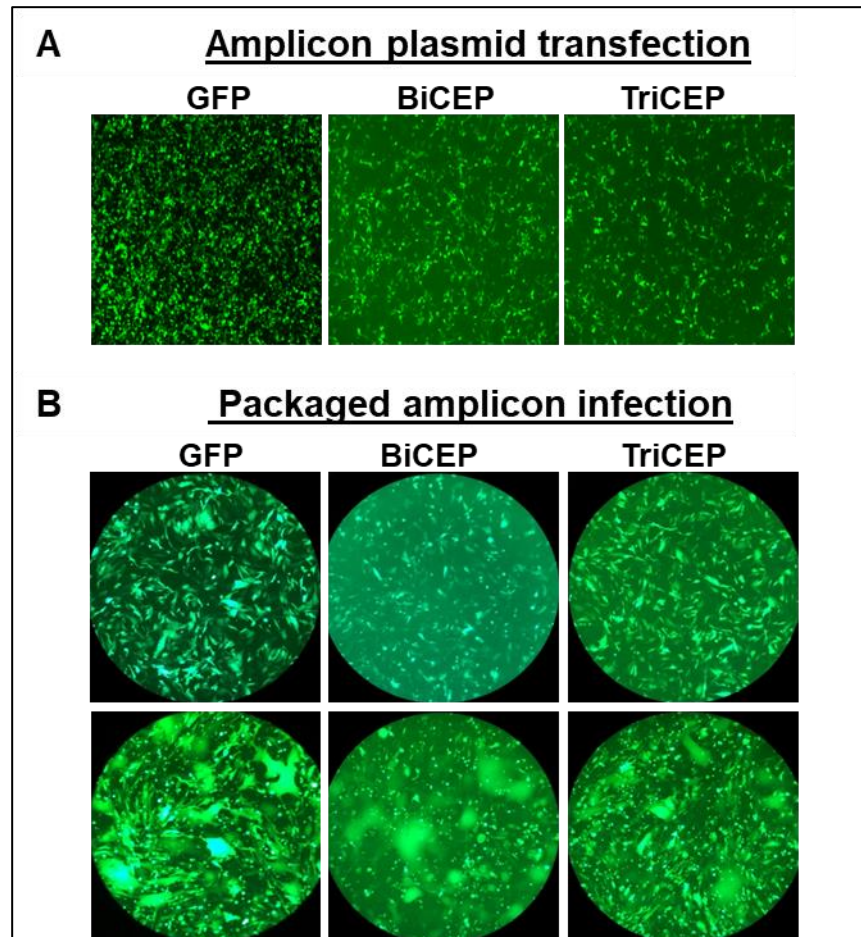


**Figure 3.4: Characterization of amplicon plasmids the chimeric engagers and production of the packaged amplicon**

**A.** Transfection efficiency as determined by EGFP expression in HEK293 cells transfected with amplicon plasmid constructs: Amplicon-GFP, Amplicon-BiCEP, or Amplicon-TriCEP (all contain the *EGFP* gene). **B.** Amplicon packaging efficiency as determined by EGFP expression in cells infected with the same packaged amplicons. For amplicon packaging, the same amplicon plasmids were transfected into BHK cells. Micrographs were taken at 24 h (the top panel) before the cells were super-infected with

Synco-2D (1 pfu/cell). The packaged amplicons were harvested 24 h later and used to infect fresh BHK cells, and the packaging efficiency was determined by the GFP expression after infection (the bottom panel). Original magnification is 10X.

#### **3.4.5 Therapeutic impact of BiCEP and TriCEP co-delivered by amplicon during Synco-2D virotherapy**

We chose the CT26-EGFR tumor model for the *in vivo* studies to evaluate the therapeutic impact of these two chimeric engagers during Synco-2D virotherapy. The experiment process is summarized in **Figure 3.5A**. Initially, CT26-EGFR tumors were subcutaneously established as reported. Once tumors reached the approximate size of 5-6 mm in diameter, they were treated with intratumoral injection of PBS, Synco2D-BiCEP, Synco2D-TriCEP, or the control amplicon expressing GFP alone (Synco-2D - GFP) at  $5 \times 10^6$  pfu of Synco-2D per mice. Tumors were measured every other day using calipers and tumor volumes were calculated as described in the Materials and Methods. The results showed that, while Synco-2D-GFP only showed a marginally therapeutic effect against this murine tumor, both Synco2D-BiCEP and Synco2D-TriCEP produced a significantly better therapeutic effect compared to the PBS control (**Figure 3.5B**). By the end of the experiment, all mice were euthanized, and the tumor explanted (**Figure 3.5C**). The measurement of explanted tumors confirmed the enhanced therapeutic efficacy by the co-delivery of both the BiCEP and TriCEP molecules. The transgene expression by the co-delivered amplicons during virotherapy was confirmed by examining the GFP expression in tumor sections collected two days after virotherapy (**Figure 3.5D**).

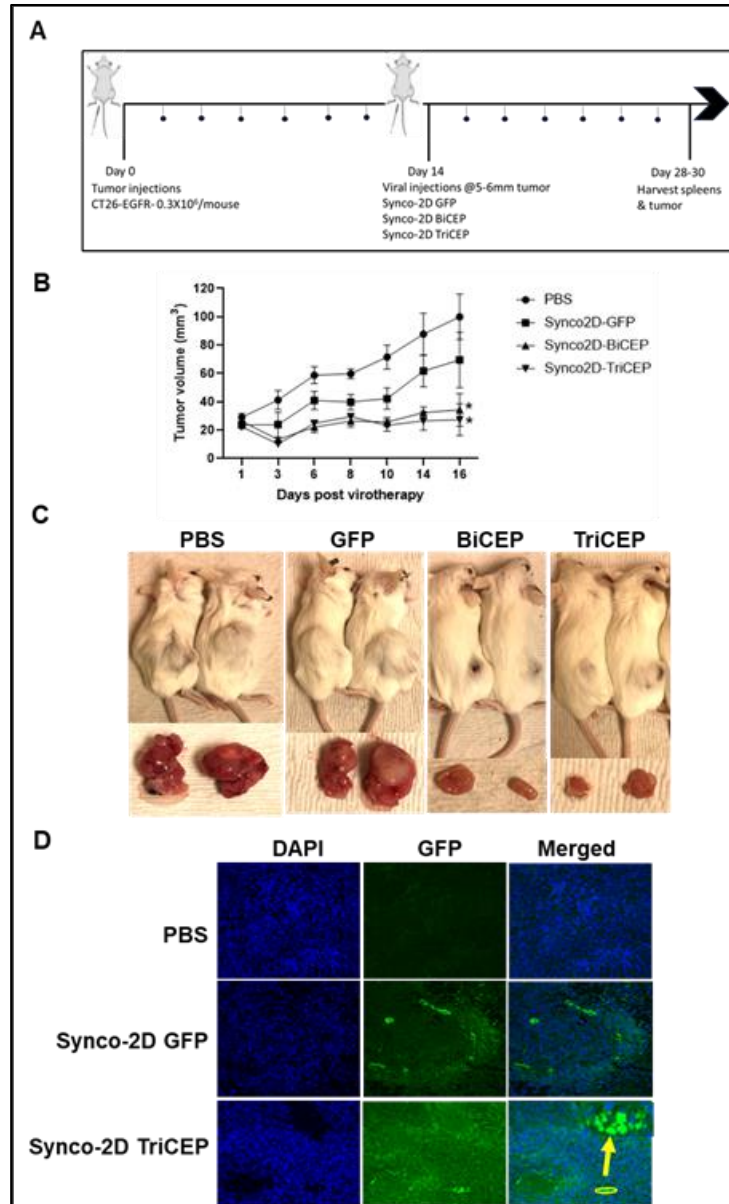


**Figure 3.5: Therapeutic evaluation of co-administration of the chimeric engagers with Synco-2D in a murine colon cancer model**

**A.** Treatment scheme of BALB/C mice bearing CT26-EGFR subcutaneous tumors.  $3 \times 10^5$  CT26-EGFR cells were injected into the right flank of 6-8 week old female BALB/C mice. When the tumors reached the approximate size of 6-8 mm, mice were randomly grouped and treated with  $5 \times 10^6$  pfu Synco-2D, Synco-2D GFP, Synco-2D BiCEP, or

Synco-2D TriCEP. PBS group served as a negative control. **B.** Tumor growth curve after virotherapy. \* $p < 0.05$  as compared with the PBS control and Synco-2D GFP treatment. **C.** Representatives of the tumor-bearing mice and the gross appearance of tumors excised at the end of the experiment. **D.** Representative immunohistochemical and histologic images from tumor sections were obtained 48 h after mice receiving the different treatment. GFP is indicative of expression of the transgene and was detected in the tumor samples from Synco-2D GFP and Synco-2D TriCEP treatment (exemplified in an enlarged inset). Original magnification: 20X.

#### **3.4.6 Characterization of immune cell landscape in TME during virotherapy with or without co-delivery of TriCEP by single-cell RNA sequence (scRNA-seq)**

The previous studies on characterizing the infiltrating immune cells during virotherapy are fragmented, as they were designed to focus on certain populations of immune cells.<sup>29</sup> Hence, we decided to use scRNA-seq to fully characterize the immune cell landscape as well as their activation status during Synco-2D virotherapy with or without the amplicon-mediated co-delivery of TriCEP. We decided not to include BiCEP in this scRNA-seq analysis as it was similarly constructed as TriCEP. The scheme for this scRNA-seq is shown in **Figure 3.6A**. BALB/c mice bearing subcutaneous CT26-EGFR tumors (approx. 8-10 mm in diameter) were injected intratumorally with either PBS, Synco2D-TriCEP, or Synco-2D-GFP at  $5 \times 10^6$  pfu per mice (**Figure 3.6A**). Forty-eight hours later, the tumors were excised from the mice and dissociated into a single-cell suspension. Due to the rarity of immune cell filtration in the TME, we initially sorted the single cells were then sorted into CD45<sup>-</sup> and CD45<sup>+</sup> populations, which were

subsequently mixed at a 3:1 ratio for single cell capture, barcoding, and sequencing by the 10X Genomics Chromium pipeline.

For characterizing the types of infiltrating immune cells in the TME of the collected tumor samples after treatment, all cells were initially clustered into unbiased cell-type classification using the Seurat package.<sup>191</sup> as shown in **Figure 3.6A**. Tumor cells were clustered by CD45<sup>-</sup> and hEGFR<sup>+</sup> expression. CD45<sup>+</sup> cells were clustered based on the assessment of known cell type markers into distinct lymphoid; monocyte/macrophage, T cells, NK cells, DCs, and neutrophils (**Figure 3.6B**). For the purpose of this study, we restricted our analysis to NK and T cells, which are the main effector cells targeted by these chimeric engagers. Cell-type specific gene expression of *Cd3d* for T cells and *Ncr1* for NK cells are shown in the violin plots (**Figure 3.6C**). The T and NK cells are further subclustered into six distinct clusters (Natural killer cells, Vd2 gd T cells, Th2 cells, T regulatory cells, Naïve CD8<sup>+</sup> T cells and Th1/Th17 cells) (**Figure 3.6D**). The sub-clustering was then stratified by samples to illustrate the relative composition of each subtype of these infiltrating NK and T cells in the different groups (**Figure 3.6E**). The data showed that Synco-2D-TriCEP treatment increased the proportion of NK cells in TME. Considering that the proportion of CD45<sup>+</sup> cells in tumors treated with Synco-2D-TriCEP was significantly higher than in the other two groups (data not shown), the increase in NK cells is quite significant. Moreover, treatment with Synco-2D-TriCEP generated more favorable T cell responses. First, it increased the proportion of Th1/Th17 cells by approximately two-fold and four-fold compared to PBS and GFP, respectively. Second, it reduced the relative presence of both Th2 (approx. two-fold and four-fold reduction compared to PBS and GFP, respectively) and Treg cells (approx.

two-fold reduction compared to both control groups). Both of these changes on T cells in TME are considered desirable for cancer immunotherapy.

To determine the activation status of the infiltrating NK and T cells in the TME, we analyzed the expression of the activation and major cytotoxic effector markers of NK and T cells, including *Klrk1* (NKG2D), *Cd69* (Cluster of Differentiation 69), *Stat3* (Signal transducer and activator of transcription 3) *Prfl* (perforin), and *Gzmb* (granzyme B). **Figure 3.8: A-E**). Among them, *Cd69* is an activation marker for both T and NK cells.<sup>220</sup> Although NKG2D is constitutively expressed on both NK and CD8<sup>+</sup> T cells, its expression is enhanced when these cells become activated.<sup>221</sup> As such, it is also considered as an activation marker for both cell types. *Stat3* is a transcription factor that is activated downstream of many key cytokine receptors expressed by lymphocytes. As such, the presence of *Stat3* is indicative of the activated status of immune cells. Moreover, it plays an important role in regulating NK cell function and is thus considered as a NK cell activation marker (**Figure 3.7C**). Perforin and granzyme B are classical markers for critical cytolytic enzymes for both NK and T cells and their expression levels indicate their cytolytic activity.<sup>222</sup> The expression of all these genes was significantly elevated in the tumors treated by Synco-2D TriCEP as compared to the other two groups with the p-value < 0.05 (**Figure 3.7D** and **E**), indicating that TriCEP directly contributed to the activation and/or effector function of NK and T cells.

In addition to the above activation markers, we also analyzed the expression of key cytokines in the infiltrated NK and T cells (shown in **Figure 3.8**), including *Icos* (**Figure 3.8A**), *Ifng* (**Figure 3.8B**) and *Tgfb1* (**Figure 3.8C**). The expression of these cytokines

is significantly elevated in NK cells, whereas significant expression of *Icos* and *Tgfb1* is only observed within the T cell clusters in the TriCEP treated group (compared to the PBS control). The p-values for the violin plots showing activation genes and cytokine genes are shown in **Table 3.1**.

**Table 3.1: p-values for the violin plots**

p- values for Fig.7		PBS vs. GFP	PBS vs. TriCEP
Klrk1	NK cells	0.037	0.004
	T cells	0.001	0.135
Cd69	NK cells	0.556	0.003
	T cells	0.012	0.000
Stat3	NK cells	0.036	0.180
	T cells	0.849	0.001
Prf1	NK cells	0.454	0.019
	T cells	0.340	0.011
Gzmb	NK cells	0.008	0.565
	T cells	0.032	0.027
Icos	NK cells	0.353	0.403
	T cells	0.000	0.000
Ifng	NK cells	0.987	0.000
	T cells	0.170	0.205
Tgfb1	NK cells	0.696	0.000
	T cells	0.593	0.000

p-values for the violin plots for **Figure 3.7** and **Figure 3.8**: are indicated with \*p < 0.05 as compared with PBS control.

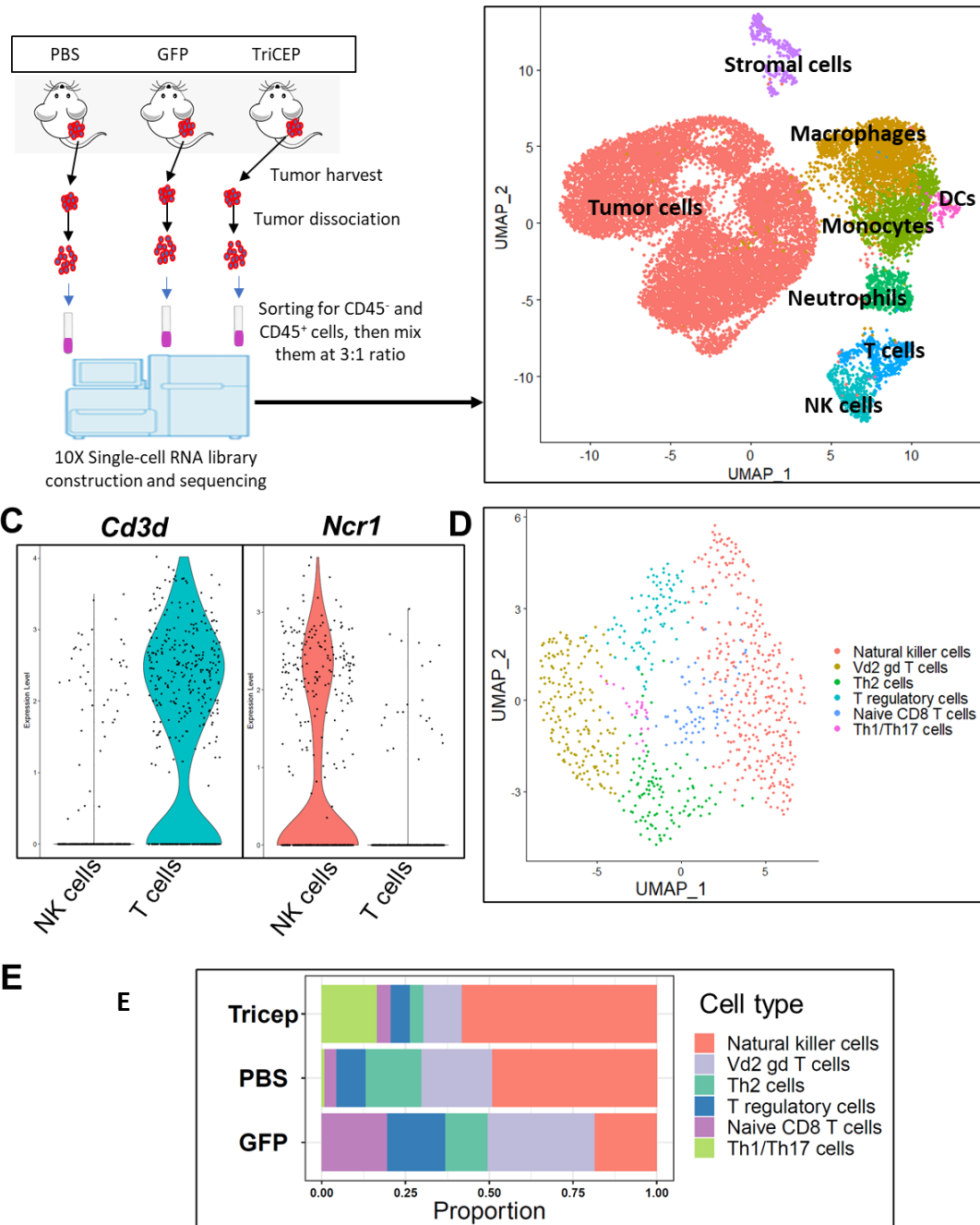


**Figure 3.6: scRNA-seq characterization of infiltrating immune cells in TME after different treatment**

**A.** Experimental setup of scRNA-seq on tumor samples. Tumors were explanted from three mice from each group 48 h after receiving the indicated treatment and pooled into

a single tube for each treatment group. The pool tumors were then digested using a tissue dissociation kit and gentleMACS tissue dissociator from Milteyni. The dissociated cells were sorted into CD45<sup>-</sup> and CD45<sup>+</sup> populations and were then mixed at a 3:1 ratio to proceed to scRNA-seq using a 10X Genomics pipeline. **B.** UMAP presentation of major cell types classified into tumor cells and six distinct clusters of immune cells are indicated. **C.** Violin plots of representative cluster-specific marker genes (*Cd3d* and *Ncr1* for T and NK cells respectively). **D.** Sub-clustering of T and NK cells annotated by mapping the scRNA seq data to Monaco Immune database. **E.** The relative composition and proportion of T and NK cell sub-clusters within each treatment group (PBS, Synco-2D- GFP (GFP), Synco-2D-TriCEP (TriCEP)).

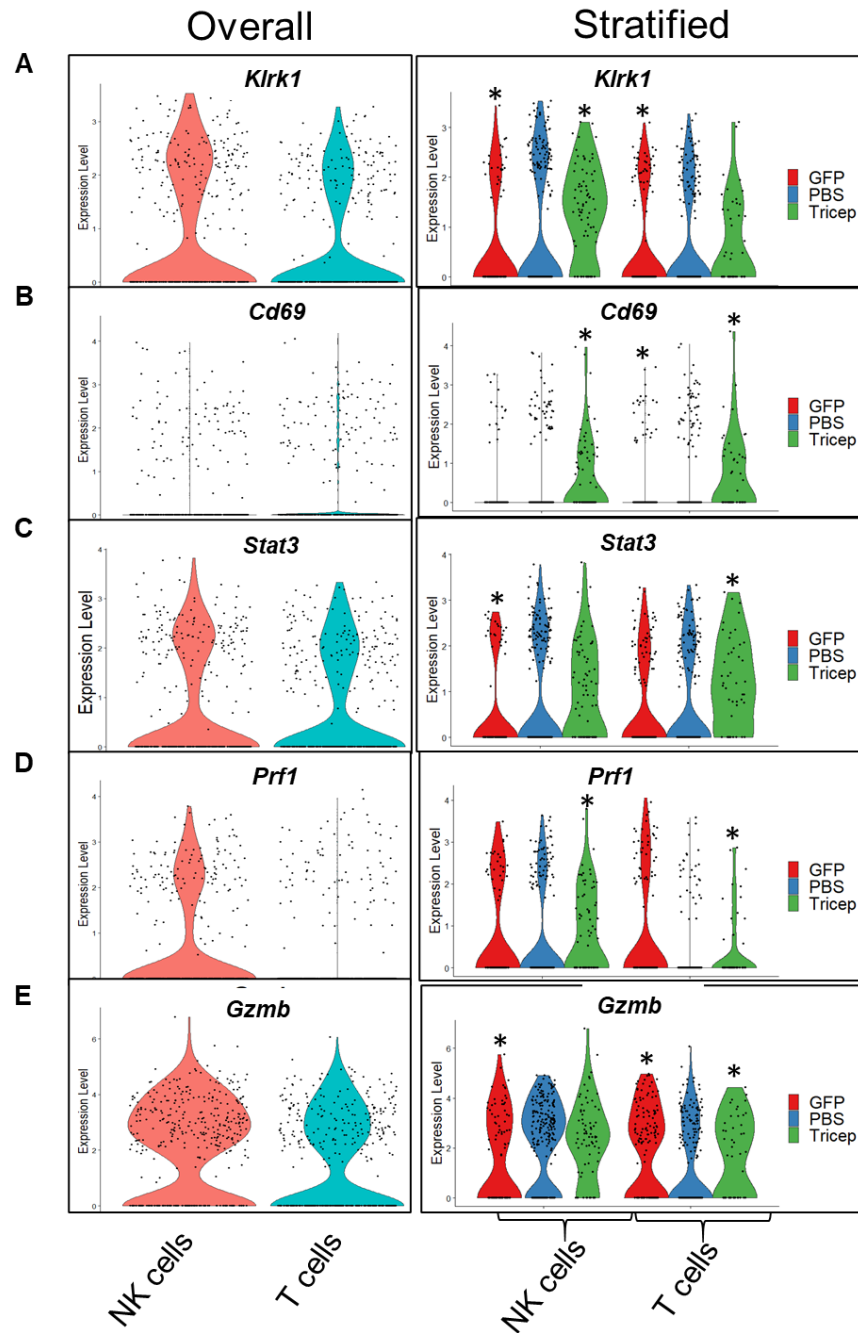


**Figure 3.7: Quantification of the signature NK and T cell activation and cytotoxic genes by scRNA-seq**

A. Violin plots showing the expression of *Klrk1* (A), *Cd69* (B), *Stat3* (C), *Prf1* (D) and *GZMB* (E) within NK and T cell cluster (overall) and further stratification as per the

treatment group (PBS, GFP or TriCEP). \* $p < 0.05$  as compared with PBS control. In a standard workflow on Seurat-v2, the expression level on y-axis in the violin plots represents the Log<sub>2</sub> transformed value (readcount+1). A higher expression level represents more read count (or percentage, as it is scaled by total read count).

### **3.4.7 Oncolytic vectors for expression of chimeric engagers**

Recombinant Herpes virus (Synco-2D) amplicon vectors were cloned to encode secretable either Bi-Specific Chimeric Engager (BiCEP) or Tri-specific Chimeric Engager (TriCEP). Upon infection, the chimeric engagers are expressed and are secreted into the tumor microenvironment (TME). We hypothesized that tumor-targeted expression of BiCEP or TriCEP by oncolytic amplicon vectors can improve the efficacy of the chimeric engagers and the oncolytic virus. This approach allows for tumor-restricted BiCEP/ TriCEP expression, thereby increasing the local concentration of the chimeric engagers. Moreover, it reduces the systemic exposure, which may result in higher therapeutic index. In addition, oncolysis by Synco-2D virus induced release of tumor associated antigens or neoantigens in an immunostimulatory context, enabling in situ tumor vaccination. Thus, the immunomodulatory effects of oncolysis in combination with locally released BiCEP/ TriCEP mediated NK/ T cell recruitment can induce a sustained anti-tumor immune response. The anticipated mechanism of action of the Synco-2D virus in combination with the amplicon vectors encoding for the chimeric engager molecules is illustrated in **Figure 3.9**.

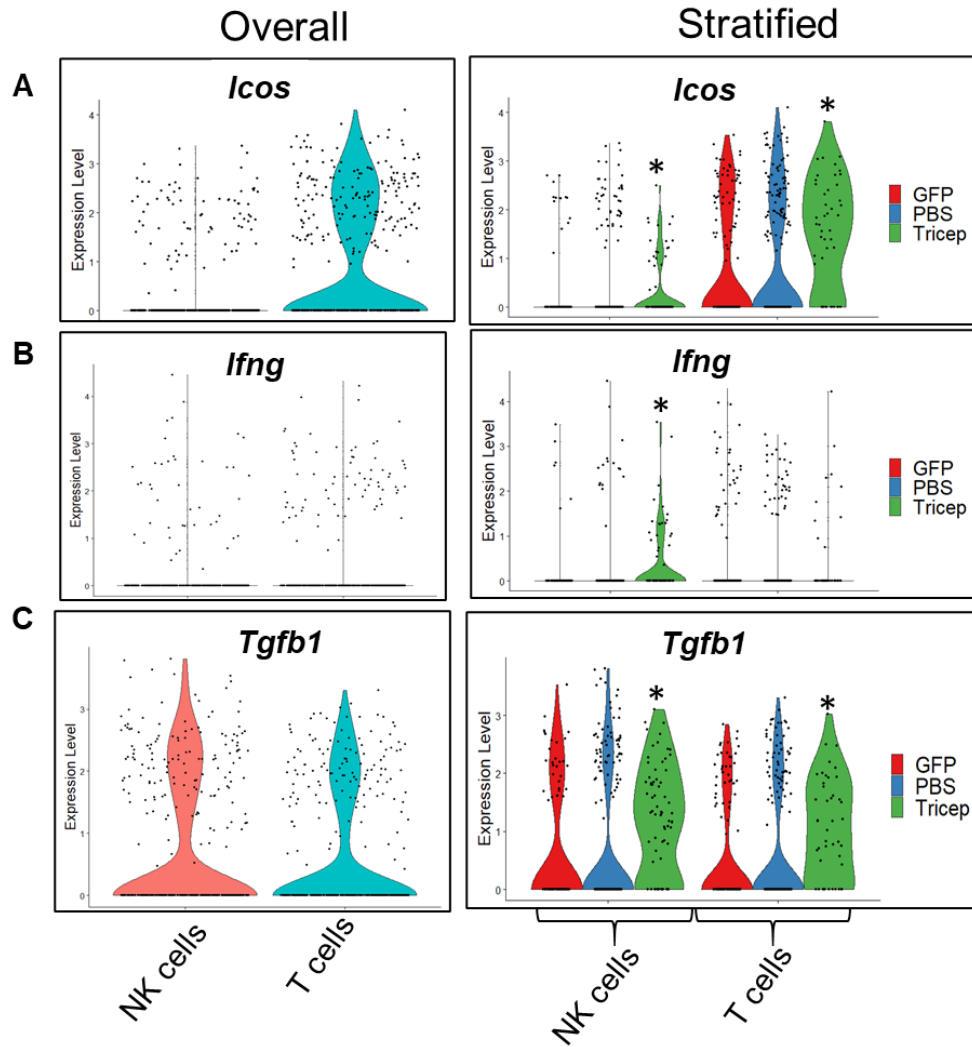


**Figure 3.8: Quantification of key cytokine genes within NK and T cell clusters by scRNA-seq**

Violin plots showing the expression of *Icos* (A), *Ifng* (B) and *Tgfb1* (C) within NK and T cell cluster (overall) and further stratification as per the treatment group (PBS, GFP or TriCEP). In a standard workflow on Seurat-v2, the expression level on y-axis in the violin plots represents the Log2 transformed value (readcount+1). A higher expression level represents more read count (or percentage, as it is scaled by total read count).

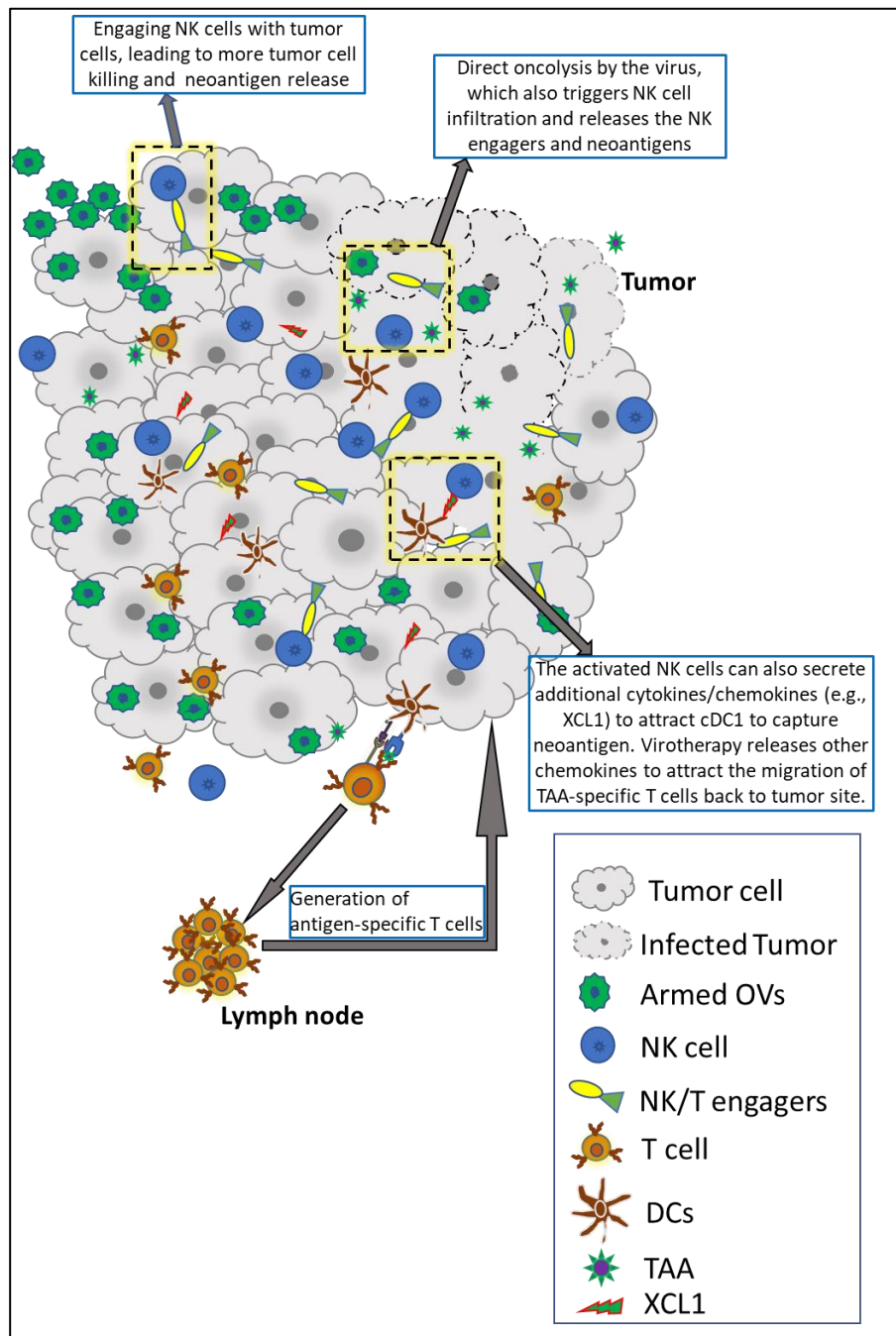


**Figure 3.9: Oncolytic Herpes viruses encoding chimeric engagers (BiCEP/TriCEP). Proposed mechanism of action of HSV amplicon vector encoding chimeric engagers**

HSV-1 amplicon virus (Synco-2D- BiCEP/ TriCEP) infected tumor cells express and secrete BiCEP and TriCEP molecules into the TME. HSV-1 (Synco-2D) infected cells form multi-nucleated syncytia, which ultimately leads to tumor cell lysis. BiCEP and TriCEP recruit NKG2D bearing NK/ T cells and mediate NKG2D mediated cytotoxicity against non-infected tumor cells as a by-stander effect.

### **3.5 Discussion**

It is becoming increasingly clear that combining virotherapy with immunotherapy can bring a synergistic therapeutic effect against solid tumors. One approach is to take advantage of the induced change in the landscape of the infiltrating immune cells during virotherapy by co-delivering bi-specific engagers that can direct T cells or NK cells to attack tumor cells. Here we report the design of a class of novel chimeric engagers – BiCEP and TriCEP. Unlike the approaches reported in previous studies that engage either T cells or NK cells separately, BiCEP and TriCEP can simultaneously engage both types of these two important immune cells for cancer immunotherapy. Additionally, we chose to engage NKG2D on the immune cells instead of CD3 that is the predominant target for most of the BiTEs reported in the literature. In addition to the abundant expression on NK cells, NKG2D is expressed on CD8<sup>+</sup> and  $\gamma\delta$  T cells in humans.<sup>223</sup> In contrast, CD3 is expressed on all T cell subsets, including regulatory T cells. As such, BiCEP and TriCEP may have the additional advantage of selectively engaging CD8<sup>+</sup> T cells and  $\gamma\delta$  T cells, potentiating their antitumor effect through co-stimulation to enhance T-cell receptor (TCR) activation.<sup>224</sup> Our in vitro data, on both tumor cells that naturally express EGFR or murine tumor cells that were transduced

with the human EGFR gene, showed that both BiCEP and TriCEP could guide cells with NK and T cell property to kill tumor cells that express the targeted tumor antigen. Co-delivery of BiCEP and TriCEP in vivo through an amplicon vector has significantly enhanced the therapeutic effect of an HSV-1-based oncolytic virus, Synco-2D, against a murine colon cancer that is otherwise only moderately permissive to the oncolytic effect of the virus. Efforts are currently underway to insert one of these engaging molecules (TriCEP) into the oncolytic viral genome, which will allow for more efficient transgene expression and hence for a better in vivo therapeutic effect. As part of the path for clinical translation of this armed strategy, the new virus will be tested in more than one tumor model that will include those expressing native EGFR.

BiTEs are commonly constructed by linking two scFvs, with one binding to a key receptor on the immune cells and the other to a TAA on tumor cells.<sup>225</sup> We chose to use two ligand-based polypeptides instead. One of them is OMCP, which can selectively bind to NKG2D of both human and rodent origin with an affinity similar to or even higher than its natural ligand.<sup>183</sup> The other one is a mutant form of EGF, m123, which can bind to EGFR of both human and murine origin with an enhanced affinity.<sup>213</sup> Our chimeric engager design on using these unique ligands instead of scFvs thus theoretically has two potential advantages. First, both ligands can bind their receptors from either human or murine origin. This allows these chimeric molecules to be tested on immune cells of both human and murine sources, making the outcomes more clinically relevant. Second, as ligands usually have lower binding affinity than scFvs, this may make these engagers less likely to induce cytokine storms during clinical application. Indeed, it has been suggested that tuning down of the binding affinity may

be necessary to increase the safety for both CAR-T cell and BiTE immunotherapy for clinical application.<sup>212</sup>

Several cell surface-expressed TAAs have been chosen as the targets for BiTE-mediated cancer immunotherapy.<sup>226</sup> EGFR is overexpressed on many carcinomas and hence is a good therapeutic target for an immune engager such as the BiCEP and TriCEP. However, EGFR is also widely expressed on many normal tissues,<sup>227</sup> which poses a risk of potential on-target off-tumor toxicity. Delivery of BiCEP and TriCEP by an HSV amplicon vector as reported in our studies can partly limit such potential toxicity as amplicon relies on the helper virus (in this case, it is the Synco-2D oncolytic virus) for further replication and packaging *in vivo*. However, for the best control of the expression of these engagers to tumor tissues, we may need to insert their coding sequences into the backbone of the viral genome of the oncolytic virus, using a strict late viral promoter. Our previous studies have shown that a strict late viral promoter such as the UL38p controls transgene expression strictly to the tumor tissues in the context of an oncolytic HSV.<sup>228</sup>

scRNA-seq, owing to its capability at revealing complex and rare cell populations, uncovering regulatory relationships between genes, and tracking the trajectories of distinct cell lineages in development,<sup>229</sup> has been widely used in recent years in many studies where these intricate characterizations are desirable.<sup>230</sup> However, to our knowledge, scRNA-seq has not yet been applied to characterize the infiltration of immune cells and their activation status during virotherapy. We thus conducted a scRNA-seq analysis of tumor samples collected from some of the treatment groups. The

data revealed that virotherapy could increase and/or alter the infiltrating immune cells in a way that is consistent with the previous report that oncolytic viruses can convert cold tumors into hot ones. Co-administration of the chimeric engagers can further enhance this effect. Most importantly, the engagers can contribute to the activation of the infiltrated immune cells, clearly indicating its role in engaging and potentiating these immune cells to attack tumor cells. Comprehensive data on scRNA-seq analysis of immune cell infiltration by comparing several oncolytic virotherapies will soon be submitted separately for publication.

### **3.6 Supporting information**

#### **3.6.1 scRNA sequencing raw and meta data**

The raw data files and the processed data files used to conduct the analysis will be loaded on GEO website.

**4. COMPREHENSIVE CHARACTERIZATION OF ONCOLYTIC  
VIRUS INFECTION WITHIN THE TUMOR  
MICROENVIRONMENT BY SINGLE CELL RNA SEQUENCING**

## 4.1 Introduction

Oncolytic viruses are promising anti-cancer agents that selectively replicate and kill cancer cells, spread within the tumor without damaging normal tissue. The oncolytic activities of the virus represent the basic biological attributes of the virus; in hijacking the host system, interacting with the host in the fight between pathogenesis and the immune system. Understanding the interplay between the oncolytic viruses and the tumor cells is critical for the development of successful therapeutic approaches. In numerous studies, the host response to tumor infection with the oncolytic virus has been characterized by measuring bulk cell populations and their further experimental validation. Collectively, these have provided rough models of the host response,<sup>231</sup> but the infected tumor is far more complex than the currently investigated in vitro models. For example, while tumor cells are known to be the main targets of the oncolytic viruses, a recent study has documented the infection of T-VEC to other cell types, such as natural killer (NK) cells, macrophages, and dendritic cells (DCs), indicating the susceptibility of immune cells to the oncolytic virus, with potential implications of intracellular infection for their functionality.<sup>197</sup> The infection of the tumor with the oncolytic virus and the generation of anti-viral and anti-tumor immune responses is complex and may be related to a wide range of viral transcriptional states within the infected cells, as well as the heterogeneity of host-response states.<sup>232</sup> Not only that, but the dual role of the metabolic machinery in supporting the host while also limiting the energetic demands of the viral life cycle adds an extra layer of complexity to the oncolytic viral infection. Yet another source of heterogeneity may derive from the possibility that only a subset of cells are infected with the OV, while most of the cells are either exposed (bystanders)

or uninfected and typically respond to defensive host signals such as type I interferons (IFNs).<sup>233</sup>

Multiple key questions related to the complexity of the oncolytic viral infection are yet to be answered. In particular, the extent and the nature of intracellular infection in different cell types within the tumor microenvironment has not been systematically elucidated. Furthermore, systemic characterization of host-responses in both uninfected/bystander and infected cells across various cell types remains uncharacterized. The progression of viral infection and subsequent activation of different host pathways upon oncolytic viral infection is of great interest. It has been challenging to characterize *in vivo* the full repertoire of viral-host interactions using conventional methods. However, recent single-cell RNA-sequencing (scRNA-seq) efforts allows for simultaneous mapping of both the host and the viral transcriptome in the same single cell,<sup>234</sup> providing an unbiased characterization of virus–host interactions in individual cells, which are masked at the population level.<sup>235, 236</sup> With this advanced technology, we can now obtain deeper insights into unique molecular signatures of specific cell subsets by increasing the sequencing depth and applying advanced analytical approaches.

Here, we profile deep transcriptomes of HSV-infected cells (FusOn-H3, an HSV-2 based oncolytic virus, constructed by replacing the ICP10 gene with the gene encoding GFP<sup>19</sup>) from tumors harvested 48 h post infection (p.i). Our results relate the progression of infection and define a precise temporal order of viral gene expression. Particularly, we investigate the relationship of HSV-2 infection and the expression of viral and host genes, which are activated and suppressed during infection, respectively. Our results

open the way to interventions in oncolytic viral therapy, suggest principles of viral-host interactions, and highlight the power of simultaneous single-cell measurements of both hosts and viral transcriptomes in delineating a comprehensive map of oncolytic viral infection in vivo. Altogether, our study provides insights into early stages of HSV-2 infection in syngeneic mouse models, and an analytical framework to study viral infections using scRNA-seq.

## **4.2 Materials and Methods**

### **4.2.1 Cell lines and oncolytic viruses**

The mouse cancer cell line H7 was obtained from ATCC and propagated in the lab. MC38gp100, a melanoma cell line, stably expressing gp100-KVP was a kind gift from Dr. Weiyi Peng. H7-Her2 and MC38gp100-Her2 cells were established by stably transducing the cells (H7 and MC38gp100, respectively) with a lentiviral vector that contains Her2 receptor. The expression of Her2 is determined by flow cytometry. All tumor cells were propagated in vitro in Dulbecco's Modified Eagle Medium (Gibco) supplemented with 10% fetal bovine serum (FBS, Gibco).

FusOn-H3 is derived from an HSV-2 based oncolytic virus, FusOn-H2. The details of FusOn-H2 construction and its antitumor properties have been described in our previous studies.<sup>26</sup> FusOn-H3 was constructed from FusOn-H2 by deleting the inserted *GFP* gene at the N-terminus of the *ICP10* gene locus.

#### **4.2.2 Tumor transplantation and treatment**

Immune-competent male C57BL/6 mice (4 - 6 weeks old) were purchased from Charles River Laboratories. All animal experiments were approved by the University's Institutional Animal Care and Use Committee (IACUC). Right flanks of mice were shaved the day before tumor cell injection. Tumor cells were washed extensively and resuspended in endotoxin-free phosphate-buffered saline (PBS) for tumor implantation in mice.  $2 \times 10^5$  cells were then injected subcutaneously to the shaved right flank the following day. Once the tumor volumes reached the approximate size of 8-10 mm in diameter, mice were randomized into different groups (n= 8) to receive either PBS control or FusOn treatment at the dose of  $5 \times 10^6$  pfu per mouse. Three mice from groups receiving the oncolytic viral treatment were euthanized on day 3 after virotherapy to collect tumor tissues for scRNA-seq and spleens for other immune assays. The rest of the mice were kept for 2 to 3 weeks to monitor tumor growth by measuring two perpendicular tumor diameters with a caliper. Tumor volume was calculated by the formula: tumor volume ( $\text{mm}^3$ ) = [length (mm)]  $\times$  [width (mm)]<sup>2</sup>  $\times$  0.52.

#### **4.2.3 Tumor dissociation and single-cell processing**

For scRNA-seq studies, the freshly collected tumors were immediately immersed in a tissue storage medium (Miltenyi, San Diego, CA) and kept at 4 °C until ready for dissociation. Within 24 h, tissues were processed to single-cell suspensions using the human tumor dissociation kit from Miltenyi and the gentleMACS apparatus and this was done by following the manufacturer's protocol. Single-cell suspensions were then stained with a fluorescently conjugated antibody specific to CD45 (BioLegend) for 30

min at 4 °C. The cells were washed with cell staining buffer (BioLegend) and CD45<sup>+</sup> live cells were sorted on a FACS Melody cell sorter (BD) into 2% FBS in PBS, which were kept on ice until the cells were further processed for scRNA-seq.

#### **4.2.4 scRNA-seq library preparation and sequencing**

Cell suspensions were washed 2–4 times and manually counted twice to assure cell viability was >90% before loading onto the Chromium platform. The libraries were created from the cells by successfully capturing cells inside gel beads in emulsion (GEM) by passing cells through a microfluidic channel. Library fragmentation size and quantification were measured before sequencing to ensure that the cDNA has been fragmented and barcoded correctly. The cDNA libraries were assessed while using an Agilent TapeStation 4200 High sensitivity DNA tape. On the day of single-cell capture and library preparation, the cells were resuspended in PBS containing 0.04% bovine serum albumin (BSA) (Ambion, Foster City, CA) to a final concentration of 200 cells per  $\mu$ L. This cell suspension was used as an input for automated single-cell capture and barcoding using the 10X Genomics Full Chromium platform. Approximately 700 single cells were captured for each sample while using the 10X Genomics Single Cell 3' Chip at the university's Seq-N-Edit Core per standard protocols. The single-cell GEMs were generated and individually barcoded. The cDNA was recovered and selected using DynaBead MyOne Silane Beads (Thermo Fisher Scientific, Carlsbad, CA) and SPRIselect beads (Beckman Coulter, Brea, CA). The sequencing libraries were constructed and the quality was assessed using a high-sensitivity DNA tape on TapeStation 4200 (Agilent, Santa Clara, CA), and the fragments were counted with

Qubit Fluorometer (Thermo Fisher Scientific, Carlsbad, CA) and Kapa Library Quantification Kit (Kapa Biosystems, Wilmington, MA) using the AriaMX instrument (Agilent, Santa Clara, CA). The libraries were sequenced on a NextSeq 500 (Illumina, San Diego, CA) in stand-alone mode to obtain pair-end sequencing 26 bp (read1) x 98 bp (read2) and a single index 8 bp in length.

#### **4.2.5 scRNA-seq data process**

Single-cell RNA sequencing data downstream analysis was performed on the Maxwell Cluster high-performance research computing center at the University of Houston, using the analytical program, Cell Ranger 4.0.0 single cell analysis pipelines (10x Genomics, Pleasanton, CA, USA). Raw base call files that were generated by NextSeq 500 were demultiplexed using the “cellranger mkfastq” function to generate FASTQ files. The reads were aligned to the mouse (mm10) genome using “cellranger count” function by STAR aligner.<sup>189</sup> The feature-barcode matrices across different samples were aggregated by “cellranger aggr” function, leading to an aggregated read count table.

#### **4.2.6 scRNA-seq data analysis**

After constructing the single-cell gene expression count matrix, we used the R package Seurat (v3.1.1) for downstream analysis on R platform (v3.5.2). Transcription noise cells were firstly filtered by several criteria, including minimal expression of 300 genes per cell and mitochondrial read percentage <30%. All cells passing quality control were merged into one count matrix and normalized and scaled using Seurat’s NormalizeData and ScaleData functions. The reduced set of consensus highly variable genes was used as the feature set for independent component analysis on ~3000 genes using Seurat’s

RunPCA function. A UMAP dimensional reduction was performed on the scaled matrix (with most variable genes only) using the first 40 components of principal component analysis (PCA) to obtain a two-dimensional representation of the cell states. Cell clustering was performed using the function FindClusters that implements SNN (shared nearest neighbor) modularity optimization-based clustering algorithm on 40 PCA components with resolution 0.8, leading to 22 clusters. For each cluster, only the genes that were expressed in >25% of cells with at least 0.25-fold difference were considered.

To aid the assignment of cell type to clusters derived from unsupervised clustering, we performed cell-type enrichment analysis. Cell-type gene signatures obtained from BlueprintENCODE, Monaco Immune references from SingleR and human cell landscape. Mouse gene symbols were capitalized to map to human gene symbols. Each gene signature obtained from our clustering was statistically evaluated for overlap with gene signatures contained in these two resources.

#### **4.2.7 Statistical analysis**

All quantitative results are displayed as the mean  $\pm$  S.D. The statistical difference between the two groups was compared using a Mann-Whitney U test or a Student's t-test. If more than two groups were compared, ANOVA was used. Statistical analysis was determined using Prism5 software (GraphPad Software, Inc., La Jolla, CA). A *p*-value of less than 0.05 was considered statistically significant.

## 4.3 Results

### 4.3.1 Dissecting oncolytic HSV infection of tumor with FusOn-H3 using combined single-cell mapping of host and viral transcriptome

To study simultaneously, in an unbiased way, both host and viral transcriptional states after oncolytic viral treatment and the potential impact of virotherapy on it, we used single cell RNA sequencing (scRNA-seq) to reveal the complex transcriptomes within the virally infected and uninfected cells from the collected tumor tissues from the two mouse tumor models. The experimental procedure is summarized in **Figure 4.1A**. We established tumors in the right flank of 6-8 week old BALB/c mice by implanting either the H7/H7-Her2/MC38gp100 and MC38gp100-Her2 murine cancer cell lines. (eight per group) H7-Her2 and MC38gp100-Her2 were generated by stably transducing with a lentiviral vector encoding the human epidermal growth factor receptor 2 (Her2). The transduced *her2* gene would allow the tumor cells to be annotated based upon the *her2* expression and thus can be clustered in an UMAP plot. When the tumors reached an approximate size of 8-10 mm in diameter, tumors were injected either with  $5 \times 10^6$  plaque-forming-unit (pfu) of FusOn-H3, a HSV-2 based oncolytic virus.<sup>24</sup> Five out of the eight mice were randomly separated for tumor reduction and the tumors were measured for 2 weeks post therapy. The therapeutic efficacy of FusOn-H3 in both H7 group and MC38 group is illustrated in **Figure 4.10A** and **B** respectively. Whereas, for scRNA seq study, the tumors from rest of the three mice were collected 48 h post virotherapy and were dissociated into single cell suspension using Miltenyi GentleMACS Octo Dissociator, following manufacturer's instructions. The single cell

preparations were then sorted into CD45<sup>-</sup> and CD45<sup>+</sup> populations. The CD45<sup>-</sup> and CD45<sup>+</sup> cells from each tumor sample were mixed at a 3:1 ratio before they were processed for single-cell RNA sequencing (scRNA-seq) on the 10x Genomics Chromium controller and sequenced by Illumina NextSeq 500 platform at recommended sequencing depth to provide information for both host and viral gene expression.

The sequencing yielded gene expression profiles from over 12,379 cells in total with a coverage of over 16,668 reads per cell after normalization. The breakdown details for the individual treatment groups are: 1) H7 (n= 1,314 cells sequenced, 39,215 mean reads per cell) 2) H7-Her2 (n= 1,954 cells sequenced, 46,003 mean reads per cell) 3) MC38gp100 (n= 2,831 cells sequenced, 23,572 mean reads per cell) and 4) MC38gp100-Her2 (n= 6,280 cells sequenced, 17,403 mean reads per cell). The data were normalized with the Seurat V4.0<sup>191</sup> and separated into two datasets for further analysis: H7 dataset comprising sequencing reads from H7 and H7-Her2 cells; MC38 group comprising the sequencing reads from MC38gp100 and MC38gp100-Her2 groups. Here in this chapter, we report the analysis from the H7 data set. In the H7 aggregated dataset, after clustering and annotation analysis, the 11 distinct cell clusters were initially classified into two distinct groups: CD45<sup>+</sup> leukocytes (containing all the immune cells) based on CD45 (*Ptprc*) expression (**Figure 4.1B**) and Her2<sup>+</sup> tumor cells based upon Her2 expression (**Figure 4.1C**). Despite the low expression level of Her2, the non-immune cells with dispersed Her2 expression are clustered together and annotated as tumor cells (similar cells tend to cluster together). The CD45<sup>+</sup> cells were reanalyzed at a high-resolution by performing sub-clustering of immune cells and

mapped them to the Monaco Immune fine reference panel. This yielded five distinct CD45<sup>+</sup> subpopulations (CD4 T cells, CD8 T cells, B cells, neutrophils, monocytes/macrophages (**Figure 4.1C**).

Next, we broadly classified the cells into virally “infected” (166 cells), “uninfected/bystanders” (1637 cells) and “Others” (1057 cells) based upon the expression of viral transcripts in each cell, from which the percentage of infection is determined to be approx..10%. The “Others” are predominantly CD45<sup>+</sup> immune cells, clustered far from the tumor cells as shown in **Figure 4.1A**. We investigated the heterogeneity of molecular phenotypes within the infected tumor cells by profiling the transcriptomes of uninfected and infected cells. The distribution of the viral gene expression per single cells indicated the progression of infection over time and to further explore the cell-to-cell variability in viral gene expression, we analyzed the relative expression of three groups of viral transcripts: immediate early (IE)- **Figure 4.2B**, early (E)- **Figure 4.2C** and late (L)- **Figure 4.2D** genes.<sup>237</sup> **Figure 4.2B-D** shows the correlation between the viral gene expression and the HSV-2 viral transcriptome load ranging from 0-45%, indicating the extreme cell-to-cell variability in the amount of viral transcripts expressed by the FusOn-H3 infected cells. The differential expression of the viral genes between infected and uninfected cells is represented in

**Figure 4.3** and the differential expression of all the viral genes between infected and uninfected cells is illustrated in **Figure 4.8**.

We were not able to detect all the late genes perhaps due the fact that those cells are probably compromised and therefore, may have been sorted out for dead/dying cells

during the sorting process, which may also be the reason for the underestimated 10% rate of infection observed.

Our scRNA-seq data indicate a wide and uneven distribution of viral gene expression during FusOn-H3 infection, with most cells expressing low levels of viral gene transcripts and a smaller group expressing much higher levels (in agreement with the ICP4 (gene-RS1) expression levels presented in **Figure 4.2B**). The vast majority of cells infected with the virus, had some level of viral gene expression, predominantly early genes, suggesting that the fraction of lowly expressing cells (and the ICP4<sup>-</sup> population noted above) are indeed abortively infected cells, rather than cells that did not encounter a virus. We note that significant cell-to-cell differences are seen even within the group of highly infected cells, with viral gene expression ranging from 1% to >45%, and that this ‘viral expression load’ is indicative of the permissiveness of tumor cells to FusOn-H3 infection.

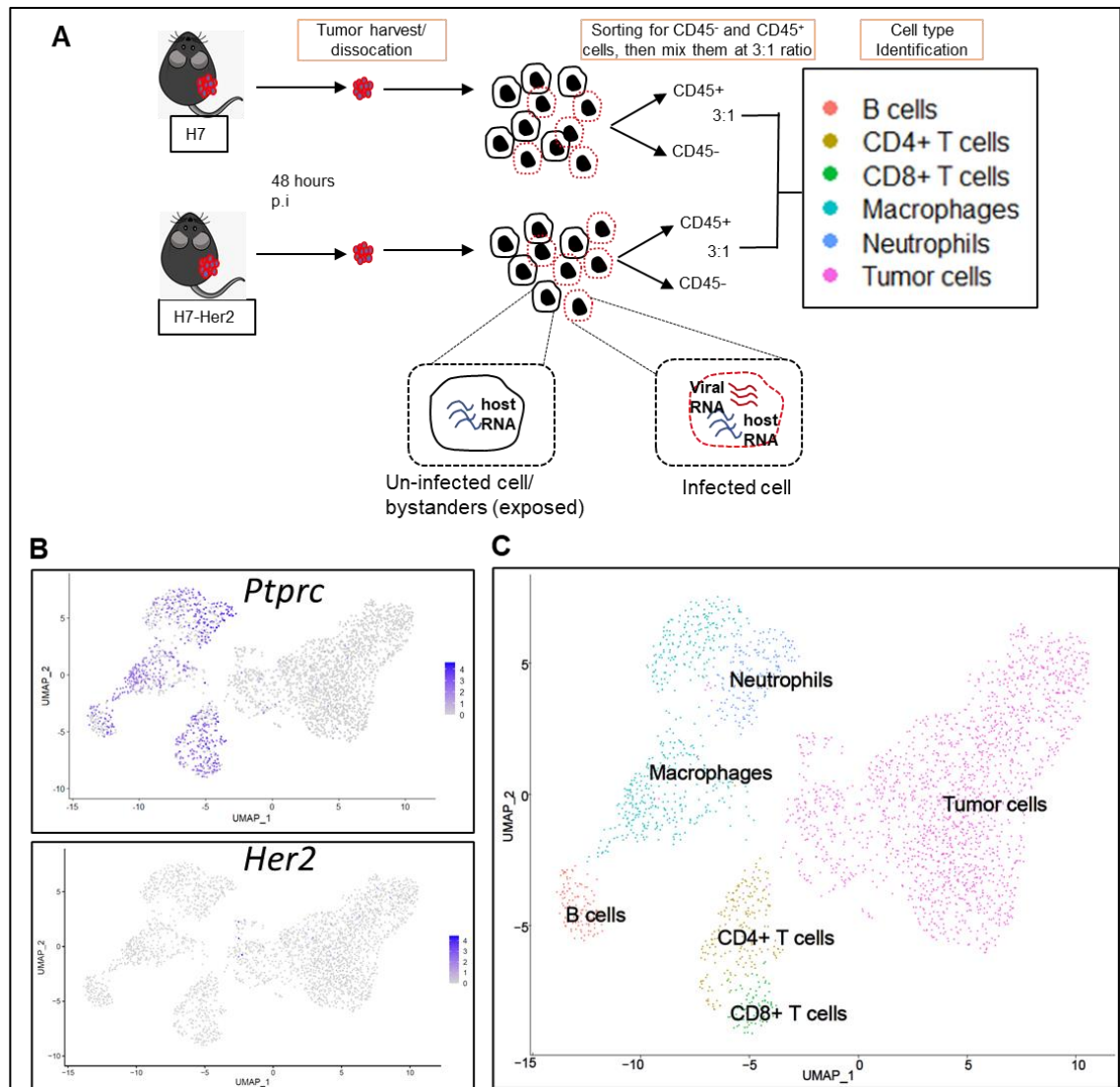


**Figure 4.1: scRNA-seq experiment and data analysis**

**A.** Tumors were explanted from three mice in each group at 48 h after receiving the FusOn-H3 treatment. pooled tumors were digested and dissociated into single cells, which were subsequently sorted into CD45<sup>-</sup> and CD45<sup>+</sup> populations and then mixed at a 3:1 ratio for scRNA-seq using a 10X Genomics pipeline and the sequenced cells were clustered into cell types using BlueENCODER database **C.** Classification of cells into immune cells (CD45<sup>+</sup>/*Ptprc*) and tumor cells (*her2*<sup>+</sup>) based on *Ptprc* and *her2*

expression, respectively. **D.** UMAP plot showing the merged data of all the immune cell types annotated as per Monaco cell immune database.

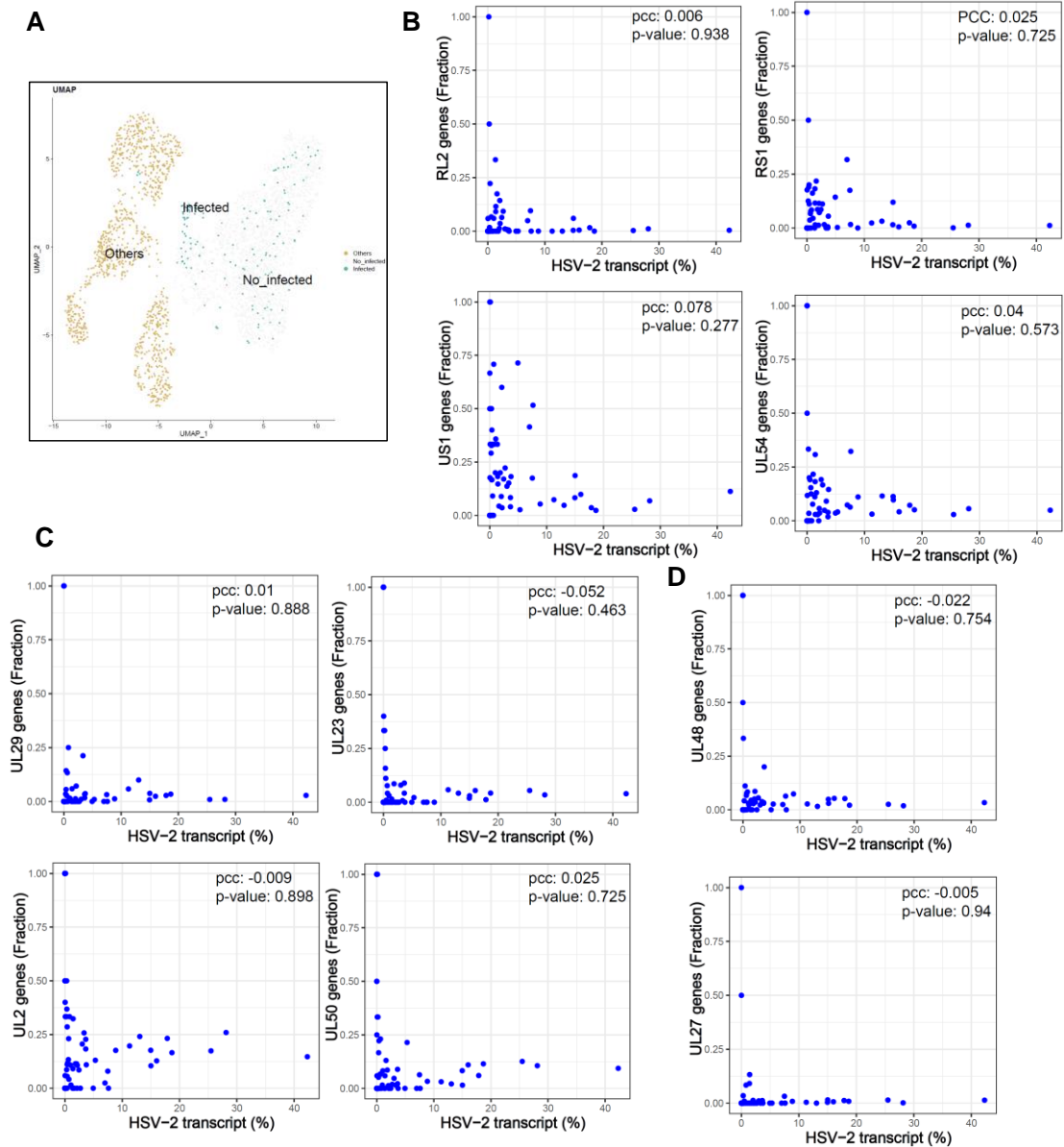


**Figure 4.2: Cell-to-cell variability in infection dynamics and viral gene expression**

**A.** UMAP plot showing the total sequenced cells classified into “infected”, “Uninfected” and “Others” based upon the expression of viral transcripts. **B.** Scatter plots of single cells showing the % of viral transcripts on the x-axis and the relative abundance

of each viral gene (Immediate early genes (B), early genes (C) and late genes (D)) on the Y-axis. pcc and p are the Pearson correlation coefficients and p-values, respectively.

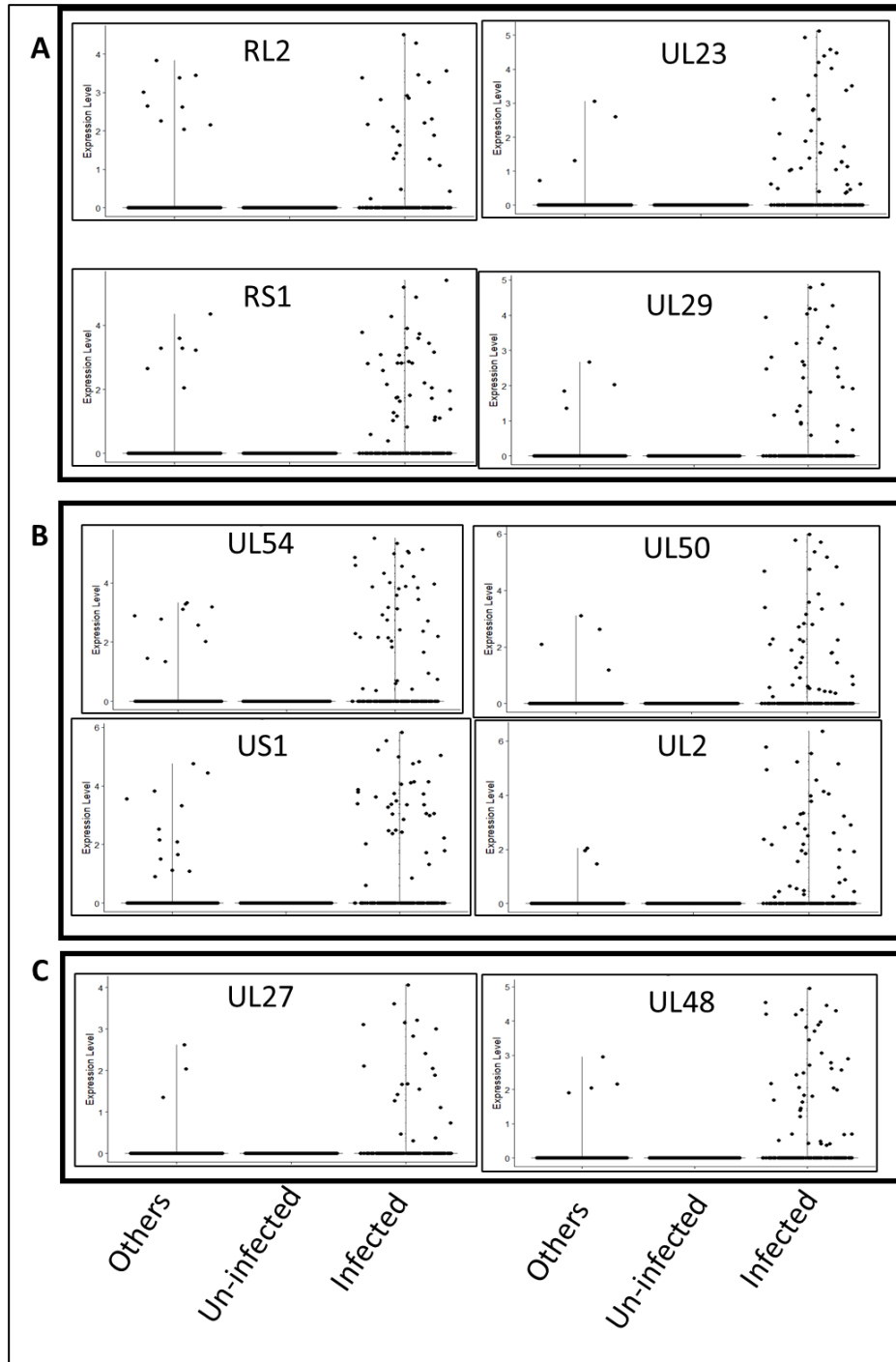


**Figure 4.3: viral gene expression according to their infection status**

A. Violin plots showing the expression of genes as per the infection status (A- immediate early genes; B- early gene; C- late genes) between the infected, uninfected and the Others group. In a standard workflow on Seurat-v2, the expression level on y-axis in the violin plots represents the Log2 transformed value (readcount+1). A higher expression level represents more read count (or percentage, as it is scaled by total read count).

#### 4.3.2 Correlation of known antiviral genes and tumor infection status

Numerous studies have reported a powerful cellular response to HSV infection, involving the activation of anti-viral genes including but not limited to IFN-responding genes,<sup>238</sup> so we hypothesized that highly infected cells should be enriched for anti-viral genes. To characterize this response systematically, we looked at the expression of some typical anti-viral genes to the tumor infection status. To our surprise, the gene expression analysis in the infected cells did not indicate the upregulation of anti-viral response. In fact, canonical anti-viral genes such as IFIT1, IFIT2, and IFIT3 were only detected in a fraction of FusOn-H3 infected cells (**Figure 4.4**). The human IFN-stimulated gene 56 (ISGs) family of genes (ISG56/IFIT1; ISG54/IFIT2 and ISG60/IFIT3) are normally silent in most cell types, but their transcription is induced by interferons, virus infection, and other molecular patterns (PAMPs).<sup>239</sup>

Next, we compared a larger panel of interferon-stimulated genes (ISGs) in infected vs uninfected cells. ISGs are usually expressed after IFN stimulation and the robust induction of ISG15 in response to viral infection implies the role of ISG15 in antiviral defense.<sup>240</sup> From **Figure 4.4**, not only infected but also uninfected tumor cells have

upregulated ISG15, indicating that, these cells were exposed to the virus and initiated the anti-viral responses, evading the attack from the virus.

Beyond obvious factors like the IFNs and ISGs, cells either exposed or infected with the virus, exhibited highly heterogeneous expression patterns of numerous other anti-viral genes likely to influence infection outcomes. For example, expression levels of NEAT1, a long non-coding RNA (lncRNA) involved in inflammasome formation, regulation of cytokine and chemokine expression, and nuclear paraspeckle formation,<sup>241,242</sup> is highly expressed across all three classified groups (**Figure 4.4**).

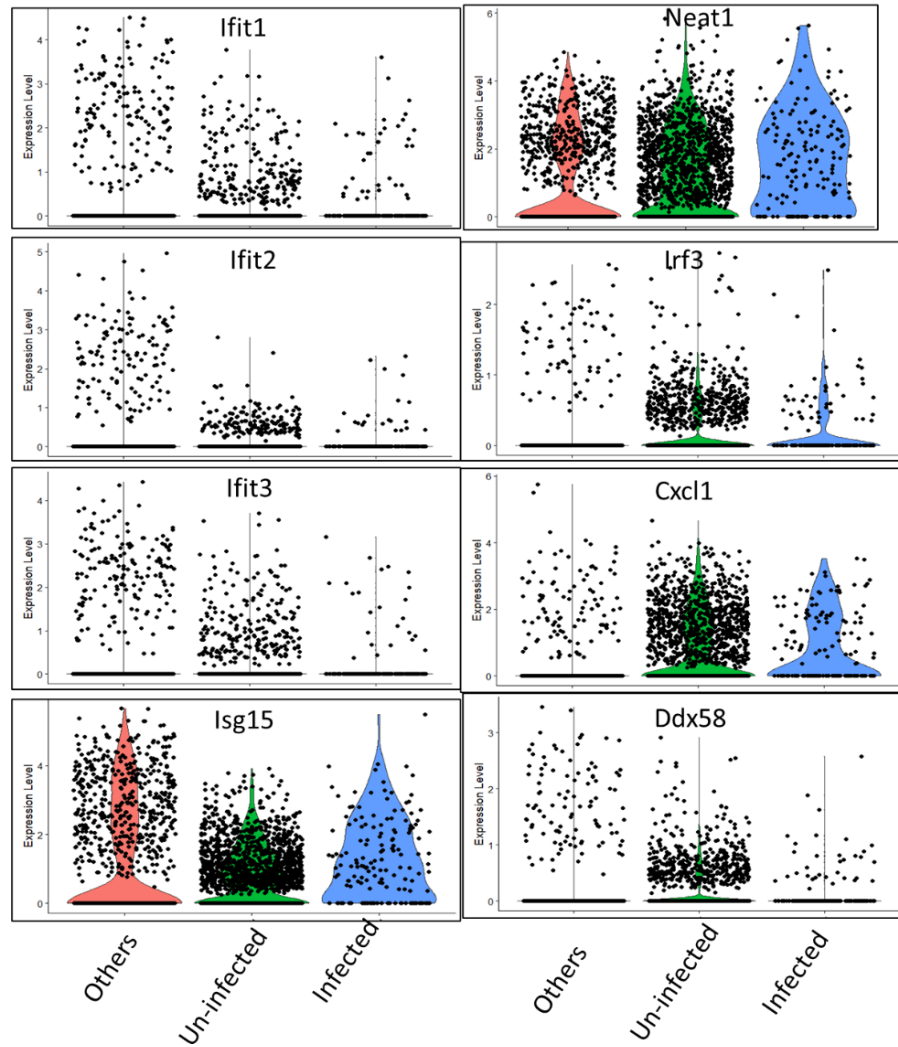


**Figure 4.4: The anti-viral program is initiated in cells irrespective of their infection status**

Violin plots showing the expression of key anti-viral genes (*Ifit1*, *Ifit2*, *Ifit3*, *Isg15*, *Neat1*, *Irf3*, *Cxcl1*, and *Ddx58*) between the infected, uninfected and the others group. In a standard workflow on Seurat-v2, the expression level on y-axis in the violin plots represents the Log2 transformed value (readcount+1). A higher expression level represents more read count (or percentage, as it is scaled by total read count).

### 4.3.3 Correlation of other cellular genes and tumor infection status

A high-resolution analysis of expression changes in infected and uninfected cells (bystanders) can convey valuable information about the host-responses against viral infection. In particular, differences in expression levels can be affected by extracellular exposure to various elements in the tumor micro-environment or may be associated with intracellular viral invasion. Previous studies have characterized many of the signaling cascades that operate in HSV infection, such as IFN and NF- $\kappa$ B signaling,<sup>243</sup> but the contribution of each stimulus to the host response was not well understood. We hypothesized that differential expression between infected and un-infected/bystander cell populations could identify transcriptional regulation associated with the intracellular virus infection as well as extracellular signals, since both subsets are essentially exposed to the same extracellular signals. For simplicity, we looked at the differential expression of host genes in between the infected and uninfected cells. **Figure 4.5** represents a volcano plot, showing differentially expressed genes between the virally infected and uninfected tumor cells. One of the upregulated genes is Gadd45g, Growth arrest and DNA Damage Inducible Gamma gene, which has been reported to be activated during HSV1 infection, reduces viral yield and is known to play a role in the suppression of innate immunity.<sup>244</sup> In agreement with the literature, where Gadd45g was activated during HSV-1 infection, FusOn-H3 upregulated the expression of Gadd45g, by favoring the viral replication. These findings and the role of Gadd45g during oncolytic viral infection will be explored. On the other hand, there were several ribosomal proteins that were significantly downregulated between the infected and the uninfected cells. In general, viruses or small pathogens recruit a variety of host factors

to survive and propagate, including RPs (Ribosomal proteins). These RPs interact with the viral mRNA and regulate the replication and infection of virus in the host cells. These interactions are essential for promoting viral infection and accumulation.<sup>245</sup> Collectively, the differentially expressed genes seem to favor the FusOn-H3 spread and activation of the host's immune responses.

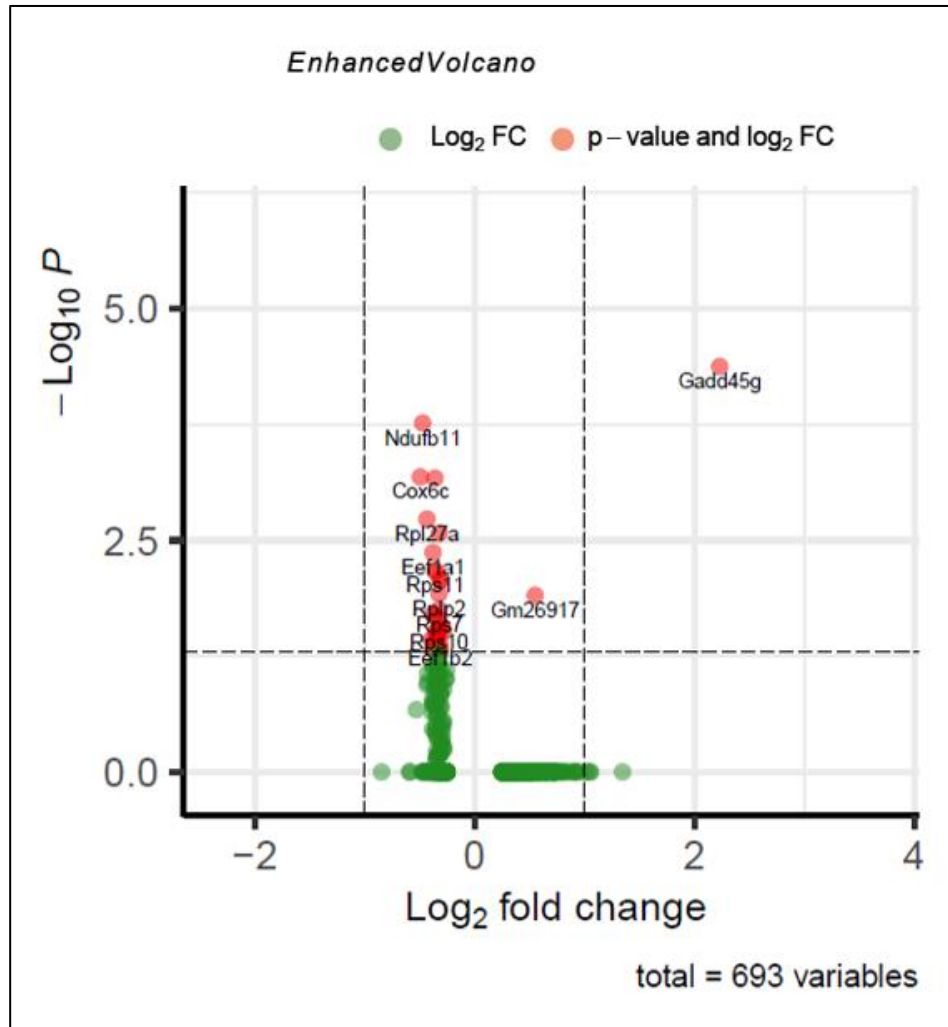


**Figure 4.5: Differential expression of cellular genes between infected and uninfected cells**

Volcano plot showing the differential expression of host genes in FusOn-H3 infected and uninfected cells. The genes indicated in red have a p value < 0.05.

#### **4.3.4 Oncolytic HSV infection of immune cells**

Next, we looked at the possibility of FusOn-H3 infecting non-malignant or immune cells. From the UMAP plot, predominantly, the infected cells are scattered over the tumor cell cluster. However, there is a small number of cells, almost negligible, within the immune cell cluster that appear to be infected. Further, classifying the cells into distinct cell populations, we looked at the expression of the viral genes across all cell clusters. From the analysis, we have observed that a small fraction of macrophages are infected with the virus, with some of the immediate, early and late gene expression detectable in these infected macrophages. None of the other immune cell subsets are infected with the virus, with no detectable levels of viral genes. On the other hand, these cells may have been exposed to the virus and we were able to notice expression of some key anti-viral genes. Although there are anti-viral responses generated by the immune cells in the TME, FusOn-H3 was able to infect and invade the tumor tissue efficiently.

This data suggests that FusOn-H3 can specifically target tumor cells (malignant cells alone) and not infecting neighboring non-malignant or immune cells. From our previous studies, we have reported that FusOn-H3 can infiltrate immune cells into the tumor microenvironment, including but not limited to T cells, B cells, macrophages, and Neutrophils. Therefore, FusOn-H3 can safely be used in the clinic in combination with other immune therapeutics, taking advantage of the infiltrated immune cells into the

tumor at the same time have no influence on the infection of immune cells by FusOn-H3.

**Table 4.1: Immediate early ( $\alpha$ ), early ( $\beta$ ), and late ( $\gamma$ ) HSV gene expression**

HSV gene expression	Gene	Protein
Immediate early ( $\alpha$ )	RL2	ICP0
	RS1	ICP4
	UL54	ICP27
	US1	ICP22
	US12	ICP47
Early ( $\beta$ )	UL23	TK
	UL29	ICP8
	UL50	dUTPase
	UL2	Uracil Deoxyglycosylase
Late ( $\gamma$ )	UL48	VP16
	UL19	VP5
	US6	gD
	UL27	gB
	UL53	gK
	UL44	gC
	UL41	vhs

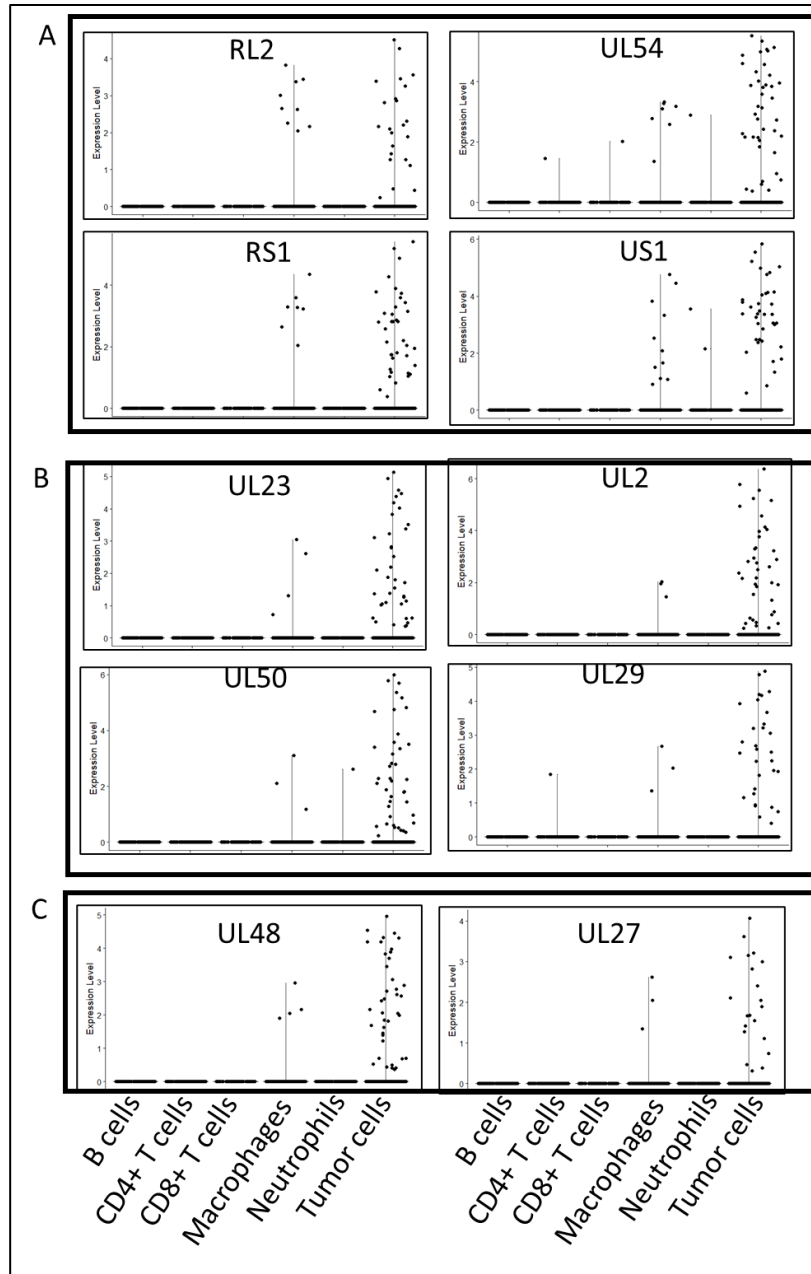


**Figure 4.6: FusOn-H3 specifically infects tumor cells sparing other cells in the TME**

Violin plots showing the expression of viral genes as per cell type (A- immediate early genes; B-early genes; C-late genes). In a standard workflow on Seurat-v2, the expression level on y-axis in the violin plots represents the Log2 transformed value

(readcount+1). A higher expression level represents more read count (or percentage, as it is scaled by total read count).

#### 4.3.5 CellChat analysis

In addition to the immunological changes in the tumor microenvironment induced by FusOn-H3 treatment described in Chapter 1 of this dissertation, and in this chapter, we show the transcriptional changes in the host cells and the activation of host's immune response both antiviral and anti-tumoral induced upon infection with FusOn-H3. It is expected that these changes can result in the alteration of the complex intercellular communication networks among these infected and uninfected tumor cells. We used CellChat prediction to compare the number of interactions and the interaction strength among different cell populations in infected and uninfected treatment groups (**Figure 4.7A**). The analysis revealed an increase although not significant in the total number of interactions and the interaction strength in the FusOn-H3 infected and uninfected cells. The predicted interaction details of the infected (**Figure 4.7D**) and the uninfected cells (**Figure 4.7D**) with the neighboring immune cells in the TME from which it is inferred that cells infected with the FusOn-H3 generally displayed a higher level of connectivity and an increased number of interactions between various cell types. In particular, the infected cells communicated with the immune cells including B cells, CD4<sup>+</sup> T cells, CD8<sup>+</sup> T cells, dendritic cells, and macrophages also with the non-immune cells (uninfected tumor cells). The intensive interaction between the infected cells with both the innate and adaptive immune cells is particularly interesting, as it is known that these

two immune components need to act coordinately for efficient generation of an effective immunity against infection or malignancy.<sup>195</sup>

Next, we compiled the information flow (i.e., the overall communication probability across the two datasets, infected vs. uninfected). This network analysis predicts the information flow for a given signaling pathway that is defined by the sum of communication probability among all pairs of cell groups in the inferred network. Intriguingly, 41 out of 77 pathways were found highly active, albeit at different levels, in the FusOn treated group (**Figure 4.7C**). Among those pathways that represented significantly enhanced information flow upon FusOn infected cells compared to the uninfected cells is Interleukin-1 family, which is a group of 11 cytokines (IL-1 $\alpha$ , IL-1 $\beta$ , IL-1R $\alpha$ , IL-18, IL-33, IL-15, IL-36 $\alpha$ , IL-36 $\beta$ , IL-37, IL-38, and IL-36R $\alpha$ ) that collectively play a central role in the regulation of immune and inflammatory responses to infections.<sup>246</sup> IL-1 family members also have important functions in activating and reinforcing the function of polarized T cells. For example, IL-18 mainly affects T helper 1 cells (T<sub>H</sub>1 cells), whereas, IL-33 affects T<sub>H</sub>2 cells and IL-1 has a key role in T<sub>H</sub>17 cell differentiation and maintenance.

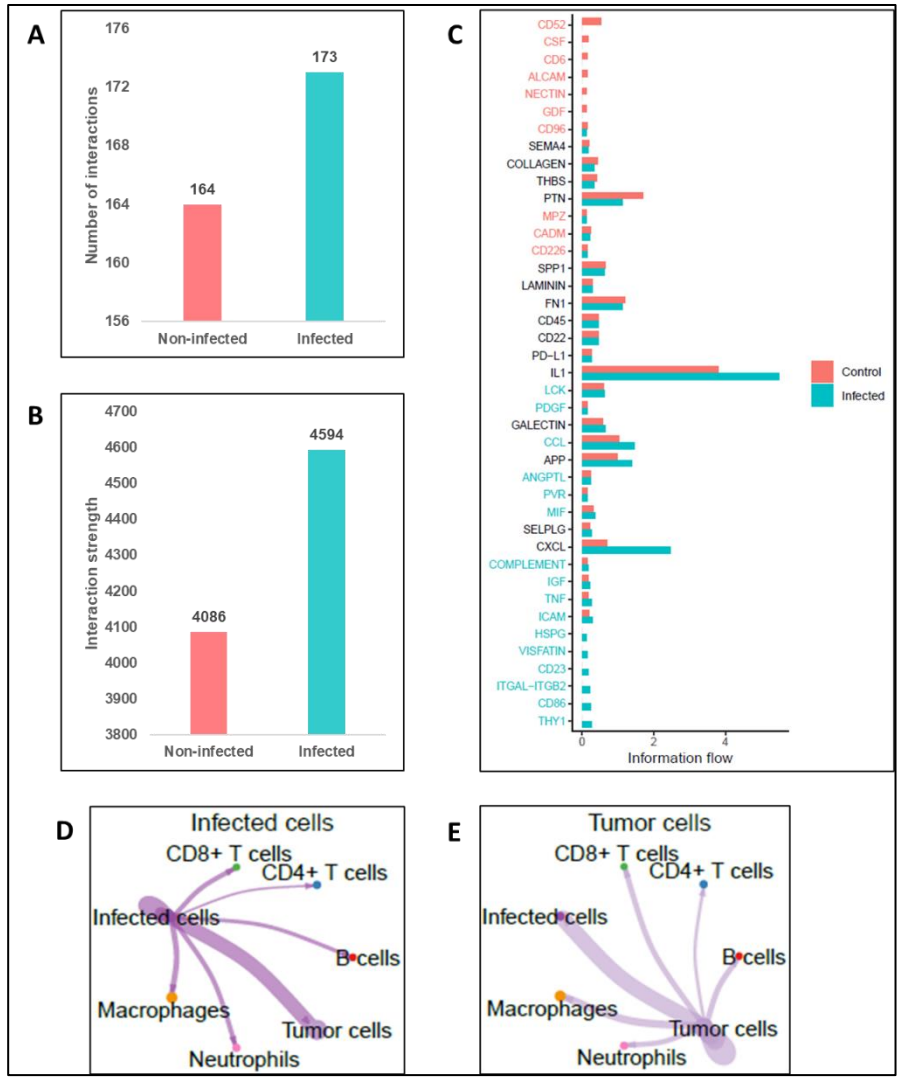


**Figure 4.7: Cell-to-cell communications among the infected and uninfected cells with the cells in the TME**

Bar plot showing the total number of interactions (A) and the interaction strength (B) of the inferred cell-cell communication networks from the infected and uninfected cells. C. the signaling pathway networks that are strongly active in either group based on the differences in the overall information flow as predicted by Cellchat. Summary chord plots showing the interactions from the infected tumor cells (D) and the uninfected tumor cells (E) with the immune cells.

#### 4.4 Discussion

In this study, we used scRNA sequencing to simultaneously study the viral and host transcriptomics in the same single cell. We find that single cells that are infected with the virus show variability across all stages of infection, with successful initiation of infection and the cellular response of the host cells. Such heterogeneity in the population of infected cells is determinantal in providing new insights into the host response against oncolytic viral infection. This property is particularly important to reconstruct the host response against the targeted tumor. From the differential analysis of host genes in response to viral infection, seemed to favor FusOn-H3 replication, spread and its capacity to induce host's immune responses. The role of these genes in the generation of anti-tumor immunity will need to be explored.

We also report the initiation of anti-viral program in both FusOn-H3 infected and uninfected cells in the TME, as revealed by increased expression of IFN $\gamma$  genes, ISGs and IFITs. Zamarin et al., 2014<sup>50</sup> found that infection with an oncolytic NDV stimulated uniform upregulation of MHC-I among infected and non-infected tumor cells. This was likely caused by increased type I IFNs, which are known to regulate MHC-I expression and were released by tumor cells infected by the same NDV.<sup>50</sup> A similar mechanism was observed in a murine lung cancer model treated with an adenovirus armed with an IFN $\beta$  transgene. IFN $\beta$  expression was shown to upregulate MHC-I expression in this tumor cell line. This alteration of the tumor cells was required for CTL-mediated tumor rejection.<sup>51</sup> These two studies suggest that the ability of IFN $\beta$  to upregulate MHC-I make it a promising tool to increase the immunogenicity of tumor cells in the context

of virotherapy.<sup>50</sup> Our findings in this study are in agreement with these studies, validating the role of FusOn-H3 in promoting antigen presentation, resulting in generation of anti-tumor immunity.

This chapter is a result of some preliminary analysis to characterize the infection of tumor cells within the TME. However, in-depth analysis will have to be conducted to dissect the anti-viral and anti-tumor properties of FusOn-H3.

## **4.5 Supporting information**

### **4.5.1 scRNA sequencing raw and meta data**

The raw data files and the processed data files will be uploaded on GEO website.

#### 4.5.2 Additional figures

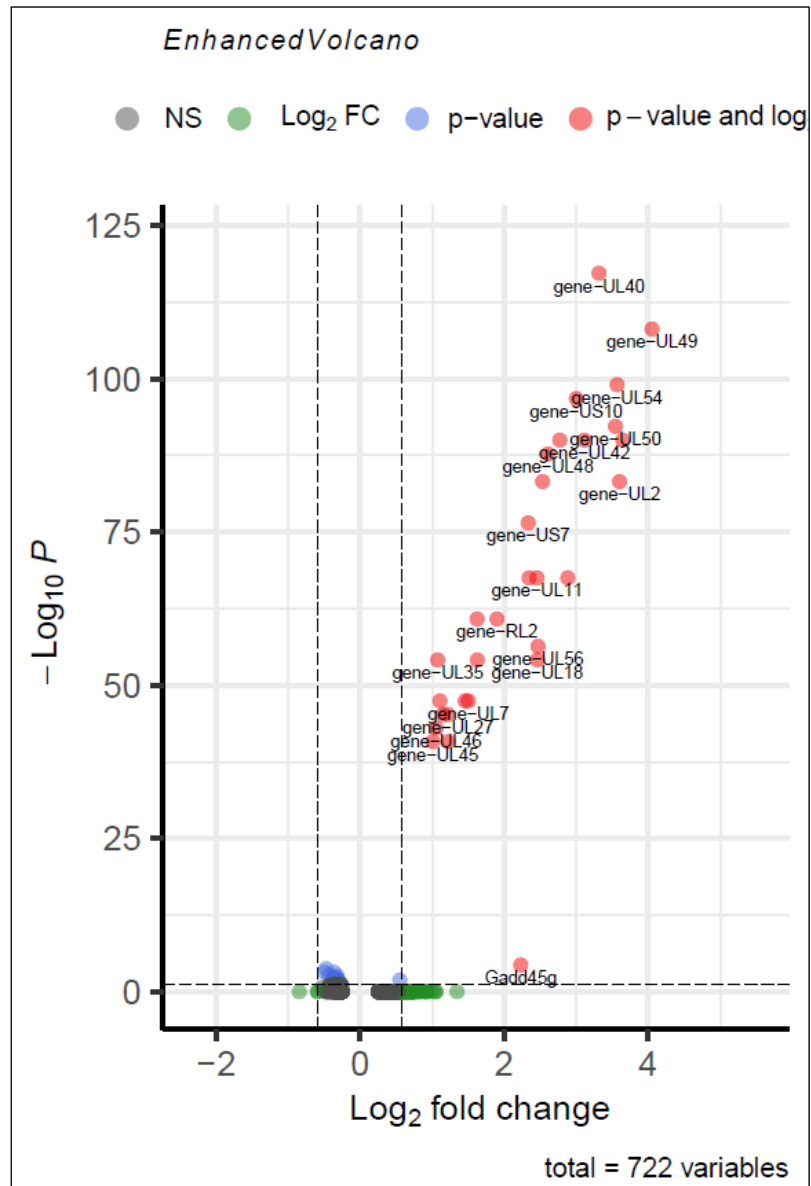


**Figure 4.8: Differential expression of viral genes between infected and uninfected cells**

Volcano plots showing the expression of viral genes in the infected cells. the genes denoted in red have a p value < 0.05.

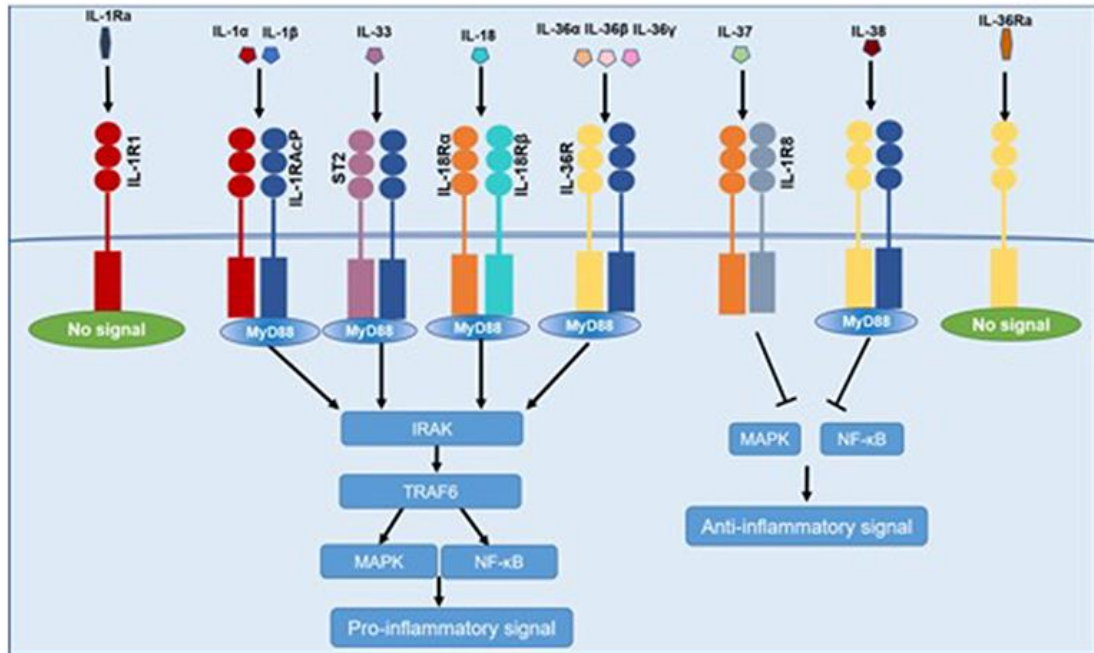


**Figure 4.9: Common signaling pathways for IL-1 family of cytokines**

IL-1 $\alpha$ , IL-1 $\beta$ , IL-18, IL-33, and IL-36 bind to IL-1R family members, and recruit MyD88 along with IRAK4, TRAF6, resulting in the activation of NF- $\kappa$ B and MAPK. This activation promotes the transcription of other inflammatory genes. IL-37 and IL-38 exert anti-inflammatory effects by inhibiting NF- $\kappa$ B and MAPK signaling. IL-1Ra and IL-36 Ra cannot recruit the signaling chain. (Reproduced from <sup>247</sup>. **Copyright** © 2019 Xu, Mu and Wei).

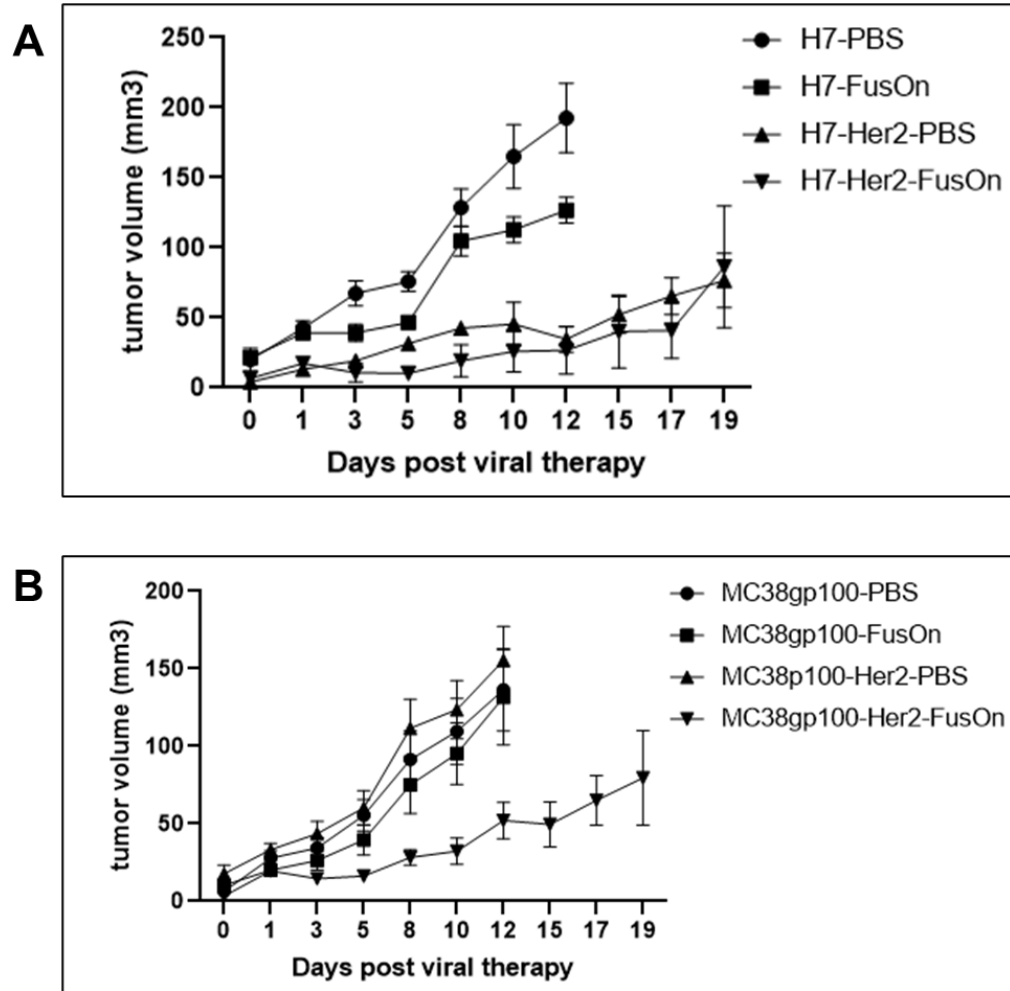


**Figure 4.10: Therapeutic impact of FusOn-H3 in two mouse tumor models**

BALB/C mice (n= 5) bearing either H7, H7-Her2 and MC38gp100, MC38gp100Her2 subcutaneous tumors of approx..6-8 mm, were randomly grouped and treated with  $5 \times 10^6$  pfu FusOn-H3 per mice. PBS group served as a negative control. **A.** Tumor growth curve after virotherapy. \* $p < 0.05$  as compared with the PBS control and FusOn-H3 treatment in the H7 group. **C.** Tumor growth curve after virotherapy. \* $p < 0.05$  as compared with the PBS control and FusOn-H3 treatment in the MC38gp100 group.

## 5 FUTURE DIRECTIONS

As described in Chapter 1 of this dissertation, both BiCEP and TriCEP were delivered by HSV amplicon vector, and due to which we were unable to evaluate the effect of these two engaging molecules without the presence of virus. In addition to the above limitation, the underlying reason for the moderate effect of the engager molecules in vitro and the relatively modest antitumor effect detected in the in vivo experiment is probably also due to a low transgene expression. This is because the amplicon (which carries the transgene of BiCEP and TriCEP) only constitutes about 10% of the total viral titer. We are currently in the process of inserting TriCEP into the backbone of the oncolytic HSV (FusOn-H3) for clinical development. This will ensure that 100% of the virus will produce this gene product, which will likely lead to a significantly better therapeutic effect.

The alternate method would be to deliver BiCEP and TriCEP in the form of either DNA or mRNA. mRNA based therapeutics have become the focus of immune-oncology and is currently explored for the treatment of cancer. For a long time, invitro transcribed mRNA encoding tumor antigens was used for the development of cancer vaccines. However, the versatility of mRNA opened new avenues beyond this application. The smart design of mRNA, attributed to its structural properties and pharmaceutical formulation, improved in vivo stability and selective targeting makes it a powerful vector for in situ delivery of therapeutic proteins. Consequently, there is a growing interest in using mRNA for the development of many cancer therapeutics. Therefore, efforts are currently made in the lab to design mRNA encoding the Bispecific and the

Trispecific engagers for in vivo delivery, Using this approach, we can investigate the efficacy of the chimeric engagers independent of the anti-tumor activity of the oncolytic virus and the amplicon.

Although EGFR is a good therapeutic target for an immune engager such as the BiCEP and TriCEP, it is also widely expressed on many normal tissues, which poses a risk of potential on-target off-tumor toxicity. In this study, we tried to restrict the expression of transgene to the tumor site by using HSV amplicon and an oncolytic virus. However, the design of the chimeric engagers offers flexibility, where we can easily replace the EGF ligand moiety with any other gene encoding a ligand specific for other tumor antigens e.g., Her2 and PSCA. As such, we can make a cocktail of engagers targeting multiple tumor antigens at the same time. This approach is highly favorable with the mRNA technology, where an mRNA cocktail encoding various engagers can easily be formulated and delivered in vivo.

We aim to conduct adequate testing to prove the efficacy of these molecules in the pre-clinical studies and may potentially be investigated in the clinic.

\*\*\*\*\*

## 6 BIBLIOGRAPHY

1. Parato KA, Senger D, Forsyth PAJ, Bell JC. Recent progress in the battle between oncolytic viruses and tumours. *NATURE REVIEWS CANCER* 2005;5(12):965-76.
2. Twumasi-Boateng K, Pettigrew JL, Kwok YYY, Bell JC, Nelson BH. Oncolytic viruses as engineering platforms for combination immunotherapy. *NATURE REVIEWS CANCER* 2018;18(7):419-32.
3. Kaufman HL, Kohlhapp FJ, Zloza A. Oncolytic viruses: A new class of immunotherapy drugs. *NATURE REVIEWS DRUG DISCOVERY* 2015;14(9):642-62.
4. Pikor LA, Bell JC, Diallo J-S. Oncolytic viruses: Exploiting cancer's deal with the devil. *TRENDS IN CANCER* 2015;1(4):266-77.
5. De Munck J, Binks A, McNeish IA, Aerts JL. Oncolytic virus-induced cell death and immunity: A match made in heaven? *JOURNAL OF LEUKOCYTE BIOLOGY* 2017;102(3):631-43.
6. Aurelian L. Oncolytic viruses as immunotherapy: Progress and remaining challenges. *ONCOTARGETS AND THERAPY* 2016;9:2627.
7. Upton JW, Chan FK-M. Staying alive: Cell death in antiviral immunity. *MOLECULAR CELL* 2014;54(2):273-80.
8. Bartlett DL, Liu Z, Sathaiah M, Ravindranathan R, Guo Z, et al. Oncolytic viruses as therapeutic cancer vaccines. *MOLECULAR CANCER* 2013;12(1):103.
9. Aghi M, Martuza RL. Oncolytic viral therapies – the clinical experience. *ONCOGENE* 2005;24(52):7802-16.
10. Johnson DB, Puzanov I, Kelley MC. Talimogene laherparepvec (t-vec) for the treatment of advanced melanoma. *IMMUNOTHERAPY* 2015;7(6):611-19.
11. Larocca CJ, Warner SG. Oncolytic viruses and checkpoint inhibitors: Combination therapy in clinical trials. *CLINICAL AND TRANSLATIONAL MEDICINE* 2018;7(1):35.
12. Zhang SX. Turning killer into cure—the story of oncolytic herpes simplex viruses. *DISCOVERY MEDICINE* 2015;20(111):303-09.
13. Bolovan CA, Sawtell NM, Thompson RL. Icp34.5 mutants of herpes simplex virus type 1 strain 17syn+ are attenuated for neurovirulence in mice and for replication in confluent primary mouse embryo cell cultures. *JOURNAL OF VIROLOGY* 1994;68(1):48-55.
14. McKie E, MacLean A, Lewis A, Cruickshank G, Rampling R, et al. Selective in vitro replication of herpes simplex virus type 1 (hsv-1) icp34.5 null mutants in primary human

cns tumours - evaluation of a potentially effective clinical therapy. BRITISH JOURNAL OF CANCER 1996;74(5):745-52.

15. Agarwalla PK, Aghi MK. Oncolytic herpes simplex virus engineering and preparation: Humana Press 2012:1-19.
16. Aghi M, Visted T, Depinho RA, Chiocca EA. Oncolytic herpes virus with defective icp6 specifically replicates in quiescent cells with homozygous genetic mutations in p16. ONCOGENE 2008;27(30):4249-54.
17. Chase M, Chung RY, Chiocca EA. An oncolytic viral mutant that delivers the cyp2b1 transgene and augments cyclophosphamide chemotherapy. NATURE BIOTECHNOLOGY 1998;16(5):444-48.
18. Liu BL, Robinson M, Han Z-Q, Branston RH, English C, et al. Icp34.5 deleted herpes simplex virus with enhanced oncolytic, immune stimulating, and anti-tumour properties. GENE THERAPY 2003;10(4):292-303.
19. Nakamori M, Fu X, Pettaway CA, Zhang X. Potent antitumor activity after systemic delivery of a doubly fusogenic oncolytic herpes simplex virus against metastatic prostate cancer. THE PROSTATE 2004;60(1):53-60.
20. Farrell KB, Tusnady GE, Eiden MV. New structural arrangement of the extracellular regions of the phosphate transporter slc20a1, the receptor for gibbon ape leukemia virus. JOURNAL OF BIOLOGICAL CHEMISTRY 2009;284(43):29979-87.
21. Nakamori M, Fu X, Meng F, Jin A, Tao L, et al. Effective therapy of metastatic ovarian cancer with an oncolytic herpes simplex virus incorporating two membrane fusion mechanisms. CLINICAL CANCER RESEARCH 2003;9(7):2727-33.
22. Fu X, Nakamori M, Tao L, Amato R, Zhang X. Antitumor effects of two newly constructed oncolytic herpes simplex viruses against renal cell carcinoma. INTERNATIONAL JOURNAL OF ONCOLOGY 2007
23. Smith CC, Nelson J, Aurelian L, Gober M, Goswami BB. Ras-gap binding and phosphorylation by herpes simplex virus type 2 rr1 pk (icp10) and activation of the ras/mek/mapk mitogenic pathway are required for timely onset of virus growth. JOURNAL OF VIROLOGY 2000;74(22):10417-29.
24. Fu X, Tao L, Cai R, Prigge J, Zhang X. A mutant type 2 herpes simplex virus deleted for the protein kinase domain of the icp10 gene is a potent oncolytic virus. MOLECULAR THERAPY 2006;13(5):882-90.
25. Li H, Dutuor A, Fu X, Zhang X. Induction of strong antitumor immunity by an hsv-2-based oncolytic virus in a murine mammary tumor model. THE JOURNAL OF GENE MEDICINE 2007;9(3):161-69.

26. Fu X, Tao L, Li M, Fisher WE, Zhang X. Effective treatment of pancreatic cancer xenografts with a conditionally replicating virus derived from type 2 herpes simplex virus. *CLINICAL CANCER RESEARCH* 2006;12(10):3152-57.
27. Fu X, Tao L, Zhang X. An oncolytic virus derived from type 2 herpes simplex virus has potent therapeutic effect against metastatic ovarian cancer. *CANCER GENE THERAPY* 2007;14(5):480-87.
28. Fu X, Nakamori M, Tao L, Amato R, Zhang X. Antitumor effects of two newly constructed oncolytic herpes simplex viruses against renal cell carcinoma. *INTERNATIONAL JOURNAL OF ONCOLOGY* 2007;30(6):1561-7.
29. Fu X, Rivera A, Tao L, Zhang X. An hsv-2 based oncolytic virus can function as an attractant to guide migration of adoptively transferred t cells to tumor sites. *ONCOTARGET* 2015;6(2):902-14.
30. Fu X, Wang H, Zhang X. High-frequency intermolecular homologous recombination during herpes simplex virus-mediated plasmid DNA replication. *JOURNAL OF VIROLOGY* 2002;76(12):5866-74.
31. Yu D-C, Chen Y, Seng M, Dilley J, Henderson DR. The addition of adenovirus type 5 region e3 enables calydon virus 787 to eliminate distant prostate tumor xenografts. *CANCER RESEARCH* 1999;59(17):4200-03.
32. Epstein AL. Hsv-1-derived amplicon vectors: Recent technological improvements and remaining difficulties - a review. *MEMÓRIAS DO INSTITUTO OSWALDO CRUZ* 2009;104(3):399-410.
33. Wang H, Fu X, Zhang X. Isomerization of a uniquely designed amplicon during herpes simplex virus-mediated replication. *JOURNAL OF VIROLOGY* 2001;75(21):10505-10.
34. Boehmer PE, Lehman IR. Herpes simplex virus DNA replication. *ANNUAL REVIEW OF BIOCHEMISTRY* 1997;66(1):347-84.
35. Kwong AD, Frenkel N. Herpes simplex virus amplicon: Effect of size on replication of constructed defective genomes containing eucaryotic DNA sequences. *JOURNAL OF VIROLOGY* 1984;51(3):595-603.
36. D'Angelica M, Karpoff H, Halterman M, Ellis J, Klimstra D, et al. In vivo interleukin-2 gene therapy of established tumors with herpes simplex amplicon vectors. *CANCER IMMUNOLOGY, IMMUNOTHERAPY* 1999;47(5):265-71.
37. Zibert A, Thomassen A, Müller L, Nguyen L, Glouchkova L, et al. Herpes simplex virus type-1 amplicon vectors for vaccine generation in acute lymphoblastic leukemia. *GENE THERAPY* 2005;12(23):1707-17.

38. Carew JF, Federoff H, Halterman M, Kraus DH, Savage H, et al. Efficient gene transfer to human squamous cell carcinomas by the herpes simplex virus type 1 amplicon vector. *THE AMERICAN JOURNAL OF SURGERY* 1998;176(5):404-08.
39. Rock KL, York IA, Saric T, Goldberg AL. Protein degradation and the generation of mhc class i-presented peptides. *ADVANCES IN IMMUNOLOGY* 2002;80:1-70.
40. Le Bon A, Etchart N, Rossmann C, Ashton M, Hou S, et al. Cross-priming of cd8+ t cells stimulated by virus-induced type i interferon. *NATURE IMMUNOLOGY* 2003;4(10):1009-15.
41. Russell SJ, Peng KW. Viruses as anticancer drugs. *TRENDS IN PHARMACOLOGICAL SCIENCES* 2007;28(7):326-33
42. Farassati F, Pan W, Yamoutpour F, Henke S, Piedra M, et al. Ras signaling influences permissiveness of malignant peripheral nerve sheath tumor cells to oncolytic herpes. *THE AMERICAN JOURNAL OF PATHOLOGY* 2008;173(6):1861-72.
43. Andtbacka RH, Kaufman HL, Collichio F, Amatruda T, Senzer N, et al. Talimogene laherparepvec improves durable response rate in patients with advanced melanoma. *J CLINICAL ONCOLOGY* 2015;33(25):2780-8.
44. Prestwich RJ, Errington F, Ilett EJ, Morgan RS, Scott KJ, et al. Tumor infection by oncolytic reovirus primes adaptive antitumor immunity. *CLINICAL CANCER RESEARCH : AN OFFICIAL JOURNAL OF THE AMERICAN ASSOCIATION FOR CANCER RESEARCH* 2008;14(22):7358-66.
45. Han Z, Assenberg M, Liu B, Wang Y, Simpson G, et al. Development of a second-generation oncolytic herpes simplex virus expressing tnfalpha for cancer therapy. *THE JOURNAL OF GENE MEDICINE* 2007;9(2):99-106.
46. Kloetzel PM. Generation of major histocompatibility complex class i antigens: Functional interplay between proteasomes and tppii. *NATURE IMMUNOLOGY* 2004;5(7):661-69.
47. Gujar S, Dielschneider R, Clements D, Helson E, Shmulevitz M, et al. Multifaceted therapeutic targeting of ovarian peritoneal carcinomatosis through virus-induced immunomodulation. *MOLECULAR THERAPY : THE JOURNAL OF THE AMERICAN SOCIETY OF GENE THERAPY* 2013;21(2):338-47.
48. Endo Y, Sakai R, Ouchi M, Onimatsu H, Hioki M, et al. Virus-mediated oncolysis induces danger signal and stimulates cytotoxic t-lymphocyte activity via proteasome activator upregulation. *ONCOGENE* 2008;27(17):2375-81.
49. Sun Y, Sijts AJ, Song M, Janek K, Nussbaum AK, et al. Expression of the proteasome activator pa28 rescues the presentation of a cytotoxic t lymphocyte epitope on melanoma cells. *CANCER RESEARCH* 2002;62(10):2875-82.

50. Zamarin D, Holmgaard RB, Subudhi SK, Park JS, Mansour M, et al. Localized oncolytic virotherapy overcomes systemic tumor resistance to immune checkpoint blockade immunotherapy. *SCI TRANSL MED* 2014;6(226):226ra32.
51. Wilderman MJ, Sun J, Jassar AS, Kapoor V, Khan M, et al. Intrapulmonary ifn-beta gene therapy using an adenoviral vector is highly effective in a murine orthotopic model of bronchogenic adenocarcinoma of the lung. *CANCER RESEARCH* 2005;65(18):8379-87.
52. Hill A, Jugovic P, York I, Russ G, Bennink J, et al. Herpes simplex virus turns off the tap to evade host immunity. *NATURE* 1995;375(6530):411-15.
53. Delamarre L, Mellman I. Harnessing dendritic cells for immunotherapy. *SEMINARS IN IMMUNOLOGY* 2011;23(1):2-11.
54. Blander JM. Regulation of the cell biology of antigen cross-presentation. *ANNUAL REVIEW OF IMMUNOLOGY* 2018;36:717-53.
55. Diamond MS, Kinder M, Matsushita H, Mashayekhi M, Dunn GP, et al. Type i interferon is selectively required by dendritic cells for immune rejection of tumors. *THE JOURNAL OF EXPERIMENTAL MEDICINE* 2011;208(10):1989-2003.
56. Fuertes MB, Kacha AK, Kline J, Woo SR, Kranz DM, et al. Host type i ifn signals are required for antitumor cd8+ t cell responses through cd8{alpha}+ dendritic cells. *THE JOURNAL OF EXPERIMENTAL MEDICINE* 2011;208(10):2005-16.
57. Caminschi I, Lahoud MH, Shortman K. Enhancing immune responses by targeting antigen to dc. *EUROPEAN JOURNAL OF IMMUNOLOGY* 2009;39(4):931-38.
58. Parlato S, Romagnoli G, Spadaro F, Canini I, Sirabella P, et al. Lox-1 as a natural ifn-alpha-mediated signal for apoptotic cell uptake and antigen presentation in dendritic cells. *BLOOD* 2010;115(8):1554-63.
59. Burke S, Shergold A, Elder MJ, Whitworth J, Cheng X, et al. Oncolytic newcastle disease virus activation of the innate immune response and priming of antitumor adaptive responses in vitro. *CANCER IMMUNOLOGY, IMMUNOTHERAPY : CII* 2020;69(6):1015-27.
60. Wang LC, Lynn RC, Cheng G, Alexander E, Kapoor V, et al. Treating tumors with a vaccinia virus expressing ifn $\beta$  illustrates the complex relationships between oncolytic ability and immunogenicity. *MOLECULAR THERAPY : THE JOURNAL OF THE AMERICAN SOCIETY OF GENE THERAPY* 2012;20(4):736-48.
61. García-Romero N, Palacín-Aliana I, Esteban-Rubio S, Madurga R, Rius-Rocabert S, et al. Newcastle disease virus (ndv) oncolytic activity in human glioma tumors is dependent on cdkn2a-type i ifn gene cluster codeletion. *CELLS* 2020;9(6):1405.

62. Greter M, Helft J, Chow A, Hashimoto D, Mortha A, et al. Gm-csf controls nonlymphoid tissue dendritic cell homeostasis but is dispensable for the differentiation of inflammatory dendritic cells. *IMMUNITY* 2012;36(6):1031-46.
63. Choi IK, Lee JS, Zhang SN, Park J, Lee K-M, et al. Oncolytic adenovirus co-expressing il-12 and il-18 improves tumor-specific immunity via differentiation of t cells expressing il-12r $\beta$  2 or il-18 $\alpha$ . *GENE THERAPY* 2011;18(9):898-909.
64. Cerullo V, Pesonen S, Diaconu I, Escutenaire S, Arstila PT, et al. Oncolytic adenovirus coding for granulocyte macrophage colony-stimulating factor induces antitumoral immunity in cancer patients. *CANCER RESEARCH* 2010;70:4297-309.
65. Deng L, Yang X, Fan J, Ding Y, Peng Y, et al. Il-24-armed oncolytic vaccinia virus exerts potent antitumor effects via multiple pathways in colorectal cancer. *ONCOLOGY RESEARCH* 2020; 16;28(6):579-590
66. Bollino D, Colunga A, Li B, Aurelian L.  $\Delta$ pk oncolytic activity includes modulation of the tumour cell milieu. *THE JOURNAL OF GENERAL VIROLOGY* 2016;97(2):496-508.
67. Hou W, Zhang Q, Yan Z, Chen R, Zeh Iii HJ, et al. Strange attractors: Damps and autophagy link tumor cell death and immunity. *CELL DEATH & DISEASE* 2013;4(12):e966.
68. Kepp O, Senovilla L, Vitale I, Vacchelli E, Adjemian S, et al. Consensus guidelines for the detection of immunogenic cell death. *ONCOIMMUNOLOGY* 2014;3(9):e955691.
69. Gaston DC, Odom CI, Li L, Markert JM, Roth JC, et al. Production of bioactive soluble interleukin-15 in complex with interleukin-15 receptor alpha from a conditionally-replicating oncolytic hsv-1. *PLOS ONE* 2013;8(11):e81768.
70. Ghiringhelli F, Apetoh L, Tesniere A, Aymeric L, Ma Y, et al. Activation of the nlrp3 inflammasome in dendritic cells induces il-1 $\beta$ -dependent adaptive immunity against tumors. *NATURE MEDICINE* 2009;15(10):1170-78.
71. Saenz R, Futralan D, Leutenez L, Eekhout F, Fecteau JF, et al. Tlr4-dependent activation of dendritic cells by an hmgb1-derived peptide adjuvant. *JOURNAL OF TRANSLATIONAL MEDICINE* 2014;12:211.
72. Berwin B, Delneste Y, Lovingood RV, Post SR, Pizzo SV. Srec-i, a type f scavenger receptor, is an endocytic receptor for calreticulin. *THE JOURNAL OF BIOLOGICAL CHEMISTRY* 2004;279(49):51250-57.
73. Miyamoto S, Inoue H, Nakamura T, Yamada M, Sakamoto C, et al. Coxsackievirus b3 is an oncolytic virus with immunostimulatory properties that is active against lung adenocarcinoma. *CANCER RESEARCH* 2012;72(10):2609-21.

74. Di Somma S, Iannuzzi CA, Passaro C, Forte IM, Iannone R, et al. The oncolytic virus dl 922-947 triggers immunogenic cell death in mesothelioma and reduces xenograft growth. *FRONTIERS IN ONCOLOGY* 2019;9:564.
75. Hong B, Muili K, Bolyard C, Russell L, Lee T, et al. Suppression of hmgb1 released in the glioblastoma tumor microenvironment reduces tumoral edema. *MOLECULAR THERAPY ONCOLYTICS* 2018;12:93-102.
76. Russell L, Swanner J, Jaime-Ramirez A, Wang Y, Sprague A, et al. Pten expression by an oncolytic herpesvirus directs t-cell mediated tumor clearance. *NATURE COMMUNICATIONS* 2018;9(1):5006.
77. Huang XF, Ren W, Rollins L, Pittman P, Shah M, et al. A broadly applicable, personalized heat shock protein-mediated oncolytic tumor vaccine. *CANCER RESEARCH* 2003;63(21):7321-29.
78. Delneste Y, Magistrelli G, Gauchat J, Haeuw J, Aubry J, et al. Involvement of lox-1 in dendritic cell-mediated antigen cross-presentation. *IMMUNITY* 2002;17(3):353-62.
79. Bai FL, Yu YH, Tian H, Ren GP, Wang H, et al. Genetically engineered newcastle disease virus expressing interleukin-2 and tnf-related apoptosis-inducing ligand for cancer therapy. *CANCER BIOLOGY & THERAPY* 2014;15(9):1226-38.
80. Xu C, Sun Y, Wang Y, Yan Y, Shi Z, et al. Cea promoter-regulated oncolytic adenovirus-mediated hsp70 expression in immune gene therapy for pancreatic cancer. *CANCER LETTERS* 2012;319(2):154-63.
81. Schmitt E, Gehrman M, Brunet M, Multhoff G, Garrido C. Intracellular and extracellular functions of heat shock proteins: Repercussions in cancer therapy. *JOURNAL OF LEUKOCYTE BIOLOGY* 2007;81(1):15-27.
82. Eisenberg D, Carpenter S, Adusumilli P, Chan M, Hendershott K, et al. Hyperthermia potentiates oncolytic herpes viral killing of pancreatic cancer through a heat shock protein pathway. *SURGERY* 2010;148(2):325-34.
83. Burch A, Weller S. Herpes simplex virus type 1 DNA polymerase requires the mammalian chaperone hsp90 for proper localization to the nucleus. *JOURNAL OF VIROLOGY* 2005;79(16):10740-49.
84. Yoo J, Hurwitz B, Bolyard C, Yu J, Zhang J, et al. Bortezomib-induced unfolded protein response increases oncolytic hsv-1 replication resulting in synergistic antitumor effects. *CLINICAL CANCER RESEARCH* 2014;20(14):3787-98.
85. Andarini S, Kikuchi T, Nukiwa M, Pradono P, Suzuki T, et al. Adenovirus vector-mediated in vivo gene transfer of ox40 ligand to tumor cells enhances antitumor immunity of tumor-bearing hosts. *CANCER RESEARCH* 2004;64(9):3281-7.

86. Townsend SE, Allison JP. Tumor rejection after direct costimulation of cd8+ t cells by b7-transfected melanoma cells. *SCIENCE (NEW YORK, NY)* 1993;259(5093):368-70.
87. Rivera-Molina Y, Jiang H, Fueyo J, Nguyen T, Shin DH, et al. Gitr1-armed delta-24-rgd oncolytic adenovirus prolongs survival and induces anti-glioma immune memory. *NEURO-ONCOLOGY ADVANCES* 2019;1(1):vdz009.
88. Ino Y, Saeki Y, Fukuhara H, Todo T. Triple combination of oncolytic herpes simplex virus-1 vectors armed with interleukin-12, interleukin-18, or soluble b7-1 results in enhanced antitumor efficacy. *CLINICAL CANCER RESEARCH : AN OFFICIAL JOURNAL OF THE AMERICAN ASSOCIATION FOR CANCER RESEARCH* 2006;12(2):643-52.
89. Cohen AD, Diab A, Perales MA, Wolchok JD, Rizzuto G, et al. Agonist anti-gitr antibody enhances vaccine-induced cd8(+) t-cell responses and tumor immunity. *CANCER RESEARCH* 2006;66(9):4904-12.
90. Côté AL, Zhang P, O'Sullivan JA, Jacobs VL, Clemis CR, et al. Stimulation of the glucocorticoid-induced tnf receptor family-related receptor on cd8 t cells induces protective and high-avidity t cell responses to tumor-specific antigens. *JOURNAL OF IMMUNOLOGY (BALTIMORE, MD : 1950)* 2011;186(1):275-83.
91. Durham NM, Holowecky N, MacGill RS, McGlinchey K, Leow CC, et al. Gitr ligand fusion protein agonist enhances the tumor antigen-specific cd8 t-cell response and leads to long-lasting memory. *JOURNAL FOR IMMUNOTHERAPY OF CANCER* 2017;5:47.
92. Shuford WW, Klussman K, Tritchler DD, Loo DT, Chalupny J, et al. 4-1bb costimulatory signals preferentially induce cd8+ t cell proliferation and lead to the amplification in vivo of cytotoxic t cell responses. *THE JOURNAL OF EXPERIMENTAL MEDICINE* 1997;186(1):47-55.
93. Wen T, Bukczynski J, Watts TH. 4-1bb ligand-mediated costimulation of human t cells induces cd4 and cd8 t cell expansion, cytokine production, and the development of cytolytic effector function. *JOURNAL OF IMMUNOLOGY (BALTIMORE, MD : 1950)* 2002;168(10):4897-906.
94. Huang J-H, Zhang S-N, Choi K-J, Choi I-K, Kim J-H, et al. Therapeutic and tumor-specific immunity induced by combination of dendritic cells and oncolytic adenovirus expressing il-12 and 4-1bb. *MOLECULAR THERAPY* 2010;18(2):264-74.
95. Zamarin D, Holmgaard RB, Ricca J, Plitt T, Palese P, et al. Intratumoral modulation of the inducible co-stimulator icos by recombinant oncolytic virus promotes systemic anti-tumour immunity. *NATURE COMMUNICATIONS* 2017;8:14340.
96. Starbeck-Miller GR, Xue HH, Harty JT. Il-12 and type i interferon prolong the division of activated cd8 t cells by maintaining high-affinity il-2 signaling in vivo. *THE JOURNAL OF EXPERIMENTAL MEDICINE* 2014;211(1):105-20.

97. Keppler SJ, Rosenits K, Koegl T, Vucikujja S, Aichele P. Signal 3 cytokines as modulators of primary immune responses during infections: The interplay of type I IFN and IL-12 in CD8 T cell responses. *PLoS ONE* 2012;7(7):e40865.
98. Vigil A, Park MS, Martinez O, Chua MA, Xiao S, et al. Use of reverse genetics to enhance the oncolytic properties of Newcastle disease virus. *CANCER RESEARCH* 2007;67(17):8285-92.
99. Hellums EK, Markert JM, Parker JN, He B, Perbal B, et al. Increased efficacy of an interleukin-12-secreting herpes simplex virus in a syngeneic intracranial murine glioma model. *NEURO-ONCOLOGY* 2005;7(3):213-24.
100. Errington F, Steele L, Prestwich R, Harrington KJ, Pandha HS, et al. Reovirus activates human dendritic cells to promote innate antitumor immunity. *THE JOURNAL OF IMMUNOLOGY* 2008;180(9):6018-26.
101. Mathios D, Park CK, Marcus WD, Alter S, Rhode PR, et al. Therapeutic administration of IL-15 superagonist complex ALT-803 leads to long-term survival and durable antitumor immune response in a murine glioblastoma model. *INTERNATIONAL JOURNAL OF CANCER* 2016;138(1):187-94.
102. Stephenson KB, Barra NG, Davies E, Ashkar AA, Lichty BD. Expressing human interleukin-15 from oncolytic vesicular stomatitis virus improves survival in a murine metastatic colon adenocarcinoma model through the enhancement of anti-tumor immunity. *CANCER GENE THERAPY* 2012;19(4):238-46.
103. Kowalsky SJ, Liu Z, Feist M, Berkey SE, Ma C, et al. Superagonist IL-15-armed oncolytic virus elicits potent antitumor immunity and therapy that are enhanced with PD-1 blockade. *MOLECULAR THERAPY : THE JOURNAL OF THE AMERICAN SOCIETY OF GENE THERAPY* 2018;26(10):2476-86.
104. Brooks DG, Trifilo MJ, Edelmann KH, Teyton L, McGavern DB, et al. Interleukin-10 determines viral clearance or persistence in vivo. *NATURE MEDICINE* 2006;12(11):1301-09.
105. Chard LS, Lemoine NR, Wang Y. New role of interleukin-10 in enhancing the antitumor efficacy of oncolytic vaccinia virus for treatment of pancreatic cancer. *ONCOIMMUNOLOGY* 2015;4(9):e1038689.
106. Vicari AP, Chiodoni C, Vaure C, Ait-Yahia S, Dercamp C, et al. Reversal of tumor-induced dendritic cell paralysis by CpG immunostimulatory oligonucleotide and anti-interleukin 10 receptor antibody. *THE JOURNAL OF EXPERIMENTAL MEDICINE* 2002;196(4):541-49.
107. Kundu N, Beaty TL, Jackson MJ, Fulton AM. Antimetastatic and antitumor activities of interleukin 10 in a murine model of breast cancer. *JOURNAL OF THE NATIONAL CANCER INSTITUTE* 1996;88(8):536-41.

108. Emmerich J, Mumm JB, Chan IH, LaFace D, Truong H, et al. Il-10 directly activates and expands tumor-resident cd8(+) t cells without de novo infiltration from secondary lymphoid organs. *CANCER RESEARCH* 2012;72(14):3570-81.
109. Groom JR, Luster AD. Cxcr3 ligands: Redundant, collaborative and antagonistic functions. *IMMUNOLOGY AND CELL BIOLOGY* 2011;89(2):207-15.
110. Eckert EC, Nace RA, Tonne JM, Evgin L, Vile RG, et al. Generation of a tumor-specific chemokine gradient using oncolytic vesicular stomatitis virus encoding cxcl9. *MOLECULAR THERAPY ONCOLYTICS* 2019;16:63-74.
111. Benencia F, Courrèges MC, Conejo-García JR, Mohamed-Hadley A, Zhang L, et al. Hsv oncolytic therapy upregulates interferon-inducible chemokines and recruits immune effector cells in ovarian cancer. *MOLECULAR THERAPY* 2005;12(5):789-802.
112. Francis L, Guo ZS, Liu Z, Ravindranathan R, Urban JA, et al. Modulation of chemokines in the tumor microenvironment enhances oncolytic virotherapy for colorectal cancer. *ONCOTARGET* 2016;7(16):22174-85.
113. Fujisawa Y, Yoshino K, Otsuka A, Funakoshi T, Uchi H, et al. Retrospective study of advanced melanoma patients treated with ipilimumab after nivolumab: Analysis of 60 japanese patients. *JOURNAL OF DERMATOLOGICAL SCIENCE* 2018;89(1):60-66.
114. Iwashiro M, Messer RJ, Peterson KE, Stromnes IM, Sugie T, et al. Immunosuppression by cd4+ regulatory t cells induced by chronic retroviral infection. *PROCEEDINGS OF THE NATIONAL ACADEMY OF SCIENCES OF THE UNITED STATES OF AMERICA* 2001;98(16):9226-30.
115. Onizuka S, Tawara I, Shimizu J, Sakaguchi S, Fujita T, et al. Tumor rejection by in vivo administration of anti-cd25 (interleukin-2 receptor alpha) monoclonal antibody. *CANCER RESEARCH* 1999;59(13):3128-33.
116. Calmels B, Paul S, Futin N, Ledoux C, Stoeckel F, et al. Bypassing tumor-associated immune suppression with recombinant adenovirus constructs expressing membrane bound or secreted gitr-l. *CANCER GENE THERAPY* 2005;12(2):198-205.
117. Bartee MY, Dunlap KM, Bartee E. Tumor-localized secretion of soluble pd1 enhances oncolytic virotherapy. *CANCER RESEARCH* 2017;77(11):2952-63.
118. Liu Z, Ravindranathan R, Kalinski P, Guo ZS, Bartlett DL. Rational combination of oncolytic vaccinia virus and pd-1 blockade works synergistically to enhance therapeutic efficacy. *NATURE COMMUNICATIONS* 2017;8:14754.
119. Sivanandam V, LaRocca CJ, Chen NG, Fong Y, Warner SG. Oncolytic viruses and immune checkpoint inhibition: The best of both worlds. *MOLECULAR THERAPY ONCOLYTICS* 2019;13:93-106.

120. Dias JD, Hemminki O, Diaconu I, Hirvinen M, Bonetti A, et al. Targeted cancer immunotherapy with oncolytic adenovirus coding for a fully human monoclonal antibody specific for ctla-4. *GENE THERAPY* 2012;19(10):988-98.
121. Rojas JJ, Sampath P, Hou W, Thorne SH. Defining effective combinations of immune checkpoint blockade and oncolytic virotherapy. *CLINICAL CANCER RESEARCH : AN OFFICIAL JOURNAL OF THE AMERICAN ASSOCIATION FOR CANCER RESEARCH* 2015;21(24):5543-51.
122. Cervera-Carrascon V, Siurala M, Santos JM, Havunen R, Tähtinen S, et al. Tnfa and il-2 armed adenoviruses enable complete responses by anti-pd-1 checkpoint blockade. *ONCOIMMUNOLOGY* 2018;7(5):e1412902.
123. Bourgeois-Daigneault MC, Roy DG, Aitken AS, El Sayes N, Martin NT, et al. Neoadjuvant oncolytic virotherapy before surgery sensitizes triple-negative breast cancer to immune checkpoint therapy. *SCIENCE TRANSLATIONAL MEDICINE* 2018;10(422):eaa01641.
124. Hwang JK, Hong J, Yun CO. Oncolytic viruses and immune checkpoint inhibitors: Preclinical developments to clinical trials. *INTERNATIONAL JOURNAL OF MOLECULAR SCIENCES* 2020;21(22):8627.
125. Puzanov I, Milhem MM, Minor D, Hamid O, Li A, et al. Talimogene laherparepvec in combination with ipilimumab in previously untreated, unresectable stage iiib-iv melanoma. *JOURNAL OF CLINICAL ONCOLOGY : OFFICIAL JOURNAL OF THE AMERICAN SOCIETY OF CLINICAL ONCOLOGY* 2016;34(22):2619-26.
126. Chesney J, Puzanov I, Collichio F, Singh P, Milhem MM, et al. Randomized, open-label phase ii study evaluating the efficacy and safety of talimogene laherparepvec in combination with ipilimumab versus ipilimumab alone in patients with advanced, unresectable melanoma. *JOURNAL OF CLINICAL ONCOLOGY : OFFICIAL JOURNAL OF THE AMERICAN SOCIETY OF CLINICAL ONCOLOGY* 2018;36(17):1658-67.
127. Curti B, Richards J, Faries M, Andtbacka RHI, Grose M, et al. The mitci (phase 1b) study: A novel immunotherapy combination of coxsackievirus a21 and ipilimumab in patients with advanced melanoma. *ANNALS OF ONCOLOGY* 2016;27:vi359–vi78.
128. Ribas A, Dummer R, Puzanov I, VanderWalde A, Andtbacka RHI, et al. Oncolytic virotherapy promotes intratumoral t cell infiltration and improves anti-pd-1 immunotherapy. *CELL* 2017;170(6):1109-19 e10.
129. Zadeh G, Lang F, Daras M, Cloughesy T, Colman H, et al. Atim-24. Interim results of a phase ii multicenter study of the conditionally replicative oncolytic adenovirus dnx-2401 with pembrolizumab (keytruda) for recurrent glioblastoma; captive study (keynote-192). *NEURO-ONCOLOGY* 2018;20(6)

130. Zugmaier G, Gökbuget N, Klinger M, Viardot A, Stelljes M, et al. Long-term survival and t-cell kinetics in relapsed/refractory all patients who achieved mrd response after blinatumomab treatment. *BLOOD* 2015;126(24):2578-84.
131. Viardot A, Goebeler M-E, Hess G, Neumann S, Pfreundschuh M, et al. Phase 2 study of the bispecific t-cell engager (bite) antibody blinatumomab in relapsed/refractory diffuse large b-cell lymphoma. *BLOOD* 2016;127(11):1410-16.
132. Kantarjian H, Stein A, Gökbuget N, Fielding AK, Schuh AC, et al. Blinatumomab versus chemotherapy for advanced acute lymphoblastic leukemia. *NEW ENGLAND JOURNAL OF MEDICINE* 2017;376(9):836-47.
133. Scott EM, Duffy MR, Freedman JD, Fisher KD, Seymour LW. Solid tumor immunotherapy with t cell engager-armed oncolytic viruses. *MACROMOLECULAR BIOSCIENCE* 2018;18(1):1700187.
134. Yu F, Wang X, Guo ZS, Bartlett DL, Gottschalk SM, et al. T-cell engager-armed oncolytic vaccinia virus significantly enhances antitumor therapy. *MOLECULAR THERAPY* 2014;22(1):102-11.
135. Freedman JD, Hagel J, Scott EM, Psallidas I, Gupta A, et al. Oncolytic adenovirus expressing bispecific antibody targets t-cell cytotoxicity in cancer biopsies. *EMBO MOLECULAR MEDICINE* 2017;9(8):1067-87.
136. Speck T, Heidbuechel JPW, Veinalde R, Jaeger D, von Kalle C, et al. Targeted bite expression by an oncolytic vector augments therapeutic efficacy against solid tumors. *CLINICAL CANCER RESEARCH* 2018;24(9):2128-37.
137. Fajardo CA, Guedan S, Rojas LA, Moreno R, Arias-Badia M, et al. Oncolytic adenoviral delivery of an egfr-targeting t-cell engager improves antitumor efficacy. *CANCER RESEARCH* 2017;77(8):2052-63.
138. Ungerechts G, Springfield C, Frenzke ME, Lampe J, Parker WB, et al. An immunocompetent murine model for oncolysis with an armed and targeted measles virus. *MOLECULAR THERAPY* 2007;15(11):1991-97.
139. Yaiw KC, Miest TS, Frenzke M, Timm M, Johnston PB, et al. Cd20-targeted measles virus shows high oncolytic specificity in clinical samples from lymphoma patients independent of prior rituximab therapy. *GENE THERAPY* 2011;18(3):313-17.
140. Paul S, Regulier E, Rooke R, Stoeckel F, Geist M, et al. Tumor gene therapy by mva-mediated expression of t-cell-stimulating antibodies. *CANCER GENE THERAPY* 2002;9(5):470-77.
141. Fu X, Tao L, Wu W, Zhang X. Arming hsv-based oncolytic viruses with the ability to redirect the host's innate antiviral immunity to attack tumor cells. *MOL THER ONCOLYTICS* 2020;19:33-46.

142. Chen X, Song E. Turning foes to friends: Targeting cancer-associated fibroblasts. *NATURE REVIEWS DRUG DISCOVERY* 2019;18(2):99-115.
143. Yu F, Hong B, Song X-T. A t-cell engager-armed oncolytic vaccinia virus to target the tumor stroma. *CANCER TRANSLATIONAL MEDICINE* 2017;3(4):122.
144. Freedman JD, Duffy MR, Lei-Rossmann J, Muntzer A, Scott EM, et al. An oncolytic virus expressing a t-cell engager simultaneously targets cancer and immunosuppressive stromal cells. *CANCER RESEARCH* 2018;78(24):6852-65.
145. de Sostoa J, Fajardo CA, Moreno R, Ramos MD, Farrera-Sal M, et al. Targeting the tumor stroma with an oncolytic adenovirus secreting a fibroblast activation protein-targeted bispecific t-cell engager. *JOURNAL FOR IMMUNOTHERAPY OF CANCER* 2019;7(1):1-15.
146. Scott EM, Jacobus EJ, Lyons B, Frost S, Freedman JD, et al. Bi- and tri-valent t cell engagers deplete tumour-associated macrophages in cancer patient samples. *JOURNAL FOR IMMUNOTHERAPY OF CANCER* 2019;7(1):1-18.
147. Porter CE, Shaw AR, Jung Y, Yip T, Castro PD, et al. Oncolytic adenovirus armed with bite, cytokine, and checkpoint inhibitor enables car t cells to control the growth of heterogeneous tumors. *MOLECULAR THERAPY* 2020;28(5):1251-62.
148. Choi BD, Yu X, Castano AP, Bouffard AA, Schmidts A, et al. Car-t cells secreting bites circumvent antigen escape without detectable toxicity. *NATURE BIOTECHNOLOGY* 2019;37(9):1049-58.
149. Kamperschroer C, Shenton J, Lebrech H, Leighton JK, Moore PA, et al. Summary of a workshop on preclinical and translational safety assessment of cd3 bispecifics. *JOURNAL OF IMMUNOTOXICOLOGY* 2020;17(1):67-85.
150. Li H, Peng K-W, Dingli D, Kratzke RA, Russell SJ. Oncolytic measles viruses encoding interferon  $\beta$  and the thyroidal sodium iodide symporter gene for mesothelioma virotherapy. *CANCER GENE THERAPY* 2010;17(8):550-58.
151. Pulido J, Kottke T, Thompson J, Galivo F, Wongthida P, et al. Using virally expressed melanoma cDNA libraries to identify tumor-associated antigens that cure melanoma. *NATURE BIOTECHNOLOGY* 2012;30(4):337-43.
152. Ramakrishna E, Woller N, Mundt B, Knocke S, Gürlevik E, et al. Antitumoral immune response by recruitment and expansion of dendritic cells in tumors infected with telomerase-dependent oncolytic viruses. *CANCER RESEARCH* 2009;69(4):1448-58.
153. Buijs P, Van Nieuwkoop S, Vaes V, Fouchier R, Van Eijck C, et al. Recombinant immunomodulating lentogenic or mesogenic oncolytic newcastle disease virus for treatment of pancreatic adenocarcinoma. *VIRUSES* 2015;7(6):2980-98.

154. Zamarin D, Vigil A, Kelly K, García-Sastre A, Fong Y. Genetically engineered newcastle disease virus for malignant melanoma therapy. *GENE THERAPY* 2009;16(6):796-804.
155. Grossardt C, Engeland CE, Bossow S, Halama N, Zaoui K, et al. Granulocyte-macrophage colony-stimulating factor-armed oncolytic measles virus is an effective therapeutic cancer vaccine. *HUMAN GENE THERAPY* 2013;24(7):644-54.
156. Prestwich RJ, Errington F, Hatfield P, Merrick AE, Ilett EJ, et al. The immune system — is it relevant to cancer development, progression and treatment? *CLINICAL ONCOLOGY* 2008;20(2):101-12.
157. Du R, Zhao H, Yan F, Li H. Il-17+ foxp3+ t cells: An intermediate differentiation stage between th17 cells and regulatory t cells. *JOURNAL OF LEUKOCYTE BIOLOGY* 2014;96(1):39-48.
158. Shin EJ, Wanna GB, Choi B, Aguila Iii D, Ebert O, et al. Interleukin-12 expression enhances vesicular stomatitis virus oncolytic therapy in murine squamous cell carcinoma. *THE LARYNGOSCOPE* 2007;117(2):210-14.
159. Niu Z, Bai F, Sun T, Tian H, Yu D, et al. Recombinant newcastle disease virus expressing il15 demonstrates promising antitumor efficiency in melanoma model. *TECHNOLOGY IN CANCER RESEARCH & TREATMENT* 2015;14(5):607-15.
160. Hock K, Laengle J, Kuznetsova I, Egorov A, Hegedus B, et al. Oncolytic influenza a virus expressing interleukin-15 decreases tumor growth in vivo. *SURGERY* 2017;161(3):735-46.
161. Li J, O'Malley M, Urban J, Sampath P, Guo ZS, et al. Chemokine expression from oncolytic vaccinia virus enhances vaccine therapies of cancer. *MOLECULAR THERAPY* 2011;19(4):650-57.
162. Parker JN, Meleth S, Hughes KB, Gillespie GY, Whitley RJ, et al. Enhanced inhibition of syngeneic murine tumors by combinatorial therapy with genetically engineered hsv-1 expressing ccl2 and il-12. *CANCER GENE THERAPY* 2005;12(4):359-68.
163. Li J, O'Malley M, Sampath P, Kalinski P, Bartlett DL, et al. Expression of ccl19 from oncolytic vaccinia enhances immunotherapeutic potential while maintaining oncolytic activity. *NEOPLASIA* 2012;14(12):1115-IN1.
164. Liu Z, Ravindranathan R, Li J, Kalinski P, Guo ZS, et al. Cxcl11-armed oncolytic poxvirus elicits potent antitumor immunity and shows enhanced therapeutic efficacy. *ONCOIMMUNOLOGY* 2015;5(3):e1091554.
165. Engeland CE, Grossardt C, Veinalde R, Bossow S, Lutz D, et al. Ctl4 and pd-1 checkpoint blockade enhances oncolytic measles virus therapy. *MOLECULAR THERAPY* 2014;22(11):1949-59.

166. Fukuhara H, Ino Y, Kuroda T, Martuza RL, Todo T. Triple gene-deleted oncolytic herpes simplex virus vector double-armed with interleukin 18 and soluble b7-1 constructed by bacterial artificial chromosome-mediated system. *CANCER RESEARCH* 2005;65(23):10663-68.
167. Kaufman HL, DeRaffele G, Mitcham J, Moroziewicz D, Cohen SM, et al. Targeting the local tumor microenvironment with vaccinia virus expressing b7. 1 for the treatment of melanoma. *THE JOURNAL OF CLINICAL INVESTIGATION* 2005;115(7):1903-12.
168. Pesonen S, Diaconu I, Kangasniemi L, Ranki T, Kanerva A, et al. Oncolytic immunotherapy of advanced solid tumors with a cd40l-expressing replicating adenovirus: Assessment of safety and immunologic responses in patients. *CANCER RESEARCH* 2012;72(7):1621-31.
169. Parviainen S, Ahonen M, Diaconu I, Hirvonen M, Karttunen Å, et al. Cd40 ligand and tdtomato-armed vaccinia virus for induction of antitumor immune response and tumor imaging. *GENE THERAPY* 2014;21(2):195-204.
170. Galivo F, Diaz RM, Thanarajasingam U, Jevremovic D, Wongthida P, et al. Interference of cd40l-mediated tumor immunotherapy by oncolytic vesicular stomatitis virus. *HUMAN GENE THERAPY* 2010;21(4):439-50.
171. Kim HS, Kim-Schulze S, Kim DW, Kaufman HL. Host lymphodepletion enhances the therapeutic activity of an oncolytic vaccinia virus expressing 4-1bb ligand. *CANCER RESEARCH* 2009;69(21):8516-25.
172. Yan L, Silva DMD, Verma B, Gray A, Brand HE, et al. Forced light expression in prostate tumors overcomes treg mediated immunosuppression and synergizes with a prostate tumor therapeutic vaccine by recruiting effector t lymphocytes. *THE PROSTATE* 2015;75(3):280-91.
173. Lorenz MGO, Kantor JA, Schlom J, Hodge JW. Anti-tumor immunity elicited by a recombinant vaccinia virus expressing cd70 (cd271). *HUMAN GENE THERAPY* 1999;10(7):1095-103.
174. Choi K-J, Zhang S-N, Choi I-K, Kim J-S, Yun C-O. Strengthening of antitumor immune memory and prevention of thymic atrophy mediated by adenovirus expressing il-12 and gm-csf. *GENE THERAPY* 2012;19(7):711-23.
175. Lee Y-S, Kim J-H, Choi K-J, Choi I-K, Kim H, et al. Enhanced antitumor effect of oncolytic adenovirus expressing interleukin-12 and b7-1 in an immunocompetent murine model. *CLINICAL CANCER RESEARCH* 2006;12(19):5859-68.
176. Choi KJ, Kim JH, Lee YS, Kim J, Suh BS, et al. Concurrent delivery of gm-csf and b7-1 using an oncolytic adenovirus elicits potent antitumor effect. *GENE THERAPY* 2006;13(13):1010-20.

177. Wang W, Ji W, Hu H, Ma J, Li X, et al. Survivin promoter-regulated oncolytic adenovirus with hsp70 gene exerts effective antitumor efficacy in gastric cancer immunotherapy. *ONCOTARGET* 2014;5(1):150-60.
178. Hou W, Sampath P, Rojas JJ, Thorne SH. Oncolytic virus-mediated targeting of pge2 in the tumor alters the immune status and sensitizes established and resistant tumors to immunotherapy. *CANCER CELL* 2016;30(1):108-19.
179. Hirvinen M, Capasso C, Guse K, Garofalo M, Vitale A, et al. Expression of dai by an oncolytic vaccinia virus boosts the immunogenicity of the virus and enhances antitumor immunity. *MOLECULAR THERAPY-ONCOLYTICS* 2016;3:16002.
180. Macedo N, Miller DM, Haq R, Kaufman HL. Clinical landscape of oncolytic virus research in 2020. *JOURNAL FOR IMMUNOTHERAPY OF CANCER* 2020;8(2):e001486.
181. Bommareddy PK, Shettigar M, Kaufman HL. Integrating oncolytic viruses in combination cancer immunotherapy. *NATURE REVIEWS IMMUNOLOGY* 2018;18(8):498-513.
182. Conry RM, Westbrook B, McKee S, Norwood TG. Talimogene laherparepvec: First in class oncolytic virotherapy. *HUMAN VACCINES & IMMUNOTHERAPEUTICS* 2018;14(4):839-46.
183. Campbell JA, Trossman DS, Yokoyama WM, Carayannopoulos LN. Zoonotic orthopoxviruses encode a high-affinity antagonist of nkg2d. *JOURNAL OF EXPERIMENTAL MEDICINE* 2007;204(6):1311-17.
184. Annunziato F, Cosmi L, Santarlasci V, Maggi L, Liotta F, et al. Phenotypic and functional features of human th17 cells. *JOURNAL OF EXPERIMENTAL MEDICINE* 2007;204(8):1849-61.
185. Thorsson V, Gibbs DL, Brown SD, Wolf D, Bortone DS, et al. The immune landscape of cancer. *IMMUNITY* 2018;48(4):812-30.e14.
186. Linette GP, Carreno BM. Tumor-infiltrating lymphocytes in the checkpoint inhibitor era. *CURRENT HEMATOLOGIC MALIGNANCY REPORTS* 2019;14(4):286-91.
187. Koch MS, Lawler SE, Chiocca EA. Hsv-1 oncolytic viruses from bench to bedside: An overview of current clinical trials. *CANCERS (BASEL)* 2020;12(12)
188. Chon HJ, Lee WS, Yang H, Kong SJ, Lee NK, et al. Tumor microenvironment remodeling by intratumoral oncolytic vaccinia virus enhances the efficacy of immune-checkpoint blockade. *CLINICAL CANCER RESEARCH* 2019;25(5):1612-23.
189. Du Y, Huang Q, Arisdakessian C, Garmire LX. Evaluation of star and kallisto on single cell rna-seq data alignment. *G3: GENES|GENOMES|GENETICS* 2020;10(5):1775-83.

190. Bangari D, Mittal S. Current strategies and future directions for eluding adenoviral vector immunity. *CURRENT GENE THERAPY* 2006;6(2):215-26.
191. Vieth B, Parekh S, Ziegenhain C, Enard W, Hellmann I. A systematic evaluation of single cell rna-seq analysis pipelines. *NATURE COMMUNICATIONS* 2019;10(1):4667.
192. Helmink BA, Reddy SM, Gao J, Zhang S, Basar R, et al. B cells and tertiary lymphoid structures promote immunotherapy response. *NATURE* 2020;577(7791):549-55.
193. Hollern DP, Xu N, Thennavan A, Glodowski C, Garcia-Recio S, et al. B cells and t follicular helper cells mediate response to checkpoint inhibitors in high mutation burden mouse models of breast cancer. *CELL* 2019;179(5):1191-206.
194. Jin S, Guerrero-Juarez CF, Zhang L, Chang I, Ramos R, et al. Inference and analysis of cell-cell communication using cellchat. *NATURE COMMUNICATIONS* 2021;12(1)
195. Janssen LME, Ramsay EE, Logsdon CD, Overwijk WW. The immune system in cancer metastasis: Friend or foe? *JOURNAL FOR IMMUNOTHERAPY OF CANCER* 2017;5(1)
196. Nakanishi Y, Lu B, Gerard C, Iwasaki A. Cd8(+) t lymphocyte mobilization to virus-infected tissue requires cd4(+) t-cell help. *NATURE* 2009;462(7272):510-13.
197. Ramelyte E, Tastanova A, Balázs Z, Ignatova D, Turko P, et al. Oncolytic virotherapy-mediated anti-tumor response: A single-cell perspective. *CANCER CELL* 2021;39(3):394-406.
198. Bishnoi S, Tiwari R, Gupta S, Byrareddy SN, Nayak D. Oncotargeting by vesicular stomatitis virus (vsv): Advances in cancer therapy. *VIRUSES* 2018;10(2)
199. Peter M, Kühnel F. Oncolytic adenovirus in cancer immunotherapy. *CANCERS (BASEL)* 2020;12(11)
200. Torres-Domínguez LE, McFadden G. Poxvirus oncolytic virotherapy. *EXPERT OPINION ON BIOLOGICAL THERAPY* 2019;19(6):561-73.
201. Msaouel P, Opyrchal M, Dispenzieri A, Peng KW, Federspiel MJ, et al. Clinical trials with oncolytic measles virus: Current status and future prospects. *CURRENT CANCER DRUG TARGETS* 2018;18(2):177-87.
202. Sun L, Funchain P, Song JM, Rayman P, Tannenbaum C, et al. Talimogene laherparepvec combined with anti-pd-1 based immunotherapy for unresectable stage iii-iv melanoma: A case series. *JOURNAL FOR IMMUNOTHERAPY OF CANCER* 2018;6(1):36.
203. Ma J, Ramachandran M, Jin C, Quijano-Rubio C, Martikainen M, et al. Characterization of virus-mediated immunogenic cancer cell death and the consequences for oncolytic virus-based immunotherapy of cancer. *CELL DEATH & DISEASE* 2020;11(1):48.

204. You Y, Cheng AC, Wang MS, Jia RY, Sun KF, et al. The suppression of apoptosis by alpha-herpesvirus. *CELL DEATH & DISEASE* 2017;8(4):e2749.
205. Kanerva A, Nokisalmi P, Diaconu I, Koski A, Cerullo V, et al. Antiviral and antitumor t-cell immunity in patients treated with gm-csf-coding oncolytic adenovirus. *CLIN CANCER RESEARCH* 2013;19(10):2734-44.
206. Zhang T, Kordish D, Suryawanshi Y, Eversole R, Kohler S, et al. Oncolytic tanapoxvirus expressing interleukin-2 is capable of inducing the regression of human melanoma tumors in the absence of t cells. *CURR CANCER DRUG TARGETS* 2017;17
207. Ghiasi H, Osorio Y, Perng GC, Nesburn AB, Wechsler SL. Overexpression of interleukin-2 by a recombinant herpes simplex virus type 1 attenuates pathogenicity and enhances antiviral immunity. *JOURNAL OF VIROLOGY* 2002;76(18):9069-78.
208. Jiang H, Rivera-Molina Y, Gomez-Manzano C, Clise-Dwyer K, Bover L, et al. Oncolytic adenovirus and tumor-targeting immune modulatory therapy improve autologous cancer vaccination. *CANCER RESEARCH* 2017;77(14):3894-907.
209. Breitbach CJ, De Silva NS, Falls TJ, Aladl U, Evgin L, et al. Targeting tumor vasculature with an oncolytic virus. *MOL THER* 2011;19(5):886-94.
210. Raulet DH. Roles of the nkg2d immunoreceptor and its ligands. *NATURE REVIEWS IMMUNOLOGY* 2003;3(10):781-90.
211. Sigismund S, Avanzato D, Lanzetti L. Emerging functions of the egfr in cancer. *MOLECULAR ONCOLOGY* 2018;12(1):3-20.
212. Yu S, Yi M, Qin S, Wu K. Next generation chimeric antigen receptor t cells: Safety strategies to overcome toxicity. *MOLECULAR CANCER* 2019;18(1):125.
213. Lahti JL, Lui BH, Beck SE, Lee SS, Ly DP, et al. Engineered epidermal growth factor mutants with faster binding on-rates correlate with enhanced receptor activation. *FEBS LETTERS* 2011;585(8):1135-9.
214. Zhang X, De Alwis M, Hart SL, Fitzke FW, Inglis SC, et al. High-titer recombinant adeno-associated virus production from replicating amplicons and herpes vectors deleted for glycoprotein h. *HUMAN GENE THERAPY* 1999;10(15):2527-37.
215. Ghasemi R, Lazear E, Wang X, Arefanian S, Zheleznyak A, et al. Selective targeting of il-2 to nkg2d bearing cells for improved immunotherapy. *NATURE COMMUNICATIONS* 2016;7:12878.
216. Wang K, Li D, Sun L. High levels of egfr expression in tumor stroma are associated with aggressive clinical features in epithelial ovarian cancer. *ONCOTARGETS & THERAPY* 2016;9:377-86.

217. Lanigan TM, Rasmussen SM, Weber DP, Athukorala KS, Campbell PL, et al. Real time visualization of cancer cell death, survival and proliferation using fluorochrome-transfected cells in an incucyte((r)) imaging system. *JOURNAL OF BIOLOGICAL METHODS* 2020;7(2):e133.
218. Kruse CA, Visonneau S, Kleinschmidt-DeMasters BK, Gup CJ, Gomez GG, et al. The human leukemic t-cell line, tall-104, is cytotoxic to human malignant brain tumors and traffics through brain tissue: Implications for local adoptive immunotherapy. *CANCER RESEARCH* 2000;60(20):5731-39.
219. He L, Hakimi J, Salha D, Miron I, Dunn P, et al. A sensitive flow cytometry-based cytotoxic t-lymphocyte assay through detection of cleaved caspase 3 in target cells. *JOURNAL OF IMMUNOLOGICAL METHODS* 2005;304(1-2):43-59.
220. Cibrián D, Sánchez-Madrid F. Cd69: From activation marker to metabolic gatekeeper. *EUROPEAN JOURNAL OF IMMUNOLOGY* 2017;47(6):946-53.
221. Jamieson AM, Diefenbach A, McMahon CW, Xiong N, Carlyle JR, et al. The role of the nkg2d immunoreceptor in immune cell activation and natural killing. *IMMUNITY* 2002;17(1):19-29.
222. Trapani JA, Smyth MJ. Functional significance of the perforin/granzyme cell death pathway. *NATURE REVIEWS IMMUNOLOGY* 2002;2(10):735-47.
223. Prajapati K, Perez C, Rojas LBP, Burke B, Guevara-Patino JA. Functions of nkg2d in cd8+ t cells: An opportunity for immunotherapy. *CELLULAR & MOLECULAR IMMUNOLOGY* 2018;15(5):470-79.
224. Bauer S, Groh V, Wu J, Steinle A, Phillips JH, et al. Activation of nk cells and t cells by nkg2d, a receptor for stress-inducible mica. *SCIENCE* 1999;285(5428):727-9.
225. Huehls AM, Coupet TA, Sentman CL. Bispecific t-cell engagers for cancer immunotherapy. *IMMUNOLOGY & CELL BIOLOGY* 2015;93(3):290-6.
226. Voynov V, Adam PJ, Nixon AE, Scheer JM. Discovery strategies to maximize the clinical potential of t-cell engaging antibodies for the treatment of solid tumors. *ANTIBODIES (BASEL)* 2020;9(4)
227. Yano S, Kondo K, Yamaguchi M, Richmond G, Hutchison M, et al. Distribution and function of egfr in human tissue and the effect of egfr tyrosine kinase inhibition. *ANTICANCER RESEARCH* 2003;23(5a):3639-50.
228. Fu X, Meng F, Tao L, Jin A, Zhang X. A strict late viral promoter is a strong tumor-specific promoter in the context of an oncolytic herpes simplex virus. *GENE THERAPY* 2003;10:1458-64.

229. Hwang B, Lee JH, Bang D. Single-cell rna sequencing technologies and bioinformatics pipelines. *EXPERIMENTAL & MOLECULAR MEDICINE* 2018;50(8):96.
230. Hedlund E, Deng Q. Single-cell rna sequencing: Technical advancements and biological applications. *MOLECULAR ASPECTS OF MEDICINE* 2018;59:36-46.
231. Drayman N, Patel P, Vistain L, Tay S. Hsv-1 single-cell analysis reveals the activation of anti-viral and developmental programs in distinct sub-populations. *ELIFE* 2019;8:e46339.
232. Hu B, Li X, Huo Y, Yu Y, Zhang Q, et al. Cellular responses to hsv-1 infection are linked to specific types of alterations in the host transcriptome. *SCIENTIFIC REPORTS* 2016;6(1):1-14.
233. McFadden G, Mohamed MR, Rahman MM, Bartee E. Cytokine determinants of viral tropism. *NATURE REVIEWS IMMUNOLOGY* 2009;9(9):645-55.
234. Jaitin DA, Kenigsberg E, Keren-Shaul H, Elefant N, Paul F, et al. Massively parallel single-cell rna-seq for marker-free decomposition of tissues into cell types. *SCIENCE* 2014;343(6172):776-79.
235. Steuerman Y, Cohen M, Peshes-Yaloz N, Valadarsky L, Cohn O, et al. Dissection of influenza infection in vivo by single-cell rna sequencing. *CELL SYSTEMS* 2018;6(6):679-91.
236. Cristinelli S, Ciuffi A. The use of single-cell rna-seq to understand virus–host interactions. *CURRENT OPINION IN VIROLOGY* 2018;29:39-50.
237. Garvey CE, McGowin CL, Foster TP. Development and evaluation of sybr green-i based quantitative pcr assays for herpes simplex virus type 1 whole transcriptome analysis. *JOURNAL OF VIROLOGICAL METHODS* 2014;201:101-11.
238. Melchjorsen J, Matikainen S, Paludan SR. Activation and evasion of innate antiviral immunity by herpes simplex virus. *VIRUSES* 2009;1(3):737-59.
239. Fensterl V, Sen GC. The isg56/ifit1 gene family. *JOURNAL OF INTERFERON & CYTOKINE RESEARCH* 2011;31(1):71-78.
240. Skaug B, Chen ZJ. Emerging role of isg15 in antiviral immunity. *CELL* 2010;143(2):187-90.
241. Hendry S, Salgado R, Gevaert T, Russell PA, John T, et al. Assessing tumor-infiltrating lymphocytes in solid tumors. *ADVANCES IN ANATOMIC PATHOLOGY* 2017;24(5):235-51.
242. Imamura K I. Longnoncoding RNA NEAT1- dependent sfpq relocation from promoter region to paraspeckle mediates il8 expression upon immune stimuli. *MOLECULAR CELL* 2014;53(3):393.

243. Marino-Merlo F, Papaiani E, Medici MA, Macchi B, Grelli S, et al. Hsv-1-induced activation of nf- $\kappa$  b protects u937 monocytic cells against both virus replication and apoptosis. *CELL DEATH & DISEASE* 2016;7(9):e2354-e54.
244. She M, Jiang H, Chen X, Chen X, Liu X, et al. Gadd45 $\gamma$  activated early in the course of herpes simplex virus 1 infection suppresses the activation of a network of innate immunity genes. *JOURNAL OF VIROLOGY* 2019;93(7)
245. Li S. Regulation of ribosomal proteins on viral infection. *CELLS* 2019;8(5):508.
246. Sims JE, Smith DE. The il-1 family: Regulators of immunity. *NATURE REVIEWS IMMUNOLOGY* 2010;10(2):89-102.
247. Xu D, Mu R, Wei X. The roles of il-1 family cytokines in the pathogenesis of systemic sclerosis. *FRONTIERS IN IMMUNOLOGY* 2019;10:2025.

## **APPENDIX I: LIST OF GLOSSARY (SOURCE: MARY CROWLEY CANCER RESEARCH)**

### **Adjuvant therapy**

Additional cancer treatment given after the primary treatment to lower the risk that the cancer will come back. Adjuvant therapy may include chemotherapy, radiation therapy, hormone therapy, targeted therapy, or biological therapy.

### **ADOPTIVE CELLULAR THERAPY**

A treatment used to help the immune system fight diseases, such as cancer and infections with certain viruses. T cells are collected from a patient and grown in the laboratory. This increases the number of T cells that are able to kill cancer cells or fight infections. These T cells are given back to the patient to help the immune system fight disease. Also called cellular adoptive immunotherapy.

### **ANGIOGENESIS**

Blood vessel formation. Tumor angiogenesis is the growth of new blood vessels that tumors need to grow.

### **ANTIGEN**

Any substance that causes the body to make an immune response against that substance. Antigens include toxins, chemicals, bacteria, viruses, or other substances that come from outside the body. Body tissues and cells, including cancer cells, also have antigens on them that can cause an immune response.

### **APOPTOSIS**

A type of cell death in which a series of molecular steps in a cell lead to its death. This is one method the body uses to get rid of unneeded or abnormal cells.

### **AUTOLOGOUS**

Taken from an individual's own tissues, cells, or DNA.

### **B-CELL**

A type of white blood cell that makes antibodies. Also called B lymphocyte.

### **BENIGN**

Not cancerous. Benign tumors may grow larger but do not spread to other parts of the body. Also called nonmalignant.

### **BIOINFORMATICS**

The science of using computers, databases, and math to organize and analyze large amounts of biological, medical, and health information.

**BIOLOGIC**

A medicinal preparation made from living organisms and their products, such as a serum or vaccine.

**BIOMARKER**

A characteristic that is objectively measured and evaluated as an indicator of normal biological processes, pathogenic processes, or pharmacologic responses to a therapeutic intervention.

**CANCER**

A disease caused by an uncontrolled division of abnormal cells in a part of the body.

**CELLULAR THERAPIES**

The transplantation of human or animal cells to replace or repair damaged tissue.

**CHEMOTHERAPY**

Treatment that uses drugs to stop the growth of cancer cells, either by killing the cells or by stopping them from dividing.

**CLINICAL TRIALS**

A research investigation involving human subjects that is designed to answer specific questions about the safety and efficacy of a biomedical intervention (drug, treatment, device) or new ways of using a known drug, treatment, or device.

**COMBINATION THERAPY**

Therapy that combines more than one method of treatment. Also called multimodality therapy.

**CYTOKINE**

A type of protein that is made by certain immune and non-immune cells and influences the immune system. Some cytokines stimulate the immune system and others slow it down.

**DENDRITIC CELL**

A special type of immune cell that is found in tissues, such as the skin, and boosts immune responses by showing antigens on its surface to other cells of the immune system. A dendritic cell is a type of phagocyte and a type of antigen-presenting cell (APC).

**EFFICACY**

The capacity of a drug or treatment to produce beneficial effects on the course or duration of a disease at the dose tested and against the illness.

**FUSION GENE**

A gene made by joining parts of two different genes. Fusion genes may occur naturally or can be made in the laboratory by combining genes or parts of genes from the same or different organisms.

**FUSION PROTEIN**

A protein made from a fusion gene, which is created by joining parts of two different genes.

**GENE THERAPY**

The insertion, alteration, or removal of genes to correct missing or defective ones that are responsible for disease development/genetic disorders.

**IMMUNE CHECKPOINT INHIBITOR**

A type of drug that blocks certain proteins made by some types of immune system cells, such as T cells, and some cancer cells. These proteins help keep immune responses in check and can keep T cells from killing cancer cells. When these proteins are blocked, the “brakes” on the immune system are released and T cells can kill cancer cells better. Examples of checkpoint proteins found on T cells or cancer cells include PD-1/PD-L1 and CTLA-4/B7-1/B7-2. Some immune checkpoint inhibitors are used to treat cancer.

**IMMUNOSUPPRESSION**

Suppression of the body's immune system and its ability to fight infections and other diseases.

**IMMUNOTHERAPY**

The treatment of disease using medicines that boost the body's natural immune response.

**IN VITRO**

In the laboratory (outside the body).

**IN VIVO**

In the body.

**LYMPHOCYTE**

A lymphocyte is a type of white blood cell. The two main types of lymphocytes are B lymphocytes and T lymphocytes. B lymphocytes make antibodies, and T lymphocytes help kill tumor cells and help control immune responses.

**MALIGNANT**

Cancerous. Malignant cells can invade and destroy nearby tissue and spread to other parts of the body.

**METASTASIS**

The spread of cancer cells from the place where they first formed to another part of the body.

**MOLECULAR IMMUNOLOGY**

Sub-discipline of immunology which investigates the molecular interaction involved in antigen recognition and processing, antibody-antigen interactions, cell-cell interactions, cell death, etc.

**NK CELL**

An NK cell is a type of immune cell that has granules (small particles) with enzymes that can kill tumor cells or cells infected with a virus.

**ONCOLYTIC VIRUS**

A type of virus that infects and lyses (breaks down) cancer cells but not normal cells. Oncolytic viruses can occur naturally or can be made in the laboratory by changing other viruses.

**TARGETED THERAPY**

A type of treatment that uses drugs or other substances to identify and attack specific types of cancer cells with less harm to normal cells. Some targeted therapies block the action of certain enzymes, proteins, or other molecules involved in the growth and spread of cancer cells. Other types of targeted therapies help the immune system kill cancer cells or deliver toxic substances directly to cancer cells and kill them. Targeted therapy may have fewer side effects than other types of cancer treatment. Most targeted therapies are either small molecule drugs or monoclonal antibodies.

**TRANSLATIONAL RESEARCH**

A term used to describe the process by which the results of research done in the laboratory are used to develop new ways to diagnose and treat disease.

**TUMOR-SPECIFIC ANTIGEN**

A protein or other molecule that is unique to cancer cells or is much more abundant in them. These molecules may be potential targets for immunotherapy or other types of anticancer treatment.

**TUMOR SUPPRESSOR GENE**

A type of gene that makes a protein called a tumor suppressor protein that helps control cell growth. Mutations (changes in DNA) in tumor suppressor genes may lead to cancer. Also called antioncogene.

**UNRESECTABLE**

Unable to be removed with surgery.

**VACCINE**

A substance or group of substances meant to cause the immune system to respond to a tumor or to microorganisms, such as bacteria or viruses.

**VIRAL THERAPY**

Treatment using a virus that has been changed in the laboratory to find and destroy cancer cells without harming healthy cells. It is a type of targeted therapy. Also called oncolytic virotherapy, oncolytic virus therapy, and virotherapy.

**VIRAL VECTOR**

A type of virus used in cancer therapy. The virus is changed in the laboratory and cannot cause disease. Viral vectors may produce tumor antigens (proteins found on a tumor cell) to stimulate an antitumor immune response in the body.